Gastroenterology Research and Practice

New Imaging in Gastrointestinal Tract

Guest Editors: Roberto Grassi, Antonio Pinto, Lorenzo Mannelli, Daniele Marin, and Maria Antonietta Mazzei

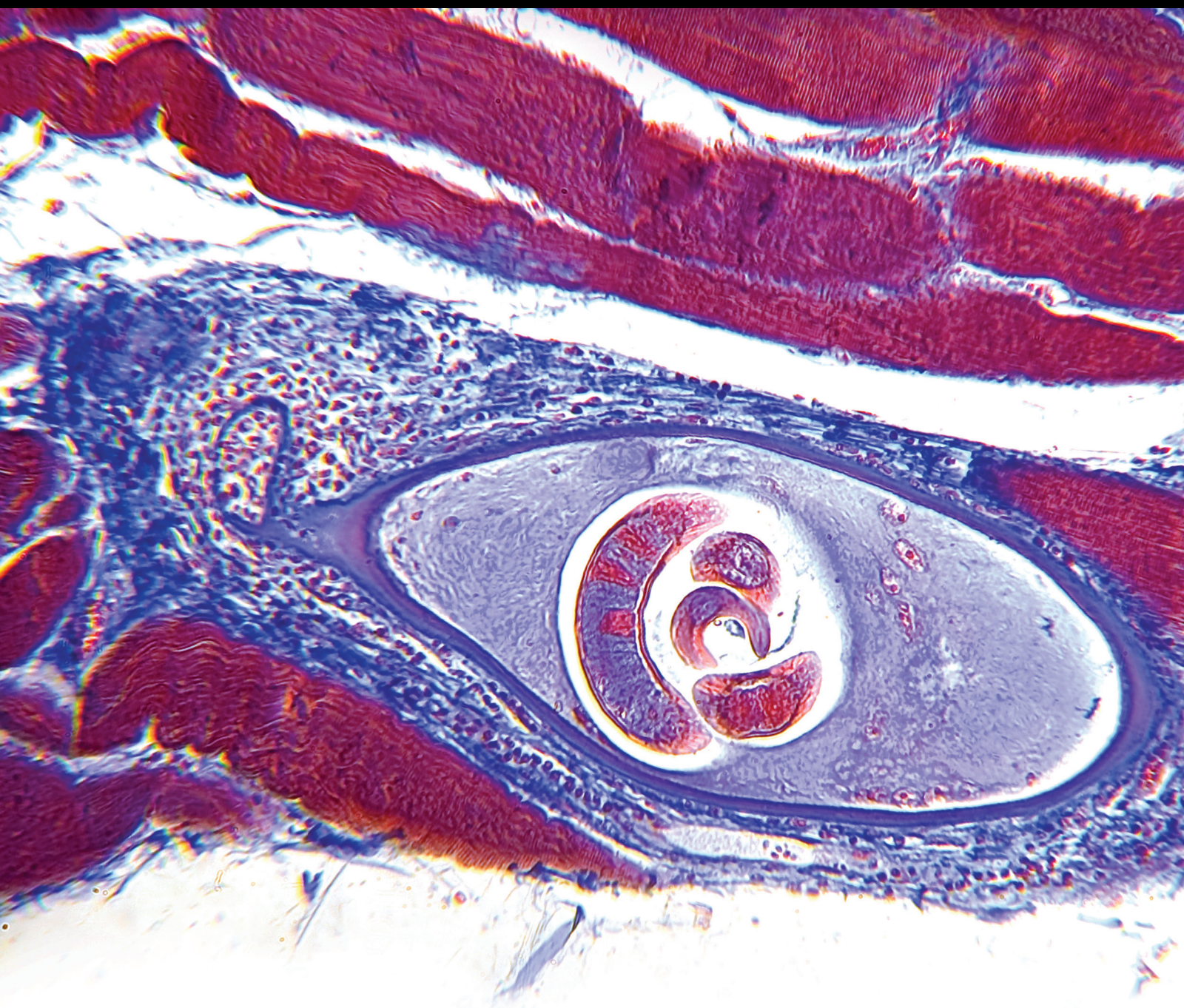

New Imaging in Gastrointestinal Tract

Gastroenterology Research and Practice

New Imaging in Gastrointestinal Tract

Guest Editors: Roberto Grassi, Antonio Pinto,
Lorenzo Mannelli, Daniele Marin, and Maria Antonietta Mazzei

Editorial Board

Contents

Hindawi Publishing Corporation
Gastroenterology Research and Practice
Volume 2016, Article ID 5785871, 2 pages
http://dx.doi.org/10.1155/2016/5785871

Editorial

New Imaging in Gastrointestinal Tract

Roberto Grassi,[1] Antonio Pinto,[2] Lorenzo Mannelli,[3] Daniele Marin,[4] and Maria Antonietta Mazzei[5]

[1]*Institute of Radiology, Second University of Naples, 80138 Naples, Italy*
[2]*Department of Radiology, Cardarelli Hospital, 80123 Naples, Italy*
[3]*Department of Radiology, Memorial Sloan Kettering Cancer Center, 1275 York Avenue, New York, NY 10065, USA*
[4]*Department of Radiology, Duke University Medical Center, Durham, NC 27710, USA*
[5]*Department of Medical, Surgical and Neuro Sciences, Diagnostic Imaging, University of Siena, Azienda Ospedaliera Universitaria Senese, Viale Bracci 10, 53100 Siena, Italy*

Correspondence should be addressed to Maria Antonietta Mazzei; mamazzei@gmail.com

Received 7 December 2015; Accepted 10 December 2015

Pathologies of gastrointestinal tract are various and affect patients of different ages. Both of these conditions influence the imaging modalities of gastrointestinal tract that underwent relevant changes during recent years. Magnetic Resonance (MR) and Computed Tomography (CT) techniques, optimised for gastrointestinal imaging, are playing today an increasing role in the evaluation of gastrointestinal disorders, and several studies have shown the advantage of these techniques over tradition barium fluoroscopic examinations secondary to improvements in spatial and temporal resolution combined with improved bowel distending agents. Based on recent literature and guidelines, there is a change of paradigms regarding the diagnosis of esophagus and gastrointestinal cancer towards CT, whereas for small bowel imaging in inflammatory disease MRI with a new focus on Diffusion Weighted Imaging (DWI) are the most important imaging modalities, because DWI can be easily implemented in standard MRI for routine use to further enhance the diagnostic accuracy in disease assessment [1–4]. CT and MRI play an important role also in functional disorders. In particular, the recent development of faster MRI pulse sequences provides rapid, real-time imaging of the gastrointestinal tract, pinpointing areas of stricture and providing valuable information on motility.

This special issue is devoted to current and emerging techniques in gastrointestinal tract, focusing on some selected topics that are both interesting and challenging: neoplastic pathologies, chronic inflammatory diseases, functional pathologies, and nontraumatic emergency causing occlusion. The first section covers cross-sectional imaging of the gastrointestinal tract in neoplastic disease, including lymphoma, both through a review ("Radiological Features of Gastrointestinal Lymphoma" by G. Lo Re et al.) and through an original paper ("Staging of Primary Abdominal Lymphomas: Comparison of Whole-Body MRI with Diffusion-Weighted Imaging and ^{18}F-FDG-PET/CT" by A. Stecco et al.) and small-bowel neoplasms ("Small-Bowel Neoplasms: Role of MRI Enteroclysis" by A. Faggian et al.). The imaging of hepatocellular carcinoma after locoregional treatments is also reviewed ("CT Appearance of Hepatocellular Carcinoma after Locoregional Treatments: A Comprehensive Review" by D. Marin et al.). Cross-sectional imaging modalities are fundamental also in the management of patients with inflammatory bowel disease (IBD) from the first diagnosis and throughout the entire course of the disease. In this sense, MRI, owing to the lack of ionizing radiation, represents the main technique in young patients with IBD who may require multiple studies over a lifetime. New imaging of chronic inflammatory pathologies is focused on Crohn's disease, where the imaging is essential also in scoring the activity of disease ("3D-EAUS and MRI in the Activity of Anal Fistulas in Crohn's Disease" by M. E. Alabiso et al.; "Assessment of Disease Activity in Small Bowel Crohn's Disease: Comparison between Endoscopy and Magnetic Resonance Enterography

Using Mria and Modified Mria Score" by A. Scardapane et al.). Some functional pathologies are also discussed: achalasia and pelvic floor disfunction ("Imaging in the Evaluation of Endoscopic or Surgical Treatment for Achalasia" by D. Palladino et al.; "MR Imaging in Diagnosis of Pelvic Floor Descent: Supine versus Sitting Position" by F. Iacobellis et al.). Finally nontraumatic emergency causing occlusion is discussed in three different papers, with emphasis on the role of MDCT and dynamic MRI ("Intussusception in Adults: The Role of MDCT in the Identification of the Site and Cause of Obstruction" by V. Valentini et al.; "A Novel Diagnostic Aid for Detection of Intra-Abdominal Adhesions to the Anterior Abdominal Wall Using Dynamic Magnetic Resonance Imaging" by D. Randall et al.; "Adhesions to Mesh after Ventral Hernia Mesh Repair are Detected by MRI but Are Not a Cause of Long Term Chronic Abdominal Pain" by O. Langbach et al.).

The contributions of this special issue could stimulate the spread of new imaging modalities in daily practice, pinpoint technical aspects, and share some strategies to optimise CT and MR protocols.

Roberto Grassi
Antonio Pinto
Lorenzo Mannelli
Daniele Marin
Maria Antonietta Mazzei

References

[1] A. G. Schreyer, J. Wessling, S. Kinner et al., "A review of scientific topics and literature in abdominal radiology in Germany—part 1: gastrointestinal tract," *RöFo*, 2015.

[2] M. Scharitzer and A. Ba-Ssalamah, "Modern MRI of the small bowel," *Der Radiologe*, vol. 55, no. 12, pp. 1067–1076, 2015.

[3] N. Seo, S. H. Park, K.-J. Kim et al., "MR enterography for the evaluation of small-bowel inflammation in Crohn disease by using diffusion-weighted imaging without intravenous contrast material: a prospective noninferiority study," *Radiology*, 2015.

[4] E. Amzallag-Bellenger, P. Soyer, C. Barbe, T. L. F. Nguyen, N. Amara, and C. Hoeffel, "Diffusion-weighted imaging for the detection of mesenteric small bowel tumours with Magnetic Resonance—enterography," *European Radiology*, vol. 24, no. 11, pp. 2916–2926, 2014.

Hindawi Publishing Corporation
Gastroenterology Research and Practice
Volume 2016, Article ID 6594152, 12 pages
http://dx.doi.org/10.1155/2016/6594152

Research Article

MR Imaging in Diagnosis of Pelvic Floor Descent: Supine versus Sitting Position

Francesca Iacobellis,[1] Antonio Brillantino,[2] Adolfo Renzi,[2] Luigi Monaco,[3] Nicola Serra,[1] Beatrice Feragalli,[4] Aniello Iacomino,[1] Luca Brunese,[5] and Salvatore Cappabianca[1]

[1]*Department of Radiology, Second University of Naples, Piazza Miraglia 2, 80138 Napoli, Italy*
[2]*"Villa delle Querce" Hospital, Via Battistello Caracciolo 48, 80136 Napoli, Italy*
[3]*"Villa Esther" Hospital, Via Due Principati 169, 83100 Avellino, Italy*
[4]*Department of Medical, Oral and Biotechnological Sciences, "G. D'Annunzio" University, Via dei Vestini, 66013 Chieti, Italy*
[5]*Department of Health Science, University of Molise, Viale Giovanni Paolo II 1, 86100 Campobasso, Italy*

Correspondence should be addressed to Francesca Iacobellis; francesca.iacobellis@libero.it

Received 15 June 2015; Accepted 13 August 2015

Academic Editor: Lorenzo Mannelli

Introduction. Functional disorders of the pelvic floor represent have a significant impact on the quality of life. The advent of open-configuration systems allowed for the evaluation of defecation with MR imaging in sitting position. The purpose of the present study is to compare the results of static and dynamic pelvic MR performed in supine position versus sitting position, using a new MR prototype machine, in the diagnosis of pelvic floor descent. *Materials and Methods*. Thirty-one patients with pelvic floor disorders were enrolled, and underwent MR Defecography in supine position with 1.5 T closed magnet (MAGNETOM Symphony, Siemens, Germany) and in sitting position with a 0.25-Tesla open magnet system (G-Scan ESAOTE, Italy). *Results*. In rest and squeezing phases, positions of bladder, vagina, and ARJ were significantly different when the patient was imaged in supine versus sitting position. In the defecation phase, a significant difference for the bladder and vagina position was detected between the two exams whereas a significant difference for the ARJ was not found. A statistically significant difference exists when the pelvic floor descent is evaluated in sitting versus supine position. *Conclusion*. Our results show that MR Defecography in sitting position may represent a useful tool to correctly diagnose and grade the pelvic organ descent.

1. Introduction

Functional disorders of the pelvic floor represent common clinical problems and have a significant impact on the quality of life. They comprise a wide range of clinical conditions, including urinary incontinence, sensory and emptying abnormalities of the lower urinary tract, fecal incontinence, defecatory dysfunction, chronic pelvic pain syndromes, and pelvic organ prolapse [1, 2]. Pelvic floor disorders often coexist and, therefore, incontinence, descensus, and organ prolapse may occur in many different combinations [3–5]. Risk factors for pelvic floor dysfunction include pregnancy, multiparity, advanced age, menopause, obesity, connective tissue disorders, smoking, and chronic obstructive pulmonary disease, as well as any other component that results in a chronic rise in intra-abdominal pressure [2, 6, 7]. Although the collection of the clinical history and the physical examination represent the first step in the evaluation of patients with pelvic floor dysfunctions [8], a multidisciplinary approach and the employment of panoramic radiological investigations with a wide and detailed view of the pelvis are needed for a more detailed diagnosis and grading of pelvic floor disorders [2, 9–11] and for the surgical planning [12–16].

Weakness of the pelvic floor can involve anterior, middle, and posterior compartments, producing an abnormal descent of the bladder, uterus, and bowel.

In case of pelvic floor weakness, traditionally diagnosed via physical exam, pelvic magnetic resonance (MR) imaging, with its superior soft-tissue contrast resolution, allows direct visualisation of the pelvic organs and their supportive structures in a single, dynamic, and noninvasive examination [1, 3, 6, 7, 10, 17]; the supine position of the patient during the examination may be a disadvantage, because it may influence the pelvic floor physiology as well as the dynamic defecation process [1, 3].

The advent of open-configuration systems allowed the evaluation of defecation with MR imaging in sitting position, and several studies were performed [5, 18–23]. However, the magnet configuration and the examination technique, as well as the accuracy of the sitting position in the diagnosis of the pelvic floor disorders, are not standardised, not completely defined, and currently debated in literature.

The purpose of the present study is to compare the results of static and dynamic pelvic MR performed in supine position versus sitting position, using a new MR prototype machine, in the diagnosis of pelvic floor descent.

2. Materials and Methods

2.1. Patients and Methods

2.1.1. Ethics. The study was approved by the institutional ethical committee. All patients gave their written informed consent to take part in this study.

From January 2012 to December 2014, all the patients referring to our Radiology Department for pelvic dynamic MRI for the evaluation of pelvic floor disorders were investigated about their clinical history and considered for enrolment in this study.

All the patients eligible for their physical prerequisites (hip circumference less than 100 cm) were asked to be enrolled in the study and so patients that gave their consent underwent sitting MR examination after supine MR examination.

2.1.2. MRI Technique. MR images were obtained after administration of contrast agent (ultrasound gel) into the rectum and vagina in both sitting and supine positions. To ensure an adequate bladder filling, all patients were invited to drink 500–700 mL of water 15–20 min before the examination. Rectum and vagina were filled with 200 mL and about 25–30 mL, respectively, of ultrasonographic gel (Aquasonic, Parker Laboratories, Fairfield, NJ, USA). Rectal cleaning was considered unnecessary.

1.5 T Dynamic MR Defecography. All supine imaging studies were performed on 1.5 T closed magnet (MAGNETOM Symphony, Siemens, Germany). All the patients were supine imaged with a four-channel body-phased-array receiver coil.

After an initial localizer in three different planes, the study protocol includes the following morphological (static) sequences: axial TSE T1-W (TR/TE 611/11; slices: 25; thickness: 5 mm; matrix: 256 × 256; flip angle: 150°), axial TSE T2-W (TR/TE 6430/114; slices: 25; thickness: 5 mm; matrix: 256 × 256; flip angle: 180°), and sagittal TSE T2-W (TR/TE 4650/127; matrix: 256 × 256; slices: 20; thickness: 4 mm; flip angle: 150°).

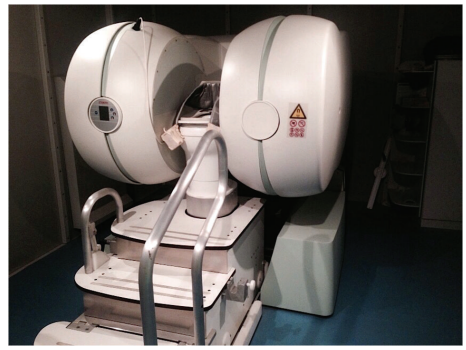

Figure 1: "Pelvic scan" prototype.

Functional dynamic sequences TRUE FISP T2-W sagittal (TR/TE 3.75/1.6; matrix: 256 × 256; slices: 1; thickness: 8 mm; flip angle: 80°) during maximal pelvic floor contraction (squeezing) and defecation phases were acquired. During the dynamic sequences of the examination, patients were instructed via headphones: they were asked first to squeeze and after to strain emptying the rectum as completely as possible. The MR-D images so obtained were assembled in cineview in postprocessing. Examination time (static and dynamic sequences) took about 25–30 min to be completed.

0.25 T Open Magnet MR Defecography. After the examination in supine position, patients were transferred to a 0.25-Tesla open magnet system (G-Scan ESAOTE) and underwent the examination in sitting position.

The adopted magnet is a prototype made modifying the G-Scan ESAOTE tilting open magnet system to carry out the examination with the patient in sitting position on a dedicated commode (Figure 1).

The G-Scan ESAOTE MRI system was originally designed to study the joints and the spine, either in a clinostatic (supine) or in an orthostatic (weight-bearing) position since magnet and patient can rotate from 0 to 90 degrees.

The prototype available in our institution was obtained, positioning the magnet at 90 degrees, increasing the distance originally existing in the G-Scan ESAOTE magnet to insert a dedicated commode equipped with a flexible single channel receiving coil. The coils were specifically designed to maximize the signal/noise ratio in the pelvic floor and they consist of a belt part with solenoidal coils arranged to optimize the signal reception from the lower trunk area, connected to a surface part with concentric coils allowing us to detect signal from the lower part of the pelvic floor. The coils were realized in two different lengths: small, 96 cm, and large, 116 cm.

This allowed patients to be studied in the physiological position adopted during defecation.

The sequence adopted for the dynamic study (2D HYCE sagittal) was specifically developed for this new prototype

Table 1: Synthesis of the measures (in cm) of pelvic organs in respect to the PCP, in rest, squeeze, and defecation phases in both sitting and supine examinations in all patients. SD: standard deviation.

	Sitting position			Supine position		
	Rest	Squeeze	Defecation	Rest	Squeeze	Defecation
Bladder						
Mean (±SD)	9.29 (1.37)	1.72 (1.26)	−1.35 (1.78)	2.41 (0.9)	2.68 (0.88)	−0.41 (2.06)
Median (range)	1.40 (3.56−−2.72)	1.80 (4.70−−2.20)	−1.37 (1.90−−4.30)	2.34 (4.90–0.48)	2.51 (5.18–1.40)	−0.70 (3.23−−4.35)
Vagina						
Mean (±SD)	3.23 (0.79)	3.70 (0.76)	0.13 (2.61)	4.47 (0.87)	4.47 (0.87)	1.48 (2.45)
Median (range)	3.27 (4.48–0.74)	3.80 (5.25–1.94)	1.04 (3.20−−5.40)	4.49 (6.21–2.57)	4.49 (6.21–2.57)	2.14 (5.95−−4.32)
ARJ						
Mean (±SD)	−2.88 (1.05)	−1.51 (1.36)	−5.15 (1.99)	−1.45 (1.78)	−0.59 (1.78)	−4.72 (1.70)
Median (range)	−3.00 (−0.97−−5.30)	−1.66 (1.30−−4.86)	−5.08 (−1.00−−8.97)	−1.87 (4.19−−5.12)	−1.87 (4.19−−5.12)	−4.96 (−1.14−−8.56)

and it is a balanced steady-state gradient-echo sequence that allows one to acquire images of the same layer previously selected by the user, repeatedly.

The rectum and vagina were filled of gel and static images were first obtained acquiring the following sequences: axial FSE T2 (TR/TE/NEX, 3140/100/1; slices: 19; thickness: 6 mm; FOV: 420 ∗ 420; oversampling: 130), sagittal FSE T2 (TR/TE/NEX, 3200/100/1; slices: 11; thickness: 6 mm; FOV: 300 ∗ 300; oversampling: 182). During squeezing and defecation, functional 2D HYCE sagittal (TR/TE/NEX 14/7/1; slices: 1, thickness: 12.5 mm, FOV: 280∗280, matrix: 208∗206) sequences were acquired in sitting position. Overall MR time for the study was approximately 25–30 minutes.

2.1.3. Image Analysis. Images were analysed in consensus by an experienced board-certified abdominal radiologist (SC) and a radiology resident with four years of experience in abdominal radiology (FI).

The degree of the pelvic organs descent was evaluated measuring the perpendicular distance between the pubococcygeal plane (PCP) and the bladder base and the posterior vaginal fornix or the vaginal vault (if the patient was hysterectomized) and the anorectal junction (ARJ) during each of the three phases: rest, squeezing, and defecation in both supine and sitting MR examinations. The reference plane used for MRI, the PCP, is defined as the plane of the pubococcygeal line (PCL) which connects the inferior margin of the symphysis pubis with the last coccygeal joint. The anorectal junction is defined as the point of taper of the distal part of the rectum as it meets the anal canal, corresponding to the posterior impression of the transition between puborectal muscle and levator plate, and it represents the point of reference for posterior compartment descent [24, 25].

According to the majority of the authors, an ARJ position lower than 3 centimetres (cm) in respect to PCP in the resting phase or a descent of more than 3 cm during the evacuation, if compared with the position at rest, is the definition of fixed and dynamic perineal descent, respectively [5, 26–30].

A descent of more than 1 cm at rest or during evacuation of the bladder base and of the posterior vaginal fornix or vaginal vault in respect to the PCP is considered suggestive for anterior and middle prolapse, respectively [5, 25]. The distances in centimetres between PCP and bladder and vaginal fornix or vaginal vault and ARJ were considered positive if they have a position above PCP, negative if they have a position under PCP, and null value if they have a position on the PCP.

Data were compared analysing the difference between the two different positions in the three different phases (rest, squeeze, and defecation), the difference in the detection of fixed and dynamic perineal descent, and the existence of possible correlation between supine and sitting positions.

2.1.4. Statistical Analysis. The statistical analyses were performed using MATLAB statistical toolbox version 2008 (MathWorks, Natick, MA, USA) for Windows at 32 bits on random sample of 31 patients, 12.90% males and 87.10% females. ANOVA test [31], Fisher's exact test, Pearson linear correlation [32], Student t-test, and Z-test [33] were used for data analysis. A p value < 0.05 was considered significant.

3. Results

Two hundred patients with clinical symptoms suggestive for pelvic floor descent referred to our Radiology Department for pelvic dynamic MRI for the evaluation of pelvic floor disorders.

Fifty patients satisfied the physical prerequisite to be examined in sitting position and they were asked to take part in the study.

Out of these, 31 patients (27 female, 473 male; mean age: 48.5 years; range: 21–74) gave the consent to participate in the study and were imaged in both positions.

The procedures were well tolerated by all the patients and were successful in all cases. The average total examinations time was 60 minutes per patient.

In all cases, the images quality was diagnostic.

In Table 1, the measures (in centimetres) of pelvic organs in respect to the PCP, in rest, squeeze, and defecation phases,

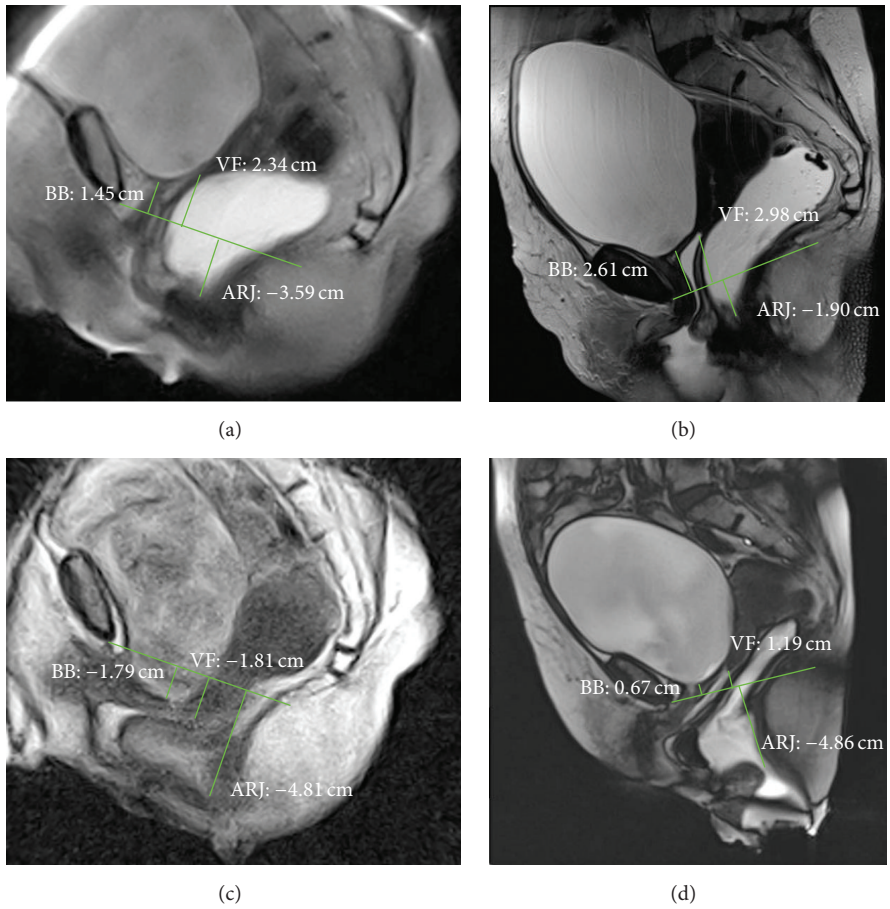

Figure 2: MR Defecography. Rest phase in sitting (a) and supine (b) position. Evacuation phase in sitting (c) and supine (d) position. The pathological fixed descent was detected only in sitting position in rest phase (a). In evacuation phase, a cystocele became evident (d), whereas the maximal descent of the ARJ is similar in both sitting and supine position (c, d). BB: bladder base; VF: vaginal fornix; ARJ: anorectal junction.

in both sitting and supine examinations in all patients are reported.

In rest phase, both positions of bladder and ARJ were significantly different when the patient was imaged in supine versus sitting position (p value ≤ 0.0001 and p value ≤ 0.001, resp.) (Figures 2(a), 2(b), 3(a), and 3(b)); also during squeezing, both positions of bladder and ARJ were significantly different when the patient was imaged in supine versus sitting position (p value = 0.0011; p value = 0.0154). In the defecation phase, a significant difference for the bladder position was detected between the two exams (p value ≤ 0.001) whereas a significant difference for the ARJ was not found (p value = 0.373) (Figures 2(c), 2(d), 4(c), and 4(d)).

In the rest phase, a fixed pelvic floor descent was detected in sitting position in 16/31 (51.6%) patients whereas only in 2/31 (0.64%) the supine MR detected a descent of more than 3 cm ($p > 0.0005$) (Figures 2(a), 2(b), 3(a), 3(b), 4(a), and 4(b)).

In rest phase, a cystocele was detected in sitting position in 4/31 (12.9%) patients whereas in 0/31 (0%) the supine MR detected a descent of more than 1 cm ($p > 0.11$).

In evacuation phase, a cystocele was detected in sitting position in 20/31 (64.5%) patients whereas in 14/31 (45.16%) the supine MR detected a descent of more than 1 cm ($p = 0.20$) (Figures 3(c) and 3(d)). The dynamic descent for the bladder and the ARJ was also evaluated and compared: a statistically major descent was detected in supine position if compared with sitting position for both bladder and the ARJ (p value = 0.04; p value = 0.0157) (Figure 2).

In Figure 5, the graphic representation of the ANOVA test is shown.

A dynamic descent was detected in sitting position in 10/31 (32.25%) patients and in 18/31 (58%) in supine position ($p = 0.3$).

The measures of pelvic organs in respect to the PCP were also examined for the female and male subgroups as shown in Table 2.

In the female subgroup ($n = 27$), in rest phase, the positions of bladder, ARJ, and vagina were significantly different (p value ≤ 0.0001) when the patient is imaged in supine versus sitting position.

In squeezing phase only for bladder and vagina, there was a statistically significant difference (p value = 0.0002

Table 2: Synthesis of the measures (in cm) of pelvic organs in respect to the PCP, in rest, squeeze, and defecation phases in both sitting and supine examinations in male and female patient subgroups. SD: standard deviation.

	Sitting position						Supine position					
	Rest		Squeeze		Defecation		Rest		Squeeze		Defecation	
	Male	Female	Male	Female	Male	Female	Male	Female	Male	Female	Male	Female
Bladder												
Mean (SD)	2.34 (0.73)	0.71 (1.28)	3.52 (1.06)	1.45 (±1.05)	0.36 (1.27)	−1.58 (±1.74)	4.11 (0.67)	2.15 (0.60)	4.37 (0.99)	2.43 (0.50)	2.20 (0.66)	−0.79 (1.91)
Median (range)	2.32 (3.15–1.59)	0.8 (2.15−−2.72)	3.59 (4.70–1.79)	1.63 (2.77−−2.20)	0.64 (1.70−−1.55)	−1.58 (1.90−−4.33)	4.33 (4.80–3.00)	2.28 (2.94–0.49)	4.82 (5.18–2.68)	2.45 (3.20–1.40)	2.04 (3.23–1.50)	−0.10 (2.15−−4.35)
ARJ												
Mean (SD)	−3.35 (1.05)	−2.81 (1.03)	−1.41 (0.23)	−1.52 (1.46)	−5.40 (2.01)	−5.11 (1.98)	−1.93 (0.61)	−1.38 (1.88)	0.25 (1.59)	−0.71 (1.45)	−3.97 (0.85)	−4.83 (1.77)
Median (range)	−3.04 (−2.34−−4.98)	−3.00 (−0.97−−5.30)	−1.47 (−1.04−−1.66)	−1.75 (1.30−−4.86)	−4.81 (−3.30−−8.70)	−5.20 (−1.00−−8.97)	−2.25 (−0.87−−2.35)	−1.80 (4.19−−5.12)	0.03 (2.26−−1.32)	−0.89 (1.78−−3.90)	−3.65 (−3.23−−5.34)	−5.00 (−1.14−−8.56)

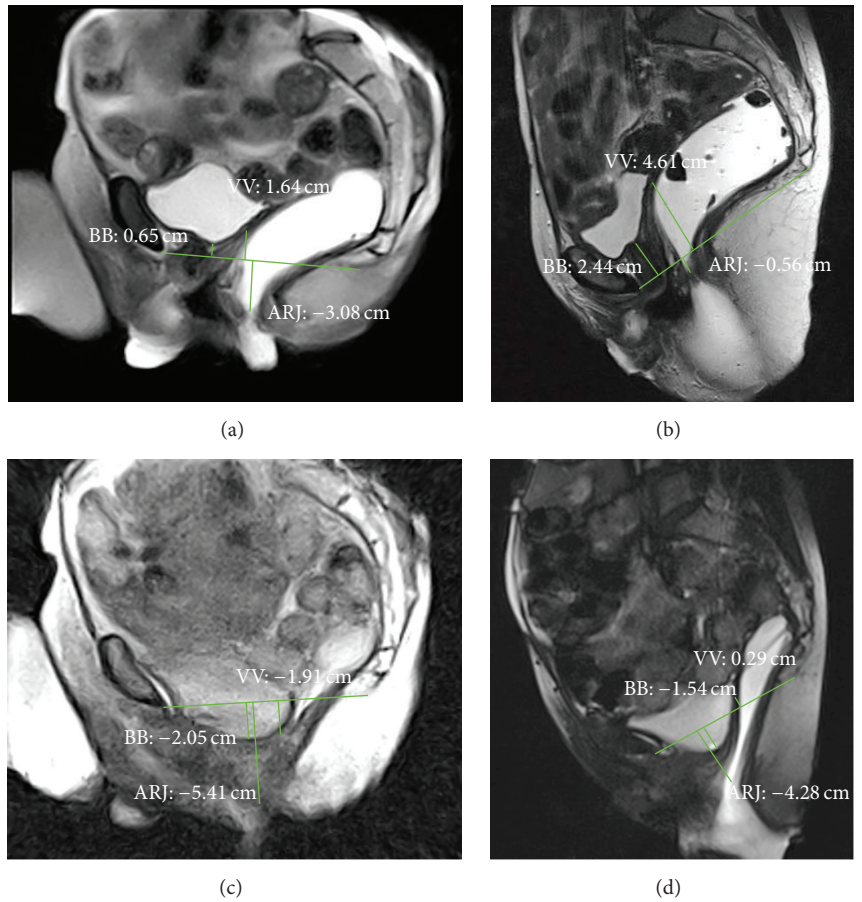

Figure 3: MR Defecography. Rest phase in sitting (a) and supine (b) position. Evacuation phase in sitting (c) and supine (d) position. The pathological fixed descent was detected only in sitting position in rest phase (a). In evacuation phase, a cystocele and a vaginal vault prolapse became evident (c), and the MR examination in supine position overestimates the dynamic descent, nonpathological in (a) and (c) and pathological in (b) and (d). BB: bladder base; VV: vaginal vault; ARJ: anorectal junction.

and p value = 0.0013) whereas for ARJ measure a significant difference was not detected with a probability more than or equal to 95% (p value = 0.0735). In the defecation phase for ARJ measures, a significant difference was not detected (p value = 0.572), whereas there was a statistically significant difference for bladder and vagina measures (p values < 0.001; p value = 0.019).

The dynamic descent of bladder, ARJ, and vagina between rest and defecation phases in both positions was also compared and for the ARJ a statistically significant major descent was detected in supine position versus sitting position (p value = 0.018). A significant difference between sitting and supine positions in the degree of descent of the bladder (p value = 0.0239) was found; a significant difference was not detected for the vagina measure with a probability more than or equal to 95% (p value = 0.278).

In Figure 6, the graphic representation of the ANOVA test for the female subgroup is shown.

In the male subgroup (reported for completeness, $n = 4$), in rest phase, there was a statistically significant difference in the bladder measures between supine and sitting positions (p value = 0.0217), whereas there were not significant differences for ARJ measures (p value = 0.09) between supine and sitting positions.

In squeezing phase, significant differences for bladder and ARJ measures between supine and sitting positions were not found (p value = 0.346 and p value = 0.124, resp.).

In the defecation phase, significant differences for both bladder and ARJ measures between supine and sitting positions were not found (p value = 0.066 and p value = 0.297, resp.).

The dynamic descent of the bladder and the ARJ between rest and defecation phases in both positions was also compared and statistically significant differences were not found for both bladder and ARJ (p value = 0.906 and p value = 0.982, resp.).

The results of the Pearson correlation test are shown in Table 3.

A strong linear correlation in the bladder measures detected in sitting and supine MR examination was found in all phases (rest, squeeze, and defecation) (Figure 7).

In the female subgroup, a moderate correlation was found for the vagina measures in rest phase and a strong correlation was detected in defecation phase (Figure 8).

Table 3: Pearson's test correlation coefficient and related p value (in parentheses).

	Rest	Sitting/supine Squeeze	Defecation
All patients			
Bladder	**0.71** (**$8.07 \cdot 10^{-6}$**)	**0.854** (**$9.64 \cdot 10^{-10}$**)	**0.753**(**$1.04 \cdot 10^{-6}$**)
ARJ	0.228 (0.217)	**0.517 (0.0029)**	**0.696** (**$1.36 \cdot 10^{-5}$**)
Female subgroup			
Bladder	**0.678** (**$1.02 \cdot 10^{-4}$**)	**0.808** (**$3.35 \cdot 10^{-7}$**)	**0.806** (**$3.82 \cdot 10^{-7}$**)
Vagina	**0.611** (**$6.77 \cdot 10^{-4}$**)	0.31 (0.176)	**0.796** (**$1.61 \cdot 10^{-5}$**)
ARJ	0.277 (0.162)	0.568 (0.002)	**0.805** (**$4.03 \cdot 10^{-7}$**)

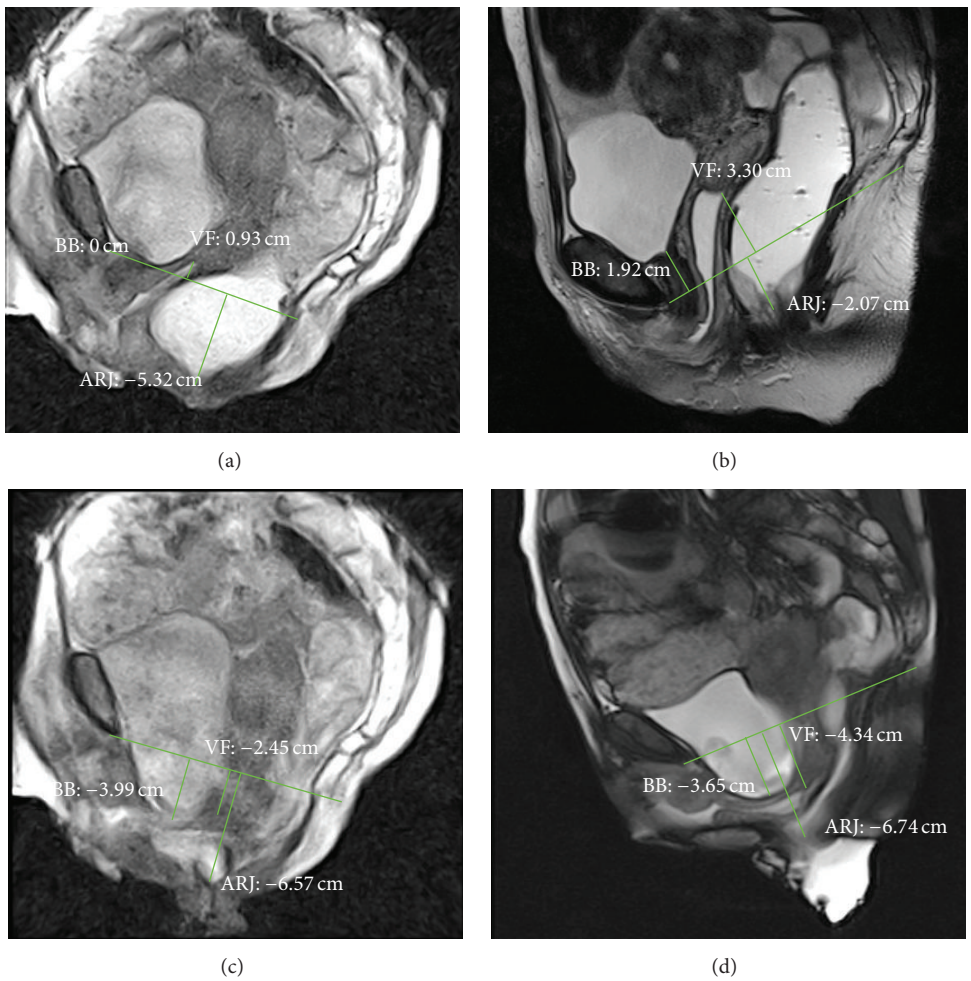

Figure 4: MR Defecography. Rest phase in sitting (a) and supine (b) position. Evacuation phase in sitting (c) and supine (d) position. The pathological fixed descent was detected only in sitting position in rest phase (a). In evacuation phase, the MR examination in supine position overestimates the dynamic descent; the rectocele is seen only in sitting position. BB: bladder base; VF: vaginal fornix; ARJ: anorectal junction.

A strong correlation for the ARJ measure was found in defecation phase, whereas it was weak in rest phase (Figure 8).

4. Discussion

Weakening of the pelvic floor is a debilitating disorder usually involving middle-aged and elderly parous women, even if pelvic floor disorders may also occur in male patients [23, 34, 35]. Weakening of the pelvic floor may result in an abnormal descent of the bladder, the uterus, or the vaginal vault and the rectum, with pelvic organ prolapse and related symptoms including urinary incontinence, fecal incontinence, or obstructed defecation syndrome. The diagnostic limitation of the pelvic examination alone has led to the need of using more direct and comprehensive diagnostic methods [3]. In the assessment of patient with pelvic floor

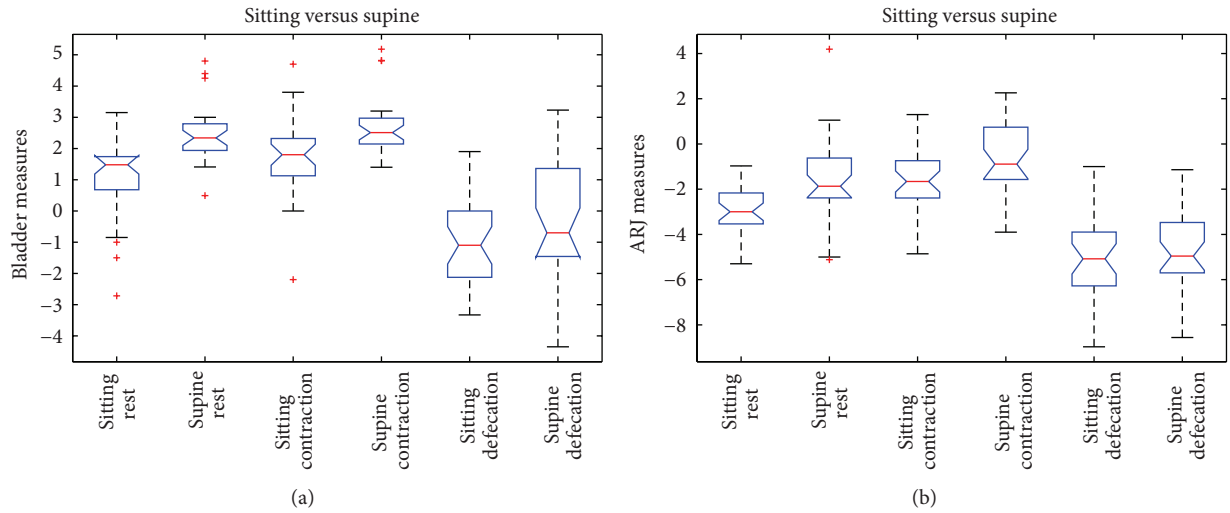

FIGURE 5: ANOVA box plot for bladder (a) and ARJ (b) measures of all the patients.

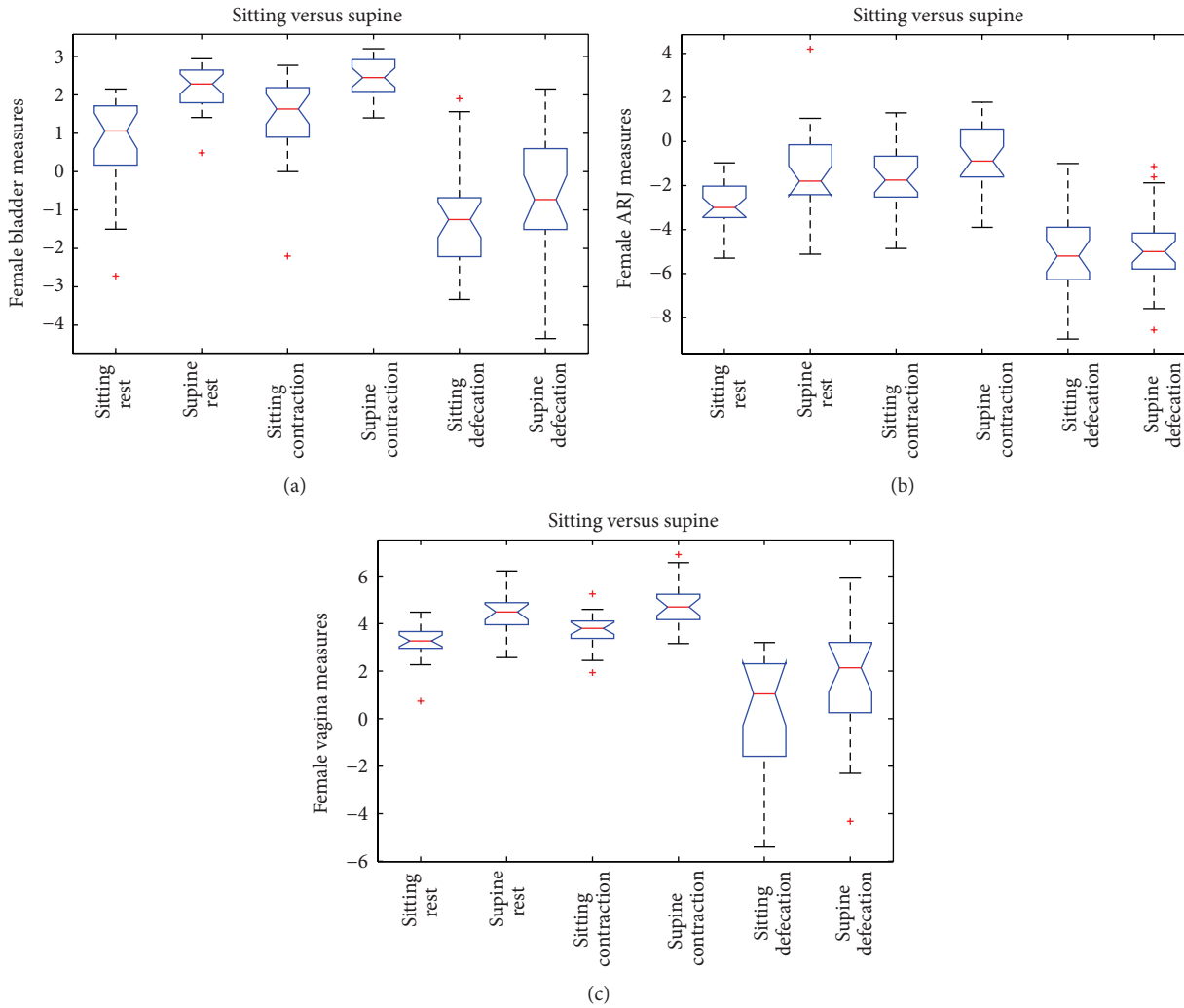

FIGURE 6: ANOVA box plot for bladder (a), vagina (b), and ARJ (c) measures of the female subgroup.

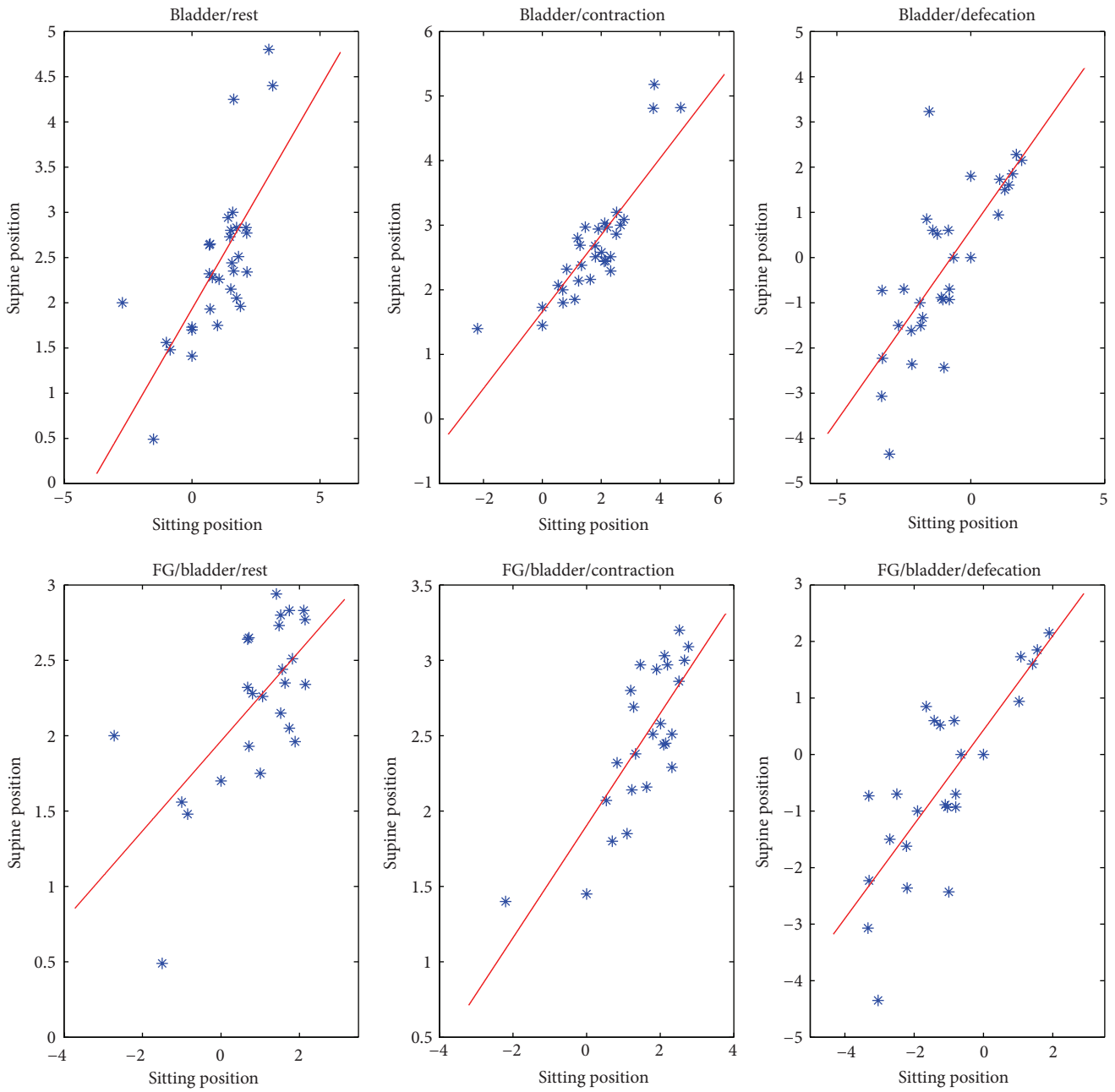

Figure 7: Strong linear correlation for bladder measures in all phases between sitting and supine positions, for all patients.

disease, several radiological investigations are used [9]: RX-Defecography is considered the "gold standard" in the evaluation of pelvic floor diseases, being a cost-effective procedure, easy to perform, and widely available. However, it is an invasive procedure due to the ionizing radiations and the administration of four contrasts and it allows one to evaluate only the opacified organs, neither muscular structures nor soft tissues of the pelvic floor [36]. Ultrasound (US) has the advantage of the lack of ionizing radiation, but this method has several limitations in evaluating pelvic organs prolapse [2]. The alternative, especially in complex combined pelvic floor disorders, is represented by dynamic MR, first described by Yang et al. in 1991, that allows for a multiplanar and multiparametric evaluation of the three pelvic compartments (anterior urinary, middle genital, and posterior digestive) and the direct and detailed visualization of the pelvic floor structures without using ionizing radiation because of its intrinsic soft-tissue contrast capability [3, 4, 12, 37, 38].

In the axial, T1 and T2 weighted, and sagittal, T2 weighted, dynamic sequences, the three different pelvic compartments are displayed to evaluate their morphology and signal characteristics and their position across the different phases (rest, straining, and evacuation) in respect to the PCL with a real-time evaluation of patterns of dysfunction;

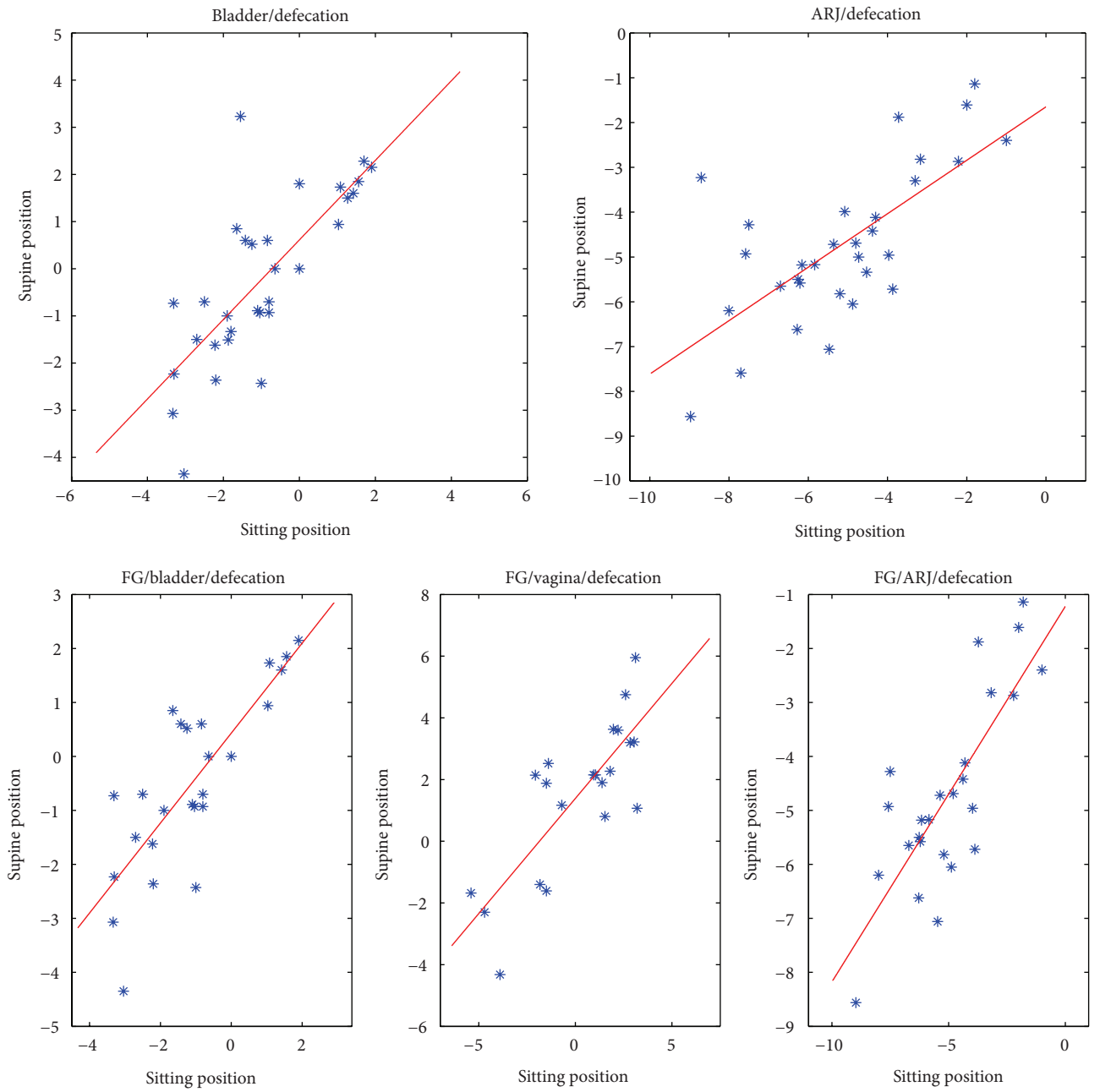

FIGURE 8: Linear correlation graphs of bladder and ARJ measures on all patients and of bladder, vagina, and ARJ measures on FG in defecation phase between sitting and supine positions.

the supporting ligaments and the muscles can be adequately investigated to detect if there are associated muscular and fascial defects, thus providing the surgeon with a road map for tailored treatment. The assessment of the peritoneal compartment (the fourth pelvic compartment) is important especially for the surgical planning and it appears clearly visible on MRI as a thin, low signal band, outlined by the high signal of fat [37].

MR evaluation of pelvic floor descent is limited by the closed architecture of conventional MR systems allowing the patient to be examined only in supine position. Pelvic floor abnormalities may not be detected or misinterpreted if the examination is not completed with evacuation phase; this can be difficult to perform in supine position, limiting the diagnosis [3, 39].

The availability of open magnet systems allows us to perform MR Defecography in sitting position: this is an ideal tool to assess pelvic floor disorders in a physiological position with the advantage of good delineation of all pelvic soft tissues [3]. The use of this technique is limited by worldwide availability. Some authors reported that to perform the examination using a state-of-the-art technique, which means dynamic

MR imaging in supine position in closed magnet at rest, during squeezing, straining, and evacuation is probably more important than to consider the patient position [11, 17, 40, 41]. In our previous experience, imaging the patients in supine position has been shown to be satisfactory in the evaluation of symptomatic pelvic floor weakness even if defects are best demonstrated when patients are sitting [42, 43]. According to this, the results of the present study show that a statistically significant difference exists when the pelvic floor descent is evaluated in sitting versus supine position, and the MR study in supine position can underestimate the fixed descent (Figures 2, 3, and 4). In our series, the percentage of patients with a pathological fixed pelvic floor descent (ARJ more than 3 cm below the PCP) evaluated in rest phase significantly differs between the two procedures.

No significant differences were found in the percentage of patients with cystocele detected in sitting position versus supine position at rest, even if the positions of the bladder significantly differ when the patient is imaged in supine versus sitting position.

In defecation phase no significant differences were found in the percentage of patients with cystocele detected in sitting position versus supine position.

No significant differences exist between the supine and sitting positions in the measures of the ARJ in the defecation phase, suggesting that the maximal level of pelvic floor descent is more influenced by the muscles elasticity and by the pelvic floor muscle voluntary contractions than by the gravity force (Figures 2, 4(c), and 4(d)).

Although the percentage of patients with pathological dynamic descent did not significantly differ between the two procedures, a statistically significant difference was found comparing the grade of dynamic descent between supine and sitting positions. This is explained considering that in supine position pelvic organs are located more cranially in respect to the PCP than in sitting position whereas in defecation phase the values in evacuation do not significantly differ between the two positions of examination. So, the MR in supine position may overestimate the grade of the dynamic descent of the pelvic floor.

The existence of a significant linear correlation between the measures detected in supine versus sitting position for most of the considered measures will encourage further studies for the definition of new cut-off values to be adopted when examining the patients in supine position, since the cut-off values currently used are taken from studies on RX-Defecography, performed in sitting position [10].

It will be also of interest to investigate if the MR in sitting position allows one to improve the detection and the accuracy in diagnosing and grading pelvic pathologies (rectocele, pelvic floor hernias).

To our knowledge, this is the largest series of patients who underwent MR Defecography both in supine 1.5 T and in sitting 0.25 T magnets; a new prototype was used allowing one to obtain diagnostic quality of the images in all the examinations. The limit of the prototype is currently due to the width of the magnet, allowing one to image only patient with hip circumference less than 100 cm. This can be optimized in the future, once the accuracy of this new system is validated.

5. Conclusion

Our results show that MR Defecography in sitting position may represent a useful tool to correctly diagnose and grade the pelvic organ descent. This is of pivotal importance in the assessment of patients with pelvic floor disorders since it may help the surgeon in the definition of the appropriate surgical therapy.

Conflict of Interests

The authors declare they have no conflict of interests.

References

[1] G. T. Bitti, G. M. Argiolas, N. Ballicu et al., "Pelvic floor failure: MR imaging evaluation of anatomic and functional abnormalities," *Radiographics*, vol. 34, no. 2, pp. 429–448, 2014.

[2] S. Cappabianca, A. Reginelli, F. Iacobellis et al., "Dynamic MRI defecography vs. entero-colpo-cysto-defecography in the evaluation of midline pelvic floor hernias in female pelvic floor disorders," *International Journal of Colorectal Disease*, vol. 26, no. 9, pp. 1191–1196, 2011.

[3] Y. Ribas, A. Hotouras, C. L. Chan, and P. Clavé, "Imaging of pelvic floor disorders: are we underestimating gravity?" *Diseases of the Colon and Rectum*, vol. 57, no. 10, pp. 1242–1244, 2014.

[4] A. Lienemann, C. Anthuber, A. Baron, P. Kohz, and M. Reiser, "Dynamic MR colpocystorectography assessing pelvic-floor descent," *European Radiology*, vol. 7, no. 8, pp. 1309–1317, 1997.

[5] K. M. Bertschinger, F. H. Hetzer, J. E. Roos, K. Treiber, B. Marincek, and P. R. Hilfiker, "Dynamic MR imaging of the pelvic floor performed with patient sitting in an open-magnet unit versus with patient supine in a closed-magnet unit," *Radiology*, vol. 223, no. 2, pp. 501–508, 2002.

[6] Y. M. Law and J. R. Fielding, "MRI of pelvic floor dysfunction: review," *American Journal of Roentgenology*, vol. 191, no. 6, supplement, pp. S45–S53, 2008.

[7] N. Bolog and D. Weishaupt, "Dynamic MR imaging of outlet obstruction," *Romanian Journal of Gastroenterology*, vol. 14, no. 3, pp. 293–302, 2005.

[8] A. Renzi, A. Brillantino, G. Di Sarno, and F. d'Aniello, "Five-item score for obstructed defecation syndrome: study of validation," *Surgical Innovation*, vol. 20, no. 2, pp. 119–125, 2013.

[9] A. C. Silva and D. D. Maglinte, "Pelvic floor disorders: what's the best test?" *Abdominal Imaging*, vol. 38, no. 6, pp. 1391–1408, 2013.

[10] A. G. Schreyer, C. Paetzel, A. Fürst et al., "Dynamic magnetic resonance defecography in 10 asymptomatic volunteers," *World Journal of Gastroenterology*, vol. 18, no. 46, pp. 6836–6842, 2012.

[11] M. Rentsch, C. Paetzel, M. Lenhart, S. Feuerbach, K. W. Jauch, and A. Fürst, "Dynamic magnetic resonance imaging defecography: a diagnostic alternative in the assessment of pelvic floor disorders in proctology," *Diseases of the Colon and Rectum*, vol. 44, no. 7, pp. 999–1007, 2001.

[12] J. R. Fielding, "Practical MR imaging of female pelvic floor weakness," *Radiographics*, vol. 22, no. 2, pp. 295–304, 2002.

[13] A. Renzi, A. Brillantino, G. Di Sarno, D. Izzo, F. D'Aniello, and A. Falato, "Improved clinical outcomes with a new contour-curved stapler in the surgical treatment of obstructed defecation syndrome: a mid-term randomized controlled trial," *Diseases of*

the Colon and Rectum, vol. 54, no. 6, pp. 736–742, 2011, Erratum in: Diseases of the Colon and Rectum, vol. 54, no. 11, pp. 1462, 2011.

[14] D. Izzo, A. Brillantino, F. Iacobellis, P. Falco, A. Renzi, and R. Rea, "Role of 0.4 % glyceryl trinitrate ointment after stapled trans-anal rectal resection for obstructed defecation syndrome: a prospective, randomized trial," *International Journal of Colorectal Disease*, vol. 29, no. 1, pp. 105–110, 2014.

[15] A. Renzi, A. Brillantino, G. Di Sarno et al., "PPH-01 versus PPH-03 to perform STARR for the treatment of hemorrhoids associated with large internal rectal prolapse: a prospective multicenter randomized trial," *Surgical Innovation*, vol. 18, no. 3, pp. 241–247, 2011.

[16] F. Selvaggi, G. Pellino, and G. Sciaudone, "Surgical treatment of recurrent prolapse after stapled haemorrhoidopexy," *Techniques in Coloproctology*, vol. 18, no. 9, pp. 847–850, 2014.

[17] N. Bolog and D. Weishaupt, "Dynamic MR imaging of outlet obstruction," *Romanian Journal of Gastroenterology*, vol. 14, no. 3, pp. 293–302, 2005.

[18] J. R. Fielding, D. J. Griffiths, E. Versi, R. V. Mulkern, M.-L. T. Lee, and F. A. Jolesz, "MR imaging of pelvic floor continence mechanisms in the supine and sitting positions," *American Journal of Roentgenology*, vol. 171, no. 6, pp. 1607–1610, 1998.

[19] V. Fiaschetti, E. Squillaci, D. Pastorelli et al., "Dynamic MR defecography with an open-configuration, low-field, tilting MR system in patients with pelvic floor disorders," *Radiologia Medica*, vol. 116, no. 4, pp. 620–633, 2011.

[20] P. R. Hilfiker, J. F. Debatin, W. Schwizer, A. W. Schoenenberger, M. Fried, and B. Marincek, "MR defecography: depiction of anorectal anatomy and pathology," *Journal of Computer Assisted Tomography*, vol. 22, no. 5, pp. 749–755, 1998.

[21] A. W. Schoenenberger, J. F. Debatin, I. Guldenschuh, T. F. Hany, P. Steiner, and G. P. Krestin, "Dynamic MR defecography with a superconducting, open-configuration MR system," *Radiology*, vol. 206, no. 3, pp. 641–646, 1998.

[22] V. Fiaschetti, D. Pastorelli, E. Squillaci et al., "Static and dynamic evaluation of pelvic floor disorders with an open low-field tilting magnet," *Clinical Radiology*, vol. 68, no. 6, pp. e293–e300, 2013.

[23] K. J. Mortele and J. Fairhurst, "Dynamic MR defecography of the posterior compartment: indications, techniques and MRI features," *European Journal of Radiology*, vol. 61, no. 3, pp. 462–472, 2007.

[24] V. Goh, S. Halligan, G. Kaplan, J. C. Healy, and C. I. Bartram, "Dynamic MR imaging of the pelvic floor in asymptomatic subjects," *American Journal of Roentgenology*, vol. 174, no. 3, pp. 661–666, 2000.

[25] M. C. Colaiacomo, G. Masselli, E. Polettini et al., "Dynamic MR imaging of the pelvic floor: a pictorial review," *Radiographics*, vol. 29, no. 3, article e35, 2009.

[26] R. G. Landmann and S. D. Wexner, "Paradoxical puborectalis contraction and increased perineal descent," *Clinics in Colon and Rectal Surgery*, vol. 21, no. 2, pp. 138–145, 2008.

[27] J. M. N. Jorge, S. D. Wexner, E. D. Ehrenpreis, J. J. Nogueras, and D. G. Jagelman, "Does perineal descent correlate with pudendal neuropathy?" *Diseases of the Colon & Rectum*, vol. 36, no. 5, pp. 475–483, 1993.

[28] A. G. Parks, N. H. Porter, and J. Hardcastle, "The syndrome of the descending perineum," *Proceedings of the National Academy of Sciences of the United States of America*, vol. 59, no. 6, pp. 477–482, 1966.

[29] P. J. Shorvon, S. McHugh, N. E. Diamant, S. Somers, and G. W. Stevenson, "Defecography in normal volunteers: results and implications," *Gut*, vol. 30, no. 12, pp. 1737–1749, 1989.

[30] D. E. Beck and S. D. Wexner, Eds., *Fundamentals of Anorectal Surgery*, WB Saunders, Philadelphia, Pa, USA, 2nd edition, 1998.

[31] R. V. Hogg and J. Ledolter, *Engineering Statistics*, MacMillan, New York, NY, USA, 1987.

[32] M. Hollander and D. A. Wolfe, *Nonparametric Statistical Methods*, Wiley, 1973.

[33] R. R. Sokal and F. J. Rohlf, *Biometry. The Principles and Practice of Statistics in Biological Research*, Freeman, New York, NY, USA, 3rd edition, 1995.

[34] A. Reginelli, M. G. Pezzullo, M. Scaglione, M. Scialpi, L. Brunese, and R. Grassi, "Gastrointestinal disorders in elderly patients," *Radiologic Clinics of North America*, vol. 46, no. 4, pp. 755–771, 2008.

[35] G. Cavallo, A. Salzano, R. Grassi, P. Zanatta, and M. Tuccillo, "Rectocele in males: clinical, defecographic, and CT study of singular cases," *Diseases of the Colon and Rectum*, vol. 34, no. 11, pp. 964–966, 1991.

[36] A. Salzano, V. Nocera, E. Rossi, G. L. Gatta, and R. Grassi, "Radiologic investigation of external rectal prolapse. Assessment in 48 patients with defecography, seven of them also with dynamic CT of the pelvis," *La Radiologia Medica*, vol. 100, no. 5, pp. 348–353, 2000.

[37] A. Maubon, Y. Aubard, V. Berkane, M.-A. Camezind-Vidal, P. Marès, and J. P. Rouanet, "Magnetic resonance imaging of the pelvic floor," *Abdominal Imaging*, vol. 28, no. 2, pp. 217–225, 2003.

[38] R. Grassi, G. Lombardi, A. Reginelli et al., "Coccygeal movement: assessment with dynamic MRI," *European Journal of Radiology*, vol. 61, no. 3, pp. 473–479, 2007.

[39] Y. Mandato, A. Reginelli, R. Galasso, F. Iacobellis, D. Berritto, and S. Cappabianca, "Errors in the radiological evaluation of the alimentary tract: part I," *Seminars in Ultrasound, CT and MRI*, vol. 33, no. 4, pp. 300–307, 2012.

[40] R. C. Bump and P. A. Norton, "Epidemiology and natural history of pelvic floor dysfunction," *Obstetrics and Gynecology Clinics of North America*, vol. 25, no. 4, pp. 723–746, 1998.

[41] R. Hausammann, T. Steffen, D. Weishaupt, U. Beutner, and F. H. Hetzer, "Rectocele and intussusception: is there any coherence in symptoms or additional pelvic floor disorders?" *Techniques in Coloproctology*, vol. 13, no. 1, pp. 17–26, 2009.

[42] A. Faggian, M. E. Alabiso, N. Serra et al., "Entero-colpodefecography vs supine entero-MRI: which one is the best tool in the differentiation of enterocele, elytrocele and edrocele?" *Journal of Biological Regulators and Homeostatic Agents*, vol. 27, no. 3, pp. 861–868, 2013.

[43] A. Reginelli, G. Di Grezia, G. Gatta et al., "Role of conventional radiology and MRi defecography of pelvic floor hernias," *BMC Surgery*, vol. 13, supplement 2, article s53, 2013.

Hindawi Publishing Corporation
Gastroenterology Research and Practice
Volume 2016, Article ID 2523768, 6 pages
http://dx.doi.org/10.1155/2016/2523768

Research Article

A Novel Diagnostic Aid for Detection of Intra-Abdominal Adhesions to the Anterior Abdominal Wall Using Dynamic Magnetic Resonance Imaging

David Randall,[1] John Fenner,[1] Richard Gillott,[2] Richard ten Broek,[3] Chema Strik,[3] Paul Spencer,[2] and Karna Dev Bardhan[2]

[1]*Medical Physics Group, Department of Cardiovascular Science, University of Sheffield, Beech Hill Road, Sheffield S10 2RX, UK*
[2]*The Rotherham NHS Foundation Trust, Rotherham Hospital, Moorgate Road, Rotherham S60 2UD, UK*
[3]*Radboud University Medical Centre, Department of Surgery, P.O. Box 9101, 6500 HB Nijmegen, Netherlands*

Correspondence should be addressed to David Randall; drandall1@sheffield.ac.uk

Received 29 May 2015; Revised 19 October 2015; Accepted 15 November 2015

Academic Editor: Maria Antonietta Mazzei

Introduction. Abdominal adhesions can cause serious morbidity and complicate subsequent operations. Their diagnosis is often one of exclusion due to a lack of a reliable, non-invasive diagnostic technique. Development and testing of a candidate technique are described below. *Method*. During respiration, smooth visceral sliding motion occurs between the abdominal contents and the walls of the abdominal cavity. We describe a technique involving image segmentation and registration to calculate shear as an analogue for visceral slide based on the tracking of structures throughout the respiratory cycle. The presence of an adhesion is attributed to a resistance to visceral slide resulting in a discernible reduction in shear. The abdominal movement due to respiration is captured in sagittal dynamic MR images. *Results*. Clinical images were selected for analysis, including a patient with a surgically confirmed adhesion. Discernible reduction in shear was observed at the location of the adhesion while a consistent, gradually changing shear was observed in the healthy volunteers. *Conclusion*. The technique and its validation show encouraging results for adhesion detection but a larger study is now required to confirm its potential.

1. Introduction

Abdominal adhesions are pathological formations of fibrous scar tissue that tether or adhere abdominal structures. As a complication of abdominal surgery they may be the cause of serious morbidity and may complicate subsequent operations. A combination of non-specific symptoms and an aversion to unnecessary surgery leads to a conservative patient management strategy that often fails to tackle the underlying condition. Surgical procedures (laparoscopy, laparotomy) are currently the only reliable way to determine if a patient has adhesions, but such intervention may induce further adhesions. A non-invasive diagnostic technique would therefore be invaluable for effective patient management and reducing surgical complications.

During the respiratory cycle the abdominal contents slide smoothly against the confines of the abdominal cavity (abdominal wall, etc.)—a process termed visceral slide. Although absence of, or disturbance to, visceral slide is considered an indicator of adhesions, the literature contains very few quantitative attempts at visceral slide measurement [1–3]. The use of dynamic MR for adhesion detection has had reported success but examination of the images in sufficient detail to detect abnormal slide has proven labour intensive and results are subject to high inter-operator variability [4–6]. We have previously presented a technique to mathematically analyse movement within the whole of the abdomen to help infer the presence of gross abnormalities (extensive adhesions) [6]. This current paper outlines a refinement of this technique using image segmentation and registration to exclusively interrogate more subtle abnormalities on the abdominal wall by examination of visceral slide.

Image registration is a mathematical process which aims to warp points in one image to match their corresponding

points in another. It has a proven value in tracking features or structures between incrementally varying images. However, sliding geometry (such as in the abdomen) is recognised to challenge registration algorithms [7–11]. To address this issue the literature has largely focused on development of highly sophisticated, bespoke registration algorithms to accurately account for sliding [7–11]. In this paper our focus is different: we intend to evaluate the sliding motion itself. We consider that there is benefit in using "off-the-shelf" registration technology combined with a protocol optimised for shear detection, and for this purpose we promote a segmentation-registration method. Such a pragmatic approach makes the technique more transparent and the technology more accessible, hopefully encouraging clinical adoption.

To the authors' knowledge nobody has accomplished quantitative characterisation/measurement of the sliding motion in the abdomen nor has a reliable technique been developed for non-invasive abdominal adhesion detection. With this in mind this paper is a "work in progress" that communicates an overview of the methodology developed and presents preliminary results.

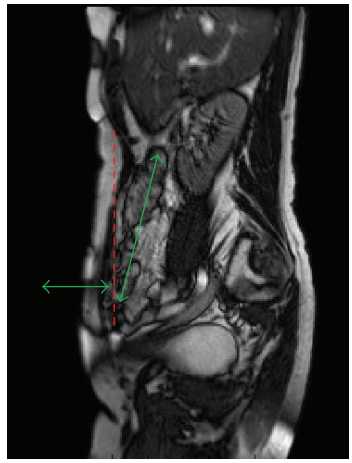

Figure 1: Schematic of the motion discontinuity in the abdomen during respiration. The horizontal green arrow indicates the predominant motion of the abdominal wall whilst the mostly vertical arrow represents the predominant motion of the abdominal contents. The dotted red line indicates the approximate location of the motion discontinuity.

2. Method

Our scanning protocol was developed independently which led to a protocol that echoed that of Lienemann et al. (2000) [4]. Dynamic MR images are acquired using a True FISP (true fast imaging with steady-state precession) MR imaging sequence. Images are obtained in the sagittal plane from the mid ascending colon to mid descending colon, which covers the full extent of the abdominal contents. Scanning parameters include a matrix size of 256 × 256, a slice thickness of 7 mm, and 10 mm gaps between slices. 30 frames are acquired at each sagittal slice location with an approximate time between frames of 0.4 seconds. Patients are scanned in the supine position and asked to bear down and breathe normally during the acquisition of each sagittal slice (for ~12 seconds) capturing approximately 3 respiratory cycles.

The focus of our method is a particular sliding motion system, characterised as one in which two adjacent structures in contact slide independently against each other. A schematic of the type of motion observed in the abdomen during respiration is shown in Figure 1.

These types of systems involve a discontinuity in the motion along the boundary separating the two moving objects. The method aims to determine the degree of sliding by quantifying shear as an analogue for the sliding motion taking place at the discontinuity. The amount of shear refers to the difference in the relative displacement of the two objects on either side of the motion discontinuity along the boundary.

The method relies on a segmentation step that requires that the boundary between the two regions of motion be defined, as shown in step 1 of Figure 2. This is done semi-automatically by manually defining the boundary on a single frame, after which the position of the boundary is tracked for all subsequent frames. The motion within the two regions can now be mathematically interrogated separately without interference from one another. Separate registrations quantify the motion in each region which are then recombined to reconstruct a full description of motion over the whole image. The motion is depicted as arrows (vectors) in step 2 of Figure 2. The relative motions along the boundary over the whole dynamic image sequence are then computed to determine the amount of shear. The result is a "sheargram": the coloured band in step 3 of Figure 2 depicting the total shear along the boundary over approximately 3 respiratory cycles.

3. Results

For the purposes of this exercise we obtained a selection of suitable MR images in which complementary surgical confirmation was available to clarify the degree of adhesive pathology. Of particular interest was a patient with a surgically confirmed adhesion to the anterior abdominal wall following a hernia repair. The result of the shear summed over approximately 3 respiratory cycles for this patient is compared to two healthy volunteers without adhesions in Figure 3.

An apparent reduction in shear is observed at the site of the surgically confirmed adhesion (highlighted by the arrow) which contrasts with the relatively uniform, gradually changing shear observed along the abdominal wall of the two healthy volunteers.

4. Validation

A critical assessment of our method demands evidence that the technique is robust and bereft of artefacts. In the absence of a clinical trial or a pilot study this section discusses two examples of validation tests, with interpretation of results and

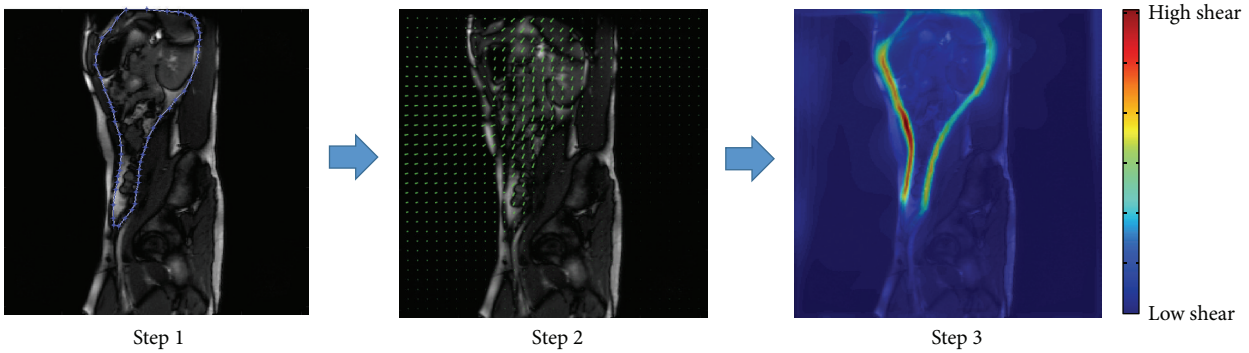

Figure 2: Flow chart describing the methodology. Step 1: typical region drawn to separate (segment) the two regions of different motion; step 2: depiction of the mathematically quantified movement; step 3: depiction of the shear taking place along the boundary in a "sheargram".

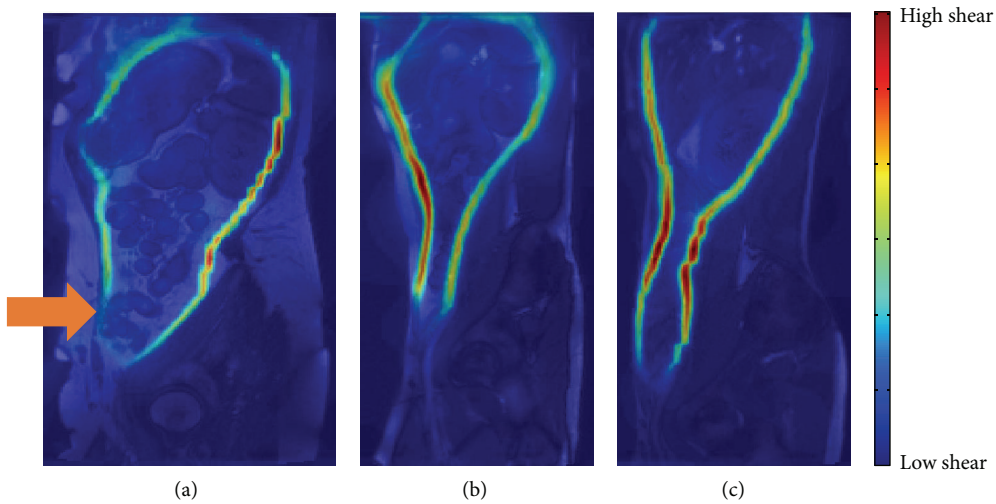

Figure 3: Comparison of the sheargrams from (a) a patient with an adhesion (arrow) and (b) and (c) two healthy volunteers.

implications for clinical use. Validation tests that have been performed to assess the robustness of the technique include:

(1) A highly idealised computer-generated stretching of a rectangular region of an MR image

(2) Imaging of a physical system involving the compression of a sponge in a syringe to generate a sliding against the syringe wall.

4.1. Test 1. A rectangular section of an abdominal MR image was artificially stretched relative to the surrounding MR image (shown in Figure 4(a)) to create a movie of discontinuous sliding with known, time-dependent shear at the boundary. The shear along the boundary was calculated with and without the segmentation step and compared to the known shear along the boundary in Figure 4(b).

The shear calculated when motion segmentation is included closely matched the known shear at the boundary of the stretched section. The largest discrepancy occurred at the top of the image (see Figure 4(b)) and is attributable to detail being stretched outside the image space. Even with the relatively small shears present in this example the measured shear agreed within approximately 5% of the actual shear. The simple nature of the deformation (uniform stretch) does not challenge the registration algorithm but it does demonstrate the inherent accuracy of the procedure in the absence of "real-world" complexities.

4.2. Test 2. The second validation test was physical rather than computationally simulated and involved the compression of a textured sponge within a syringe (Figure 5). The plunger was used to gradually compress the sponge while images were taken with a standard DSLR camera (Cannon EOS 1100D). Two separate sets of acquisitions were made: in the first, the sponge was allowed to be freely compressed; for the second, an adhesive piece of double sided sticky tape was added to the inside of the syringe to create a localised resistance to the sponge's "motion" thereby disrupting slide (an analogue for an adhesion). The images in Figures 5(a) and 5(b) show the uncompressed and compressed sponge while the images in Figures 5(c) and 5(d) used our segmentation-registration protocol to depict the shear summed over the whole compression with and without the presence of the adhesive tape. This test offers a more realistic challenge for

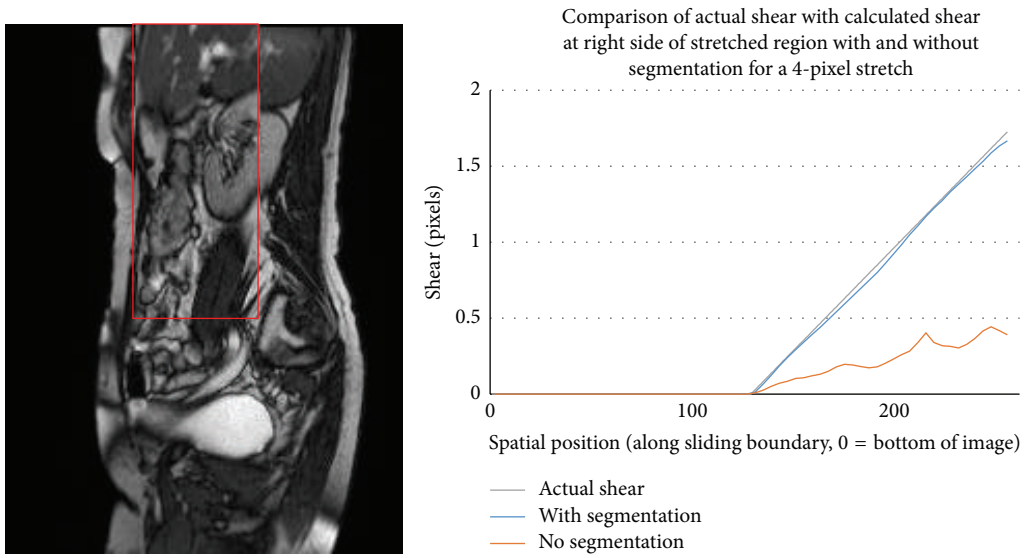

FIGURE 4: Validation experiment 1 with an idealised stretch of the portion of a MR image shown in (a) and shear results compared to actual shear in the system in (b).

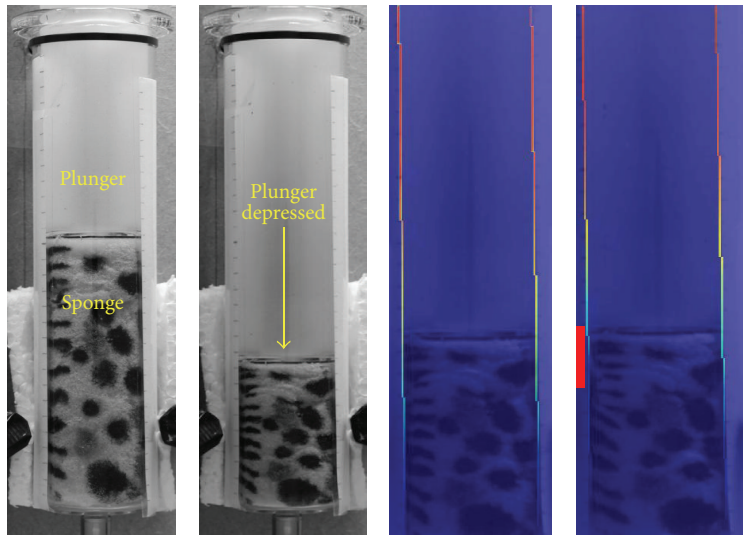

FIGURE 5: Syringe test object displaying (a) uncompressed sponge, (b) compressed sponge, (c) shear result without adhesive tape, and (d) shear result with adhesive tape (indicated by red block).

the algorithm as it includes non-uniform deformation and localised variations in sliding motion. It not only assesses the technique's ability to quantify shear but also its ability to detect an adhesive area along the boundary—proof of principle for adhesion detection.

When qualitatively observing the sponge's motion unaided by the sheargram, determining the location of the adhesion was extremely challenging. When combined with the images in Figures 5(c) and 5(d), a sufficient reduction in shear around the location of the adhesion was observed to accurately raise awareness of its presence.

5. Discussion

Intra-abdominal adhesions can form anywhere in the abdomen, vary in shape and size, and therefore cause a spectrum of symptoms: little or none at one end to severe, frequent pain at the other. A proportion of patients with adhesions are forced to repeatedly seek medical attention for their unexplained abdominal pain. In current clinical practice a patient with severe abdominal pain and suspected bowel obstruction will undergo non-invasive imaging [12–15]. Planar X-ray, fluoroscopy, CT or MRI may be used in an attempt

to detect a proximal region of distended bowel with an abrupt reduction in bowel calibre to a collapsed distal region [13]. Importantly, the radiological features determine the site of obstruction but not necessarily the cause: an adhesion may be likely but not proven. The only definitive method to prove the presence of adhesions is by surgery (laparotomy or laparoscopy) which itself is often the primary cause of adhesions [16]. As a result they place a significant burden on healthcare worldwide [16–18] and the lack of a reliable non-invasive diagnostic technique results in conservative patient management and prolonged patient discomfort [12].

It is recognised that improved diagnostic methods are required to reliably inform patient management strategies for adhesive bowel obstruction [12] but additionally we propose a requirement for diagnosis of adhesions in symptomatic patients *without* intestinal obstruction. A potential diagnostic technique is radiological examination of cine-MRI to observe the motion of the abdominal contents. This was first described by Lienemann et al. in 2000 [4] and has led to several further publications [5, 19, 20] from the same group. The cine-MRI acquisition acquires slices in the transverse and sagittal planes and requires a radiologist to identify regions of absence of movement which could correspond to adhesive pathology. The technique has shown promise and reported impressive accuracies, identifying up to 89% of surgically confirmed adhesions [19].

However, in our experience, radiological assessment of cine-MR images is limited by its difficulty, high inter-operator variability, and excessive reporting time. These factors led to our previous publication which described mathematical mapping and depiction of movement in the abdomen to aid the radiologist [6]. This current paper offers a refinement to our previous approach by presenting shear measurements as a diagnostic metric for the presence and location of more subtle adhesive pathologies around the perimeter of the abdominal cavity. The measurement of shear could be used to influence decisions on whether to operate, facilitate more efficient surgery due to improved adhesion localisation, and reduce the risk of serious surgical complications such as bowel perforation during incisions.

5.1. Non-Clinical Validation. The validation tests were idealised and non-clinical but permitted the analysis method to be verified, offering a proof of principle for the detection of adhesive regions. The result of Test 1 (stretched MRI region) showed a close match between the output of the computer analysis and actual shear, indicating correct shear calculation. This was echoed equally well in the less idealised experiment of Test 2 (textured sponge). Although a small amount of shear was observed at the site of the adhesion (see Figure 5), this was visibly attributable to the weakness in bonding between tape and sponge as a small amount of slippage occurred. A more subtle observation is the reduction in shear on the opposite wall to the adhered region in Figure 5(d) when compared to the acquisition without an adhesion in Figure 5(c). Close examination of the images and registration deformation field confirm that this is not a failing in the shear analysis but rather the adhesion influenced the deformation at the right-hand boundary as well as the left. With the region below the adhesion remaining largely uncompressed some sponge moved laterally into this space rather than sliding vertically downward against the syringe wall.

The results of both tests offer support for the technique showing that it accurately captured shear and that this could be used to detect an area disturbed by an adhesive influence.

5.2. Clinical Test. Application to a handful of clinical examples has thus far continued to produce promising results. In the case reported here reduced shear was observed at the site of a surgically confirmed adhesion while in a sample of healthy abdominal scans ($n = 4$) a smoother more gradual change in shear was observed. The combined evidence of the clinical outcome and the validation tests provides reassurance that the technique has merit. Developing our system for clinical use requires two major steps: retrospective application to a larger patient cohort with surgical confirmation and a prospective programme.

The clinical results in Figure 3 also reveal areas of reduced shear which do not correspond to a confirmed adhesion (e.g., upper left Figure 3(a) and at the very base of the abdomen in all images). Inspection of movement in these areas reveals that this is not a failure of the technique to measure shear correctly but rather confirms that sliding is genuinely reduced in these areas. At this stage of development the aim of this technique is not to provide a standalone diagnostic outcome but to draw the eye of the radiologist toward specific suspect areas, which when combined with other diagnostic information can enable an informed decision to be made. This initial extra investment by the radiologist is potentially more than offset by increased accuracy of diagnosis and reduction in examination time. It is likely that there will be common sites of shear reduction which, with experience, should be easily identified and interpreted appropriately. A future ambition is the production of a shear "atlas" to provide a typical map of shear in health and disease to help clarify such issues.

5.3. Challenges and Future Work. This paper has reported on a work in progress and there remain challenges which must be addressed before the proposed diagnostic protocol for anterior wall adhesions can be considered reliable. The principal concerns relate to (i) sensitivity of the results to position of boundary placement between the moving regions and (ii) possible artefacts introduced by structures moving through the 2D imaging plane. With reference to (i), our experience confirms that the placement of the boundary is relatively consistent due to high contrast anatomy; consequently reproducible results are achievable. With respect to (ii), through plane motion in 2D is most effectively addressed by 3D imaging. However, advantages gained from the 2D implementation are the high temporal resolution not available in 3D imaging and the simplicity and speed of implementation. Also, notably, movement within the abdomen is mostly superior-inferior; therefore objects largely remain in the sagittal imaging plane. It is for these reasons that complementary 2D and 3D analyses are being pursued.

As a final comment, the protocol is intentionally designed to support the use of different "off-the-shelf" registration algorithms. Currently the majority of work has been

performed using the Sheffield Image Registration Toolkit (ShIRT) but ANTs (Advanced Normalisation Toolkit, an open source registration algorithm) has also been successfully incorporated and used.

6. Conclusion

A technique to measure shear to infer the amount of visceral slide along the extremities of the abdominal cavity has been proposed, investigated, and validated. Despite the acknowledged limitations of the current implementation, the preliminary results have shown the adopted methodology to be successful in determining and detecting the locations of adhesions. Clinical application is currently limited by the small number of patients examined but an additional study is being pursued with a larger cohort of patients for further assessment.

Conflict of Interests

The authors declare that there is no conflict of interest regarding the publication of this paper.

Acknowledgments

The authors would like to thank the Bardhan Research and Education Trust of Rotherham (BRET) for supporting this work. They are also grateful to Frank Joosten (Rijnstate Ziekenhuis, Department of Radiology) and Harry van Goor (Radboud University Medical Center, Department of Surgery) for their support in this work.

References

[1] J. A. Caprini, J. A. Arcelus, J. Swanson et al., "The ultrasonic localization of abdominal wall adhesions," *Surgical Endoscopy*, vol. 9, no. 3, pp. 283–285, 1995.

[2] B. Sigel, R. M. Golub, L. A. Loiacono et al., "Technique of ultrasonic detection and mapping of abdominal wall adhesions," *Surgical Endoscopy*, vol. 5, no. 4, pp. 161–165, 1991.

[3] N. B. Zinther, A. Zeuten, E. Marinovskij, M. Haislund, and H. Friis-Andersen, "Detection of abdominal wall adhesions using visceral slide," *Surgical Endoscopy*, vol. 24, no. 12, pp. 3161–3166, 2010.

[4] A. Lienemann, D. Sprenger, H. O. Steitz, M. Korell, and M. Reiser, "Detection and mapping of intraabdominal adhesions by using functional cine MR imaging: preliminary results," *Radiology*, vol. 217, no. 2, pp. 421–425, 2000.

[5] R. A. Lang, S. Buhmann, A. Hopman et al., "Cine-MRI detection of intraabdominal adhesions: correlation with intraoperative findings in 89 consecutive cases," *Surgical Endoscopy and Other Interventional Techniques*, vol. 22, no. 11, pp. 2455–2461, 2008.

[6] J. Fenner, B. Wright, J. Emberey et al., "Towards radiological diagnosis of abdominal adhesions based on motion signatures derived from sequences of cine-MRI images," *Physica Medica*, vol. 30, no. 4, pp. 437–447, 2014.

[7] V. Vishnevskiy, T. Gass, G. Szekely, and O. Goksel, "Total variation regularization of displacements in parametric image registration," in *Abdominal Imaging. Computational and Clinical Applications*, vol. 8676 of *Lecture Notes in Computer Science*, pp. 211–220, Springer, 2014.

[8] V. Delmon, S. Rit, R. Pinho, and D. Sarrut, "Registration of sliding objects using direction dependent B-splines decomposition," *Physics in Medicine and Biology*, vol. 58, no. 5, pp. 1303–1314, 2013.

[9] D. F. Pace, M. Niethammer, and S. R. Aylward, "Sliding geometries in deformable image registration," in *Abdominal Imaging. Computational and Clinical Applications*, vol. 7029 of *Lecture Notes in Computer Science*, pp. 141–148, Springer, Berlin, Germany, 2012.

[10] Y. Xie, M. Chao, and G. Xiong, "Deformable image registration of liver with consideration of lung sliding motion," *Medical Physics*, vol. 38, no. 10, pp. 5351–5361, 2011.

[11] B. W. Papiez, M. P. Heinrich, J. Fehrenbach, L. Risser, and J. A. Schnabel, "An implicit sliding-motion preserving regularisation via bilateral filtering for deformable image registration," *Medical Image Analysis*, vol. 18, no. 8, pp. 1299–1311, 2014.

[12] T. R. van Oudheusden, B. A. C. Aerts, I. H. J. T. de Hingh, and M. D. P. Luyer, "Challenges in diagnosing adhesive small bowel obstruction," *World Journal of Gastroenterology*, vol. 19, no. 43, pp. 7489–7493, 2013.

[13] E. Amzallag-Bellenger, A. Oudjit, A. Ruiz, G. Cadiot, P. A. Soyer, and C. C. Hoeffel, "Effectiveness of MR enterography for the assessment of small-bowel diseases beyond crohn disease," *Radiographics*, vol. 32, no. 5, pp. 1423–1444, 2012.

[14] D. P. Beall, B. J. Fortman, B. C. Lawler, and F. Regan, "Imaging bowel obstruction: a comparison between fast magnetic resonance imaging and helical computed tomography," *Clinical Radiology*, vol. 57, no. 8, pp. 719–724, 2002.

[15] A. S. Kumar, J. Coralic, R. Vegeler et al., "Magnetic resonance enterography: the test of choice in diagnosing intestinal 'Zebras'," *Case Reports in Gastrointestinal Medicine*, vol. 2015, Article ID 206469, 8 pages, 2015.

[16] R. P. G. ten Broek, Y. Issa, E. J. P. van Santbrink et al., "Burden of adhesions in abdominal and pelvic surgery: systematic review and met-analysis," *British Medical Journal*, vol. 347, no. 7929, Article ID f5588, 2013.

[17] B. Tingstedt, J. Isaksson, and R. Andersson, "Long-term follow-up and cost analysis following surgery for small bowel obstruction caused by intra-abdominal adhesions," *British Journal of Surgery*, vol. 94, no. 6, pp. 743–748, 2007.

[18] N. F. Ray, W. G. Denton, M. Thamer, S. C. Henderson, and S. Perry, "Abdominal adhesiolysis: inpatient care and expenditures in the United States in 1994," *Journal of the American College of Surgeons*, vol. 186, no. 1, pp. 1–9, 1998.

[19] S. Buhmann-Kirchhoff, R. Lang, C. Kirchhoff et al., "Functional cine MR imaging for the detection and mapping of intraabdominal adhesions: method and surgical correlation," *European Radiology*, vol. 18, no. 6, pp. 1215–1223, 2008.

[20] S. Kirchhoff, R. Ladurner, C. Kirchhoff, T. Mussack, M. F. Reiser, and A. Lienemann, "Detection of recurrent hernia and intraabdominal adhesions following incisional hernia repair: a Functional Cine MRI-Study," *Abdominal Imaging*, vol. 35, no. 2, pp. 224–231, 2010.

Hindawi Publishing Corporation
Gastroenterology Research and Practice
Volume 2016, Article ID 1895694, 8 pages
http://dx.doi.org/10.1155/2016/1895694

Research Article

3D-EAUS and MRI in the Activity of Anal Fistulas in Crohn's Disease

Maria Eleonora Alabiso,[1] Francesca Iasiello,[2] Gianluca Pellino,[3] Aniello Iacomino,[2] Luca Roberto,[2] Antonio Pinto,[4] Gabriele Riegler,[5] Francesco Selvaggi,[3] and Alfonso Reginelli[2]

[1]*Department of Radiology, Ascalesi Hospital, 80100 Naples, Italy*
[2]*Department of Internal and Experimental Medicine, Second University of Naples, 80100 Naples, Italy*
[3]*Unit of Colorectal Surgery, Department of Medical, Surgical, Neurologic, Metabolic and Ageing Sciences, Second University of Naples, 80100 Naples, Italy*
[4]*Department of Radiology, Cardarelli Hospital, 80100 Naples, Italy*
[5]*Unit of Gastroenterology, Department of Medical, Surgical, Neurologic, Metabolic and Ageing Sciences, Second University of Naples, 80100 Naples, Italy*

Correspondence should be addressed to Alfonso Reginelli; alfonsoreginelli@hotmail.com

Received 18 June 2015; Revised 14 August 2015; Accepted 19 August 2015

Academic Editor: Fernando de la Portilla

Aim. This study aspires to assess the role of 3D-Endoanal Ultrasound (3D-EAUS) and Magnetic Resonance Imaging (MRI) in preoperative evaluation of the primary tract and internal opening of perianal fistulas, of secondary extensions and abscess. *Methods.* During 2014, 51 Crohn's disease patients suspected for perianal fistula were enrolled. All patients underwent physical examination with both the methods and subsequent surgery. *Results.* In the evaluation of CD perianal fistulas, there are no significant differences between 3D-EAUS and MRI in the identification of abscess and secondary extension. Considering the location, 3D-EAUS was more accurate than MRI in the detection of intersphincteric fistulas (p value = 10^{-6}); conversely, MRI was more accurate than 3D-EAUS in the detection of suprasphincteric fistulas (p value = 0.0327) and extrasphincteric fistulas (p value = $4 \oplus 10^{-6}$); there was no significant difference between MRI and 3D-EAUS in the detection of transsphincteric fistulas. *Conclusions.* Both 3D-EAUS and MRI have a crucial role in the evaluation and detection of CD perianal fistulas. 3D-EAUS was preferable to MRI in the detection of intersphincteric fistulas; conversely, in the evaluation of suprasphincteric and extrasphincteric fistulas the MRI was preferable to 3D-EAUS.

1. Introduction

Perianal fistula is a chronic inflammatory condition defined as an abnormal perianal tract that connects two epithelial surfaces, usually the anal canal and the perianal skin [1]. This condition is often highly recurrent and may require repeated surgical treatments [2, 3]. Perianal fistulas predominantly affect young males with a male-to-female ratio of 2 : 1 [2, 4]. The most common symptom is discharge, but local pain is also frequent [3]. Patients suffering from Crohn's disease (CD) often experience perianal disease and have complex perianal sepsis requiring repeated treatments [5]. Surgery still plays a relevant role in perianal CD, with a significant prevalence of recurrence [4]. Accurate preoperative assessment of a fistula and its complications, such as secondary extensions or abscess, is mandatory to perform a successful surgery [6] while preserving anal function and continence, but no single tool can effectively depict the anatomy of perianal fistulas in these patients. Overly aggressive fistulotomy can lead to postoperative fecal incontinence, whereas inappropriate conservative treatment could lead to fistula recurrence [5]. Preoperative imaging modalities can alert

the surgeon to fistula characteristics that might otherwise be missed. Aim of this study is to assess the role of 3D-Endoanal Ultrasound (3D-EAUS) and Magnetic Resonance Imaging (MRI) in diagnosing primary tract, and secondary extension, in localizing internal opening of perianal fistulas and identifying the relation between the anal fistula and anal sphincters.

2. Methods

2.1. Study Design and Population. Between January 2014 and December 2014, 51 patients with known CD (37 M; 14 F; age range: 28–56 years; mean: 42 years), suspected for perianal fistula, were enrolled. All patients were referred to our department after a previous clinical diagnosis of perianal fistula and were preoperatively evaluated with 3D-EAUS and MRI and subsequently underwent surgery. In accordance with our institute guidelines, every patient received and signed written consent forms. The eventual diagnosis of the fistula anatomy was made after combining the findings of all of the modalities (3D-EAUS, MRI, and surgery).

2.1.1. 3D-EAUS. The examinations were performed with a Bruel and Kjaer ProFocus system Ultra View-2202 (Mileparken 34, 2730 Herlev, Denmark) with a model 2050 transducer equipped with a double multifrequency crystal (range: 6–16 MHz), with 360° mechanical rotation at a speed of 1.9–2.8 rotations/s, focus range up to 45 mm, dimensions 550 × 270 × 40 × 17 mm, and automatic extraction and field depth up to 10 cm. All patients were examined in the lateral decubitus position without any prior bowel preparation and without any anesthesia. The transducer was covered with a condom and, after adequate lubrication, placed inside the anal canal. The transducer was firstly advanced as far as the rectal ampulla before continuing with more caudal scans; it was then automatically withdrawn to the superficial perianal plane. Images were viewed in planes perpendicular to the transducer, which was kept with the same orientation so that the anterior wall was always visualized at the 12 o'clock position, the left wall at 3 o'clock, the posterior wall at 6 o'clock, and the right wall at 9 o'clock.

Three scan planes were acquired:

(1) The deeper plane corresponded to the proximal extremity of the anal canal, where there is the typical U-shaped sling appearance of the hyperechoic puborectalis muscle with the wider end towards the pubis.

(2) The intermediate plane included the hypoechoic internal anal sphincter (IAS), the perianal body, and the transverse perianal muscle.

(3) The superficial plane corresponded to the level of the distal extremity of anal canal and included the hyperechoic layer of the submucosal portion of the external anal sphincter (EAS).

All images were retrospectively analyzed by two observers (reader 1 and reader 2), who were unaware of the MRI results. The two observers evaluated the data independently of each other without knowing the test results. To avoid discrepancy, both observers examined the case together until agreement was reached.

Radiological examination aimed to determine the following fistula characteristics: (1) the primary tract, defined according to the criteria of Parks et al. [7] as intersphincteric, transsphincteric, extrasphincteric, or suprasphincteric; in the intersphincteric fistulas the submucosal fistulas were included, lying in the superficial submucosal plane lateral to the subcutaneous portion of the external anal sphincter; (2) the internal opening, localized with respect to a clock face as described above; and (3) secondary extension, including horseshoe tract and abscess formation. The anatomic location of any secondary extension arising from the primary fistula track was recorded as intersphincteric, ischiorectal, or supralevator. A horseshoe extension was defined as any extension from the primary track that appeared to extend to both sides of the internal opening, and such an extension was classified as intersphincteric or ischiorectal.

Fistula tracks were visualized as tube-like, hypoechoic lesions. The internal fistula opening was identified as a hypoechoic area in the intersphincteric plane, as a defect in the internal anal sphincter, or as a subepithelial breach that connected to the fistulous tract through an internal sphincter defect [8].

After the EAUS procedures, the characteristics of the fistula were classified according to the same criteria used in the clinical evaluation.

2.1.2. MRI. MR imaging studies were performed on a 1.5 T closed magnet (Magnetom Symphony, Siemens, Germany). The patients were placed in the supine position.

T2-weighted turbo spin-echo (TSE) sequences (TR 5370, TE 126, averages 2, flip angle 150, slice thickness 4, bandwidth 130, and FOV READ 230 mm) were acquired in sagittal plane, which was used as reference to obtain para-axial planes (perpendicular to the anal canal) and paracoronal planes (parallel to the anal canal). In the para-axial planes the following sequences were acquired: T1-weighted TSE (TR 611 ms, TE 11 ms, averages 2, flip angle 150 deg, slice thickness 5 mm, bandwidth 130, and FOV READ 270 mm), T2-weighted TSE (TR 7710 ms, TE 114 ms, averages 2, flip angle 180 deg, slice thickness 3.5 mm, bandwidth 130, and FOV READ 334 mm), and T2-weighted Haste with and without suppression of fat signal (TR 9860 ms, TE 114 ms, averages 2, flip angle 180 deg, slice thickness 3.5 mm, bandwidth 130, and FOV READ 250 mm). In the paracoronal plane T2-weighted TSE with suppression of fat signal was acquired (TR 2500 ms, TE 104 ms, averages 2, flip angle 150 deg, slice thickness 4 mm, bandwidth 130, and FOV READ 300 mm).

Two radiologists (reader 3; reader 4) evaluated the images without knowing the results of the 3D-EAUS. Each component of the anal fistula was categorized and recorded using the similar criteria of 3D-EAUS. Fistula tracks were visualized as tube-like, hyperintense or hypointense lesions. The internal fistula opening was identified as a hyperintense or hypointense area in the intersphincteric plane, as a defect in the internal anal sphincter, or as a subepithelial breach that connected to the fistulous tract through an internal sphincter defect.

Table 1: Type of perianal fistulas, according to Parks classification, observed with 3D-EAUS and MRI.

Location	3D-EAUS Number of patients (%)	MRI Number of patients (%)	Hypothesis	McNemar's exact test (p value)
Intersphincteric	23 (45.10)	3 (5.88)	MRI < 3D-EAUS	10^{-6}
Transsphincteric	12 (23.53)	10 (19.61)	MRI < 3D-EAUS	0.344
Suprasphincteric	4 (7.84)	11 (21.57)	MRI > 3D-EAUS	0.0327
Extrasphincteric	3 (5.88)	21 (41.18)	MRI > 3D-EAUS	$4 \oplus 10^{-6}$
Absence of pathology	9 (17.65)	6 (11.76)	MRI < 3D-EAUS	0.187
Total	**51 (100)**	**51 (100)**	MRI > 3D-EAUS	

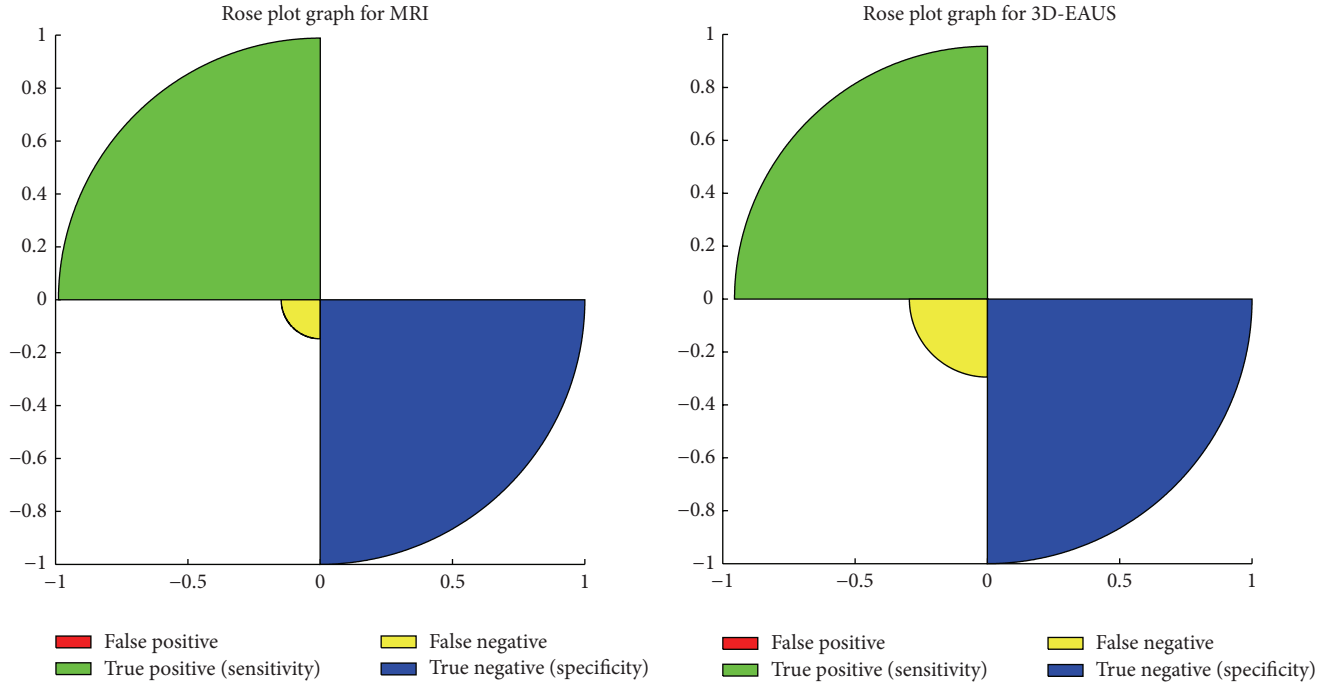

Figure 1: Rose plot graphs of sensitivity and specificity for MRI and 3D-EAUS.

2.2. Statistical Methods. The statistical analyses were performed using Matlab statistical toolbox version 2008 (MathWorks, Natick, MA, USA) for Windows at 32 bits. McNemar's exact test [9] and χ^2 test with Yates correction [10] were performed to determine the higher accuracy between 3D-EAUS and MRI in the individualization of primary tract, according to Parks classification, and in the identification of secondary extensions and abscess.

In addition the sensitivity and specificity with confidence intervals at 95% [11] were defined for the diagnostic procedures. All tests with p value < 0.05 were considered as significant.

3. Results

All patients well tolerated the exam and there were no side effects reported. The analysis of radiological examinations of 51 patients, respectively, for MRI and 3D-EAUS, showed the presence of intersphincteric fistulas in 5.88% (3/51) of cases versus 45.10% (23/51), transsphincteric fistulas in 19.61% (10/51) versus 23.53% (12/51), suprasphincteric fistulas in 21.57% (11/51) versus 7.84% (4/51), and extrasphincteric fistulas in 41.18% (21/51) versus 5.88% (3/51) and absence of pathology in 11.76% (6/51) versus 17.65% (9/51) (Table 1).

Table 2: Differences between MRI and 3D-EAUS.

Parameters	3D-EAUS		MRI	
	Value %	IC 95%	Value	IC 95%
Sensitivity	97.80	(87.9, 100.0)	91.11	(79.2, 97.6)
False negative	2.20	(2.0, 17.1)	8.89	(3.0, 20.2)
Specificity	100.00	(91.3, 100.0)	100.0	(91.3, 100.0)
False positive	0.00	(0.2, 6.8)	0.00	(0.2, 6.8)
Accuracy	98.00	(88.2, 100.0)	92.20	(80.3, 98.2)

There was no significant difference between MRI and 3D-EUAS (Table 2 and Figure 1) in specificity (100% versus 100%) and sensitivity (91.30%, with IC = 79.2%–97.6% versus 97.80%,

Table 3: Proportion of positive patients to 3D-EAUS and MRI in the diagnosis of primary tract of anal fistulas, secondary extensions, and abscess and χ^2 test with Yates correction.

	MRI %	3D-EAUS %	Hypothesis	χ^2 test (p value)
Primary tract	58.82 (30)	52.94 (27)	MRI > 3D-EAUS	0.55
Secondary extension	86.27 (44)	80.39 (41)	MRI > 3D-EAUS	0.42
Abscess	15.69 (8)	5.88 (3)	MRI > 3D-EAUS	0.11

with IC = 87.9%–100%) (Table 2). McNemar's exact test confirmed that there was no significant difference between MRI and 3D-EAUS in the evaluation of patients with pathology (p value = 0.187). Considering each location, according to Parks classification, 3D-EAUS result was more accurate than MRI in the detection of intersphincteric fistulas (p value = 10^{-6}); conversely, MRI was more accurate than 3D-EAUS in the detection of suprasphincteric fistulas (p value = 0.0327) and extrasphincteric fistulas (p value = $4 \oplus 10^{-6}$), while there was no significant difference between MRI and 3D-EAUS in the detection of transsphincteric fistulas.

In Table 3 we showed the different accuracy between MRI and 3D-EAUS in the identification of primary tract, secondary extension, and abscess, considering that one patient could be affected from more symptoms too. The χ^2 test with Yates correction showed that in the evaluation of primary tract, secondary extension, and abscess there were no significant differences between MRI and 3D-EAUS (58.82% versus 52.94% with p value = 0.55; 86.27% versus 80.39% with p value = 0.42; 15.69% versus 5.88% with p value = 0.11, resp.). Concerning secondary extensions, there were 27 patients (61.4%) with concomitant abscesses and 17 (38.6%) with horseshoe extension. No differences were observed concerning detection of each of these findings between the two modalities (abscess, 27 versus 25, $p = 0.15$; horseshoe track, 17 versus 16, $p = 0.31$ MRI versus 3D-EAUS).

4. Discussion

Anal fistulas are a significant cause of morbidity associated with a severe reduction of quality of life. It represents a common clinical problem affecting approximately 0.01% of the general population, predominantly young adults, and, differently from pelvic floor disorders, afflicts men two times more often than women [2, 4, 12]. Up to 60% of CD patients have perianal disease, of whom 30% have perianal fistula [5]. Ten percent of CD can have perianal fistula as first presenting symptom, before receiving CD diagnosis.

Anal fistula is defined by an abnormal perianal tract that connects two epithelized surfaces: the anal canal to the perianal skin. Some fistulas have a tendency to recur, despite seemingly curative surgery. Recurrence is usually due to infection that has gone undetected and untreated [1]. The most common symptom is discharge (65% of the cases), but local pain due to inflammation is also common. Perianal fistulas may be caused by several inflammatory conditions and events, including CD [13, 14]. The aetiology of perianal disease in CD is debated, and no single factor can be identified as responsible of subsequent anorectal sepsis, probably resulting from a combination of microbiological, immunological, and genetic factors [5]. The most widely used one is Parks et al. classification system that was derived from analysis of 400 consecutive patients referred for specialist evaluation of perianal fistulas. Parks et al. [7] classified fistulas into four main groups. Intersphincteric fistulas were the most commonly noted (45%) and are characterized by a primary tract that courses in the intersphincteric space without penetrating the external sphincter. In the intersphincteric fistulas we included the submucosal fistulas, lying in the superficial submucosal plane lateral to the subcutaneous portion of the external anal sphincter; transsphincteric fistulas were slightly less common (30%) and traverse the external sphincter and pass into the ischioanal fossa, below the level of the puborectalis muscle. Suprasphincteric fistulas (20%) extend within the intersphincteric plane superior to the puborectalis before penetrating the levator musculature to course within the ischioanal fossa. Extrasphincteric fistulas (5%) course within the ischioanal fossa and penetrate the levator musculature without traversing either the internal or the external sphincters opening directly into the rectum [4, 7]. All of these fistula types may be complicated by abscesses and by secondary tracks. In addition fistulas can spread circumferentially in the intersphincteric space, ischioanal fossa, or supralevator space. Circumferential branches or abscesses that extend on both sides of the interior opening are known as horseshoe branches or abscesses [7].

Incorrect classification and/or determination of extent increases risk of incomplete healing, recurrent fistula, and inadvertent sphincter injury.

3D-EAUS is a valuable tool to represent the normal anatomy of the anal canal and it is simple, cheap, readily available, less demanding for the patient, and with high diagnostic accuracy. It allows rapid evaluation for specialized equipment, is easy to perform and easily reproducible and painless, and does not require patient preparation.

It provides excellent imaging of the rectal wall, of the internal and external sphincters and of the intersphincteric plane, of muscle mobility, and of the position of the internal opening, essential for planning surgical approach to reduce the risk of incontinence. This method can be very useful also in the follow-up of anal diseases, both to study surgical drainages and in the postoperative study of anal fistulae. 3D-EAUS represents the first investigation in patients with perianal fistulas that allows real-time visualization; it has the potential to become the initial and most cost-effective investigation for fistula disease, which may alleviate the need

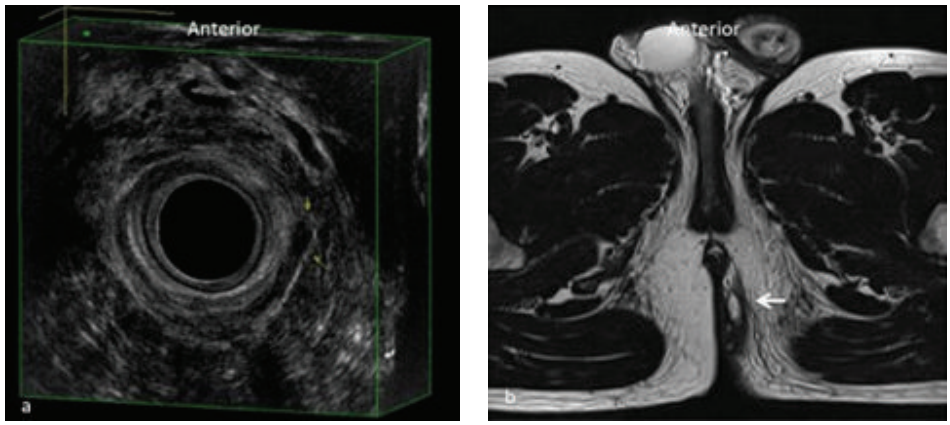

(a) (b)

Figure 2: Submucosal fistula in the superficial plane corresponding to the level of the distal extremity of anal canal. In (a) 3D-EAUS, including the hyperechoic layer of the submucosal portion of the external anal sphincter (EAS), shows a submucosal fistula extending from 3 o'clock to 5 o'clock, lying external to the submucosal portion of the EAS (yellow arrows). The same plane on MRI (b), which could be avoided in this kind of fistulas (white arrow); 3D-EAUS is often sufficient as a preoperative diagnostic method.

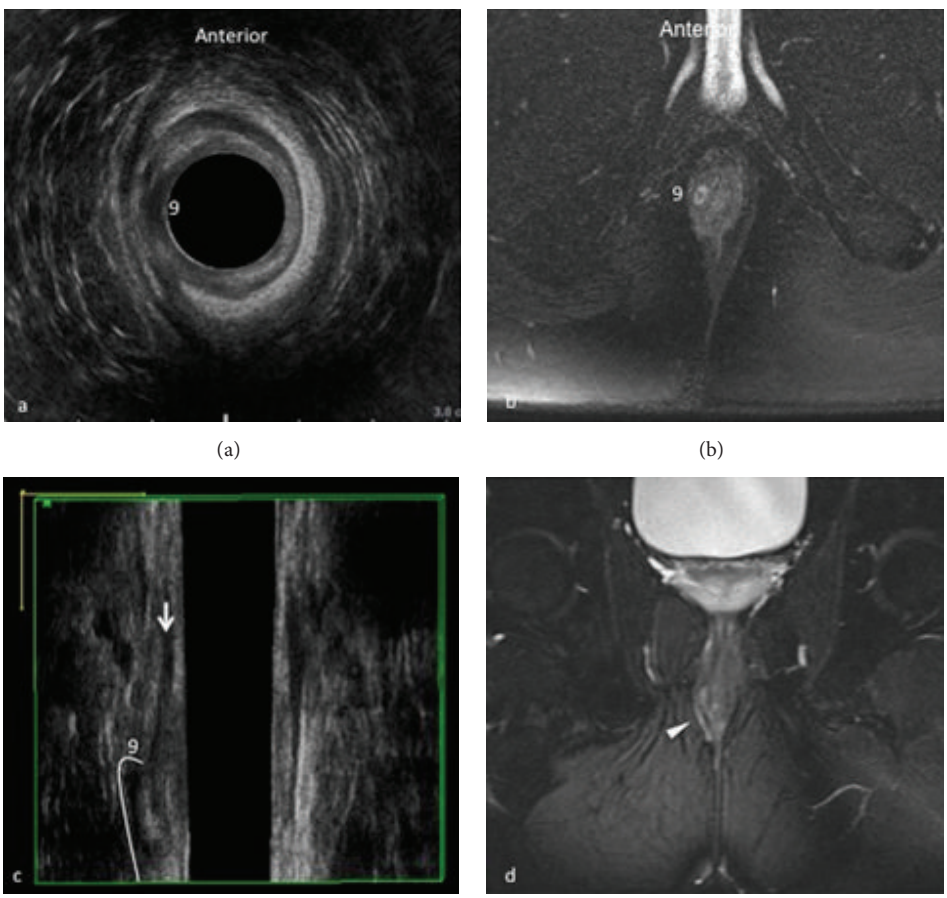

(a) (b)

(c) (d)

Figure 3: Intersphincteric fistula at 9 o'clock. 3D-EAUS demonstrates the proximal origin of the fistulous tract from the internal anal sphincter and its location in the intersphincteric plane on both axial (a) and coronal plane (c), better depicting the fistulous tract in the intersphincteric space than MRI (b, d).

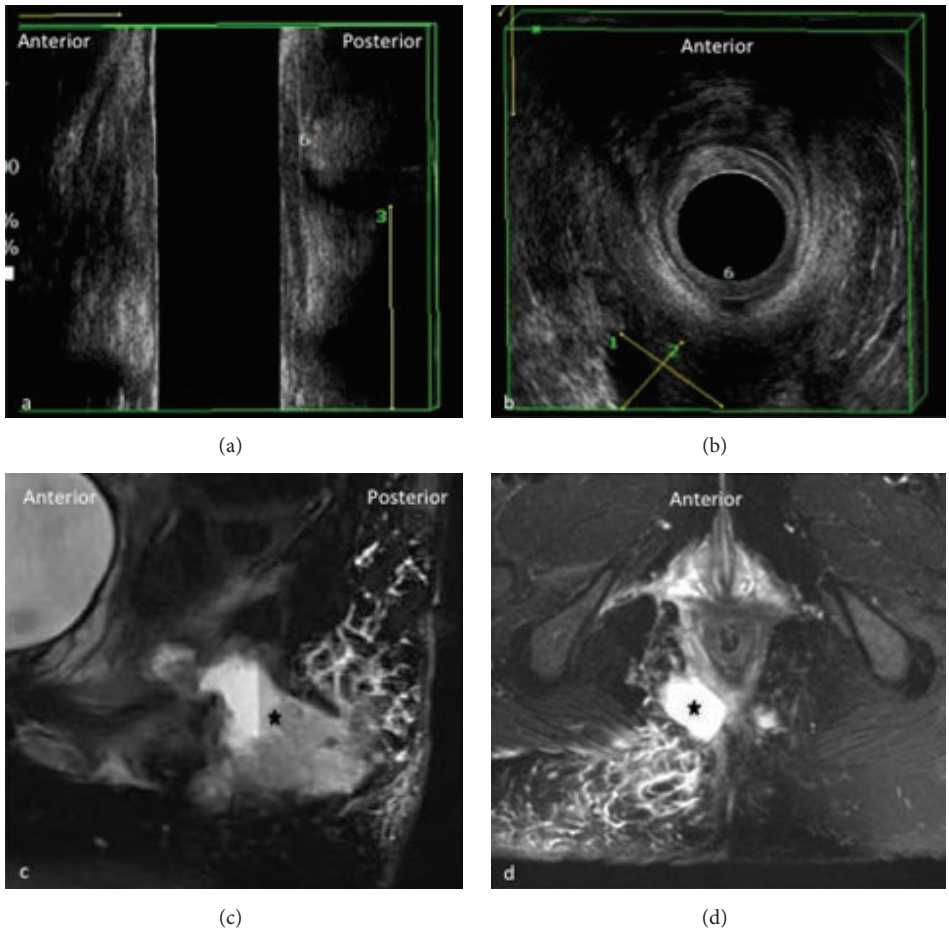

Figure 4: Extrasphincteric fistula at 6 o'clock with abscess. Sagittal (a) and axial (b) view of anal canal on 3D-EAUS showing at 6 o'clock (6) the proximal origin of an extrasphincteric fistula which drains into a big extrasphincteric abscess (calibers 1–3). On (c) and (d) sagittal and axial view, respectively, of anal and perianal region on MRI which is indispensable to demonstrate the complete extension of the extrasphincteric abscess (black star) and the appearance of edematous surrounding tissues.

for MRI in most patients. It is fully sufficient as a preoperative diagnostic method in most patients with intersphincteric and transsphincteric/submucosal fistula above all with single tract and without abscess, better depicting the intersphincteric plane and both the internal and external sphincters (Figures 2 and 3). 3D-EAUS has some limitations since it is highly operator dependent, it has limited ability to resolve ischioanal and supralevator infections, and it does not allow a reliable distinction between infection and fibrosis [4, 6, 15–18].

MRI has the advantage of an excellent intrinsic soft-tissue resolution, thus showing the fistula tract in the context of the surrounding structures. It has a wider FOV than 3D-EAUS and it is more suited for the assessment of complex branching tracts, the lateral extension into the perianal spaces, and the cranial extension above the levator ani (Figure 4) [19, 20].

It is useful to improve treatment by correct assessment of the extent of disease, in the treatment response/monitoring of perianal fistulas, especially in CD; it is also valuable to differential diagnosis between infections from fibrosis, ischioanal and supralevator infections, and supra- and infralevator extension. It could be a valid second-level examination in case of abscesses or complex tracts and also through the pelvic diaphragm and finally where internal opening cannot be simply shown [20–25].

In our series we were able to demonstrate that both MRI and 3D-EAUS can be used to assess transsphincteric fistulas. However, basing on 3D-EUAS exams alone, up to 14% of suprasphincteric fistulas can be overlooked or not correctly diagnosed (Table 1, Figure 5).

In conclusion, both EAUS and MRI have a crucial role in the evaluation and detection of perianal fistulas. 3D-EUAS is more accurate in comparison to MRI in the individuation of intersphincteric/submucosal fistulas, where it could be fully sufficient as a preoperative diagnostic method, better depicting the intersphincteric plane and both the internal and external sphincters. In fact, the introduction of 3D technique has optimized US evaluation. MRI is more accurate in comparison to 3D-EUAS in the individuation of suprasphincteric and extrasphincteric fistulas with the reported advantage of an excellent intrinsic soft-tissue resolution and higher panoramicity, thus showing the fistula track in the context of the surrounding structures. 3D-EUAS and MRI

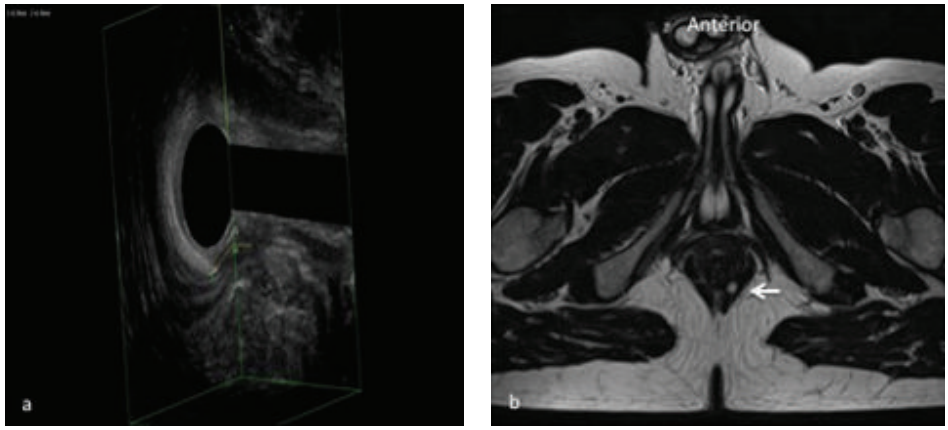

(a) (b)

Figure 5: Transsphincteric fistula at 5 o'clock. Both 3D-EAUS (calibers) (a) and MRI (white arrow) (b) are accurate in the detection of transsphincteric fistulas. Thanks to 3D technique 3D-EAUS may show the entire extension of the fistula while on MRI it appears on two different planes.

are statistically equivalent in the detection of transsphincteric fistulas and in the evaluation of abscess and secondary extension.

Conflict of Interests

The authors declare that there is no conflict of interests regarding the publication of this paper.

References

[1] G. N. Buchanan, S. Halligan, C. I. Bartram, A. B. Williams, D. Tarroni, and C. R. G. Cohen, "Clinical examination, endosonography, and MR imaging in preoperative assessment of fistula in ano: comparison with outcome-based reference standard," *Radiology*, vol. 233, no. 3, pp. 674–681, 2004.

[2] J. De Miguel Criado, L. G. del Salto, P. F. Rivas et al., "MR imaging evaluation of perianal fistulas: spectrum of imaging features," *Radiographics*, vol. 32, no. 1, pp. 175–194, 2012.

[3] S. Halligan, "Imaging fistula-in-ano," *Clinical Radiology*, vol. 53, no. 2, pp. 85–95, 1998.

[4] M. R. M. Sun, M. P. Smith, and R. A. Kane, "Current techniques in imaging of fistula in ano: three-dimensional endoanal ultrasound and magnetic resonance imaging," *Seminars in Ultrasound, CT and MRI*, vol. 29, no. 6, pp. 454–471, 2008.

[5] G. Pellino and F. Selvaggi, "Surgical treatment of perianal fistulizing crohn's disease: from lay-open to cell-based therapy—an overview," *The Scientific World Journal*, vol. 2014, Article ID 146281, 8 pages, 2014.

[6] S. Halligan and J. Stoker, "Imaging of fistula in ano," *Radiology*, vol. 239, no. 1, pp. 18–33, 2006.

[7] A. G. Parks, P. H. Gordon, and J. D. Hardcastle, "A classification of fistula in ano," *British Journal of Surgery*, vol. 63, no. 1, pp. 1–12, 1976.

[8] D.-Y. Cho, "Endosonographic criteria for an internal opening of fistula-in-ano," *Diseases of the Colon and Rectum*, vol. 42, no. 4, pp. 515–518, 1999.

[9] Q. McNemar, "Note on the sampling error of the difference between correlated proportions or percentages," *Psychometrika*, vol. 12, no. 2, pp. 153–157, 1947.

[10] R. R. Sokal and F. J. Rohlf, *Biometry. The Principles and Practices of Statistics in Biological Research*, W.H. Freeman Publishers, New York, NY, USA, 3rd edition, 1995.

[11] R. G. Newcombe, "Improved confidence intervals for the difference between binomial proportions based on paired data," *Statistics in Medicine*, vol. 17, no. 22, pp. 2635–2650, 1998.

[12] G. Cavallo, A. Salzano, R. Grassi, P. Zanatta, and M. Tuccillo, "Rectocele in males: clinical, defecographic, and CT study of singular cases," *Diseases of the Colon & Rectum*, vol. 34, no. 11, pp. 964–966, 1991.

[13] G. Gatta, G. Di Grezia, V. Di Mizio et al., "Crohn's disease imaging: a review," *Gastroenterology Research and Practice*, vol. 2012, Article ID 816920, 15 pages, 2012.

[14] R. Grassi, P. F. Rambaldi, G. Di Grezia et al., "Inflammatory bowel disease: value in diagnosis and management of MDCT-enteroclysis and ^{99m}Tc-HMPAO labeled leukocyte scintigraphy," *Abdominal Imaging*, vol. 36, no. 4, pp. 372–381, 2011.

[15] M. R. S. Siddiqui, H. Ashrafian, P. Tozer et al., "A diagnostic accuracy meta-analysis of endoanal ultrasound and MRI for perianal fistula assessment," *Diseases of the Colon and Rectum*, vol. 55, no. 5, pp. 576–585, 2012.

[16] V. A. Sahni, R. Ahmad, and D. Burling, "Which method is best for imaging of perianal fistula?" *Abdominal Imaging*, vol. 33, no. 1, pp. 26–30, 2008.

[17] A. Reginelli, Y. Mandato, C. Cavaliere et al., "Three-dimensional anal endosonography in depicting anal-canal anatomy," *Radiologia Medica*, vol. 117, no. 5, pp. 759–771, 2012.

[18] L. Brunese, M. Amitrano, V. Gargano et al., "Role of anal endosonography in inflammation and trauma of the anal canal," *Radiologia Medica*, vol. 92, no. 6, pp. 742–747, 1996.

[19] J. C. Colitis, "Imaging techniques for assessment of inflammatory bowel disease: joint ECCO and ESGAR evidence-based consensus guidelines," *Journal of Crohn's and Colitis*, vol. 7, no. 7, pp. 556–585, 2013.

[20] J. Panes, Y. Bouhnik, W. Reinisch et al., "Imaging techniques for assessment of inflammatory bowel disease: joint ECCO and ESGAR evidence-based consensus guidelines," *Journal of Crohn's and Colitis*, vol. 7, no. 7, pp. 556–585, 2013.

[21] R. Grassi, A. Rotondo, O. Catalano et al., "Endoanal ultrasonography, defecography, and enema of the colon in the radiologic study of incontinence," *Radiologia Medica*, vol. 89, no. 6, pp. 792–797, 1995.

[22] S. Halligan and C. I. Bartram, "MR imaging of fistula in ano: are endoanal coils the gold standard?" *American Journal of Roentgenology*, vol. 171, no. 2, pp. 407–412, 1998.

[23] P. J. Lunniss, P. G. Barker, A. H. Sultan et al., "Magnetic resonance imaging of fistula-in-ano," *Diseases of the Colon & Rectum*, vol. 37, no. 7, pp. 708–718, 1994.

[24] S. A. Taylor, S. Halligan, and C. I. Bartram, "Pilonidal sinus disease: MR imaging distinction from fistula in ano," *Radiology*, vol. 226, no. 3, pp. 662–667, 2003.

[25] R. Nelson, "Anorectal abscess fistula: what do we know?" *Surgical Clinics of North America*, vol. 82, no. 6, pp. 1139–1151, 2002.

Hindawi Publishing Corporation
Gastroenterology Research and Practice
Volume 2016, Article ID 2657876, 4 pages
http://dx.doi.org/10.1155/2016/2657876

Research Article

Imaging in the Evaluation of Endoscopic or Surgical Treatment for Achalasia

Diego Palladino,[1] Andrea Mardighian,[2] Marilina D'Amora,[3] Luca Roberto,[3] Francesco Lassandro,[4] Claudia Rossi,[3] Gianluca Gatta,[3] Mariano Scaglione,[5] and Guglielmi Giuseppe[2]

[1]*Radiology Department, IRCCS "Casa Sollievo della Sofferenza", San Giovanni Rotondo, Foggia, Italy*
[2]*Radiology Department, University of Foggia, Foggia, Italy*
[3]*Radiology Department, Second University of Naples, Napoli, Italy*
[4]*Radiology Department, "V. Monaldi" Hospital, Napoli, Italy*
[5]*Radiology Department, Pineta Grande Medical Center, Castel Volturno, Caserta, Italy*

Correspondence should be addressed to Gianluca Gatta; ggatta@sirm.org

Received 19 June 2015; Accepted 13 September 2015

Academic Editor: Lorenzo Mannelli

Purpose. Aim of the study is to evaluate the efficacy of the endoscopic (pneumatic dilation) versus surgical (Heller myotomy) treatment in patients affected by esophageal achalasia using barium X-ray examination of the digestive tract performed before and after the treatment. *Materials and Methods.* 19 patients (10 males and 9 females) were enrolled in this study; each patient underwent a barium X-ray examination to evaluate the esophageal diameter and the height of the barium column before and after endoscopic or surgical treatment. *Results.* The mean variation of oesophageal diameter before and after treatment is −2.1 mm for surgery and 1.74 mm for pneumatic dilation (OR 0.167, CI 95% 0.02–1.419, and *P*: 0.10). The variations of all variables, with the exception of the oesophageal diameter variation, are strongly related to the treatment performed. *Conclusions.* The barium X-ray study of the digestive tract, performed before and after different treatment approaches, demonstrates that the surgical treatment has to be considered as the treatment of choice of achalasia, reserving endoscopic treatment to patients with high operative risk and refusing surgery.

1. Introduction

Achalasia is the most frequent primary motor disorder of the esophagus. It is still a rare disease that may occur in both sexes at any age with a prevalence of less than 1/10,000 and with a new cases' incidence of 0.6–1/100,000 citizens/year [1]. At the base of this disease there is a primitive neuromuscular alteration with a myenteric plexus degeneration causing a pathophysiological disorder consisting in the failure of the lower esophageal sphincter (LES) relaxation during swallowing and the complete loss of peristaltic coordination of the esophagus body [2]. Dysphagia is the typical symptom, consisting in the difficulty in swallowing food; usually the patients have a very long and often unrelated history [3]. Other times the patients may show a sudden onset and, rarely, the symptomatology may be "paradoxical," more pronounced for liquids than solids. Patients may also feel chest pain and regurgitation. Pain is a less frequent symptom and it is usually observed in the early stages of the disease. It is probably related to the smooth muscles contraction of the esophageal body. Regurgitation is the symptom occurring in later stages, when the esophagus is dilated, and may be misdiagnosed as a gastroesophageal reflux disease, leading to diagnosis delay. In this phase, aspirations of food material may be also present leading to "ab ingestis pneumonia" in 12% of cases [1]. Other times, finally, the only sign of this disease can be a persistent halitosis, due to stagnation of endoesophageal food material. The diagnosis is usually made with X-rays of the digestive tract with barium contrast medium (cm) administration and esophageal manometry [4]. The therapeutic approach may be pharmacological, endoscopic, and surgical [5].

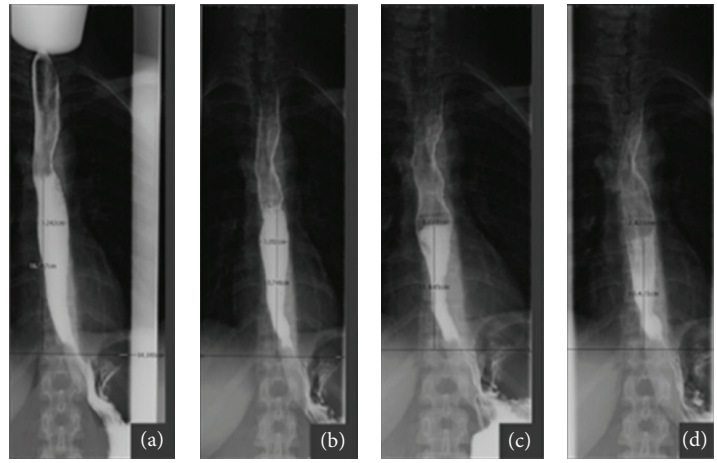

Figure 1: X-rays show the height of barium column 0, 1, 2, and 5 minutes after barium oral administration.

Aim of the study is to evaluate the efficacy of the endoscopic (pneumatic dilation) versus surgical (Heller myotomy) treatment in patients affected by esophageal achalasia through the analysis of parameters deriving from the barium X-ray examination, performed before and after surgical or endoscopic treatment.

2. Materials and Methods

The study was approved by the Institutional Ethical Committee and conducted according with the ethical principles of the Declaration of Helsinki. Written informed consent was obtained in all patients.

From January 2009 to December 2014 all the patients referring to our radiology departments for radiological evaluation of achalasia, based on previous esophageal manometry, and planned for surgical or endoscopic treatment were investigated about their clinical history and eligible patients were considered for enrolment in this study. Patients with concomitant systemic neurological and/or rheumatologic disease (e.g., Parkinson disease, scleroderma) were excluded.

Each patient underwent barium X-rays evaluation before and after endoscopic or surgical treatment.

The examination was performed with Siemens AXIOM Luminos DRF equipment. Pronto Bario HD (Bracco, Milan, Italy) has been used as contrast medium; each patient received 98,45 g of powder for oral suspension diluted in 90 mL of water and administered as a single bolus prior to the execution of swellings at 0, 1, 2, and 5 minutes (Figure 1). The esophageal diameter and the height of the barium column were evaluated at the different times after the barium administration. The procedure was successful and was well tolerated in all patients and no complications were reported during the exam execution.

2.1. Statistical Analysis. To obtain the logistic model we calculated, for each variable, the mean change was observed after the intervention of the total sample. For each patient were introduced five dichotomous variables (one for each initial variable), assuming value 1 if the reduction found in a particular patient results to be greater than or equal to the average reduction and 0 otherwise. Finally, for each variable, we evaluated the possible relationship with the treatment and we calculated odds ratio.

3. Results

Fifty-two patients were initially considered for the study, 12 patients were excluded due to the presence of concomitant systemic neurological disease, 17 did not give their consent, and 4 patients were lost to the evaluation after treatment. Nineteen patients were finally enrolled: 10 males and 9 females, age range was 27–76 y.o. for men and 41–75 for women. Eleven patients underwent surgical Heller myotomy treatment and Dor fundoplication and 8 had endoscopic pneumatic dilation treatment performed, due to the high operative risk and refusal of surgical treatment.

The mean variation of esophageal diameter before and after treatment is −2.1 mm for surgery and 1.74 mm for pneumatic dilation (OR 0.167, CI 95% 0.02–1.419, and P: 0.10). Table 1 shows the variation of esophageal diameter and the height of barium column before and after surgical or endoscopic treatment at 0, 1, 2, and 5 minutes after barium administration. Table 2 shows the odds ratio calculated with the logistic regression model to demonstrate postoperation mean changes in relation to the two treatments.

4. Discussion

The standard in diagnosing and classifying achalasia is represented by the esophageal manometry documenting the impaired relaxation of the LES and the absence or the alteration of peristaltic waves in the distal esophagus [4, 6–9].

Upper endoscopy is usually performed to rule out cancer or a peptic stricture and, particularly in patients older than 50 years with dysphagia and weight loss, attention should be paid on the possible presence of a tumor underlying achalasia (pseudoachalasia) [10, 11]. Cytohistological samples should always be taken in the cardiac region and in the suspicious areas, to find possible neoplastic degeneration [12, 13]. Chest

Table 1: Table shows the variation of esophageal diameter and the height of barium column before and after surgical or endoscopic treatment at 0, 1, 2, and 5 minutes after barium administration.

	Surgery Myotomy 11 patients			Endoscopy Pneumatic dilation 8 patients		
	Before	After	Δ	Before	After	Δ
Esophagus diameter (cm)	5.20	3.10	−2.10	4.80	6.54	+1.74
Column baryta height						
0′	23.95	11.9	−12.05	26.50	14.66	−11.89
1′	21.30	7.31	−14.00	25.85	12.61	−13.24
2′	19.64	4.84	−14.79	24.42	11.56	−12.86
5′	16.69	3.75	−12.94	23.06	8.61	−14.45

Table 2: Table shows OR, CI 95%, and P value calculated with logistic regression model to evaluate statistical significance of the variation between pneumatic dilation and myotomy treatment in patients with diagnosis of achalasia.

	Odd ratio	Confidence interval (95%)		P value
Reduction > mean				
Esophagus	0.167	0.02	1.419	0.1011
Column baryta height				
0′	0.625	0.093	4.222	0.6297
1′	0.625	0.093	4.222	0.6297
2′	0.429	0.062	2.972	0.3911
5′	0.9	0.133	6.080	0.9139

and abdominal CT scan without and with intravenous cm may be helpful in specific, not so common cases [9, 14].

The barium X-ray examination allows to confirm the diagnosis and to assess the degree of esophageal dilation, the axis of the esophagus, and the presence of an associated epiphrenic diverticulum [6], the esophagus appears dilated, aperistaltic, or with uncoordinated peristaltic contractions, sometimes stuffed of food previously ingested and with the "tail mouse" characteristic appearance of the cardiac region [6].

In the early stages, the only sign may be the endoluminal stagnation of cm, with a progressive increase in the height of the barium column until its pressure causes the forced opening and subsequent rapid emptying of the LES.

The cause for an initial reduction of inhibitory neurons in achalasia is unknown; then etiological therapies still do not exist, but only symptomatic treatments [9]. These treatments are designed to solve the lack of LES relaxation. The therapeutic approaches may be pharmacological, endoscopic, or surgical. Drug therapy is not very effective, because, even in the early stages of the treatment, the benefits can be seen only in about 2/3 of the patients, with a chronic drug intake that may cause a reduction in the pharmacological effects with tolerance and addiction phenomena; the possible presence of side effects, such as low blood pressure and related headaches, has to be considered [15]. Some studies have shown a partial efficacy of calcium channel blockers and nitrated derivatives [16], but the use of these medical therapies should be reserved for those patients who cannot tolerate surgical approaches or to who refuse to use them.

Another type of treatment consists of endoscopic therapy that includes the botulinum toxin injection (BTI) and the pneumatic dilation (PD) [17, 18].

BTI is based on a botulinum toxin endoscopic injection in the cardia leading to an inhibition of release of acetylcholine from the myenteric plexus resulting in reduction of smooth muscle contraction of the cardiac region. The effects of a single treatment can persist for six months or more (up to 2-3 years).

The PD consists in the endoscopic introduction, through the mouth, of special dilators, on a metal guide introduced until after the cardia, with the patient maintained under sedation. The dilators consist in cylindrical balloon length of about 12 cm and with variable diameter (2.5 to 4 cm), progressively positioned in the cardiac region. Once placed, it is swollen for 1 minute at 15 PSI pressure. Usually one or two dilations are sufficient to obtain a good result. In 3% of cases, however, there is a cumulative risk of incurring postoperative complications such as tearing and/or perforation of the esophagus. With this method 60–70% of good results may be obtained [19]. The surgical Heller extramucosal myotomy represents the surgical treatment of choice [20]. The intervention consists in the longitudinal section of the cardial esophageal smooth musculature for 6-7 cm; then, an antireflux Dor fundoplication is associated, protecting the esophageal mucosa from the gastroesophageal reflux. According to the available literature, good or excellent results may be obtained in up to 90% of the cases [21].

In our study, the barium X-ray examination of the esophagus (Figure 1) in patients with achalasia, performed before and after the surgical and endoscopic pneumatic treatments, has shown that the average reduction of barium column height observed in patients surgically treated was more noticeable if compared with those treated with pneumatic endoscopic dilation as well as the reduction in the esophageal caliber. The barium X-ray examination was a good test to evaluate the outcome after surgery or endoscopic dilation, being well tolerated and poorly invasive and allowing objectively defining, with a quantitative analysis of the esophageal caliber and morphology. In conclusion, the surgical treatment represents the treatment of choice of achalasia, giving better and more stable results in comparison with endoscopic pneumatic dilation reserved for patients with high operative risk and who refuse surgery; the esophagus X-ray barium study is the modality of choice in the preoperative and postoperative imaging evaluation of these patients.

Conflict of Interests

The authors declare that there is no conflict of interests regarding the publication of this paper.

References

[1] J. E. Pandolfino and A. J. Gawron, "Achalasia: a sistematic review," *The Journal of the American Medical Association*, vol. 313, no. 18, pp. 1841–1852, 2015.

[2] S. P. Bowers, "Esophageal motility disorders," *Surgical Clinics of North America*, vol. 95, no. 3, pp. 467–482, 2015.

[3] M. I. Yasawy, "Diagnosis and treatment of achalasia patients: a ten-year review of the clinical features," *Hepatogastroenterology*, vol. 61, no. 134, pp. 1611–1616, 2014.

[4] A. Moonen and G. Boeckxstaens, "Current diagnosis and management of achalasia," *Journal of Clinical Gastroenterology*, vol. 48, no. 6, pp. 484–490, 2014.

[5] A. Dobrowolsky and P. M. Fisichella, "The management of esophageal achalasia: from diagnosis to surgical treatment," *Updates in Surgery*, vol. 66, no. 1, pp. 23–29, 2014.

[6] I. Gockel, V. F. Eckardt, T. Schmitt, and T. Junginger, "Pseudoachalasia: a case series and analysis of the literature," *Scandinavian Journal of Gastroenterology*, vol. 40, no. 4, pp. 378–385, 2005.

[7] L. Abbes, M. Leconte, R. Coriat, B. Dousset, S. Chaussade, and M. Gaudric, "Achalasia: role of endoscopic therapy and surgery," *Presse Medicale*, vol. 42, no. 5, pp. 814–818, 2013.

[8] G. Zuccaro Jr., "Esophagoscopy and endoscopic esophageal ultrasound in the assessment of esophageal function," *Seminars in Thoracic and Cardiovascular Surgery*, vol. 13, no. 3, pp. 226–233, 2001.

[9] A. R. Choi, N. R. Chon, Y. H. Youn, H. C. Paik, Y. H. Kim, and H. Park, "Esophageal cancer in esophageal diverticula associated with achalasia," *Clinical Endoscopy*, vol. 48, no. 1, pp. 70–73, 2015.

[10] S. Maeyaert, J. Pringot, J. L. Samain, L. Ghijseling, and P. Matthys, "Cancer of the oesophagus in achalasia," *Journal Belge de Radiologie—Belgisch Tijdschrift voor Radiologi*, vol. 96, no. 1, p. 46, 2013.

[11] M. Ramirez and M. G. Patti, "Changes in the diagnosis and treatment of achalasia," *Clinical and Translational Gastroenterology*, vol. 6, no. 5, article e87, 2015.

[12] J. E. Richter, "High-resolution manometry in diagnosis and treatment of achalasia: help or hype," *Current Gastroenterology Reports*, vol. 16, no. 12, article 420, 2014.

[13] M. Müller, "Impact of high-resolution manometry on achalasia diagnosis and treatment," *Annals of Gastroenterology*, vol. 28, no. 1, pp. 3–9, 2015.

[14] J. E. Pandolfino and A. J. Gawron, "Achalasia: a systematic review," *Journal of the American Medical Association*, vol. 313, no. 18, pp. 1841–1852, 2015.

[15] M. F. Vela, "Management strategies for achalasia," *Neurogastroenterology & Motility*, vol. 26, no. 9, pp. 1215–1221, 2014.

[16] Z. H. Wen, E. Gardener, and Y. P. Wang, "Nitrates for achalasia," *Cochrane Database of Systematic Reviews*, no. 4, Article ID CD002299, 2002.

[17] D. A. Katzka and D. O. Castell, "Review article: an analysis of the efficacy, perforation rates and methods used in pneumatic dilation for achalasia," *Alimentary Pharmacology & Therapeutics*, vol. 34, no. 8, pp. 832–839, 2011.

[18] Z. Ramzan and A. B. Nassri, "The role of Botulinum toxin injection in the management of achalasia," *Current Opinion in Gastroenterology*, vol. 29, no. 4, pp. 468–473, 2013.

[19] M. E. Allaix and M. G. Patti, "Endoscopic dilatation, heller myotomy, and peroral endoscopic myotomy: treatment modalities for achalasia," *Surgical Clinics of North America*, vol. 95, no. 3, pp. 567–578, 2015.

[20] G. Torres-Villalobos and L. A. Martin-del-Campo, "Surgical treatment for achalasia of the esophagus: laparoscopic Heller myotomy," *Gastroenterology Research and Practice*, vol. 2013, Article ID 708327, 5 pages, 2013.

[21] A. Kolinioti, B. Kayani, C. Skouras, A. Fovos, O. Aziz, and E. Zacharakis, "Does laparoscopic Heller's myotomy provide superior results compared to endoscopic dilatation for oesophageal achalasia?" *International Journal of Surgery*, vol. 11, no. 3, pp. 238–243, 2013.

Hindawi Publishing Corporation
Gastroenterology Research and Practice
Volume 2016, Article ID 5623718, 10 pages
http://dx.doi.org/10.1155/2016/5623718

Review Article

Intussusception in Adults: The Role of MDCT in the Identification of the Site and Cause of Obstruction

Viola Valentini,[1] Grazia Loretta Buquicchio,[1] Michele Galluzzo,[1] Stefania Ianniello,[1] Graziella Di Grezia,[2] Rosa Ambrosio,[2] Margherita Trinci,[1] and Vittorio Miele[1]

[1]*Department of Emergency Radiology, S. Camillo Hospital, Circonvallazione Gianicolense 87, 00152 Rome, Italy*
[2]*Department of Radiology, Second University of Naples, Piazza Miraglia 2, 80138 Naples, Italy*

Correspondence should be addressed to Vittorio Miele; vmiele@sirm.org

Received 11 June 2015; Accepted 10 August 2015

Academic Editor: Haruhiko Sugimura

Unlike pediatric intussusception, intestinal intussusception is infrequent in adults and it is often secondary to a pathological condition. The growing use of Multi-Detector Computed Tomography (MDCT) in abdominal imaging has increased the number of radiological diagnoses of intussusception, even in transient and nonobstructing cases. MDCT is well suited to delineate the presence of the disease and provides valuable information about several features, such as the site of intussusception, the intestinal segments involved, and the extent of the intussuscepted bowel. Moreover, MDCT can demonstrate the complications of intussusceptions, represented by bowel wall ischemia and perforation, which are mandatory to promptly refer for surgery. However, not all intussusceptions need an operative treatment. In this paper, we review the current role of MDCT in the diagnosis and management of intussusception in adults, focusing on features, as the presence of a leading point, that may guide an accurate selection of patients for surgery.

1. Introduction

Intestinal intussusception in adults is considered uncommon, accounting for an estimated 5% of all intussusceptions and representing only 1% of intestinal obstructions [1, 2]. Unlike pediatric intussusception, which is usually idiopathic, adult intussusception is most often secondary to an identifiable cause [3]. Many pathological conditions [4, 5], such as malignant or benign neoplasms, polyps, Meckel's diverticulum, and postoperative adhesions, may act as leading points by altering bowel peristalsis. Association with malignant tumors is more common in large bowel intussusception (65–70% of cases), while small bowel intussusceptions are secondary to a malignancy in 30–35% of cases only.

Before the widespread use of Multi-Detector Computed Tomography (MDCT), the diagnosis was based on surgical findings in patients with obstructive symptoms [4]. The significant advancements in CT technology, along with the progressive use of MDCT in the diagnosis of abdominal emergencies, have determined an increment in the detection of intestinal intussusceptions [6, 7]. The typical bowel-within-bowel appearance [1, 8–10] is often found in asymptomatic patients, with transient intussusception and no underlying disease [11–13]. Although surgical intervention is considered necessary in symptomatic patients with leading point intussusception [14], not every patient with CT evidence of intestinal intussusception may require surgery [15, 16]. The distinction between lead point and non–lead point intussusception, as well as the detection of obstructive complications on MDCT, is important in determining the appropriate treatment, avoiding unnecessary surgery. In this paper, we review the current role of MDCT in the diagnosis and management of intussusception, focusing on features that may guide an accurate selection of adult patients for surgery, both in small bowel and large bowel intussusceptions.

2. Anatomy, Pathophysiology, and Classification

Intussusception results from altered intestinal motility, determining the telescoping of one bowel segment (*intussusceptum*) into the lumen of the contiguous intestinal tract (*intussuscipiens*) [1, 8]. Although this invagination can occur

anywhere along the gastrointestinal tract, most intussusceptions occur in the junctions between mobile and retroperitoneal fixed intestinal segments.

Intussusceptions can be classified into three types based on the location:

(i) Enteroenteric, when confined to the small bowel.

(ii) Colocolonic, when involving the large bowel.

(iii) Enterocolonic, which can be ileocaecal or ileocaecocolonic.

According to the literature, ileocaecal intussusceptions are the most common of all the gastrointestinal intussusceptions, followed by enteroenteric intussusceptions, which can account for up to 40% of cases. Colocolonic intussusceptions are the less common type of intussusceptions [11].

Intussusception in an adult can be further classified on the basis of whether a lead point is present. Intussusceptions without a lead point tend to be transient, self-limiting, and nonobstructing. Patients present with nonspecific symptoms if any, like vague abdominal pain. In asymptomatic patients, the diagnosis of intussusception is often an incidental finding on MDCT performed for other reasons [17]. In these cases, most of the time, the small bowel intussusception is self-limited; the length of intussusception is the most reliable predictive indicator of the outcome. Intussusception shorter than 3.5 cm rarely requires surgery [16].

Clinical diagnosis can be difficult even in symptomatic patients with a leading point intussusception, because of the variety of clinical findings at presentation (crampy abdominal pain, nausea, vomiting, and bloody mucoid stools), depending on the underlying cause. Complicated intussusceptions, with bowel wall engorgement due to impaired mesenteric circulation and signs of parietal ischaemia, are associated with a higher risk of perforation and peritonitis [3, 5].

3. Role of Imaging

Abdominal MDCT has been shown to be the imaging modality of choice for the detection and assessment of adult bowel intussusception, with a reported accuracy of 58–100% [1, 18]. MDCT is well suited to delineate the presence of the disease and provides valuable information about several features, such as the site of intussusception, the intestinal segments involved, and the extent of the intussuscepted bowel [19]. MDCT has the ability to differentiate between presence and lack of a leading point.

Moreover, MDCT can demonstrate the complications of intussusceptions, represented by bowel wall ischemia and perforation, which are mandatory to promptly refer for surgery.

Merine et al. [15] in 1987 described three CT patterns of intussusception as corresponding to different stages of the disease: the target-like pattern, the reniform pattern, and the sausage-shaped pattern. The first appearance, the target-like pattern, described as a round mass with intraluminal soft-tissue and eccentric fat density, was thought to correspond to an early intussusception with no or minimal obstruction and without signs of ischemia [9]. The second appearance, the reniform pattern, appearing as a bilobed mass with central low attenuation and peripheral higher density, was thought to result from ischemic thickening of the intussusceptum's bowel wall. The latter appearance, the sausage-shaped pattern, was thought to result from alternating areas of low and high attenuation related to the bowel wall, mesenteric fat and fluid, intraluminal fluid, contrast material, or air.

Actually, intussusception often appears as a complex soft-tissue mass on MDCT images. It is composed of a central intussusceptum and outer intussuscipiens, separated by mesenteric fat, which appears as a low-attenuation layer. Enhanced vessels are often seen within the mesenteric fat (Figure 1). The image pattern varies according to location, axis of section, bowel wall thickness, and lumen patency. The appearance of an intussusception on CT images is similar to that of a "target" mass when the CT beam is perpendicular to the longitudinal axis of the intussusception and to that of a "sausage" mass when the CT beam is parallel or oblique to the longitudinal axis [10] (Figure 2). The presence of a lead point, the configuration of the lead mass, the degree of bowel wall edema, and the amount of invaginated mesenteric fat all affect the radiological aspect of an intussusception. Intussusception with a lead point usually appears as an abnormal target-like mass with a cross-sectional diameter greater than that of the normal bowel and may be associated with proximal bowel obstruction (Figure 3). It is often not easy to distinguish the distinct anatomic features of the lead mass, because of poor recognisability of the edematous intestinal wall and the lead mass. If there is bowel wall edema due to impaired circulation of the mesenteric vessels, it is difficult to differentiate a lead mass from inflammation because the former may appear amorphous (Figure 4). Even when a leading mass is seen, it is not always possible to reliably distinguish a malignant from benign neoplasm.

4. Imaging Features: Enteroenteric Intussusception

Adult enteroenteric intussusceptions are thought to be relatively rare. They can be classified as duodenojejunal, jejunojejunal, or jejunoileal. Duodenojejunal intussusception is rare, because of anatomic fixation of a large portion of the duodenum. Retrograde jejunal intussusceptions, in which retrograde peristalsis determines the telescoping of a distal bowel segment into the adjacent proximal segment, are reported as postoperative complications of Roux-en-Y anastomoses [20].

Most cases of small bowel intussusceptions are secondary to benign intra- or extraluminal lesions, such as inflammatory lesions, Meckel's diverticulum [21], postoperative adhesions, lipoma (Figure 5), and adenomatous polyps [3], but they can also be iatrogenic (placement of intestinal tube, gastrojejunostomy) or caused by abdominal trauma [22] (Figure 6). Malignant pathologies, accounting for 15% of cases, include adenocarcinoma, malignant GIST, metastasis from various primary sites (lung or breast, malignant melanoma, osteosarcoma, and lymphoma), and primary lymphoma [3] (Figure 7).

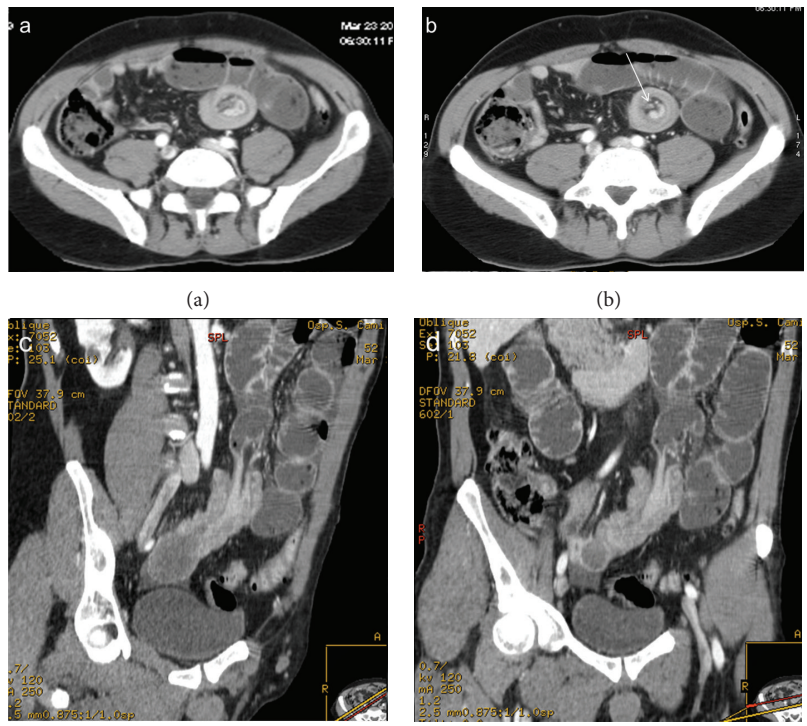

(a) (b)

(c) (d)

Figure 1: Enteroenteric intussusception. Axial CT images (a, b) demonstrate a round mass with "target" pattern and central hypodense area of mesenteric fat in which vessels are seen as linear enhanced structures (arrow). Oblique CT reformatted images (c, d) oriented parallel to the longitudinal axis of the intussusception depict intussusception as a large "sausage-shaped" mass, showing length of involvement. Gas-fluid levels in the dilated proximal loops are signs of small bowel obstruction.

Enteroenteric intussusceptions without a lead point tend to be nonobstructing and are usually smaller in transverse diameter and shorter in length than intussusception with a lead point (Figure 8). In some cases, the enteroenteric intussusception is due to increased peristalsis of the intestinal loops caused by distal obstruction, such as a stenosis caused by a neoplasm of the colon (Figure 9). Obstructing enteroenteric intussusceptions, often caused by a lead point, may present at CT with thickening and alterated enhancement of the bowel wall and engorgement of mesenteric vessels (Figure 10).

5. Imaging Features: Colocolonic Intussusception

Unlike small-bowel intussusception, more than half of large bowel intussusceptions are associated with malignant lesions. Adenocarcinoma is the most common malignant neoplasm associated with colocolonic intussusception, followed by lymphoma and metastatic disease [1]. Among about 30% of large bowel intussusceptions caused by benign lesions, lipomas are the most common cause, followed by GISTs, adenomatous polyps (Figure 11), and other benign conditions like endometriosis and a previous anastomosis [8]. Idiopathic intussusception occurs less often than those of the small bowel, accounting for approximately 10% of intussusceptions [5].

Sigmoid-rectal intussusception (Figure 12) is a very rare condition in which concentric invagination of distal sigma progresses towards rectal ampulla but does not protrude through the anus [23].

6. Imaging Features: Enterocolonic Intussusception

In enterocolonic intussusception, the lead point can be located in the small bowel, in the large bowel, often in the caecum (Figure 13), or in the appendix. Enterocolonic intussusception can be further classified as ileocaecal, in which the ileocaecal valve is in site, or ileocaecocolonic (Figure 14), in which the ileocaecal valve is displaced. Appendiceal intussusception is rare and difficult to diagnose radiologically [24].

7. Conclusions

Because of significant advancements in MDCT scanners along with increasing use of MDCT in abdominal emergency imaging, the detection of enteroenteric intussusceptions by CT has increased. Intussusceptions are now being detected incidentally on MDCT in patients being scanned for unrelated reasons [8] or in asymptomatic patients, often with transient intussusceptions and without an identifiable lead point. The radiologist can readily make a correct diagnosis,

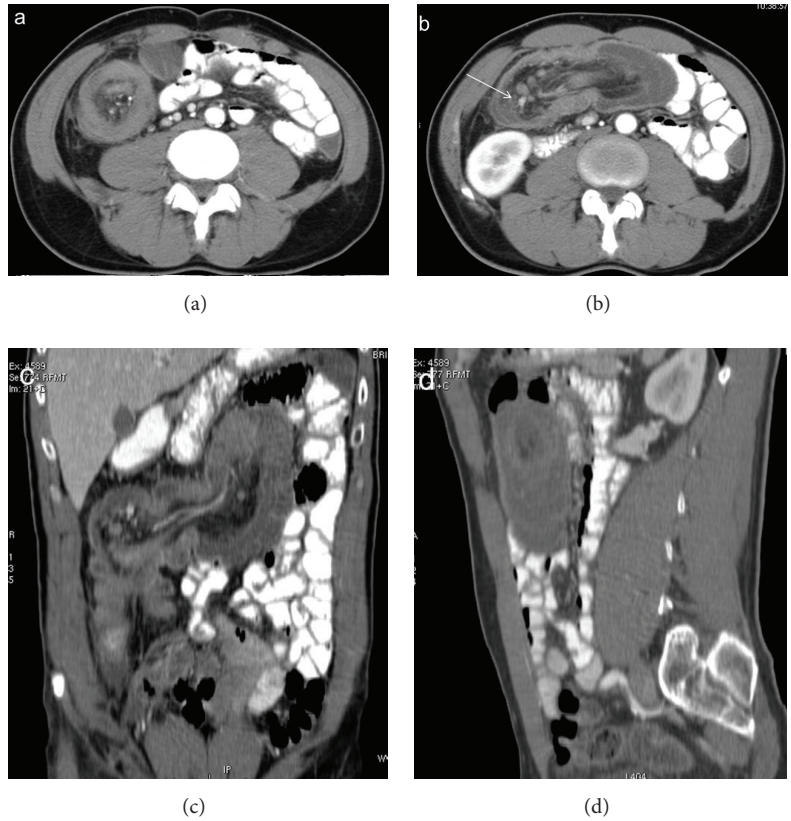

Figure 2: Enterocolonic (ileocaecocolonic) intussusception. Intussusception may present as a target (a), reniform bilobed (b, c), and a sausage-shaped (d) mass depending on the different axial CT scans or reformatted planes. Mesenteric vessels appear as enhanced linear structures between hypodense mesenteric fats (arrow). Dilated proximal bowel loops are opacified with oral contrast.

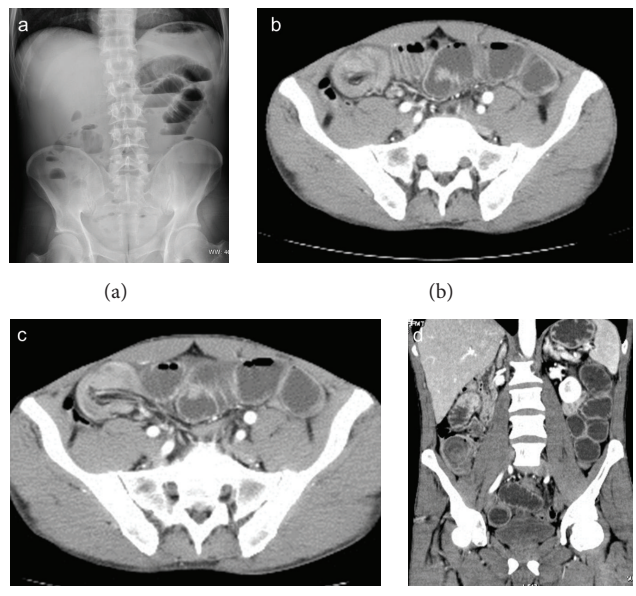

Figure 3: Enterocolonic (ileocaecocolonic) intussusception caused by intestinal lymphoma, with proximal bowel obstruction. Plain abdominal radiography (a) shows gas-fluid levels within distended small bowel loops. Intussusception is well depicted on axial CT scans (b, c) and coronal reformatting (d).

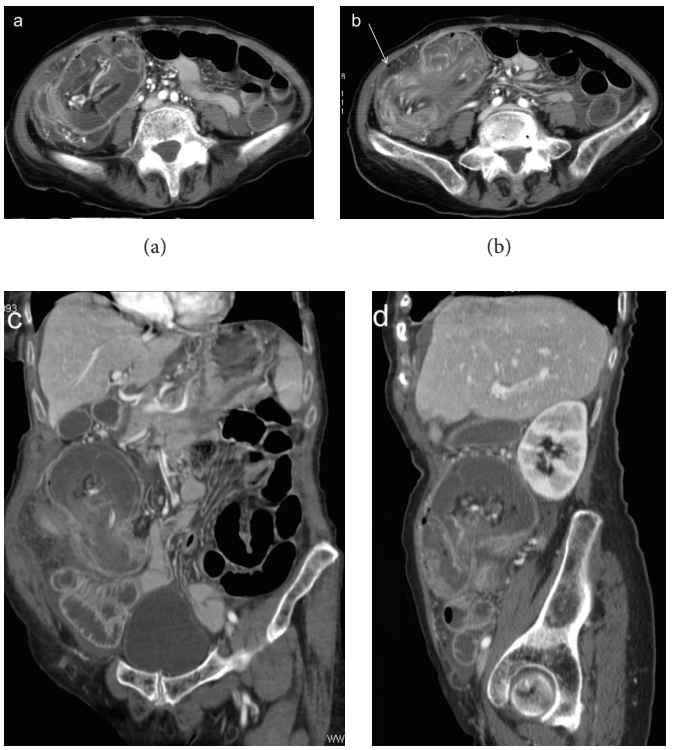

(a) (b)

(c) (d)

Figure 4: Enterocolic (ileocaecocolonic) intussusception due to a caecal carcinoma. CT images on axial scans (a, b) and oblique reformatting (c, d) show lymph nodes and vascular engorgement in the intussuscepted mesentery and fluid distention of the intussuscipiens. Extraparietal air indicates local perforation (arrow).

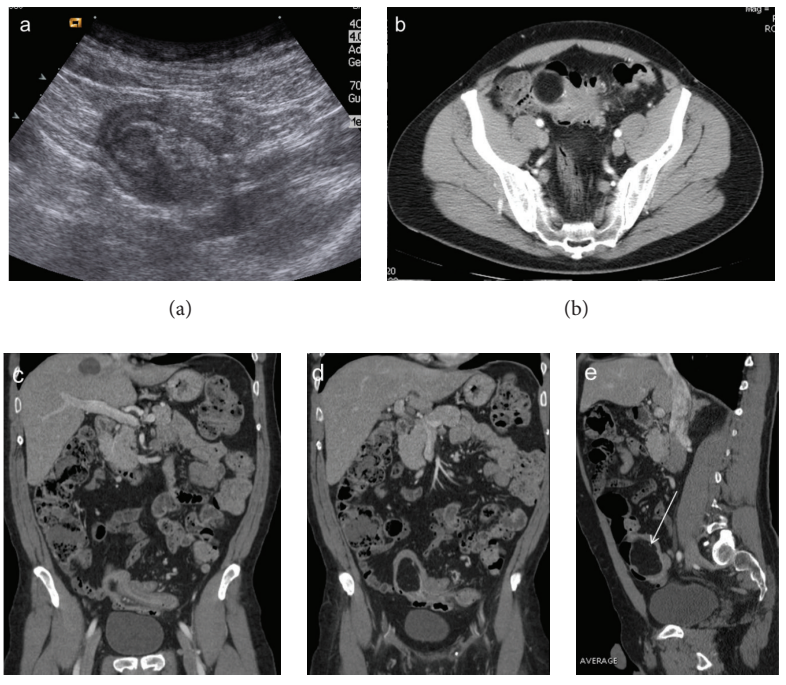

(a) (b)

(c) (d) (e)

Figure 5: Colocolonic (sigmoid) intussusception caused by a lipoma. Ultrasound scan (a) shows a pelvic layered ovoid mass. CT images on axial (b) and oblique reformatting (c, d) demonstrate an intraluminal lesion with fat attenuation (arrow) that serves as the intussusception lead point.

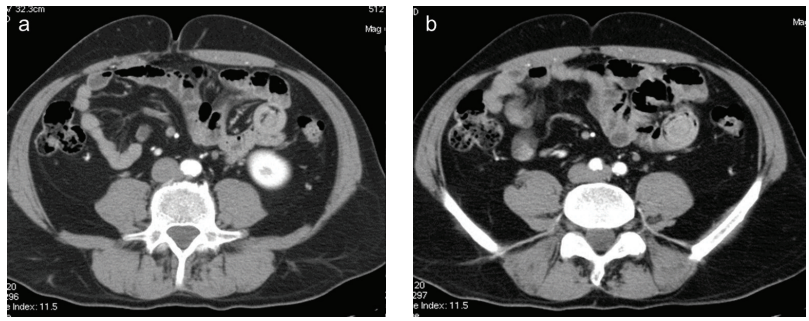

(a) (b)

Figure 6: Enteroenteric (ileoileal) transient intussusception in a traumatized patient. Axial CT images oriented perpendicular to the longitudinal plane of the intussusception demonstrate the typical multilayered appearance of small bowel intussusception. Heterogeneous "target" mass with the intussuscipiens, intussusceptum, and vessels within the invaginated mesenteric fat. No signs of significative obstruction, only mild stasis in the small bowel.

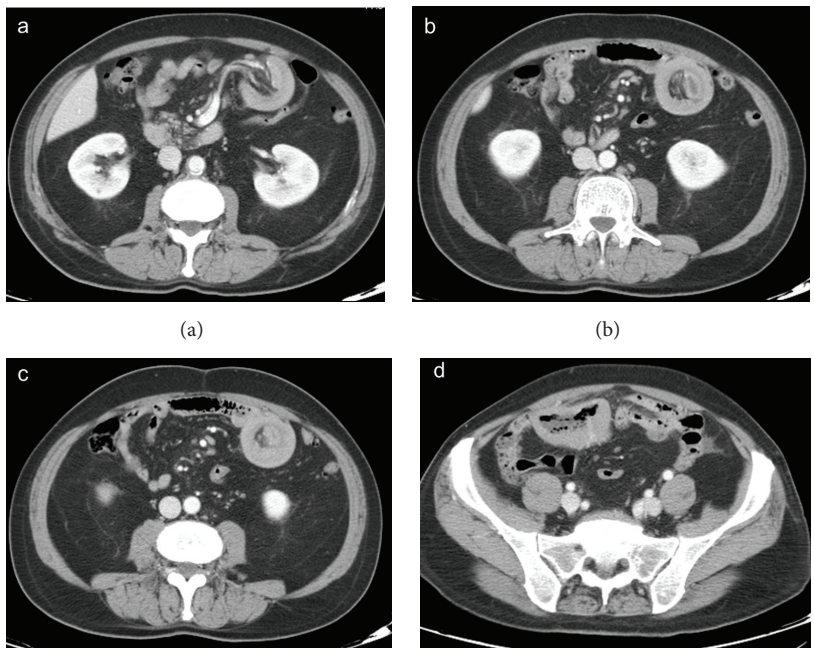

(a) (b)

(c) (d)

Figure 7: Enteroenteric (ileoileal) intussusception caused by lymphoma. Axial CT images show the typical appearance of small bowel intussusception (a, b, and c). Marked circumferential thickening of the wall of a distal ileum loop (d) is due to lymphoma, which is responsible for intussusception.

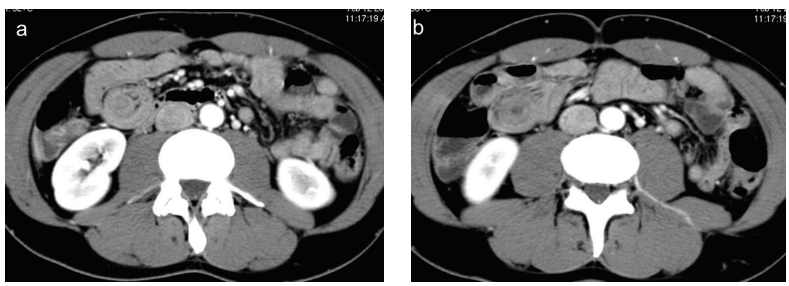

(a) (b)

Figure 8: Enteroenteric (ileoileal) intussusception. Target-like mass on axial CT images. Transient intussusception with no signs of intestinal obstruction or intestinal ischemia.

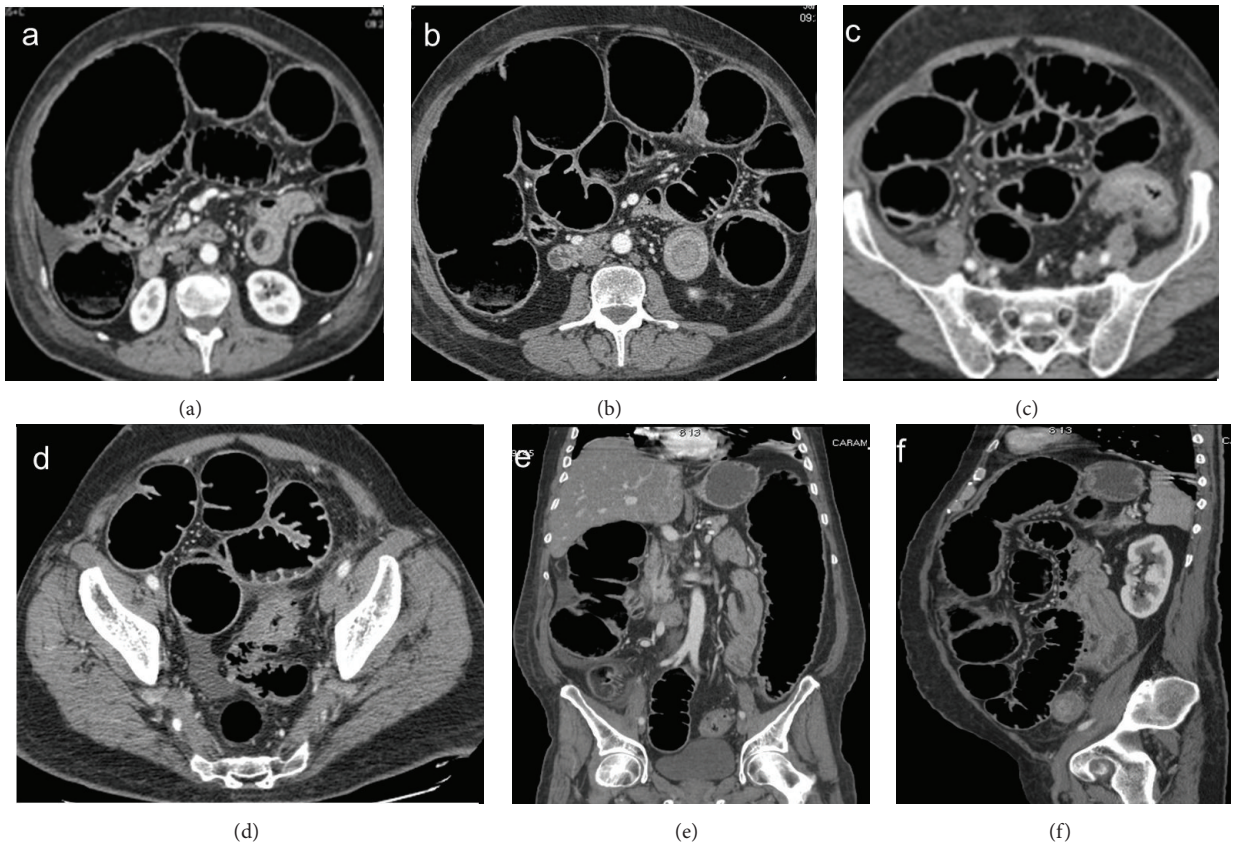

Figure 9: Enteroenteric (ileoileal) intussusception secondary to colic obstruction caused by a sigmoid cancer. Intussusception appears as a small target mass (a, b) in a condition of intestinal obstruction with massive small and large bowel dilatation, due to stenosing sigmoid cancer (d). Coronal (e) and sagittal (f) reformatting better depict the site and the extent of intussusception.

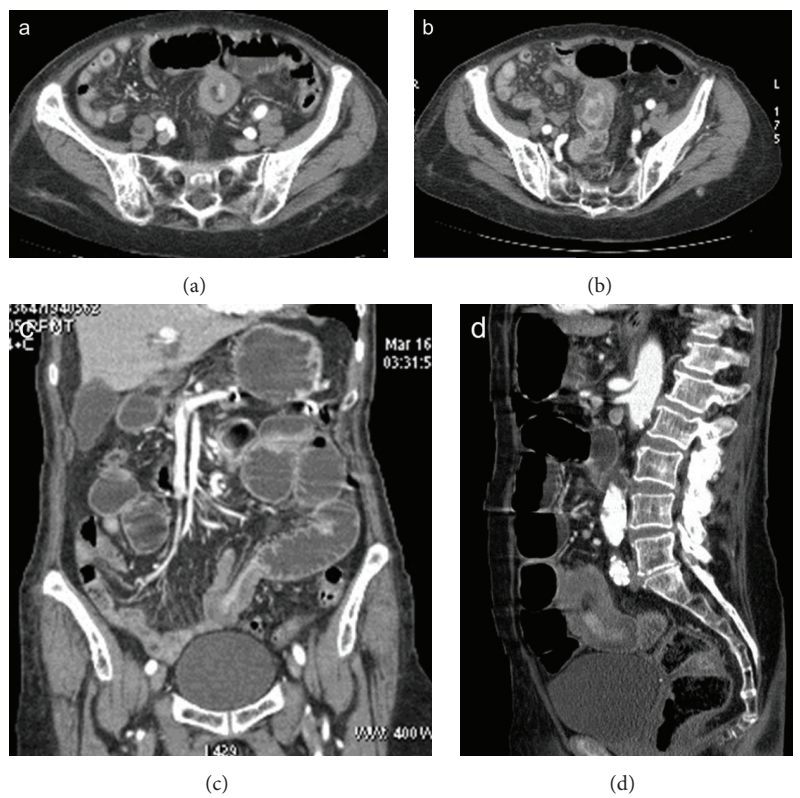

Figure 10: Enteroenteric (ileoileal) intussusception. Bowel wall of intussusception is thickened and enhanced. Signs of small bowel obstruction are seen on axial scans (a, b) and coronal (c) and sagittal (d) reformatting.

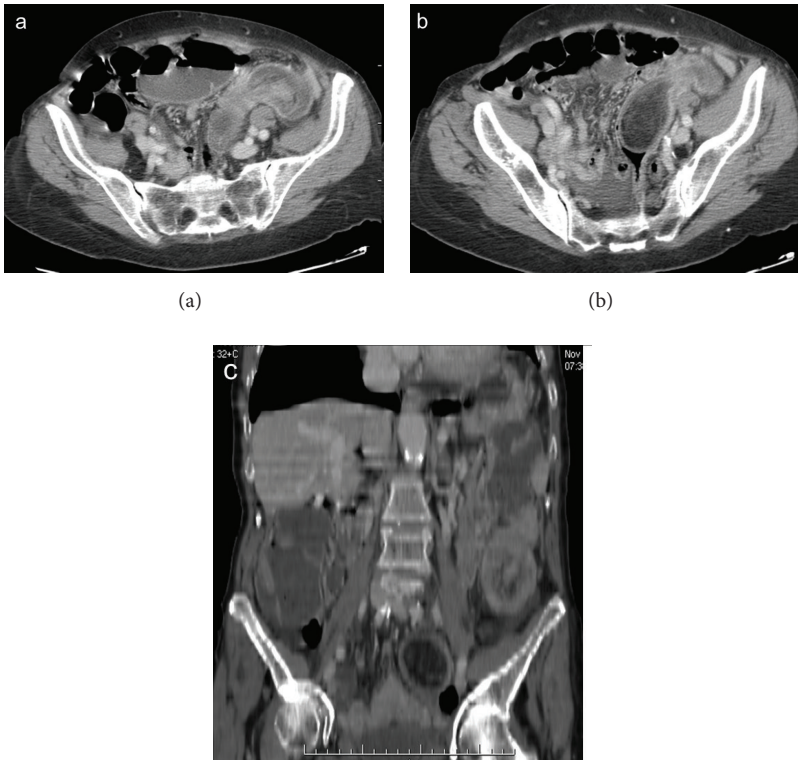

Figure 11: Colocolonic intussusception caused by a sigmoid lipoma. The intussusception is well depicted on axial CT scan (a). Both axial scan (b) and coronal reformatting (c) show the hypodense polypoid mass that acts as the lead point.

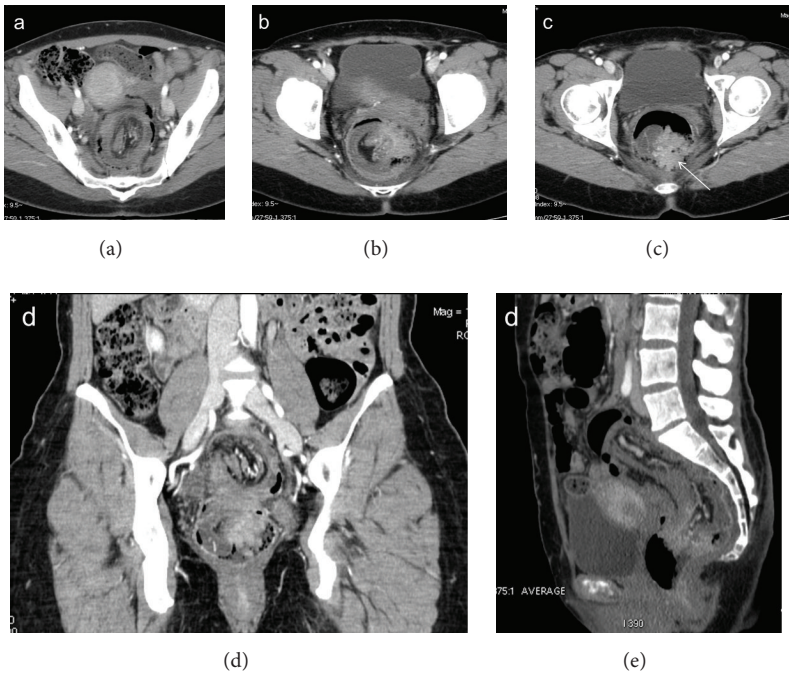

Figure 12: Colocolonic (sigmoid-rectal) intussusception (a) caused by sigmoid adenocarcinoma. The enhanced neoplastic mass, which acts as the lead point, is located in the rectum (arrow), at the tip of intussusceptum (b, c, d, and e).

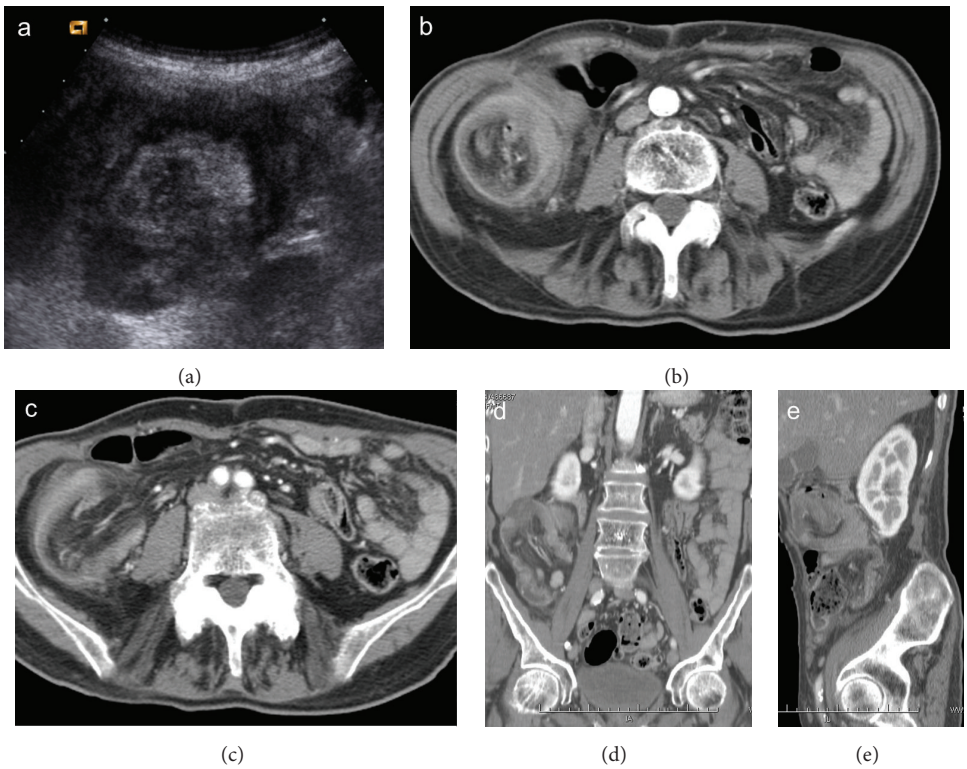

(a) (b) (c) (d) (e)

Figure 13: Enterocolic (ileocaecocolonic) intussusception caused by a caecal carcinoma. Ultrasound scan (a) shows a heterogeneous target-like mass located in right flank. CT images on axial scans (b, c) and coronal and oblique reformatting (d, e) demonstrate lead point intussusception with invaginated mesenteric fat, vessels, and lymph nodes.

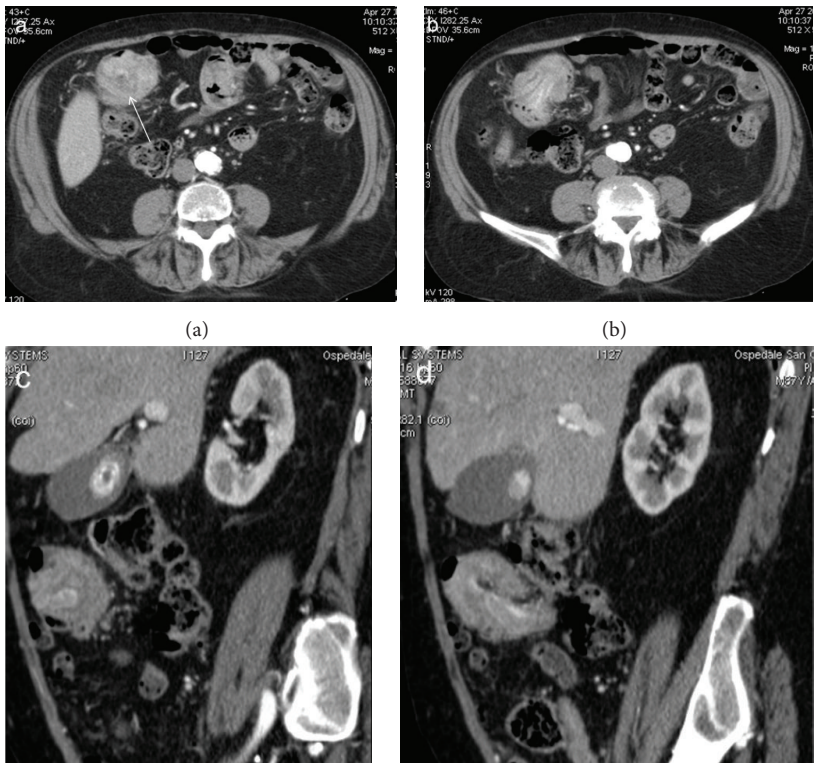

(a) (b) (c) (d)

Figure 14: Enterocolonic (ileocaecocolonic) intussusception caused by a polyp. Axial CT images (a, b) demonstrate a soft-tissue density round mass with thin eccentric hypodensity (arrow). Oblique CT reformatting (c, d) clearly shows the enhancement of the lead mass, which facilitates its identification.

detecting specific MDCT findings such as the bowel-within-bowel appearance. Some findings on CT may be helpful in guiding management and reducing the prevalence of unnecessary surgery. The radiologist's aim is not only to recognize intussusception, but also to define its location, enteroenteric, colocolonic, or enterocolonic, to evaluate underlying pathology, and to identify complicated intussusceptions, associated with obstruction or ischemia, which represent indications for surgical exploration.

Conflict of Interests

The authors declare that there is no conflict of interests regarding the publication of this paper.

References

[1] T. Azar and D. L. Berger, "Adult intussusception," *Annals of Surgery*, vol. 226, no. 2, pp. 134–138, 1997.

[2] A. Zubaidi, F. Al-Saif, and R. Silverman, "Adult intussusception: a retrospective review," *Diseases of the Colon and Rectum*, vol. 49, no. 10, pp. 1546–1551, 2006.

[3] F. Somma, A. Faggian, N. Serra et al., "Bowel intussusceptions in adults: the role of imaging," *Radiologia Medica*, vol. 120, no. 1, pp. 105–117, 2014.

[4] E. M. Haas, E. L. Etter, S. Ellis, and T. V. Taylor, "Adult intussusception," *American Journal of Surgery*, vol. 186, no. 1, pp. 75–76, 2003.

[5] D. G. Begos, A. Sandor, and I. M. Modlin, "The diagnosis and management of adult intussusception," *The American Journal of Surgery*, vol. 173, no. 2, pp. 88–94, 1997.

[6] S. Baleato-González, J. C. Vilanova, R. García-Figueiras, I. B. Juez, and A. M. de Alegría, "Intussusception in adults: what radiologists should know," *Emergency Radiology*, vol. 19, no. 2, pp. 89–101, 2012.

[7] J. D. Rea, M. E. Lockhart, D. E. Yarbrough, R. R. Leeth, S. E. Bledsoe, and R. H. Clements, "Approach to management of intussusception in adults: a new paradigm in the computed tomography era," *The American Surgeon*, vol. 73, no. 11, pp. 1098–1105, 2007.

[8] D. M. Warshauer and J. K. T. Lee, "Adult intussusception detected at CT or MR imaging: clinical–imaging correlation," *Radiology*, vol. 212, no. 3, pp. 853–860, 1999.

[9] Y. H. Kim, M. A. Blake, M. G. Harisinghani et al., "Adult intestinal intussusception: CT appearances and identification of a causative lead point," *Radiographics*, vol. 26, no. 3, pp. 733–744, 2006.

[10] G. Gayer, R. Zissin, S. Apter, M. Papa, and M. Hertz, "Pictorial review: adult intussusception—a CT diagnosis," *The British Journal of Radiology*, vol. 75, no. 890, pp. 185–190, 2002.

[11] O. Catalano, "Transient small bowel intussusception: CT findings in adults," *British Journal of Radiology*, vol. 70, pp. 805–808, 1997.

[12] R. Zissin, G. Gayer, O. Konen, and M. Shapiro-Feinberg, "Transient colocolic intussusception," *Clinical Imaging*, vol. 24, no. 1, pp. 8–9, 2000.

[13] K. M. Horton and E. K. Fishman, "MDCT and 3D imaging in transient enteroenteric intussusception: clinical observations and review of the literature," *American Journal of Roentgenology*, vol. 191, no. 3, pp. 736–742, 2008.

[14] N. Erkan, M. Haciyanli, M. Yildirim, H. Sayhan, E. Vardar, and A. F. Polat, "Intussusception in adults: an unusual and challenging condition for surgeons," *International Journal of Colorectal Disease*, vol. 20, no. 5, pp. 452–456, 2005.

[15] D. Merine, E. K. Fishman, B. Jones, and S. S. Siegelman, "Enteroenteric intussusception: CT findings in nine patients," *American Journal of Roentgenology*, vol. 148, no. 6, pp. 1129–1132, 1987.

[16] N. Lvoff, R. S. Breiman, F. V. Coakley, Y. Lu, and R. S. Warren, "Distinguishing features of self-limiting adult small-bowel intussusception identified at CT," *Radiology*, vol. 227, no. 1, pp. 68–72, 2003.

[17] P. Jain and S. W. Heap, "Intussusception of the small bowel discovered incidentally by computed tomography," *Australasian Radiology*, vol. 50, no. 2, pp. 171–174, 2006.

[18] G. Gayer, S. Apter, C. Hofmann et al., "Intussusception in adults: CT diagnosis," *Clinical Radiology*, vol. 53, no. 1, pp. 53–57, 1998.

[19] L. C. Dawes, R. Hunt, J. K. Wong, and S. Begg, "Multiplanar reconstruction in adult intussusception: case report and literature review," *Australasian Radiology*, vol. 48, no. 1, pp. 74–76, 2004.

[20] J. O. Waits, R. W. Beart Jr., and J. W. Charboneau, "Jejunogastric intussusception," *Archives of Surgery*, vol. 115, no. 12, pp. 1449–1452, 1980.

[21] K. M. Elsayes, C. O. Menias, H. J. Harvin, and I. R. Francis, "Imaging manifestations of Meckel's diverticulum," *American Journal of Roentgenology*, vol. 189, no. 1, pp. 81–88, 2007.

[22] Z. T. Stockinger and N. McSwain Jr., "Intussusception caused by abdominal trauma: case report and review of 91 cases reported in the literature," *Journal of Trauma*, vol. 58, no. 1, pp. 187–188, 2005.

[23] M. Assenza, G. Ricci, A. Antoniozzi et al., "Sigmoidorectal intussusception in adults: a case report," *Clinica Terapeutica*, vol. 161, no. 1, pp. 65–67, 2010.

[24] A. J. Siddiqi, O. Arafat, P. Nikolaidis, and V. Yaghmai, "MDCT diagnosis of ileocolic intussusception secondary to an appendiceal mucocele: value of multiplanar reformation," *Emergency Radiology*, vol. 13, no. 5, pp. 273–275, 2007.

Hindawi Publishing Corporation
Gastroenterology Research and Practice
Volume 2016, Article ID 9686815, 6 pages
http://dx.doi.org/10.1155/2016/9686815

Research Article

Small-Bowel Neoplasms: Role of MRI Enteroclysis

Angela Faggian,[1] Maria Rosaria Fracella,[2] Grazia D'Alesio,[2] Maria Eleonora Alabiso,[3] Daniela Berritto,[1] Beatrice Feragalli,[4] Vittorio Miele,[5] Francesca Iasiello,[3] and Roberto Grassi[1]

[1]*Institute of Radiology, Second University of Naples, Piazza Miraglia 2, 80138 Naples, Italy*
[2]*Department of Radiology, San Paolo Hospital, Contrada Caposcardicchio, 70123 Bari, Italy*
[3]*Department of Radiology, IGEA Sant'Antimo, Italy*
[4]*Department of Oral Science, Nano and Biotechnology, University G. d'Annunzio of Chieti-Pescara, Italy*
[5]*Department of Emergency Radiology, S. Camillo Hospital, Circonvallazione Gianicolense 87, 00152 Rome, Italy*

Correspondence should be addressed to Angela Faggian; angela.faggian@libero.it

Received 18 June 2015; Accepted 3 September 2015

Academic Editor: Rami Eliakim

Small-bowel neoplasms are the 3%–6% of all gastrointestinal tract neoplasms. Due to the rarity of these lesions, the low index of clinical suspicion, and the inadequate radiologic examinations or incorrect interpretation of radiologic findings, a delay in diagnosis of 6–8 months from the first symptoms often occurs. Even if conventional enteroclysis and capsule endoscopy are the most common procedures used to accurately depict the bowel lumen and mucosal surface, their use in evaluating the mural and extramural extents of small-bowel tumors is limited. Instead multidetector computed tomographic enteroclysis and magnetic resonance enteroclysis have the potential to simultaneously depict intraluminal, mural, and extraintestinal abnormalities. In particular MR enteroclysis has an excellent soft tissue contrast resolution and multiplanar imaging capability. It can provide anatomic, functional, and real time information without the need of ionizing radiation. MR findings, appearances of the lesions, combined with the contrast-enhancement behavior and characteristic of the stenosis are important to differentiate small-bowel neoplasm from other nonneoplastic diseases.

1. Introduction

Small-bowel neoplasms are the 3%–6% of all gastrointestinal tract neoplasms, although the small-bowel represents 75% of the length and 90% of the mucosal surface of the gastrointestinal tract. They can develop from all the various tissue components of the wall: mucosa, submucosa, and muscle layers [1]. Patients may present obscure GI bleeding and nonspecific symptoms such as abdominal pain, nausea and vomiting, weight loss, diarrhea, anaemia, and intestinal obstruction. However, many patients may remain asymptomatic until the late stages of disease [2].

Due to the rarity of these lesions, the low index of clinical suspicion, and inadequate radiologic examinations or incorrect interpretation of radiologic findings, a delay in diagnosis of 6–8 months from the first symptoms often occurs, conditioning surgical therapy and survival of patients [3].

Conventional enteroclysis and capsule endoscopy are the most common procedures used to accurately depict the bowel lumen and mucosal surface, but their use in evaluating the mural and extramural extents of small-bowel tumors is limited. Multidetector computed tomographic (CT) enteroclysis and magnetic resonance (MR) enteroclysis have the potential to simultaneously depict intraluminal, mural, and extraintestinal abnormalities.

Multidetector CT enteroclysis involves the use of ionizing radiation, limiting repeated imaging, which is important in determining whether an area of intestinal narrowing is due to a contraction in the intestinal or to fixed strictures [2, 4–6]. MR enteroclysis has an excellent soft tissue contrast resolution, multiplanar imaging capability, and a lack of ionizing

radiation. The possibility to repeat data acquisition over time and the ability to perform real time functional imaging permit functional evaluation of small-bowel mobility [7, 8]. The purposes of our study were to retrospectively evaluate the accuracy of MR enteroclysis, using histological findings as the reference standards, and to assess the interobserver variability for detection of small-bowel neoplasms.

2. Materials and Methods

2.1. Study Design and Population. Between March 2009 and December 2014 a retrospective study was performed evaluating exams of 67 patients (male/female ratio 3 : 1; mean age: about 57 years) with a clinical suspicion of intestinal neoplasia. Patients had already performed a gastroscopy and/or colonoscopy. Clinical suspicion was represented by intermittent bouts of intestinal obstruction and abdominal pain (N_9), obscure GI bleeding or chronic anemia (N_35), protein-losing enteropathy (N_7), and asthenia (N_16). All patients underwent MR enteroclysis. Diagnostic confirmation was obtained by histological examination of the surgical specimen or biopsy specimen or by follow-up with colonoscopy, videocapsule endoscopy, enteroclysis, or conventional enteroclysis RM after 6 months.

2.2. MR Enteroclysis. Three days before the exam each patient reduces or totally eliminates fiber, from the afternoon of the day before the exam, an isosmolar laxative (SELG ESSE 1000) diluted in 4 liters of water was prescribed, and only fluid diet was allowed.

MR imaging studies were performed with phased-array coil on a 1.5-T closed magnet (Magnetom Symphony, Siemens, Germany). In accordance with our institute guidelines, every patient received and signed written consent forms. After fluoroscopically guided nasojejunal intubation, while the patient lay prone inside the magnet, the small bowel is distended with 1,500–2,000 mL of polyethylene glycol- (PEG-) water solution using an electric infusion pump with a speed of injection of 120–150 mL/min. The MR protocol consists of MR fluoroscopy using RARE (T2-weighted half-Fourier rapid acquisition with relaxation enhancement) single-shot sequences in real time, starting at the beginning of the infusion and repeated every 8 seconds during normal breathing until the PEG-water solution reached the ascending colon and the entire small bowel was adequately distended. Then 20 mg of hyoscine butylbromide (Buscopan; Boehringer-Ingelheim, Ingelheim, Germany) was administered intravenously to reduce small_bowel peristalsis and prolong small-bowel distention and the MR examination was completed with cross-sectional imaging. Axial, sagittal, and coronal single-shot HASTE, TrueFISP with and without fat suppression (repetition time msec/echo time msec 3.6–3.8/1.5–1.7; matrix 192 × 340; section thickness/gap mm 5/0) were performed for morphological study of small bowel. Then VIBE T1 Flash 3D FAT-SAT sequences (repetition time msec/echo time msec, 3.24/1.24; field of view, 400 mm, even if it depends on the size of the patient; matrix, 288 × 512; flip angle, 10°; one signal is acquired; section thickness, 2.50 mm) in multiple breath-hold series repeated at least seven times in a row in expiratory apnea were obtained at 0°, 30′, 60′, 90′, and 120′ after contrast injection (0.1 mmol/kg gadolinium at 2 mL/sec). Diffusion-weighted MR imaging (DW-MRI) was also performed in the true axial plane using a single-shot spin-echo echo-planar imaging (SE-EPI) sequence with b values of 50, 400, and 800 s/mm^2 (repetition time msec/echo time msec, 5600/80; field of view, 500 mm, even if it depends on the size of the patient; matrix, 288 × 512; section thickness, 6 mm) in multiple breath-hold series repeated at least seven times in a row. Apparent diffusion coefficient (ADC) measurement by DW-MRI was done.

Images were analyzed by two experienced observer board-certified abdominal radiologists (Maria Rosaria Fracella and Roberto Grassi) with 25- and 30-year experience. Both reviewers were blinded to clinical details, results of previous investigations.

2.3. Statistical Analysis. For each reader, sensitivity, specificity, positive predictive value (PPV), negative predictive value (NPV), and the diagnostic accuracy have been calculated. Furthermore interobserver agreement was assessed (con il test κ di cohen) with κ statistics. A κ value greater than or equal to 0.75 was considered to represent excellent agreement.

3. Results

MR enteroclysis was successfully performed in all patients. For one reader MR enteroclysis revealed 24 lesions (35.8%) and 23 for the second one (34.3%). Diagnosis was confirmed in 23 patients. Malignant neoplasms were diagnosed in 17 cases: 3 adenocarcinomas, 6 lymphomas, 3 small-bowel metastases, 1 neuroendocrine tumor, and 4 GIST. Benign neoplasms were diagnosed in 6 cases: 2 leiomyomas, 1 adenoma, and 3 hamartomatous polyps.

False positives were due to two adhesions and a substenosis with wall thickening. False negatives were cases of hamartomatous polyps and jejunal metastases.

Sensitivity of MR enteroclysis in the diagnosis of small-bowel neoplasms in our sample data was 87.5% and 91.6%, while specificity was 93 and 97.6%, respectively, for readers 1 and 2 (Table 1).

There was excellent agreement between the readers, with a κ value > 0.9 for MR enteroclysis diagnosis of small-bowel neoplasm.

4. Discussion

The lack of ionizing radiation, the possibility of combining the morphologic information of cross-sectional imaging with functional information, the excellent soft-tissue contrast, and a relatively safe intravenous contrast agent profile make MR imaging the method of choice for the study of the small intestine. Moreover the opportunity of visualizing the entire thickness of the bowel wall and studying the surrounding structures makes MR imaging an excellent method not only for diagnosis but also for staging and prognosis [9–11]. Our results confirm that MR enteroclysis is an accurate modality with which to diagnose or exclude small-bowel

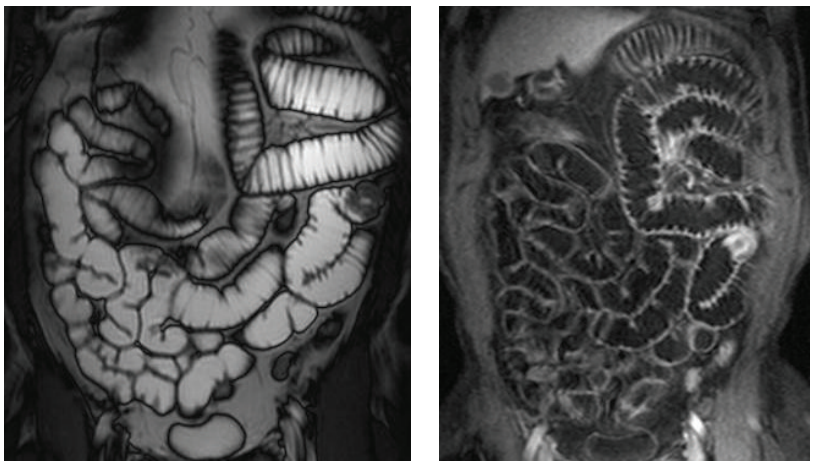

(a) (b)

Figure 1: MRI, TrueFISP coronal sequence (a): a circumferential thickening protruding in the intestinal lumen with tendency to invagination is detected, in absence of local infiltration. In the VIBE sequences after the i.v. contrast medium administration (b), there is an inhomogeneous contrast enhancement. Definitive histology: adenocarcinoma.

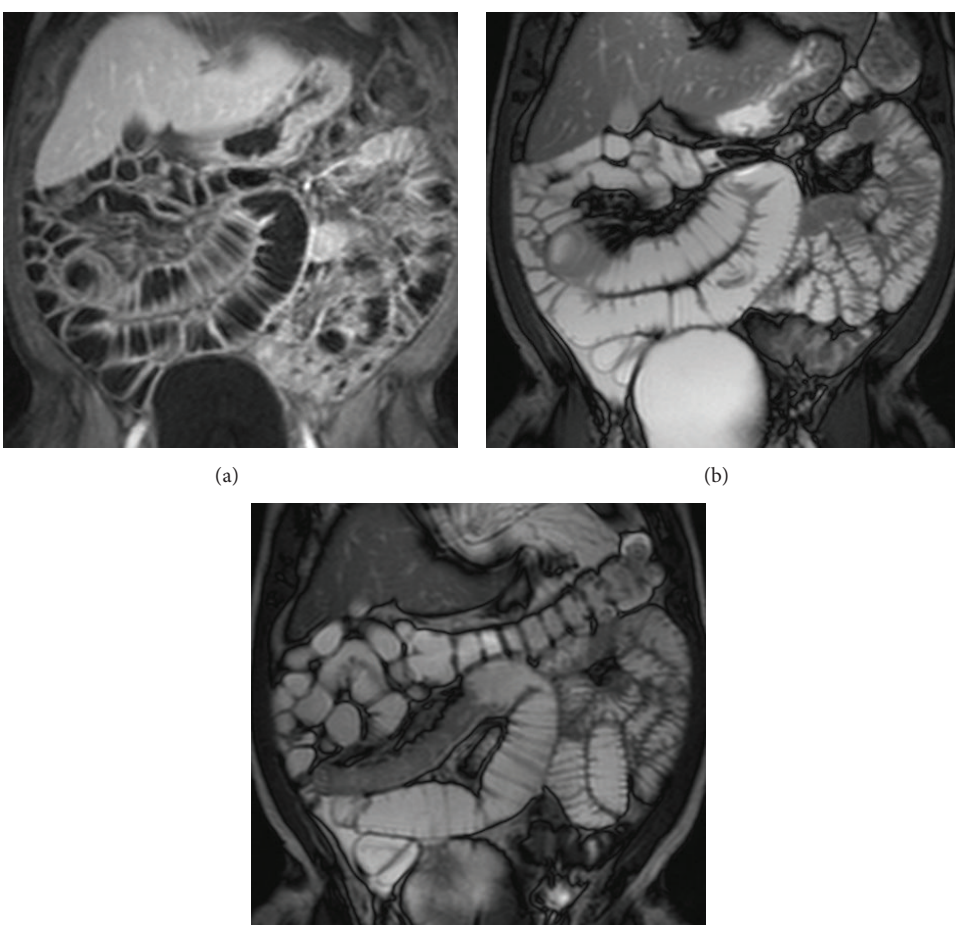

(a) (b)

(c)

Figure 2: Lesion with nodular aspect protruding into the intestinal lumen with infiltrative growth. A significant desmoplastic reaction and fibrosis of adjacent loop are also present. Definitive histology: neuroendocrine tumor.

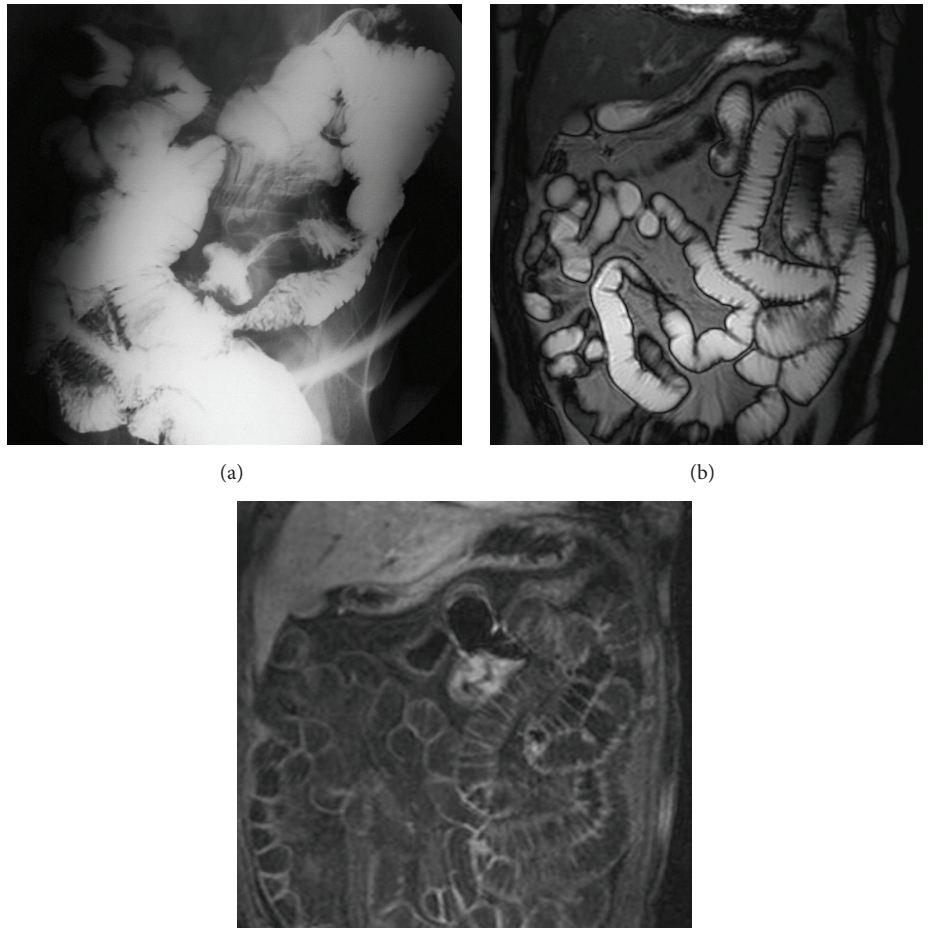

(a) (b) (c)

Figure 3: Lesion with infiltrative pattern, protruding into the intestinal lumen, with intense contrast enhancement in the VIBE sequences after the i.v. contrast medium administration (c). No evident lymphadenopathy. Definitive histology: lymphoma.

Table 1: Results of MR enteroclysis in the diagnosis of small-bowel neoplasms in our sample data for readers 1 and 2.

	Reader 1	Reader 2
Number of true-positive cases	21	22
Number of false-positive cases	3	1
Number of true-negative cases	40	42
Number of false-negative cases	3	2
Sensitivity (%)	87.5	91.6
Specificity (%)	93	97.6
PPV (%)	87.5	95.6
NPV (%)	93	95.4
Diagnostic accuracy	91	95
interobserver agreement	κ value* > 0.9	

*Interobserver agreement regarding lesion detection was excellent (κ > 0.85).
NPV: negative predictive value; PPV: positive predictive value.

neoplasms [1, 12]. Bowel cleansing and optimal distention of the small-bowel loops are crucial for the correct evaluation of the bowel wall because collapsed bowel loops can hide lesions or mimic disease by suggesting an abnormality-related thickened bowel wall in collapsed segments [13, 14].

Small-bowel distention was obtained with nasojejunal. Although this procedure was not always well accepted by patients and was characterized by longer time of the examination, as well as the use of X-rays, it improves the quality of the investigation since distension of bowel loops is controlled and uniform in contrast to the result obtained with the administration of contrast per os during procedures of MR enterography (Figures 1 and 2) [1, 15]. The use of coronal single-shot spin-echo (MR fluoroscopy) sequences is important for determining the distensibility of narrowed areas and facilitating the differentiation of contractions from strictures in the evaluation of prestenotic dilatation, of small-bowel mobility. The excellent soft tissue contrast allows evaluation of the layers of the wall and then the mucosal, submucosal or extraparietal origin of the diseaseof the disease [1, 8, 16, 17]. Furthermore ADC measurement by DW-MRI provided useful information to better characterize small lesions. An additional result was the excellent interobserver

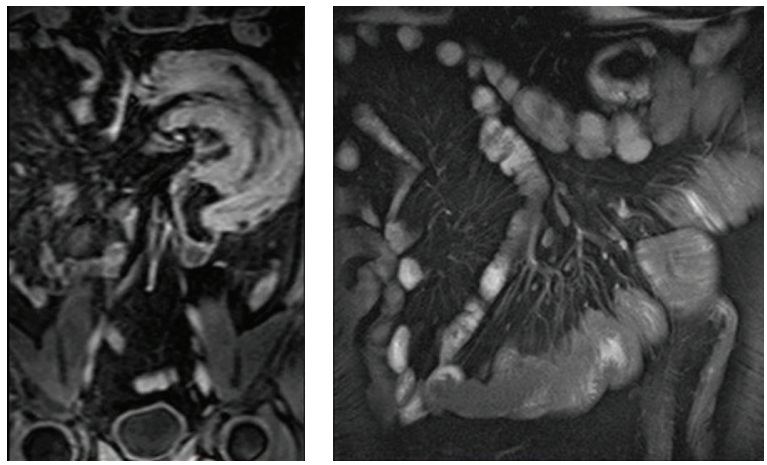

(a) (b)

Figure 4: MRI, VIBE sequences after the i.v. contrast medium administration (a) and HASTE sequences (b): large mass with endophytic growth with intense and heterogeneous enhancement. Small lymph nodes are evident in the root of the mesentery. Definitive histology: metastases from melanoma.

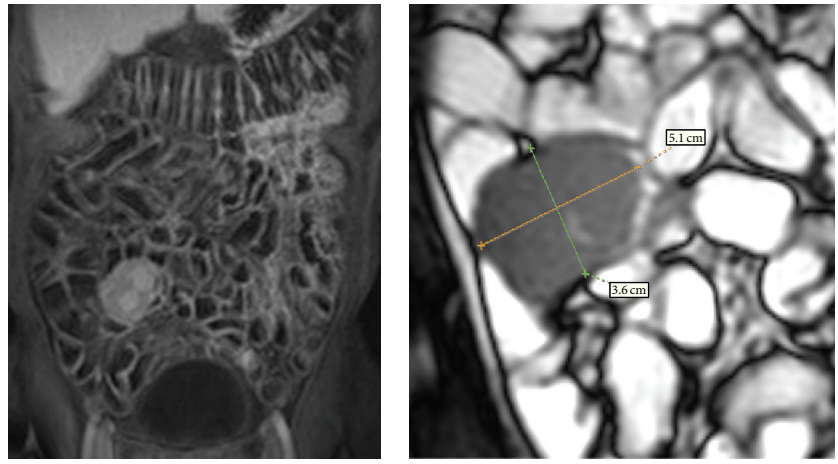

(a) (b)

Figure 5: Round lesion, with regular contours, in patients with frequent occlusive syndromes. It shows moderate enhancement in post-gadolinium sequences (a). Definitive histology: leiomyoma.

agreement achieved with MR enteroclysis, which indicates that this procedure can enable reproducible evaluation of small-bowel abnormalities.

Lymphomas represented the most common malignant tumors in our results, even if in the literature it is reported that they are about 20% of primary malignancies of the small intestine (Figure 3) [10]. B-cell lymphoma (4 cases) and follicular lymphoma (2 cases) were identified in our sample data. The first were located in the distal ileum, in agreement with the most frequent site described in the literature [16, 18] and appeared as polypoid lesions that protruded into the lumen and in one case ulceration and fistula were associated. Follicular lymphoma was located in the duodenum and appeared as thick walls without proximal obstruction, as the neoplasm does not elicit a desmoplastic response, and discreet parietal enhancement after intravenous contrast medium.

Cases of primitive adenocarcinoma were all localized in jejunal (2 cases of proximal jejunum, 1 case of distal jejunum), even if the incidence is the highest in the duodenum [19].

Characteristics of these lesions were sub-stenosis and concentric wall thickening with length between 2.7 and 3.3 cm (2 cases) and irregular intraluminal vegetation (1 case), with moderate enhancement after administration of contrast medium. In all cases a marked restriction of the diffusion signal was observed. In one case there was perivisceral adenopathy. One neuroendocrine tumor was identified with the appearance of focal and asymmetric bowel-wall thickening in the medium ileum (maximum diameter of 3 cm) with desmoplastic reaction infiltrating the adjacent ileal loops.

Gist appeared as well-circumscribed masses with intramural submucosal location and exophytic growth in three cases; in one case mucosal association was present and in another case a focal intraluminal polypoid mass was identified. For all these lesions after intravenous administration of gadolinium the solid portions enhanced in a peripheral heterogeneous fashion.

Three metastases was observed in our sample data. Two of these were caused by haematogenous spread from small cells lung cancer and melanoma (Figure 4) and appeared as round polypoid mass; the last one was an intraperitoneal metastasis from colon cancer that appeared as thick walls on the antimesenteric border of the small-bowel wall. In these three patients lymph nodes were identified at the mesenteric root.

Leiomyoma (Figure 5) was identified as an oval mass with regular margins in the distal ileum and intense uniform enhancement. Adenoma and the hamartomatous polyps appeared as solid polypoid pedunculated masses, with regular margins and the maximum diameter of 2 cm.

5. Conclusion

According to the literature our results show that MR enteroclysis is an accurate modality for detecting small-bowel neoplasm. It can provide anatomic, functional, and real time information without the need of ionizing radiation. MR findings, appearances of the lesions, combined with the contrast-enhancement behavior and characteristic of the stenosis are important to differentiate small-bowel neoplasm from other nonneoplastic disease [1, 20, 21].

Conflict of Interests

The authors declare that there is no conflict of interests regarding the publication of this paper.

References

[1] G. Masselli, E. Polettini, E. Casciani, L. Bertini, A. Vecchioli, and G. Gualdi, "Small-bowel neoplasms: prospective evaluation of MR enteroclysis," *Radiology*, vol. 251, no. 3, pp. 743–750, 2009.

[2] G. Masselli, E. Casciani, E. Polettini, F. Laghi, and G. Gualdi, "Magnetic resonance imaging of small bowel neoplasms," *Cancer Imaging*, vol. 13, no. 1, pp. 92–99, 2013.

[3] P. D. McLaughlin and M. M. Maher, "Primary malignant diseases of the small intestine," *American Journal of Roentgenology*, vol. 201, no. 1, pp. W9–W14, 2013.

[4] F. La Seta, A. Buccellato, L. Tesè et al., "Multidetector-row CT enteroclysis: Indications and clinical applications," *Radiologia Medica*, vol. 111, no. 2, pp. 141–158, 2006.

[5] R. Di Mizio, G. A. Rollandi, M. Bellomi, G. B. Meloni, S. Cappabianca, and R. Grassi, "Multidetector-row helical CT enteroclysis," *Radiologia Medica*, vol. 111, no. 1, pp. 1–10, 2006.

[6] S. Romano, E. De Lutio, G. A. Rollandi, L. Romano, R. Grassi, and D. D. T. Maglinte, "Multidetector computed tomography enteroclysis (MDCT-E) with neutral enteral and IV contrast enhancement in tumor detection," *European Radiology*, vol. 15, no. 6, pp. 1178–1183, 2005.

[7] D. D. T. Maglinte, G. N. Bender, D. E. Heitkamp, J. C. Lappas, and F. M. Kelvin, "Multidetector-row helical CT enteroclysis," *Radiologic Clinics of North America*, vol. 41, no. 2, pp. 249–262, 2003.

[8] H. W. Umschaden, D. Szolar, J. Gasser, M. Umschaden, and H. Haselbach, "Small-bowel disease: comparison of MR enteroclysis images with conventional enteroclysis and surgical findings," *Radiology*, vol. 215, no. 3, pp. 717–725, 2000.

[9] N. C. Gourtsoyiannis, J. Grammatikakis, G. Papamastorakis et al., "Imaging of small intestinal Crohn's disease: comparison between MR enteroclysis and conventional enteroclysis," *European Radiology*, vol. 16, no. 9, pp. 1915–1925, 2006.

[10] G. Masselli, E. Polettini, F. Laghi, R. Monti, and G. Gualdi, "Noninflammatory conditions of the small bowel," *Magnetic Resonance Imaging Clinics of North America*, vol. 22, no. 1, pp. 51–65, 2014.

[11] G. Gatta, G. Di Grezia, V. Di Mizio et al., "Crohn's disease imaging: a review," *Gastroenterology Research and Practice*, vol. 2012, Article ID 816920, 2012.

[12] S. J. B. Van Weyenberg, M. R. Meijerink, M. A. J. M. Jacobs et al., "MR enteroclysis in the diagnosis of small-bowel neoplasms," *Radiology*, vol. 254, no. 3, pp. 765–773, 2010.

[13] E. R. Ryan and I. S. E. Heaslip, "Magnetic resonance enteroclysis compared with conventional enteroclysis and computed tomography enteroclysis: a critically appraised topic," *Abdominal Imaging*, vol. 33, no. 1, pp. 34–37, 2008.

[14] A. Reginelli, Y. Mandato, A. Solazzo, D. Berritto, F. Iacobellis, and R. Grassi, "Errors in the radiological evaluation of the alimentary tract: part II," *Seminars in Ultrasound, CT and MRI*, vol. 33, no. 4, pp. 308–317, 2012.

[15] S. Cappabianca, V. Granata, G. Di Grezia et al., "The role of nasoenteric intubation in the MR study of patients with Crohn's disease: our experience and literature review," *Radiologia Medica*, vol. 116, no. 3, pp. 389–406, 2011.

[16] J. Fidler, "MR imaging of the small bowel," *Radiologic Clinics of North America*, vol. 45, no. 2, pp. 317–331, 2007.

[17] G. Masselli, A. Vecchioli, and G. F. Gualdi, "Crohn disease of the small bowel: MR enteroclysis versus conventional enteroclysis," *Abdominal Imaging*, vol. 31, no. 4, pp. 400–409, 2006.

[18] M. S. Levine, S. E. Rubesin, L. Pantongrag-Brown, J. L. Buck, and H. Herlinger, "Non-Hodgkin's lymphoma of the gastrointestinal tract: radiographic findings," *American Journal of Roentgenology*, vol. 168, no. 1, pp. 165–172, 1997.

[19] H. El Fattach, A. Dohan, Y. Guerrache et al., "MDCT and MR imaging of the jejunum," *Diagnostic and Interventional Imaging*, vol. 96, no. 3, pp. 227–237, 2015.

[20] G. Masselli, A. Picarelli, and G. Gualdi, "Celiac disease: MR enterography and contrast enhanced MRI," *Abdominal Imaging*, vol. 35, no. 4, pp. 399–406, 2010.

[21] G. Masselli and G. Gualdi, "CT and MR enterography in evaluating small bowel diseases: when to use which modality?" *Abdominal Imaging*, vol. 38, no. 2, pp. 249–259, 2013.

Hindawi Publishing Corporation
Gastroenterology Research and Practice
Volume 2016, Article ID 2631598, 7 pages
http://dx.doi.org/10.1155/2016/2631598

Research Article

Adhesions to Mesh after Ventral Hernia Mesh Repair Are Detected by MRI but Are Not a Cause of Long Term Chronic Abdominal Pain

Odd Langbach,[1] Stein Harald Holmedal,[2] Ole Jacob Grandal,[3] and Ola Røkke[1,4]

[1]*Department of Gastroenterologic Surgery, Akershus University Hospital, P.O. Box 1000, 1478 Lorenskog, Norway*
[2]*Department of Radiology, Akershus University Hospital, P.O. Box 1000, 1478 Lorenskog, Norway*
[3]*Department of Radiology, Norwegian Radium Hospital, Oslo University Hospital, P.O. Box 4953, Nydalen, 0424 Oslo, Norway*
[4]*Faculty of Medicine, University of Oslo, 0316 Oslo, Norway*

Correspondence should be addressed to Odd Langbach; odd.langbach@ahus.no

Received 26 May 2015; Accepted 21 July 2015

Academic Editor: Marcello Picchio

Aim. The aim of the present study was to perform MRI in patients after ventral hernia mesh repair, in order to evaluate MRI's ability to detect intra-abdominal adhesions. *Materials and Methods*. Single-center long term follow-up study of 155 patients operated for ventral hernia with laparoscopic (LVHR) or open mesh repair (OVHR), including analyzing medical records, clinical investigation with patient-reported pain (VAS-scale), and MRI. MRI was performed in 124 patients: 114 patients (74%) after follow-up, and 10 patients referred for late complaints after ventral mesh repair. To verify the MRI-diagnosis of adhesions, laparoscopy was performed after MRI in a cohort of 20 patients. *Results*. MRI detected adhesions between bowel and abdominal wall/mesh in 60% of the patients and mesh shrinkage in 20–50%. Adhesions were demonstrated to all types of meshes after both LVHR and OVHR with a sensitivity of 70%, specificity of 75%, positive predictive value of 78%, and negative predictive value of 67%. Independent predictors for formation of adhesions were mesh area as determined by MRI and Charlson index. The presence of adhesions was not associated with more pain. *Conclusion*. MRI can detect adhesions between bowel and abdominal wall in a fair reliable way. Adhesions are formed both after open and laparoscopic hernia mesh repair and are not associated with chronic pain.

1. Introduction

Ventral hernia mesh repair is a common surgical procedure and may be performed by open or laparoscopic technique. Most patients have favorable outcome after surgery, but some patients experience problems such as pain, discomfort, and hernia recurrences [1]. Hernia recurrence may explain some of the complaints and can be diagnosed by clinical investigation with the supplement of ultrasonography or computed tomography (CT). In many cases, however, there is no detectable cause of the patient's symptoms. The problems in these patients are often assumed to come from neuralgias caused by sutures, inflammatory reaction to mesh fixation materials or mesh, or even intra-abdominal adhesions, even if such causes are difficult to verify. The MRI technology is a sensitive method to diagnose abdominal wall pathology, but also adhesions [2] and is increasingly used in the diagnosis of abdominal disease. Although ultrasound is a dynamic tool, its capacity to detect adhesions is limited to the subsurface of the abdominal wall. CT can detect seroma and can also demonstrate typical adhesion-related complications like strangulated obstruction or bowel ischemia. Even with contrast-enhanced CT scan, adhesions cannot be detected directly in most cases but can be assumed due to scar tissue, bowel conglomerations, and luminal changes. Liberal use of dynamic CT-imagines, however, should be selective due to the radiation exposure.

The aim of the present study was to perform MRI in a clinically defined group of patients after LVHR and OVHR, respectively, in order to evaluate to what extent MRI is able to detect the mesh implant and adhesions between the bowel and the mesh or the abdominal wall. We also wanted to find if adhesions could explain chronic pain after ventral hernia mesh repair.

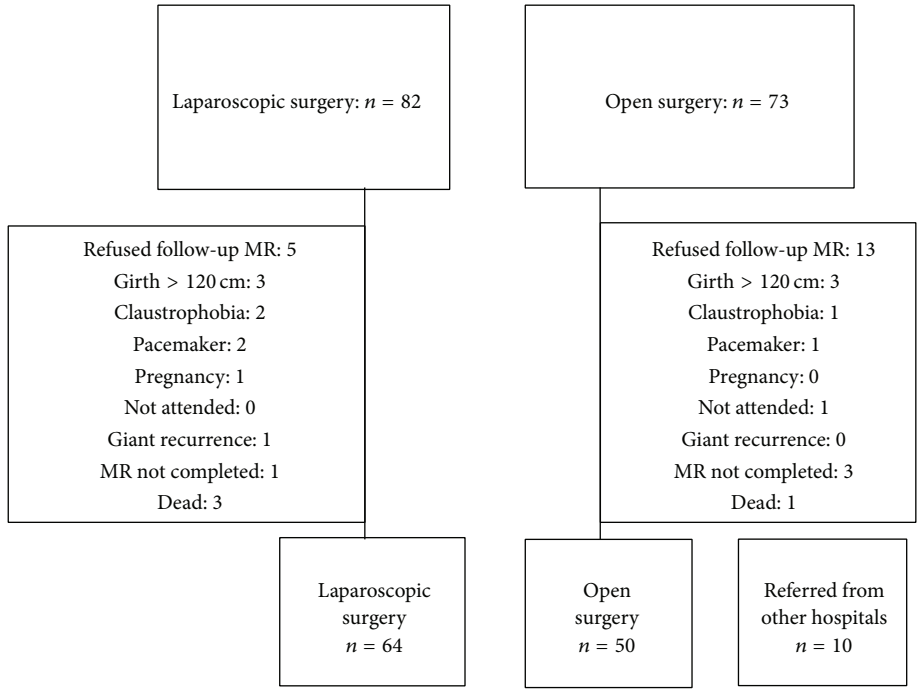

Figure 1: Consort diagram of 124 patients who attended MR-investigation.

2. Materials and Methods

We conducted a single-center follow-up study of 155 patients after LVHR (n = 82/53%) or OVHR (n = 73/47%) from January 2000 until November 2010. The follow-up included registration of perioperative data from medical records, clinical investigation of the patients, and evaluation of patient-reported pain in relation to different activity levels. Pain was assessed by using a 100 mm VAS scale, 0 meaning no pain and 100 worst imaginable pain.

Comorbidity was classified according to Charlson et al. [3]. All patients were invited to a magnetic resonance imaging- (MRI-) examination. MRI was finally performed in 114 of these patients (74%), 50 (44%) after OVHR, and 64 (56%) after LVHR, whereas 41 patients were excluded as shown in Figure 1. To increase the number of diagnostic MRI-examinations, another 10 patients, previously undergone ventral hernioplasty with mesh, were included. In these patients data from medical records were not obtained. Thus, MRI was performed in a total of 124 patients.

The MRI study was performed with a 1.5 tesla system (Achieva, Philips Medical Systems, the Netherlands). No premedication or contrast media were administered. First an axial TSE T2-weighted series throughout the abdomen was performed (field of view, 400 mm; matrix, 288 × 200 mm; flip angle, 90°; slice thickness 5 mm) to get an anatomical overview, identify the mesh, and diagnose adhesions between abdominal wall/mesh and bowel. The study was then followed by a cine-MRI, balanced FFE (field of view, 300 mm; matrix, 192×224; flip angle, 50°; slice thickness 15 mm). One sequence consisted of 30 dynamic scans in the same position. The patients were asked to increase intra-abdominal pressure and to relax repeatedly throughout this examination. Transverse series covered the abdomen in a craniocaudal direction, sagittal series covering the abdomen from right to left and a few coronal series covered the anterior abdominal wall in an anterior-posterior direction. The distance between every sequence was 15 mm. Depending on the patients size, the number of dynamic scans varied from 400 to 600. The mean examination time was 30 minutes.

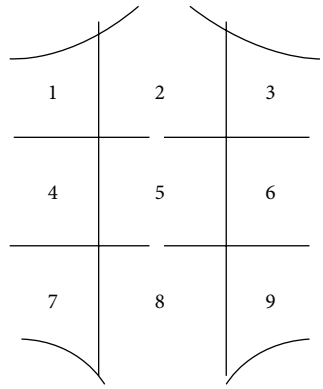

Figure 2: Abdominal map with field segmentation (segments 1–9).

A nine-segment map (Figure 2) was used as localization reference of the abdominal wall. Two experienced radiologists evaluated the MRI-studies in consensus. They were informed that the patients had been operated with mesh hernioplasty for ventral hernia but were blinded to other clinical and per-operative findings. Restricted visceral slide between bowel and adjacent abdominal wall or surgical mesh, with a missing separation between them, had been used as MRI criteria for diagnosis of adhesion. The adhesions were

Table 1: Characteristics of 114 patients investigated with MRI.

	Laparoscopic ($n = 64$)	Open ($n = 50$)	p
Age at hernia repair (y)	55.2 ± 14.1	55.1 ± 11.7	0.959
Gender (male : female)	24 : 40	25 : 25	0.181
Charlson score	0.3 ± 0.7	0.4 ± 0.8	0.613
Charlson index	1.6 ± 1.4	1.6 ± 1.4	0.914
BMI at hernia repair (kg/m^2), mean ± SD	30.1 ± 5.5	29.0 ± 5.0	0.289
BMI at follow-up (kg/m^2), mean ± SD	29.7 ± 6.1	28.5 ± 5.8	0.241
Area of hernia (cm^2)	55 ± 59	40 ± 45	0.123
Area implanted mesh (cm^2)	227 ± 115	180 ± 129	0.101
Area mesh determined MR (cm^2)	131 ± 79	106 ± 73	0.145
Days in hospital	2.4 ± 1.6	2.4 ± 2.2	0.932
Time from surgery to follow-up (y)	3.8 ± 1.4	4.6 ± 2.3	0.035
Time from follow-up to MRI (y)	0.9 ± 1.3	1.3 ± 2.5	0.222

classified according to the location and involved structures. Adhesions between different bowel loops or other organs were not evaluated. Other unrelated abdominal pathology was also recorded.

MRI's true ability of detecting adhesions was validated in a prospective double-blinded study of a cohort of 20 of these patients, in whom laparoscopy was performed after the MRI-scans due to hernia recurrence with complaints.

3. Statistics

The analyses were performed on the per-protocol basis. Data in text and tables are given as mean ± standard deviation. Analyses of categorical data were performed by the Pearsons Chi-square test (2-sided) ($n \geq 5$ in all subgroups) and Fisher's 2-sided exact test ($n < 5$ in any subgroup). The Student's t-test was used in analyses of continuous distributed data. Variables associated with the formation of adhesions at the $p < 0.1$ level in the bivariate analyses were included in multivariate analyses using a binary logistic regression model to estimate independent predictors, the odds ratio, and 95% confidence interval. Pearson correlation was used to establish association between variables. Differences between groups are given as actual p value and considered different at p values below 0.05. The analyses were performed using the SPSS version 22.

4. Results

MRI was performed in 124 patients. Patient characteristics are shown in Table 1. The mesh type used and the technique for mesh repair in 114 patients are shown in Table 2.

The ability of MRI to detect and assess the location of the implanted meshes was dependent on mesh type, with detection rates between 50% and 100%. Information of detectable mesh type and size was available in 68 patients (52%). Size-reduction/shrinkage of mesh occurred in most mesh types and varied between mesh types as shown in Table 3.

106 of the 124 MRI-examinations were evaluable with regard to adhesions between bowel and abdominal wall/mesh. There were variations in patients compliance with respect to deep breath during cine MRI. The breath procedure by the patient was inadequate in 18 patients (15%), in whom evaluation of adhesions could not be performed. Adhesions between bowel and abdominal wall/mesh were described in 63 out of 106 patients (59%) (Table 4) and mostly occurred in the middle and lower midline sectors (sectors 5 and 8). The upper (sectors 1, 2, and 3) and lateral sectors (sectors 4, 6, 7, and 9) had few detectable adhesions as shown in Table 5. 43 patients (41%) were devoid of adhesion on MRI.

Table 2: Detection of mesh by MRI in 114 patients treated with mesh hernioplasty.

	Laparoscopic ($n = 64$)		Open ($n = 50$)		All ($n = 114$)	
	n	%	n	%	n	%
Parietex composix	29/32	91	6/6	100	35/38	92
Polypropylene	1/1	100	11/20	55	12/21	57
Bard Comp.	12/14	86	2/4	50	14/18	78
Goretex dual mesh	7/8	88	6/9	67	13/17	72
Proceed	7/7	100	0	—	7/7	100
Marlex	0	—	3/6	50	3/6	50
TiMESH	2/2	100	1/1	100	3/3	100
Unknown	0	—	1/4	25	1/4	25
SUM	58/64	91	30/50	60	88/114	77

In 60 patients, there was available information about the size of the implanted mesh, and MRI could define both the mesh size and the presence or absence of adhesions. In these patients there was a significant correlation between mesh shrinkage and adhesion formation ($p = 0.003$, $R = 0.374$).

The placement of mesh in open surgery was onlay ($n = 8/16\%$), sublay (13/26%), and open IPOM ($n = 29/58\%$). Adhesions between bowel and abdominal wall/mesh were detected in 59 of 97 patients (60.8%) with evaluable MRI-scans and clinical data. Adhesions were demonstrated regardless of mesh type, however with a variation between 33% and 75% (Table 6). There was no significant difference between laparoscopic and open mesh repair with regard to formation of adhesions. Adhesions were identified in 67% of the patients

Table 3: Size of implanted mesh compared to mesh size at follow-up determined by MRI in patients with clinical data ($n = 68$).

	Area of implanted mesh	Area by MRI	% shrinkage	p
All ($n = 68$)	223 cm^2 ± 115 cm^2	133 cm^2 ± 79 cm^2	−30%	0.000
Parietex composix ($n = 34$)	227 cm^2 ± 128 cm^2	117 cm^2 ± 72 cm^2	−49%	0.000
Polypropylene ($n = 4$)	99 cm^2 ± 52 cm^2	101 cm^2 ± 96 cm^2	+1%	0.941
Bard composix ($n = 13$)	240 cm^2 ± 96 cm^2	153 cm^2 ± 74 cm^2	−36%	0.003
Goretex dual mesh ($n = 9$)	263 cm^2 ± 123 cm^2	202 cm^2 ± 95 cm^2	−23%	0.110
Proceed ($n = 4$)	217 cm^2 ± 81 cm^2	136 cm^2 ± 56 cm^2	−37%	0.082
Marlex ($n = 1$)	236 cm^2	65 cm^2	−72%	—
TiMESH ($n = 3$)	157 cm^2 ± 34 cm^2	75 cm^2 ± 20 cm^2	−52%	0.040

Table 4: Adhesions between bowel and abdominal wall and/or mesh as determined by MRI in 106 evaluable MRI-investigations.

Adhesions	n	%
Small bowel and mesh	32	30
Small bowel and mesh and abdominal wall	4	4
Colon and mesh	4	4
Small bowel and colon and mesh	8	8
Small bowel and colon and mesh and abdominal wall	2	2
Small bowel and abdominal wall	11	10
Small bowel and colon and abdominal wall	2	2
No adhesions	43	40
All	106	100
Not evaluable	18	

Table 5: Adhesions between bowel and abdominal wall and/or mesh as determined by MRI in 106 evaluable MRI-investigations.

Region	No adhesions		Adhesions between bowel and abdominal wall/mesh	
	n	%	n	%
1	103	98%	2	2%
2	96	91%	9	9%
3	103	97%	3	3%
4	104	98%	2	2%
5	59	55%	46	45%
6	103	97%	3	3%
7	99	93%	7	7%
8	71	67%	35	33%
9	105	99%	1	1%

after LVHR and in 49% after OVHR (Table 7). Adhesions to mesh were detected in 14/29 (48%) of the patients with "open IPOM."

The diagnosis of adhesions by MRI was validated by laparoscopy in 20 patients (Table 8). Laparoscopy was considered the "gold standard." 18 patients in this group had evaluable MRI-investigations. In the cohort where the results of MRI were investigated by subsequent laparoscopy, adhesions between bowel and abdominal wall were diagnosed by MRI in nine patients. At laparoscopy, 10 patients had adhesions between bowel and abdominal wall/mesh. MRI diagnosed adhesions between bowel and abdominal wall/mesh in two patients that did not have adhesions at laparoscopy. MRI failed to diagnose adhesions in three patients with adhesions at laparoscopy (Table 8). From this limited cohort, sensitivity of MRI was calculated to 7/10 = 70%, specificity 6/8 = 75%, and positive predictive value. 7/9 = 78%, negative predictive value: 6/9 = 67%. MRI was unable to detect adhesion between the omentum and the abdominal wall. At laparoscopy, 17 patients had such adhesions, mostly in region 5. Furthermore, some kind of adhesions was detected in all patients in one or more regions. Thus, the MRI underestimated the presence of adhesions.

To identify predictors for the genesis of adhesions, factors considered as important were investigated. In univariate analysis, the Charlson index, hernia width, mesh area, and operative time was associated with the presence of adhesions as determined by MRI (Table 9). When tested in a multivariate model, mesh area as determined by MRI and Charlson index were independent predictors of adhesions (Table 10).

The patient-reported pain during average-, normal-, moderate-, and maximal activity at follow-up was determined by the VAS-scale. In the laparoscopic hernia repair group we used nonabsorbable tackers ($n = 37/58\%$), nonabsorbable sutures ($n = 14/22\%$), or both ($n = 13/20\%$). We could not find any significant correlation between type of mesh fixation and chronic pain. There were similar results in patients with adhesions compared to patients without adhesions, except during normal activity, where patients with adhesions reported less pain than patient with adhesions (Table 11). Of the 114 patients, eight (7%) patients reported chronic pain (VAS > 30) during normal activity, six (5%) during average activity, 15 (13%) during moderate activity, 30 (36%) during maximal activity, and seven (6%) reported pain at follow-up. The number of patients with chronic pain during normal activity was lower in the group with adhesions (2%) compared to the group without adhesions (15%) (Table 12).

5. Discussion

In the present study, MRI could identify mesh in 77% of patients, with a rage of 50–100% depending on mesh type. Polypropylene allows for tissue ingrowth to an extent that makes detection difficult. Many of the recent meshes, however, like polytetrafluoroethylene mesh (ePTFE), are well detected on MRI. In 28 patients, laparoscopically inserted ePTFE were all visible, whereas inserted polypropylene

Table 6: Adhesions between bowel and mesh as determined by MRI in 97 patients with medical records from the operation and evaluable MR-investigations.

	Adhesions to mesh		Adhesions to abdominal wall		No adhesions		Evaluable		Not evaluable	
	n	%	*n*	%	*n*	%	*n*	%	*n*	%
Goretex	6	46	1	8	6	46	13	100	4	23
Parietex composix	20	61	3	9	10	30	33	100	5	13
Titan	1	33	0	0	2	67	3	100	0	100
Proceed	2	29	2	29	3	42	7	100	0	100
Bard composix	9	60	1	7	5	33	15	100	3	17
Polypropylene	6	38	2	12	8	50	16	100	5	25
Marlex	1	17	1	17	4	66	6	100	0	100
Unknown	1	25	2	50	1	25	4	100	0	100
SUM	46	47	12	12	39	40	97	100	17	15

Table 7: Adhesions between bowel and mesh/abdominal wall as determined by MRI in 114 patients with medical records after laparoscopic or open mesh repair.

	Laparoscopic		Open		All		*p*
	n	%	*n*	%	*n*	%	
Adhesions to mesh	32	55	14	36	46	47	0.063
Adhesions to abdominal wall	7	12	5	13	12	13	
No adhesions	19	33	20	51	39	40	
All evaluable	58	100	39	100	97	100	
Not evaluable	6	9	11	22	17	15	
All	64		50		114		

Table 8: Comparison between laparoscopy (considered as gold standard) and MRI.

MRI	Laparoscopy		Sum
	Adhesions	No adhesions	
Adhesions (positive)	7 (true positive)	2 (false positive)	9
No adhesions (negative)	3 (false negative)	6 (true negative)	9
SUM	10	8	18

meshes were not detectable [4]. Laparoscopically placed mesh may be more easily detected than mesh placed by open surgery [5]. In the present study, 57% of the polypropylene meshes were detected, possibly due to a more sensitive MRI-machine.

By MRI, we could demonstrate a size-reduction of 20–50% in mesh-implants depending on mesh types. Parietex composix showed about 50% shrinkage. This is in accordance with previous studies, reporting 20–40% shrinkage [6, 7]. In an experimental study in goats, Zinther et al. could demonstrate a 40% shrinkage of Parietex and 20% shrinkage of DynaMesh three months after insertion, with no further shrinkage thereafter [8]. In a study of polypropylene mesh with radioopaque markers, CT, after mesh insertion and two years postoperatively, demonstrated no shrinkage in 46 out of 50 patients and 3–22% shrinkage in the rest [9]. The observed size-reduction in our study might therefore have other causes than true shrinkage, like bulging and doubling, as previously described [10].

Intra-abdominal adhesions may have deleterious effects, like intestinal obstruction followed by chronic pain and reduced quality of life [1]. Previous studies using MRI after hernia mesh repair have reported adhesion rates of 70–100% [4, 11–13]. Adhesion seems to be associated with abdominal pain and discomfort [11]. The question however remains if these adhesions, in the absence of bowel obstruction, are capable of eliciting pain. In the present study, the rates of MRI diagnosed adhesions between bowel loops and abdominal wall/mesh are in agreement with others [12]. Adhesions to mesh were demonstrated in all mesh types, and there were no differences between patients operated with laparoscopic or open mesh repair. Larger mesh size at MRI was associated with higher degree of adhesions. Adhesions are thought to be caused by inflammation. In the present study, many factors were recorded and tested that might contribute to the formation of adhesions. We could demonstrate a significant correlation between mesh shrinkage and presence of adhesions. The implanted mesh may induce an inflammatory reaction, inducing shrinkage and creating adhesions, which in turn may amplify mesh shrinkage. The area of mesh as determined by MRI and Charlson comorbidity index was independent predictors of adhesion formation. Notably, laparoscopic and open mesh repair had similar rates of adhesion formation.

The MRI-investigation was designed to detect adhesions between bowel and abdominal wall/mesh and not between bowel segments. In 15% of patients, the MRI-investigation was not evaluable. During the MRI-scan period for 20–25 minutes, the patient must continuously use the abdominal muscles, which weakens in several patients during the procedure, followed by reduction in intestinal motility, and difficulty in interpretations. In some previous reports, a MRI-slice-thickness of 5–15 mm has been used [1]. To increase patient compliance, the MRI-slice-thickness of 15 mm was selected in the present study to reduce the scan-time, which in theory could overestimate the presence of adhesions.

The presence of adhesions was also associated with experience of pain during normal activity. Surprisingly, patients

Table 9: Univariate analysis of clinical parameters of possible importance for creations of adhesions in 97 patients with clinical data and evaluable MR-scans.

	Adhesions $n = 58$	No adhesions $n = 39$	p
Age at surgery (years)	57.8 ± 12.1	50.4 ± 13.9	0.007
Charlson score	0.41 ± 0.75	0.21 ± 0.62	0.153
Charlson index	1.8 ± 1.4	1.1 ± 1.4	0.012
BMI (kg/m^2), mean ± SD	29.0 ± 4.8	29.1 ± 5.3	0.978
Hernia length (preoperative measure) (cm)	6.5 ± 3.7	5.3 ± 3.5	0.121
Hernia width (preoperative measure) (cm)	6.2 ± 3.4	4.7 ± 2.3	0.018
Mesh area (cm^2)	233.6 ± 130.6	173.6 ± 68.8	0.036
Number of tacker rows	2.25 ± 0.7	2.47 ± 0.7	0.133
Operative time (min)	113.4 ± 56.1	88.2 ± 41.3	0.021
Postoperative stay (d)	2.7 ± 2.3	2.0 ± 1.2	0.064
Time from surgery to follow-up (y)	4.37 ± 1.77	3.92 ± 2.14	0.258
Time from surgery to MRI (y)	5.1 ± 1.8	5.0 ± 2.7	0.971
Area of mesh determined by MRI (cm^2)	134.7 ± 79.9	92.6 ± 55.8	0.023
Gender (male/female)	30/28	15/24	0.199
LVHR/OVHR	39/19	19/20	0.141
Postoperative complications (no/yes)	40/18	27/12	0.420

Table 10: Multivariate analysis of clinical parameters of possible independent importance for creation of adhesions in 97 patients with clinical data and evaluable MR-scans.

	B	S.E.	Wald	p	Exp(B)
Age at hernia mesh repair	0.039	0.065	0.361	0.548	1.040
Charlson index	−1.813	0.898	4.073	0.044	0.163
Hernia width	0.088	0.195	0.205	0.651	1.092
Mesh area determined at mesh repair	−0.002	0.007	0.113	0.736	0.998
Mesh area determined by MRI	−0.019	0.010	3.851	0.050	0.981
Operative time	−0.006	0.011	0.298	0.585	0.994
Postoperative stay	0.078	0.473	0.027	0.869	1.081

Table 11: VAS-scores in patients with and without adhesions between bowel and abdominal wall as determined by MRI in 97 evaluable patients with registered VAS-scores.

	Adhesions ($n = 58$)	No adhesions ($n = 39$)	p
Average pain	2.4 ± 7.0	4.5 ± 13.2	0.317
Pain during normal activity	3.8 ± 8.3	9.9 ± 17.6	0.025
Pain during moderate activity	7.7 ± 12.2	14.0 ± 21.8	0.072
Maximal pain in last 30 days	17.6 ± 20.5	20.9 ± 22.8	0.488
Pain at follow-up (today)	3.9 ± 8.5	6.5 ± 12.6	0.217

Table 12: Number of patients with chronic pain (VAS ≥ 30) in 97 evaluable patients with or without adhesions.

	Adhesions ($n = 58$)	No adhesions ($n = 39$)	p
Average pain	1 (2%)	4 (10%)	0.154
Pain during normal activity	1 (2%)	6 (15%)	0.016
Pain during moderate activity	5 (9%)	9 (23%)	0.075
Maximal pain in last 30 days	16 (28%)	12 (31%)	0.820
Pain at follow-up (today)	2 (3%)	4 (10%)	0.216

with adhesions experienced less pain than patients without adhesions. This is in contradiction to the general hypothesis today that adhesions may cause pain. Patients with abdominal pain thought of as being caused by adhesions are often scheduled for surgical adhesiolysis. Some support for this was found in a study by Demco, where laparoscopy was performed in 20 sedated but awake patients, and a systematic traction of adhesions was performed, which induced pain depending on type of adhesions [14]. In the present study, MRI was able to detect adhesions between bowel and abdominal wall. About 6% developed chronic pain at long term follow-up. Patients with adhesions did not have more pain than patients without adhesions. Thus, the present study does not support that adhesions produce pain. This is in accordance with a study by Swank et al., who randomized patients with chronic abdominal pain and adhesions to either laparoscopy with adhesiolysis or laparoscopy alone. There was no difference between the groups, except for more complications after adhesiolysis [15]. Adhesions between

omentum and abdominal wall could also be of importance in pain generation, but these adhesions could not be detected with MRI. The study was also not designed to detect adhesions between bowel loops, or between female internal genitals and bowel loops, which also may generate pain. Previous studies have validated the use of MRI. In one study, with intraoperative validation of the MRI's ability to detect adhesions, a prevalence of 96%, an accuracy of 90%, a sensitivity of 93%, a positive predictive value of 96%, and a specificity of 25% were found [16]. The low specificity was explained by the very low number of patients found without adhesions both with cine-MRI and intraoperatively. In a study of preoperative MRI before planned laparotomy, MRI could detect adhesions with a sensitivity of 21.5%, with a specificity of 87% [12]. In the present study the sensitivity was better, and specificity about the same. Interestingly, the *absence* of adhesions may be more accurately defined by ultrasound than by MRI [12], but the *presence* of adhesions is best detected with MRI compared to high-resolution ultrasonography. In a study, intra-abdominal adhesions were determined in 53 patients with MRI and 3 with ultrasonography, where most adhesions were between small bowel and abdominal wall, thereafter bowel-bowel adherences [16]. Only adhesions between intestines and abdominal wall could be detected in the present study. The use of 15 mm slices versus 10 mm slices may be an explanation.

6. Conclusion

MRI is a sensitive tool to detect various types of implanted mesh, as well as adhesions between bowel and abdominal wall/mesh with a fair sensitivity and specificity. There is no difference between the tendency to form adhesions after open or laparoscopic mesh repair. The area covered by the mesh is associated with formation of adhesions. Adhesions between bowel and abdominal wall cannot explain chronic pain after laparoscopic or open hernia mesh repair.

Conflict of Interests

The authors declare that there is no conflict of interests regarding the publication of this paper.

Acknowledgment

The paper was supported by grants from Akershus University Hospital.

References

[1] N. B. Zinther, J. Fedder, and H. Friis-Andersen, "Noninvasive detection and mapping of intraabdominal adhesions: a review of the current literature," *Surgical Endoscopy and Other Interventional Techniques*, vol. 24, no. 11, pp. 2681–2686, 2010.

[2] R. A. Lang, S. Buhmann, A. Hopman et al., "Cine-MRI detection of intraabdominal adhesions: correlation with intraoperative findings in 89 consecutive cases," *Surgical Endoscopy*, vol. 22, no. 11, pp. 2455–2461, 2008.

[3] M. E. Charlson, P. Pompei, K. L. Ales, and C. R. MacKenzie, "A new method of classifying prognostic comorbidity in longitudinal studies: development and validation," *Journal of Chronic Diseases*, vol. 40, no. 5, pp. 373–383, 1987.

[4] T. Fischer, R. Ladurner, A. Gangkofer, T. Mussack, M. Reiser, and A. Lienemann, "Functional cine MRI of the abdomen for the assessment of implanted synthetic mesh in patients after incisional hernia repair: initial results," *European Radiology*, vol. 17, no. 12, pp. 3123–3129, 2007.

[5] S. Kirchhoff, R. Ladurner, C. Kirchhoff, T. Mussack, M. F. Reiser, and A. Lienemann, "Detection of recurrent hernia and intraabdominal adhesions following incisional hernia repair: a functional cine MRI-study," *Abdominal Imaging*, vol. 35, no. 2, pp. 224–231, 2010.

[6] U. Klinge, B. Klosterhalfen, M. Müller, A. P. Öttinger, and V. Schumpelick, "Shrinking of polypropylene mesh in vivo: an experimental study in dogs," *European Journal of Surgery*, vol. 164, no. 12, pp. 965–969, 1998.

[7] J. Conze, C. J. Krones, V. Schumpelick, and U. Klinge, "Incisional hernia: challenge of re-operations after mesh repair," *Langenbeck's Archives of Surgery*, vol. 392, no. 4, pp. 453–457, 2007.

[8] N. B. Zinther, P. Wara, and H. Friis-Andersen, "Shrinkage of intraperitoneal onlay mesh in sheep: coated polyester mesh versus covered polypropylene mesh," *Hernia*, vol. 14, no. 6, pp. 611–615, 2010.

[9] C. Langer, H. Forster, F. Konietschke et al., "Mesh shrinkage in hernia surgery: data from a prospective randomized double-blinded clinical study," *Chirurg*, vol. 81, no. 8, pp. 735–745, 2010.

[10] J. R. Eriksen, "Pain and convalescence following laparoscopic ventral hernia repair," *Danish Medical Bulletin*, vol. 58, no. 12, 2011.

[11] T. Mussack, T. Fischer, R. Ladurner et al., "Cine magnetic resonance imaging vs high-resolution ultrasonography for detection of adhesions after laparoscopic and open incisional hernia repair: a matched pair pilot analysis," *Surgical Endoscopy and Other Interventional Techniques*, vol. 19, no. 12, pp. 1538–1543, 2005.

[12] N. B. Zinther, A. Zeuten, E. Marinovskij, M. Haislund, and H. Friis-Andersen, "Detection of abdominal wall adhesions using visceral slide," *Surgical Endoscopy and Other Interventional Techniques*, vol. 24, no. 12, pp. 3161–3166, 2010.

[13] N. B. Zinther, P. Wara, and H. Friis-Andersen, "Functional cine MRI and transabdominal ultrasonography for the assessment of adhesions to implanted synthetic mesh 5–7 years after laparoscopic ventral hernia repair," *Hernia*, vol. 14, no. 5, pp. 499–504, 2010.

[14] L. Demco, "Pain mapping of adhesions," *Journal of the American Association of Gynecologic Laparoscopists*, vol. 11, no. 2, pp. 181–183, 2004.

[15] D. J. Swank, S. C. G. Swank-Bordewijk, W. C. J. Hop et al., "Laparoscopic adhesiolysis in patients with chronic abdominal pain: a blinded randomised controlled multi-centre trial," *The Lancet*, vol. 361, no. 9365, pp. 1247–1251, 2003.

[16] B. A. Wormer, A. L. Walters, J. F. Bradley III et al., "Does ventral hernia defect length, width, or area predict postoperative quality of life? Answers from a prospective, international study," *Journal of Surgical Research*, vol. 184, no. 1, pp. 169–177, 2013.

Hindawi Publishing Corporation
Gastroenterology Research and Practice
Volume 2016, Article ID 2498143, 9 pages
http://dx.doi.org/10.1155/2016/2498143

Review Article

Radiological Features of Gastrointestinal Lymphoma

Giuseppe Lo Re, Vernuccio Federica, Federico Midiri, Dario Picone, Giuseppe La Tona, Massimo Galia, Antonio Lo Casto, Roberto Lagalla, and Massimo Midiri

Radiology Section, DIBIMED, University of Palermo, Via del Vespro 129, 90127 Palermo, Italy

Correspondence should be addressed to Vernuccio Federica; federicavernuccio@gmail.com

Received 7 July 2015; Accepted 20 September 2015

Academic Editor: Haruhiko Sugimura

Gastrointestinal lymphomas represent 5–20% of extranodal lymphomas and mainly occur in the stomach and small intestine. Clinical findings are not specific, thus often determining a delay in the diagnosis. Imaging features at conventional and cross-sectional imaging must be known by the radiologist since he/she plays a pivotal role in the diagnosis and disease assessment, thus assisting in the choice of the optimal treatment to patients. This review focuses on the wide variety of imaging presentation of esophageal, gastric, and small and large bowel lymphoma presenting their main imaging appearances at conventional and cross-sectional imaging, mainly focusing on computed tomography and magnetic resonance, helping in the choice of the best imaging technique for the disease characterization and assessment and the recognition of potential complications.

1. Introduction

Gastrointestinal (GI) lymphoma accounts for 5–20% of extranodal lymphomas [1, 2]: the stomach is the most common site, followed by small intestine (ileum (60–65%), jejunum (20%–25%), and duodenum (6%–8%) and then colorectal lymphomas (6–12%)) [3–8].

GI lymphomas most commonly occur around the sixth decade of life and, although rare in childhood, they are the most common GI tumours in this age [9, 10].

Etiology is usually unknown although the increase of the incidence of non-Hodgkin lymphoma has been related to the increase of congenital and acquired immunodeficiency [1, 11].

Risk factors implicated in the pathogenesis of GI lymphoma are some infections due to *Helicobacter pylori*, human immunodeficiency virus infection, *Campylobacter jejuni*, Epstein-Barr virus, hepatitis B virus, human T-cell lymphotropic virus-1, and some inflammatory conditions as celiac disease, inflammatory bowel disease, atrophic gastritis, and parasitic infection [2, 9].

Clinical findings are not specific and this causes a delay in the diagnosis. The most common symptoms are epigastric pain, weight loss, and anorexia; nausea and vomiting in case of gastric lymphoma is uncommon, except in the later stage of the disease [9]. Other symptoms encountered in these patients are GI bleeding and the presence of an abdominal mass and bowel perforation, mainly in the small bowel [9].

Concerning the histological diagnosis, the appearance of GI lymphomas is an accumulation of lymphocytic tumour cells with a uniform pattern with an admixture of mature and immature elements [9].

The majority of GI lymphomas are of B-cell origin, while just 8%–10% show a T-cell origin [9]. Most low-grade B-cell GI lymphomas are of mucosa-associated lymphoid tissue (MALT) type, while enteropathy-associated T-cell lymphoma is the most common primary gastrointestinal T-cell lymphoma. GI lymphomas represent a heterogeneous group of entities originating from different cell lineage, with lymphoid cell at different stage of development, and with different biologic behaviour [10]. Certain histological subtypes most commonly occur in a precise location as MALT lymphoma in stomach, mantle cell lymphoma in terminal ileum, jejunum, and colon, enteropathy-associated T-cell lymphoma in jejunum, and follicular lymphoma in duodenum [2].

After a diagnosis of GI lymphoma is confirmed, the extent of disease has to be determined. Laboratory studies should include a complete blood count, HIV, HBV, and HCV serology, and liver and renal function blood tests and electrolytes.

Imaging plays a pivotal role both in the diagnostic phase and in the recognition of potential complications, as perforation, obstruction, and fistulas of the involved GI wall with the adjacent structures [12].

GI lymphoma has a wide variety of morphological imaging features at conventional and cross-sectional imaging. Primary GI lymphomas are best classified according to the classification of the Consensus Conference in Lugano in 1993 [13]: stage I is defined when the tumour is confined to GI tract, while in stage II, the most common one, the tumour is extended into the abdominal cavity with nodal involvement that can be either local (II1) or distant (II2). When the tumour penetrates through serosa involving adjacent structures, it is classified as stage III, while when a disseminated extranodal involvement or a GI tract lesion with supradiaphragmatic nodal involvement occurs it is classified as stage IV.

GI lymphoma must be differentiated from other primary GI tumours and from primary nodal lymphomas because they require different treatment management and they have a substantial different prognosis [9].

2. Esophageal Lymphoma

Primary *esophageal* lymphomas account for less than 1% in all primary GI lymphomas, while usually result from lymph node metastasis of the lymphomas from the cervical or mediastinal region [14]. Both findings on barium studies, as irregular filling defects, and on CT, as thickened esophageal wall with narrowed lumen, are nonspecific and mimic esophageal adenocarcinoma [14]. However, CT may be useful to differentiate primary esophageal lymphoma from lymph node involvements in the cervical or mediastinal regions, in staging of the disease and in evaluating response to therapy [14].

3. Gastric Lymphoma

Concerning *gastric lymphoma*, the most accepted hypothesis is that a chronic infection of the stomach by *Helicobacter pylori* causes lymphoid proliferation in the gastric mucosa, with subsequent development of gastric MALT lymphoma [5, 6]. Diffuse infiltrates of small centrocyte-like cells invading the epithelial lining of glands or crypts are the classical lymphoepithelial lesions of low-grade MALT lymphoma [15, 16]. In high-grade MALT lymphoma, confluent clusters or sheets with or without areas of low-grade component can be recognized [17]. Endoscopic ultrasonography (EUS) turns to be quite useful to demonstrate all the components of the gastric wall, the thickening of the intermediate anatomic layers (submucosa, muscularis propria), extramural infiltration, and lymph node involvement [18]. Yet, it has been proposed for evaluating the extension of gastric tumours.

Three different EUS patterns can be detected in gastric lymphomas [18]:

(i) Giant rigid gastric folds, sometimes determining a polypoid appearance.

(ii) Localized or extended hypoechoic infiltration.

(iii) Thickening with superficial stellate-shaped ulcerations.

For the differential diagnosis of lymphoma with gastric carcinomas, on EUS a more echogenic pattern and a different trend of diffusion can be demonstrated in patients with gastric carcinoma (the pattern of growth may be fungating or ulcerative and infiltrative) (no extended longitudinal hypoechoic infiltration of the superficial layers or extended hypoechoic transmural infiltration) [18].

The impact of EUS on clinical outcome is consistent, as it can predict MALT remission after the simple eradication therapy of *Helicobacter pylori* [19]. EUS is superior to CT for the staging and the assessment of the T and N parameters [6, 20]. However, compared to CT it cannot demonstrate the true extraluminal extent of the disease (M) or the involvement of distant lymph nodes.

Regarding *conventional X-ray*, the role of barium studies is limited to the detection of a lesion and to the demonstration of its location and extent.

The most common radiological signs on barium meal vary from normal to bull's eye appearance due to central ulceration, filling defects, thickened gastric mucosal folds, and linitis plastica.

Moreover, it is possible to distinguish the predominant features of early and advanced gastric lymphomas: the first usually present as shallow ulcerations or uneven mucosa with enlarging radiation folds [21]; the second are usually revealed as multiple masses or ulcerations, diffuse thickening of the folds, extensive submucosal infiltration, extension across the pylorus or the esophagogastric junction, large tumours over 10 cm in diameter, and preservation of pliability of the gastric wall due to a lack of the desmoplastic reaction [22, 23].

Though barium studies may demonstrate subtle lesions not seen at CT, they do not demonstrate the true extraluminal extent of the disease and are of little value in staging [7].

The most common *CT* patterns of gastric lymphoma are the presence of diffuse or segmental wall thickening of 2–5 cm with low contrast enhancement and extensive lateral extension of the tumour due to submucosal spread (Figure 1) [24]; moreover, CT can assess the presence of lymphadenopathies. Less commonly, gastric lymphoma may present on CT as a polypoidal mass, an ulcerative lesion, or a mucosal nodularity.

Considering the CT features of lymphoma, in low-grade ones there is less severe gastric wall thickening than in high-grade lymphoma, and abdominal lymphadenopathy is less common [25, 26]. The absence of abnormality or the presence of just minimal gastric wall thickening or a shallow lesion at CT suggests low-grade MALT lymphoma [26]; yet, CT is of limited value in its diagnosis [7]. A greater thickening may indicate transformation to a higher grade lymphoma [24].

Comparing EUS and CT, EUS is better in the evaluation of parietal extension of the tumour while CT better assesses the extraparietal involvement. Moreover, as previously stated, CT has several limitations in the detection of low-grade and MALT lymphomas; yet for their diagnosis and staging EUS is the best imaging technique since it can accurately assess

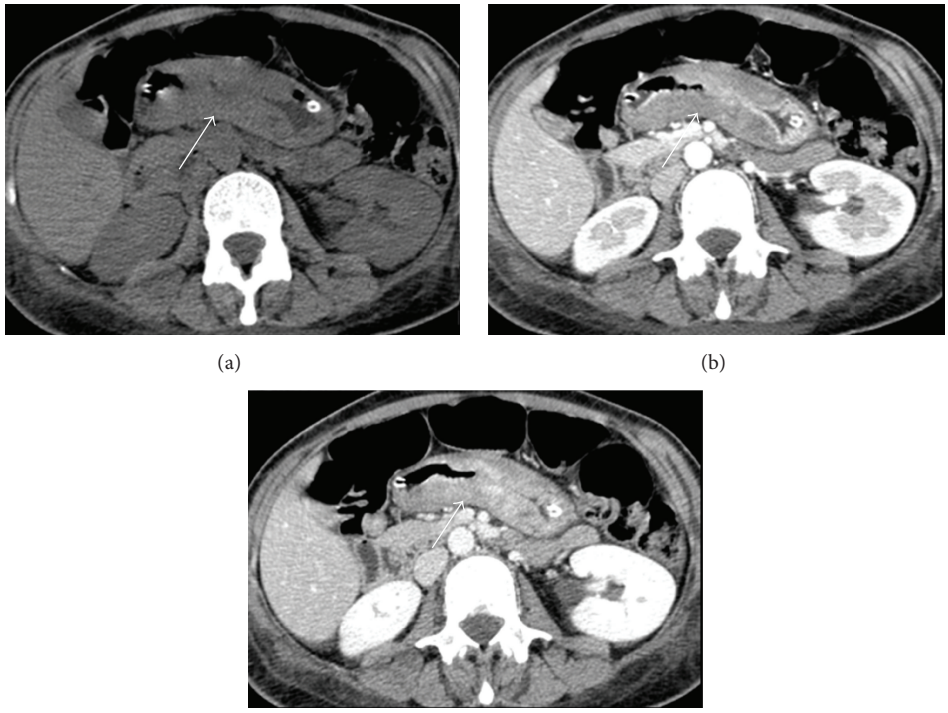

(a) (b)

(c)

Figure 1: Abdominal CT scan in a 48-year-old female with gastric lymphoma. Axial pre- (a) and postcontrastographic CT scan in the arterial (b) and portal venous (c) phase show diffuse segmental (length: 9 cm) wall thickening (thickness: 1,8 cm) (arrows) of the gastric corpus and antrum with mild contrast enhancement. The patient underwent gastrectomy with ileal-jejunum anastomosis.

the intramural infiltration, local node involvement, and response to therapy [27].

Comparing MR and CT, they show a similar diagnostic capability and overlapping radiological features [27], but due to high costs, long time required for each examination, and possible artifacts, MR is used just when the patient cannot be submitted to CT.

4. Small Bowel Lymphoma

Concerning *small bowel lymphoma*, small bowel is usually studied through endoscopic or radiological imaging techniques. Video capsule endoscopy is the preferred imaging technique for the visualization of mucosal abnormalities in patients with obscure bleeding when gastroscopy and colonoscopy are negative; however, this method is not always able to identify the source of bleeding and is contraindicated in suspected stenosis or obstruction, because of the risk of retention of the video capsule [28, 29].

Single or double balloon enteroscopy partially displays the bowel and allows biopsies; however, it is limited by its invasiveness, the long timing of the examination, and the technical difficulties [7]. Conventional radiological imaging techniques, such as the study of the small intestine through enterography or enteroclysis, allow the diagnosis of mucosal abnormalities, masses, and/or invaginations but provide only indirect information on the intestinal wall and on the surrounding structures; yet, they are actually considered obsolete [2]. CT and MR enteroclysis and enterography have an increasingly important role in the study of small intestine tumours. Thanks to their high spatial resolution, they allow a direct visualization of both the wall (assessing any luminal anomaly) and surrounding structures (mesentery, adjacent adipose tissue, lymph nodes, and peritoneal spaces) [3, 30, 31].

MR, thanks to its multiplanarity, has an excellent contrast resolution, does not use ionizing radiation, and provides both anatomical and functional information about bowel loops, allowing distinguishing organic stenosis from normal peristaltic waves [32].

CT is particularly useful both for staging and in the follow-up after surgery or chemoradiotherapy. Nowadays, CT allows the evaluation of wall thickness, mesenteric vasculature, and any associated extramural findings [7, 29]. Small bowel CT, or entero-CT, performed through a multislice CT scanner has led to considerable advances in the detection and staging of intestinal diseases. The advantage of this technique lies in its panoramic view, which allows the evaluation of the intestinal wall thickness, the degree of bowel distension, and the circular folds. Yet, ileal loops and also those of the deep pelvis, the mesentery, the surrounding adipose tissue, and other abdominal organs are studied (Figure 2) [20, 33].

CT-enterography is more and more used in place of conventional double contrast enteroclysis. It is performed with the patient in supine/prone position, and with craniocaudal scans, after oral administration of an isotonic solution, in order to obtain an adequate distension of small bowel

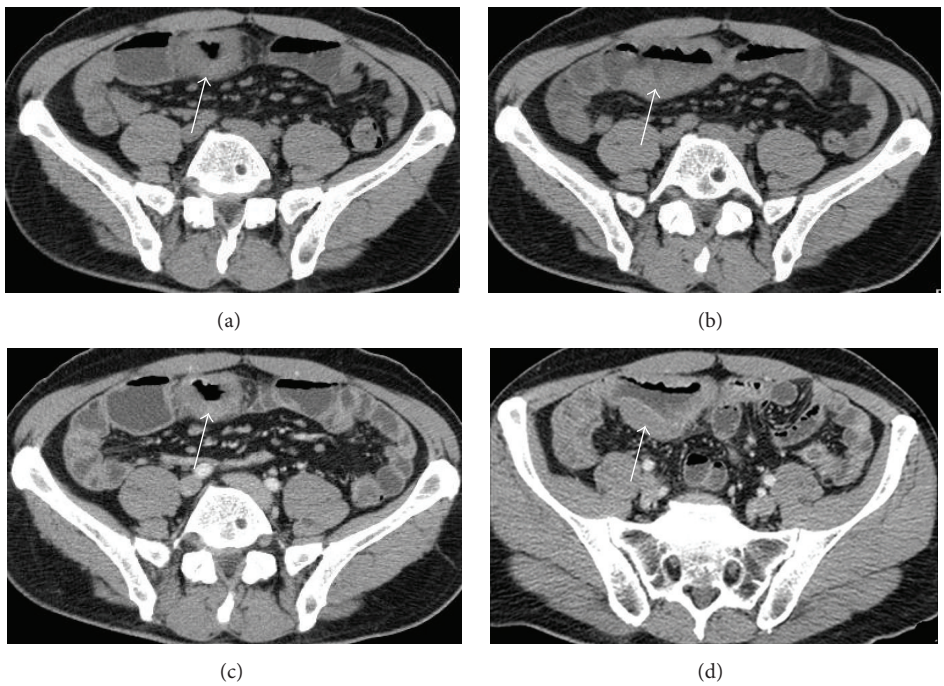

Figure 2: Abdominal CT scan in a 46-year-old male with celiac disease who developed an ileal lymphoma. Abdominal CT scan in the precontrastographic phase ((a) and (b)) and in the postcontrastographic phase ((c) and (d)) shows diffuse segmental (length: 8 cm) wall thickening (thickness: 1,5 cm) (arrows) with mild contrast enhancement in an ileal loop. Multiple subcentimetric lymph nodes are detected near the affected loop in the mesenteric fat.

wall. Less frequently, an enteroclysis CT is performed, after nasal-jejunal intubation, and subsequent introduction of a diluted barium solution. Neutral contrast media (i.e., PEG) are generally preferred for the assessment of bowel wall, particularly after intravenous contrast medium injection since the water density of the solution is opposed to that of the wall that is enhanced in the vascular phase, mainly in inflammatory diseases [20, 29, 33].

MR has played a secondary role for years compared to CT, especially due to the increased length of time of acquisition and the motion artifacts [11, 34]. However, the rapid development of the technical innovations, the introduction of new equipment, and higher gradients magnetic fields has allowed the development of fast T1- and T2-weighted sequences, single-shot fast spin-echo, or gradient-echo, acquired during a single apnoea, which enabled the development of MR protocols for the study of small bowel using an intraluminal contrast medium (enterography-MR) [29]. The absence of ionizing radiation makes this method particularly suitable in the follow-up [11, 34]. At MR a diagnosis of small bowel lymphoma is suggested by the presence of an infiltrative lesion with patency of bowel lumen or a nonstenotic bowel mass, mesenteric involvement with enlarged lymph nodes, splenomegaly, and mesenteric and retroperitoneal lymphadenopathy (Figure 3) [35].

However, the imaging diagnosis of small bowel lymphoma is still based on the use of enterography CT [33, 36].

The most common CT/MR patterns of small bowel lymphoma are 5 [34, 37]:

(i) Polypoid/nodular pattern.

(ii) Infiltrative pattern.

(iii) Aneurismal pattern.

(iv) Exophytic mass.

(v) Stenosing mass (rare).

The *polypoid* pattern is characterized by the presence of a solid nodule, with a homogeneous signal density/intensity, that develops in the submucosa and protrudes into the lumen appearing as a polypoid mass. There is no wall thickening and/or lymph adenopathy and the mucosa is intact. This mass may cause intussusception.

The *infiltrative* form is characterized by segmental symmetrical or slightly asymmetrical infiltrating lesions with a medium diameter of 1.5 cm and 2 cm, associated with mild circumferential thickening of the small bowel wall. Usually, the infiltrative lesions show ill-defined margins and a homogeneous contrast enhancement; the latter may rarely be inhomogeneous because of the presence of hypodense/hypointense areas due to development of necrosis and/or ischemia in the context of the lesion. These lesions may extend to the whole bowel thickness, from the endoluminal mucosa to the tunica serosa. The length of the thickened small bowel segment is variable.

The *aneurismal* pattern (diameter of dilatation of the lumen over 4 cm), firstly diagnosed by Cupps et al. in 1969 [4], represents 31% of small bowel lymphomas (Figure 4). It usually coexists with the infiltrative form since it can represent

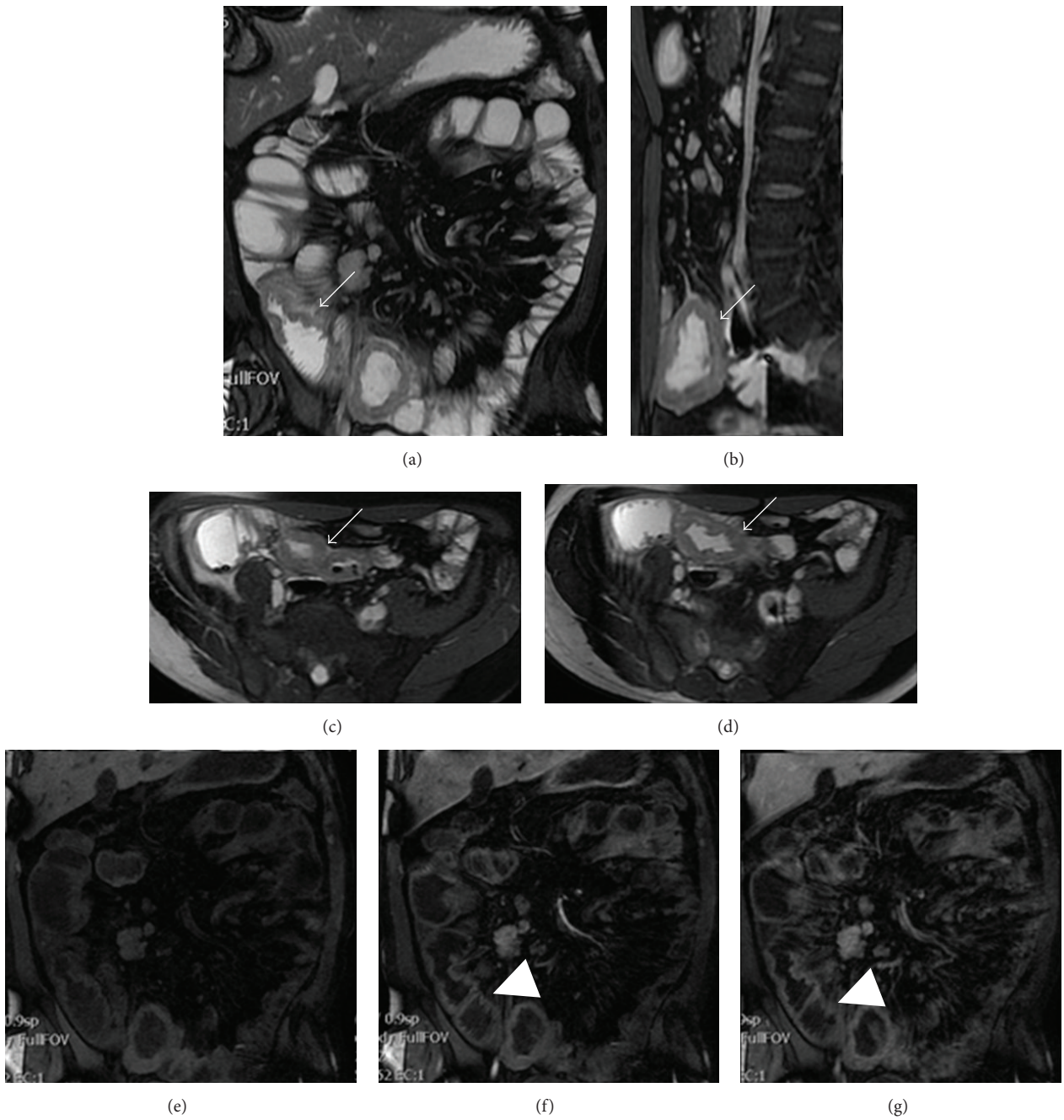

Figure 3: Abdominal MR enterography in the same patient of Figure 2. MR enterography shows the presence of a circumferential thickening of an ileal bowel loop (arrows) in the coronal (a), sagittal (b), and axial ((c) and (d)) planes, before contrast medium injection. Compared to the coronal precontrastographic phase (e), this thickening shows mild contrast enhancement in the arterial (f) and portal venous phase (g) (arrowheads).

its natural evolution [38, 39]. Several factors are responsible for the aneurismal dilation secondary to infiltrative growth of neoplastic lesion, as a progressive destruction of myenteric plexus, destruction of muscle layers with stretching of the muscle fibers, and loss of contractile cells; on the other hand, the infiltration of arterial and lymphatic vessels determines anoxia and necrosis within the lesion. According to some authors, this tumour necrosis could lead to cavitation and be also responsible for the aneurismal dilatation [38, 39].

The *stenosing* form is a rare form of presentation of intestinal lymphoma. This pattern generally occurs in Hodgkin's lymphoma. The growth of the tumour determines concentric fibrotic stenosis of the affected loop, resulting in dislocation of the contiguous loops. It is thought that this pattern is

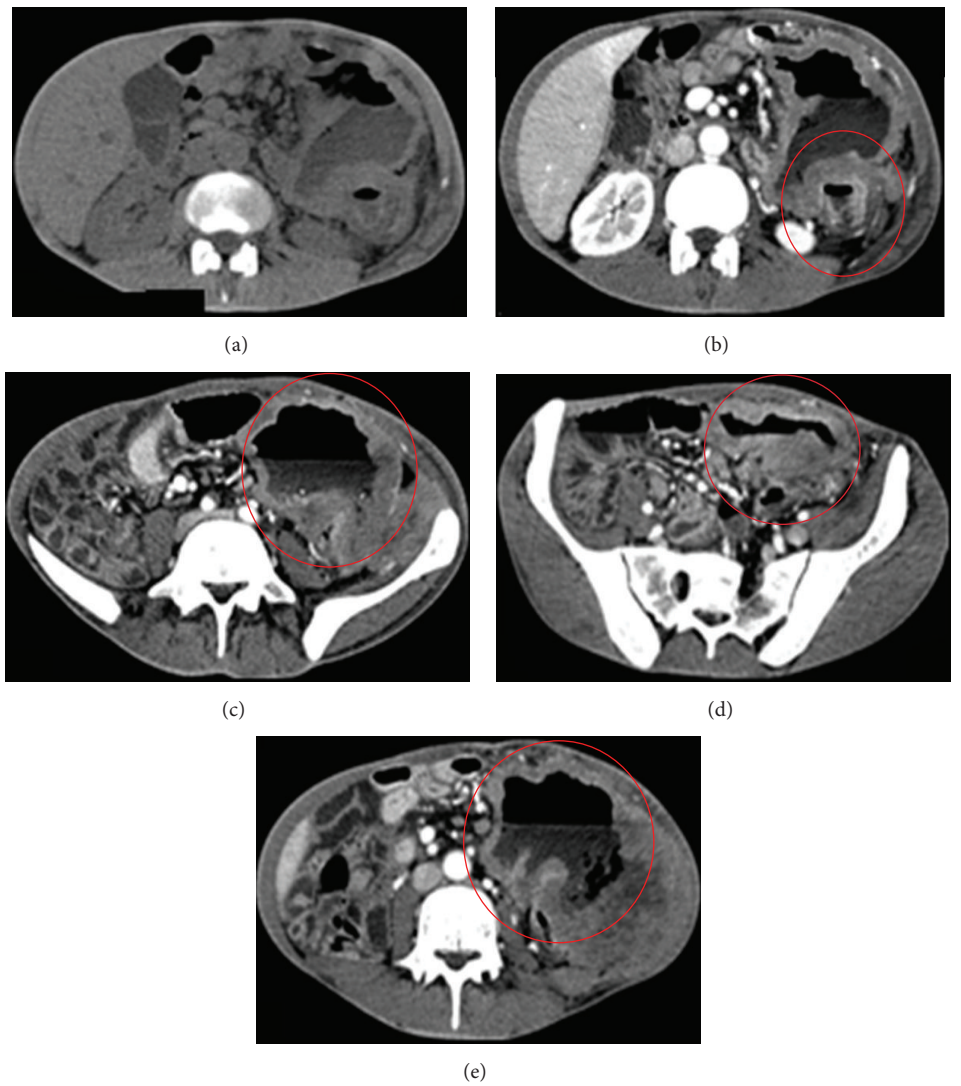

Figure 4: Aneurismatic jejunal lymphoma in a 43-year-old female. (a, b, c) Precontrastographic and postcontrastographic axial CT scan show severe circumferential wall thickening (thickening 17 mm), inhomogeneously hyperdense after contrast medium injection, of a jejunal ileal loop (length: 20 cm) located in the left side and left upper quadrant (red circle). Moreover, endoluminal dilatation and air-fluid level inside and enlarged lymph nodes and the surrounding mesenteric fat can be noticed (arrowheads). (d) Infiltration of the left colonic and sigmoid bowel wall (arrow). (e) Thickened bowel walls are entwined with a newly formed lymphomatous mass of the left abdominal wall that infiltrates the left abdominal wall muscles and the superior edge of the left iliac muscle.

associated with a greater fibrotic component. Compared to the stenosis occurring in other malignancies, the one observed in stenosing lymphoma determines just a minimal, if any, dilation of the upstream bowel segments, and this is due to the absence of a desmoplastic reaction.

The *mesenteric* pattern is characterized by the development of lymphoid tissue outside of the intestinal wall through the adventitia, extending in the context of nearby structures, in particular in the mesentery. In this form, lymphomas present as large exophytic masses (bulky appearance) with secondary involvement of surrounding tissues. The diameter of 70% of these tumours is at diagnosis larger than 5 cm [34, 37]. In the larger masses, larger ulcerative complications, tissue necrosis, perforation, and enteroenteric fistula formation are not uncommon [37].

Differential diagnosis includes all inflammatory, neoplastic, and metastatic lesions involving the small bowel. Primary carcinoma, metastases (especially those from melanoma and renal cancer), and the intestinal leiomyosarcoma are characterized by large necrotic/colliquative cavitations. In rare cases, inflammatory conditions, such as Crohn's disease and intestinal tuberculosis, have to be differentiated: the significant thickening of the bowel wall (greater than 2 cm), the presence of lymphomatous nodules, and the coexistence of perivisceral multiple lymph nodes are CT features that are suggestive for a lymphoproliferative process. On the other

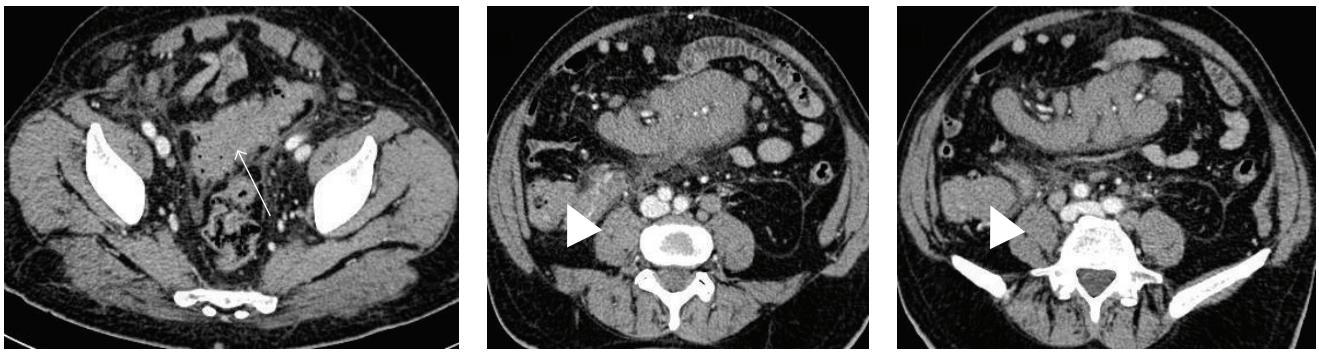

(a) (b) (c)

Figure 5: Abdominal CT scan of ileal and sigmoid lymphoma in a 78-year-old male. Axial CT scan in the portal venous phase shows a non-Hodgkin lymphoma seen as abnormal circumferential bowel thickening of the sigmoid colon ((a) arrow) and of the last ileal loop ((b) and (c) arrowheads). Enhanced lymphomatous small bowel loops (b) represent the halves of a sandwich, enveloping enhanced vessels (the sandwich filling). The patient underwent chemotherapy with marked reduction of the thickening at the follow-up CT scan.

hand, discontinuous, segmental circumferential thickening (thickness of approximately 0.5–2 cm), with symmetrical and circumferential contrast enhancement, characterized by alternation of hyperdense mucosa, a submucosal hypodense halo (halo-sign), and a hyperdense outer layer, suggests inflammatory diseases [40].

5. Large Bowel Lymphoma

Primary lymphoma of the *large bowel* accounts for 0.4% of all tumours of the colon, and colorectal lymphomas constitute 6%–12% of gastrointestinal lymphomas [26]. The cecum and rectum are most commonly affected parts compared to other tracts of the large bowel [5].

Primary large bowel lymphoma may appear as localized, large, extraluminal masses or constricting simulating annular-type carcinomas and may present with *different radiological patterns* that are often quite similar to other large bowel tumours or inflammatory diseases, thus leading to a difficult differential diagnosis [3]. These patterns include bulky polypoidal mass, focal infiltrative tumour, and aneurismal dilatation [3].

On barium studies and on CT the most common pattern is the polypoid one: polyps may vary from few millimetres to 20 centimetres and are mainly located in the ileocecal valve. Usually, bulky lymphomatoid polypoid masses are larger than the ones that can be encountered in colorectal adenocarcinomas and may extend beyond the bowel wall, thus presenting as enormous peritoneal masses, that can also be cavitated [27].

Colorectal lymphomas may also present as a concentric circumferential bowel wall thickening (with or without ulceration) or as exophytic tumours, mucosal nodularity, and fold thickening (Figure 5) [26]. Furthermore, focal strictures, aneurismal dilatation, or ulcerative forms with fistula formation may be encountered [26]. However, some features as well-defined margins with preserved fat planes, absence of involvement of adjacent structures, and perforation without any desmoplastic response may help in the differential diagnosis of lymphoma from adenocarcinoma [7]. The latter feature is responsible for the fact that obstruction is less frequent in lymphoma compared to adenocarcinoma [7].

Colonic lymphoma usually presents with larger lesions and involves a longer segment compared to adenocarcinoma; moreover, colonic lymphoma is usually located near the ileocaecal valve and grows into the terminal ileum, not invading or obstructing neighbouring viscera [41].

However, there are no imaging findings pathognomonic for lymphoma.

GI lymphoma has a wide variety of morphological imaging features at conventional and cross-sectional imaging. The goal of the radiologist when there is a clinical suspicion of GI lymphoma is to provide a diagnosis according to the WHO classification in order to provide an optimal treatment to patients. Fiberoptic endoscopy of the GI tract has still a pivotal role in the evaluation of lymphoma occurring in the oesophagus or in the stomach; however it does not allow the evaluation of concomitant localization of the lymphoma in the GI tract, as CT does.

In patients with obscure bleeding with negative gastroscopy and colonoscopy, video capsule endoscopy is usually the preferred imaging technique for the detection of mucosal abnormalities; however, it is contraindicated to use video capsule in suspected stenosis or obstruction, because of the risk of its retention, while CT can be performed in these patients.

Moreover, while conventional imaging provides just suggestive findings of the presence of the disease, cross-sectional imaging plays an emerging role in the diagnosis and staging of GI lymphoma.

The main imaging appearance of GI lymphoma may be summarized as follows:

(i) Diffuse infiltrative form, which is characterized by a circumferential wall thickening of the involved GI wall, leading to destruction of the muscularis propria and autonomic plexus and subsequent dilatation of the involved segment.

(ii) Focal GI involvement, which may appear as a solitary or multiple nodular involvement.

(iii) Ulcerative form.

Thanks to CT it is possible to study not only the GI tract using enterography technique, but also local and distant lymph nodes and other thoracic and abdominal organs that can be affected also by the disease, thus allowing an imaging staging of the disease according to the classification of the Consensus Conference of Lugano [13].

The role of CT is also considered pivotal in the evaluation of complications of the disease, as perforation, fistulisation, and obstruction, and in the differential diagnosis with other neoplastic or inflammatory conditions, which may also coexist with the lymphoma [42].

Lastly, CT must be actually considered also the preferred technique for the evaluation of response to therapy when medical therapy with targeted therapy is used; in this case according to the used drug, the imaging appearance may be substantially different.

However, CT has still many limitations for staging, restaging, and response to therapy assessment of lymphoma [43]. To date, 2-[fluorine-18]fluoro-2-deoxy-d-glucose (FDG) positron emission tomography (PET) is considered the imaging modality of choice for staging and follow-up in Hodgkin disease and most non-Hodgkin lymphomas [44]. In particular, considering GI lymphoma, FDG uptake is different according to the different location: esophageal lymphoma manifests as circumferential thickening of the esophageal wall with increased FDG uptake; gastric lymphoma presents with a variable, usually diffuse FDG uptake that can involve all portions of the stomach and that is usually higher than the liver one; small bowel lymphoma is characterized on FDG PET/CT by the presence of multiple foci of intense radiotracer activity arranged in a curvilinear pattern; finally, large bowel lymphoma manifests with a characteristic pattern of uptake consisting of focal, nodular, or diffuse hypermetabolic activity [44]. However, normal peristaltic activity, normal gastrointestinal lymphoid tissue, and granulomatous or inflammatory conditions represent a limit of the PET/CT for the evaluation of possible lymphomatous involvement in both small and large bowel lymphoma [44].

On the other hand, MR provides a better evaluation of the bowel wall and of the local infiltration by the disease. Whole-body MR with diffusion weighted imaging proved to be useful in nodal and bone marrow staging of lymphoma [45]. Concerning GI lymphoma, diffusion weighted imaging proved to be useful in the detection of gastric lymphoma, since the latter shows an increased signal on diffusion weighted imaging sequence and decreased signal on apparent diffusion coefficient maps, and in the differentiation from adenocarcinoma with significantly lower apparent diffusion coefficient values of adenocarcinoma compared to lymphoma [46]. According to our opinion, also for small bowel lymphoma, diffusion weighted imaging may help in its detection. However, MR study is mainly focused on the evaluation of the gastrointestinal tract, not allowing an accurate evaluation of the thoracic and other abdominal organs.

However, although findings of the different imaging techniques may be suspicious for lymphoma, tissue biopsy is always necessary for a specific diagnosis.

Conflict of Interests

The authors declare that there is no conflict of interests regarding the publication of this paper.

References

[1] H. Bäck, B. Gustavson, B. Ridell, S. Rödjer, and J. Westin, "Primary gastrointestinal lymphoma incidence, clinical presentation, and surgical approach," *Journal of Surgical Oncology*, vol. 33, no. 4, pp. 234–238, 1986.

[2] P. Ghimire, G.-Y. Wu, and L. Zhu, "Primary gastrointestinal lymphoma," *World Journal of Gastroenterology*, vol. 17, no. 6, pp. 697–707, 2011.

[3] M. S. Levine, S. E. Rubesin, L. Pantongrag-Brown, J. L. Buck, and H. Herlinger, "Non-Hodgkin's lymphoma of the gastrointestinal tract: radiographic findings," *American Journal of Roentgenology*, vol. 168, no. 1, pp. 165–172, 1997.

[4] R. E. Cupps, J. R. Hodgson, M. B. Dockerty, and M. A. Adson, "Primary lymphoma in the small intestine: problems of roentgenologic diagnosis," *Radiology*, vol. 92, no. 6, pp. 1354–1362, 1969.

[5] J. M. W. Van de Water, S. A. G. M. Cillessen, O. J. Visser, W. H. M. Verbeek, C. J. L. M. Meijer, and C. J. J. Mulder, "Enteropathy associated T-cell lymphoma and its precursor lesions," *Best Practice and Research: Clinical Gastroenterology*, vol. 24, no. 1, pp. 43–56, 2010.

[6] A. D. G. Krol, S. le Cessie, S. Snijder, J. C. Kluin-Nelemans, P. M. Kluin, and E. M. Noordijk, "Primary extranodal non-Hodgkin's lymphoma (NHL): the impact of alternative definitions tested in the Comprehensive Cancer Centre West population-based NHL registry," *Annals of Oncology*, vol. 14, no. 1, pp. 131–139, 2003.

[7] S. Ghai, J. Pattison, S. Ghai, M. E. O'Malley, K. Khalili, and M. Stephens, "Primary gastrointestinal lymphoma: spectrum of imaging findings with pathologic correlation," *Radiographics*, vol. 27, no. 5, pp. 1371–1388, 2007.

[8] G. Masselli, E. Polettini, E. Casciani, L. Bertini, A. Vecchioli, and G. Gualdi, "Small-bowel neoplasms: prospective evaluation of MR enteroclysis," *Radiology*, vol. 251, no. 3, pp. 743–750, 2009.

[9] C. Smith, R. A. Kubicka, and C. R. Thomas Jr., "Non-Hodgkin lymphoma of the gastrointestinal tract," *RadioGraphics*, vol. 12, no. 5, pp. 887–899, 1992.

[10] R. B. Lewis, A. K. Mehrotra, P. Rodríguez, M. A. Manning, and M. S. Levine, "From the radiologic pathology archives: gastrointestinal lymphoma: radiologic and pathologic findings," *RadioGraphics*, vol. 34, no. 7, pp. 1934–1953, 2014.

[11] A. Laghi and R. Passariello, "La risonanza magnetica nello studio del piccolo intestino," *La Radiologia Medica*, vol. 106, pp. 1–17, 2003.

[12] K. Sandrasegaran, A. Rajesh, J. Rydberg, D. A. Rushing, F. M. Akisik, and J. D. Henley, "Gastrointestinal stromal tumors: clinical, radiologic, and pathologic features," *American Journal of Roentgenology*, vol. 184, no. 3, pp. 803–811, 2005.

[13] A. Rohatiner, F. d'Amore, B. Coiffier, and et al, "Report on a workshop convened to discuss the pathological and staging

classifications of gastrointestinal tract lymphoma," *Annals of Oncology*, vol. 5, no. 5, pp. 397–400, 1994.

[14] J. C. Peng, L. Zhong, and Z. H. Ran, "Primary lymphomas in the gastrointestinal tract," *Journal of Digestive Diseases*, vol. 16, no. 4, pp. 169–176, 2015.

[15] P. G. Isaacson and D. H. Wright, "Extranodal malignant lymphoma arising from mucosa-associated lymphoid tissue," *Cancer*, vol. 53, no. 11, pp. 2515–2524, 1984.

[16] P. G. Isaacson, J. Spencer, and T. Finn, "Primary B-cell gastric lymphoma," *Human Pathology*, vol. 17, no. 1, pp. 72–82, 1986.

[17] P. G. Isaacson, "Gastrointestinal lymphoma," *Human Pathology*, vol. 25, no. 10, pp. 1020–1029, 1994.

[18] L. Bolondi, P. Casanova, G. C. Caletti, W. Grigioni, L. Zani, and L. Barbara, "Primary gastric lymphoma versus gastric carcinoma: endoscopic US evaluation," *Radiology*, vol. 165, no. 3, pp. 821–826, 1987.

[19] G. Caletti, P. L. Zinzani, P. Fusaroli et al., "The importance of endoscopic ultrasonography in the management of low-grade gastric mucosa-associated lymphoid tissue lymphoma," *Alimentary Pharmacology & Therapeutics*, vol. 16, no. 10, pp. 1715–1722, 2002.

[20] E. J. Balthazar, M. Noordhoorn, A. J. Megibow, and R. B. Gordon, "CT of small-bowel lymphoma in immunocompetent patients and patients with AIDS: comparison of findings," *American Journal of Roentgenology*, vol. 168, no. 3, pp. 675–680, 1997.

[21] T. Sato, Y. Sakai, S. Ishiguro, and H. Furukawa, "Radiologic manifestations of early gastric lymphoma," *American Journal of Roentgenology*, vol. 146, no. 3, pp. 513–518, 1986.

[22] L. S. Menuck, "Gastric lymphoma, a radiologic diagnosis," *Gastrointestinal Radiology*, vol. 1, no. 2, pp. 157–161, 1976.

[23] H. Hricak, R. F. Thoeni, A. R. Margulis, W. R. Eyler, and I. R. Francis, "Extension of gastric lymphoma into the esophagus and duodenum," *Radiology*, vol. 135, no. 2, pp. 309–312, 1980.

[24] J. N. Buy and A. A. Moss, "Computed tomography of gastric lymphoma," *American Journal of Roentgenology*, vol. 138, no. 5, pp. 859–865, 1982.

[25] M.-S. Park, K. W. Kim, J.-S. Yu et al., "Radiographic findings of primary B-cell lymphoma of the stomach: low-grade versus high-grade malignancy in relation to the mucosa-associated lymphoid tissue concept," *American Journal of Roentgenology*, vol. 179, no. 5, pp. 1297–1304, 2002.

[26] D. Choi, H. K. Lim, S. J. Lee et al., "Gastric mucosa-associated lymphoid tissue lymphoma: helical CT findings and pathologic correlation," *American Journal of Roentgenology*, vol. 178, no. 5, pp. 1117–1122, 2002.

[27] G. Guglielmi, F. Schiavon, and T. Cammarota, Eds., *Radiologia geriatrica*, Springer, 2006.

[28] D. D. T. Maglinte, "Capsule imaging and the role of radiology in the investigation of diseases of the small bowel," *Radiology*, vol. 236, no. 3, pp. 763–767, 2005.

[29] A. K. Hara, J. A. Leighton, V. K. Sharma, R. I. Heigh, and D. E. Fleischer, "Imaging of small bowel disease: comparison of capsule endoscopy, standard endoscopy, barium examination, and CT," *Radiographics*, vol. 25, no. 3, pp. 697–711, 2005.

[30] I. M. Dawson, J. S. Cornes, and B. C. Morson, "Primary malignant lymphoid tumors of the intestinal tract. Report of 37 cases with a study of factors influencing prognosis," *British Journal of Surgery*, vol. 49, pp. 80–89, 1961.

[31] S. H. Swerdlow, E. Campo, N. L. Harris et al., Eds., *WHO Classification of Tumours of Haematopoietic and Lymphoid Tissues*, International Agency for Research on Cancer, Lyon, France, 4th edition, 2008.

[32] T. Heye, D. Stein, D. Antolovic, M. Dueck, H.-U. Kauczor, and W. Hosch, "Evaluation of bowel peristalsis by dynamic cine MRI: detection of relevant functional disturbances—initial experience," *Journal of Magnetic Resonance Imaging*, vol. 35, no. 4, pp. 859–867, 2012.

[33] L. M. Minordi, A. Vecchioli, P. Mirk, E. Filigrana, G. Poloni, and L. Bonomo, "Multidetector CT in small-bowel neoplasms," *Radiologia Medica*, vol. 112, no. 7, pp. 1013–1025, 2007.

[34] F. Crusco, F. Pugliese, A. Maselli et al., "Malignant small-bowel neoplasms: spectrum of disease on MR imaging," *Radiologia Medica*, vol. 115, no. 8, pp. 1279–1291, 2010.

[35] G. Masselli, M. C. Colaiacomo, G. Marcelli et al., "MRI of the small-bowel: how to differentiate primary neoplasms and mimickers," *British Journal of Radiology*, vol. 85, no. 1014, pp. 824–837, 2012.

[36] J. A. Buckley and E. K. Fishman, "CT evaluation of small bowel neoplasms: spectrum of disease," *Radiographics*, vol. 18, no. 2, pp. 379–392, 1998.

[37] C. Smith, R. A. Kubicka, and C. R. Thomas Jr., "Non-hodgkin lymphoma of the gastrointestinal tract," *Radiographics*, vol. 12, no. 5, pp. 887–899, 1992.

[38] J. Norfray, L. Calenoff, and B. Zanon Jr., "Aneurysmal lymphoma of the small intestine," *American Journal of Roentgenology*, vol. 119, no. 2, pp. 335–341, 1973.

[39] Z. V. Maizlin, J. A. Brown, M. R. E. Buckley et al., "Case of the season: aneurysmal dilatation of the small bowel (not only lymphoma)," *Seminars in Roentgenology*, vol. 41, no. 4, pp. 248–249, 2006.

[40] G. Lo Re, M. Cappello, C. Tudisca et al., "CT enterography as a powerful tool for the evaluation of inflammatory activity in Crohn's disease: relationship of CT findings with CDAI and acute-phase reactants," *Radiologia Medica*, vol. 119, no. 9, pp. 658–666, 2014.

[41] C. Beaton, M. Davies, and J. Beynon, "The management of primary small bowel and colon lymphoma—a review," *International Journal of Colorectal Disease*, vol. 27, no. 5, pp. 555–563, 2012.

[42] M. Galia, F. Agnello, L. La Grutta et al., "Computed tomography of bowel obstruction: tricks of the trade," *Expert Review of Gastroenterology & Hepatology*, vol. 9, pp. 1115–1125, 2015.

[43] L. Kostakoglu and S. J. Goldsmith, "Fluorine-18 fluorodeoxyglucose positron emission tomography in the staging and follow-up of lymphoma: is it time to shift gears?" *European Journal of Nuclear Medicine*, vol. 27, no. 10, pp. 1564–1578, 2000.

[44] F. M. Paes, D. G. Kalkanis, P. A. Sideras, and A. N. Serafini, "FDG PET/CT of extranodal involvement in non-Hodgkin lymphoma and Hodgkin disease," *Radiographics*, vol. 30, no. 1, pp. 269–291, 2010.

[45] J. Gu, T. Chan, J. Zhang, A. Y. H. Leung, Y.-L. Kwong, and P.-L. Khong, "Whole-body diffusion-weighted imaging: the added value to whole-body MRI at initial diagnosis of lymphoma," *American Journal of Roentgenology*, vol. 197, no. 3, pp. W384–W391, 2011.

[46] S. Avcu, H. Arslan, O. Unal, C. Kotan, and M. Izmirli, "The role of diffusion-weighted MR imaging and ADC values in the diagnosis of gastric tumors," *JBR-BTR*, vol. 95, no. 1, pp. 1–5, 2012.

Hindawi Publishing Corporation
Gastroenterology Research and Practice
Volume 2015, Article ID 670965, 10 pages
http://dx.doi.org/10.1155/2015/670965

Review Article

CT Appearance of Hepatocellular Carcinoma after Locoregional Treatments: A Comprehensive Review

Daniel Marin,[1] Salvatore Cappabianca,[2] Nicola Serra,[2] Assunta Sica,[2] Francesco Lassandro,[3] Roberto D'Angelo,[4] Michelearcangelo La Porta,[5] Francesco Fiore,[4] and Francesco Somma[2]

[1]*Department of Radiology, Duke University, Durham, NC 27701, USA*
[2]*Department of Radiology, Second University of Naples, 80131 Naples, Italy*
[3]*Department of Radiology, Monaldi Hospital, 80131 Naples, Italy*
[4]*Department of Interventional Radiology, National Cancer Institute, "Fond. Pascale", 80131 Naples, Italy*
[5]*Department of Radiology, UOC San Severo Hospital, 71016 San Severo, Italy*

Correspondence should be addressed to Francesco Somma; fra1585@hotmail.it

Received 15 June 2015; Revised 9 September 2015; Accepted 14 September 2015

Academic Editor: Mitsuro Kanda

Hepatocellular carcinoma (HCC) is a major health problem worldwide, affecting more than 600,000 new patients per year. Curative treatments are available in a small percentage of patients, while most of them present in stages requiring locoregional treatments such as thermoablation, transarterial chemoembolization, and/or radioembolization. These therapies result in specific imaging features that the general radiologist has to be aware of in order to assess the response to treatment and to correctly manage the follow-up of treated patients. Multiphasic helical computed tomography has become a popular imaging modality for detecting hypervascular tumors and characterizing liver lesions. On this basis, many staging and diagnostic systems have been proposed for evaluating response to all different existing strategies. Radiofrequencies and microwaves generate thermoablation of tumors, and transarterial chemoembolization exploits the double effect of the locoregional administration of drugs and embolizing particles. Eventually radioembolization uses a beta-emitting isotope to induce necrosis. Therefore, the aim of this comprehensive review is to analyze and compare CT imaging appearance of HCC after various locoregional treatments, with regard to specific indications for all possible procedures.

1. Introduction

Hepatocellular carcinoma (HCC) is a major health problem worldwide, affecting more than 600,000 new patients per year [1]. Curative treatments are hepatic resection, liver transplantation, and percutaneous ablation [2]. Unfortunately, such treatments are generally indicated in less than 20% of patients [3, 4], while most of them present with advanced-stage disease or multifocal tumor, contraindicating any radical treatment option [5]. To date, several alternative approaches have been proposed, both systemic or locoregional [6]. Some of them such as transarterial chemoembolization (TACE) or radioembolization (TARE) are also used as a bridge to liver transplantation or to downstage tumors exceeding Milan criteria [7–11]. Some others, such as thermoablation using microwaves or radiofrequency, are designed to destroy tumors by heating tissue to temperatures higher than 60°C [12–14]. Irrespective of which locoregional treatment is performed, imaging plays a pivotal role in the follow-up of hepatic tumors, as it is the means by which local treatment efficacy, recurrent disease, and therapy-induced complications are evaluated [15]. Nowadays, multidetector computed tomography (MDCT) is still the most widely used imaging technique to describe the appearance of hepatic tumors treated with locoregional therapies. Moreover, it allows us to accurately assess the response to therapy through the evaluation of tumor size, tumor margins, tumor necrosis, and early detection of residual or recurrent tumor and new

tumor. The evaluation of treatment success is crucial in the next treatment decisions and for prognosis [16]. Therefore, the aim of this paper is to review and compare CT imaging appearance of HCC after various locoregional treatments.

2. Locoregional Treatment Options for HCC

The Barcelona Clinic Liver Cancer classification has been widely accepted as guideline for all therapies available in different stages of HCC [17]. This staging system links the stage of the disease to a specific treatment strategy, such as curative treatments or palliative therapies. Very early-stage (BCLC Stage 0) and early-stage HCC (BCLC Stage A) are still amenable to potentially curative therapies, such as hepatic resection, liver transplantation [2], providing best 5-year survival of more than 50% [18]. In case of focused disease with no extrahepatic spread, resection is the first-choice treatment, even if transplantation is preferred by many authors because, if possible, it removes underlying diseased liver that predisposes to the development of new hepatic lesions [19]. However, most patients show intermediate (BCLC Stage B) or advanced HCC (BCLC Stage C) at presentation, thus making sorafenib or locoregional treatments recommended [20]. These therapies have the advantages of preserving a larger part of hepatic parenchyma with overall less morbidity and mortality compared with resection, thanks to reduced intraoperative blood loss [21–24]. The most used locoregional treatment is the imaging-guided percutaneous thermal ablation using radiofrequency (RFA) or microwaves, transarterial chemoembolization (TACE), and radioembolization (TARE). Moreover, RFA is also used during nonconventional liver resection to obtain parenchymal dissection by creating a zone of coagulative necrosis along the transection plane [25]. This technique is indicated in patients with preserved liver function and single HCC, ideally in subcapsular position [26], reducing the risk of intraoperative blood loss when compared with conventional liver resection [25, 27]. Instead, percutaneous RFA is indicated for early-stage HCC in patients who are not suitable candidates for resection. In particular, this technique showed being more efficient than percutaneous ethanol ablation in tumors with a diameter greater than 3 cm [28]. Differently from ethanol, thermal ablation is not chemical but uses high temperatures to induce cellular disruption and tissue coagulation necrosis [29]. Patients with very early-stage HCC show complete response rates of 97% with 5-year survival rates of 68% [30]. However, vessels greater than 3 mm in diameter surrounding the site of ablation may limit RFA action, due to heat loss caused by perfusion-mediated tissue cooling [10]. This is not a limit for methods using microwaves. Indeed, despite the little amount of studies on effectiveness, microwave methods are currently emerging thanks to the many advantages, such as larger tumor ablation volumes, faster tumor ablation, and the resistance to tissue cooling due to adjacent vessels [31]. Intermediate-stage and advanced-stage HCC with no extrahepatic spread are rather suitable for transarterial therapies, such as TACE or TARE. Contrary to normal liver, HCC receives blood supply almost entirely by hepatic artery, thus making transarterial therapies effective on HCC lesions only. Iodized oil acts as a drug carrier, while embolizing particles occlude the tumor feeding arteries. On the basis of randomized controlled trials [32–34], TACE has been recommended by BCLC as the standard of choice in case of multiple or big lesions with no vascular invasion or extrahepatic spread and for lesions not accessible percutaneously. This method consists of a transarterial administration of chemotherapy, mostly Doxorubicin, mixed with iodized oil (Lipiodol, Guerbet, France), followed by the superselective injection of embolizing particles (polyvinyl alcohol (PVA)) [35]. On the other hand, TARE has emerged for the treatment of advanced-stage HCCs, that is, in patients nonresponding to TACE, in elderly patients with large HCCs, in case of vascular invasion, and prior to liver resection in order to downstage tumor [36] (Figure 1). It consists of releasing microspheres containing yttrium-90, a β-emitting isotope, straight in the tumor feeding arteries after superselective catheterization. In this way, high-energy, low-penetration radiation causes tumor destruction by coagulative necrosis and avascularity [37]. Some studies have shown the efficacy of this therapy to be similar to TACE, with lower toxicity [38–40]. TARE has also shown an overall survival outcome similar to sorafenib, in particular in patients with segmental and main portal vein tumor thrombosis [41, 42].

3. MDCT Technique for HCC Evaluation

Multiphasic helical CT has become a popular imaging modality for detecting hypervascular tumors and characterizing liver lesions. In patients with cirrhosis, MDCT performed during the hepatic arterial phase and portal venous phase is often used as the first-line diagnostic modality for detection of HCC, follow-up after local treatment or surgical excision, and assessment of hemodynamic changes in the liver [43]. Despite its high reliability in examining patients with HCC, it is unclear whether biphasic MDCT is the best technique to evaluate the effects of locoregional therapies and the possibility of tumor recurrence. Contrast-enhanced magnetic resonance imaging (MRI) has also been assessed as a valuable method to study patients with HCC, especially after transcatheter arterial therapies, such as TACE and TARE [44]. In particular, lesions treated with RFA or TACE typically undergo coagulative hemorrhagic necrosis that may appear hyperintense on unenhanced T1-weighted imaging, making contrast-enhanced evaluation difficult [45]. Image subtraction techniques with MRI have been shown to be beneficial in depicting residual enhancement, with excellent correlation with histopathologic degree of tumor necrosis [46]. However, the increased cost and comparative lack of availability of this modality make MDCT the mainstay of liver and HCC imaging for both initial tumor characterization and posttreatment follow-up for response assessment [47–49]. MDCT uses 16, 62, 128, or even more contiguous detectors to increase effective pitch without consequent loss of spatial resolution along the axis of scanning, thus allowing thin-section images to be obtained in a single breath-hold with greatly improved speed and longitudinal resolution, resulting in high-resolution multiplanar reformations. For patients with HCC eligible for liver transplantation, the United Network for

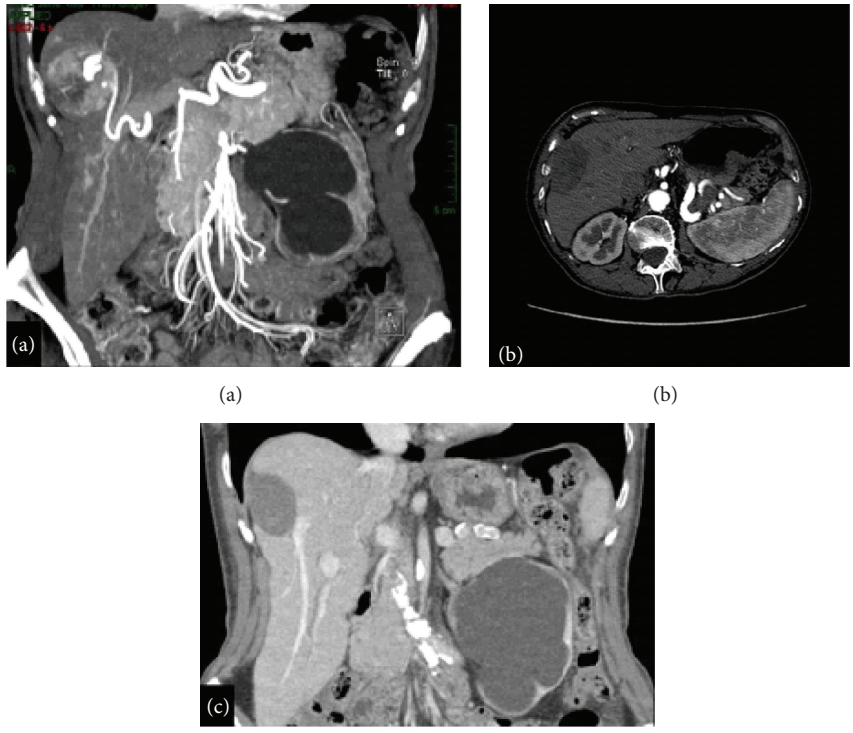

Figure 1: RFA. HCC of the 7th segment treated with RFA: (a) before treatment, MDCT arterial phase with multiplanar reconstruction; (b) 6 months after treatment, MDCT arterial phase; (c) 12 months after treatment, MDCT portal phase with multiplanar reconstruction.

Organ Sharing currently recommends the use of a quadruple-phase CT protocol that includes unenhanced images (to characterize residual enhancement in posttreatment cases), a single late arterial phase based on a bolus-tracking method (for accurate peak arterial enhancement), a portal venous phase, and a late venous phase, respectively, at 70 and 120 seconds after iodine contrast injection at a rate of 4-5 mL/s [50] (Figure 2).

4. Assessment of Tumor Response in HCC

In the past, tumor response evaluation systems have focused on anatomic biomarkers. The Response Evaluation Criteria in Solid Tumors (RECIST) considered the largest diameter of the lesion and was intended to evaluate changes in tumor size over months to years after systemic treatments, without taking into account changes in tumor tissue composition [51, 52]. Similarly, the World Health Organization (WHO) guidelines consider bidimensional perpendicular measurements [53]. However, these systems fail in evaluating the outcome of locoregional therapies, because the aim of these treatments is to obtain the tumor necrosis rather than the lesion removal. Indeed, after these therapies, HCC is likely to increase in size because of intratumoral edema, hemorrhage, or necrosis [54]. Due to these limitations, new criteria have been proposed by European Association for the Study of the Liver (EASL) [26], which modified the previous bidimensional measurements proposed by the WHO guidelines. More recently, the modified RECIST has been introduced in order to address many shortcomings affecting older evaluation systems [55]. As the unmodified RECIST, the modified version uses the single largest diameter of the tumor, considering only the component enhancing during the arterial phase [52]. This system is based on dynamic MDCT examination performed 1 month after locoregional therapy and has been endorsed by EASL and European Organization for Research and Treatment of Cancer (EORTC) [56].

However, even modified RECIST has some limitations, especially in the assessment of response after RFA and TARE, since these criteria are difficult to apply with confidence in the measurement of diffusely necrotic lesions with interspersed viable components [57]. Therefore, a previous study proposed a reduction in volume as standard of reference for tumor response [51], with partial response representing a volume reduction of 65% according to standard oncologic criteria.

5. Appearance of Treated HCC

5.1. Overall Considerations. Due to the exceedingly complex therapeutic approach to HCC, a therapy-tailored imaging evaluation of tumor response in HCC is mandatory [58]. Indeed, the correct evaluation of posttherapeutic changes in tumor viability and vascularization may alter the management of the patient, with regard to the treatments to perform. This is particularly true in case of locoregional treatments, whose ultimate goal is the tumor cell death and necrosis, with sparing of healthy surrounding tissue [59].

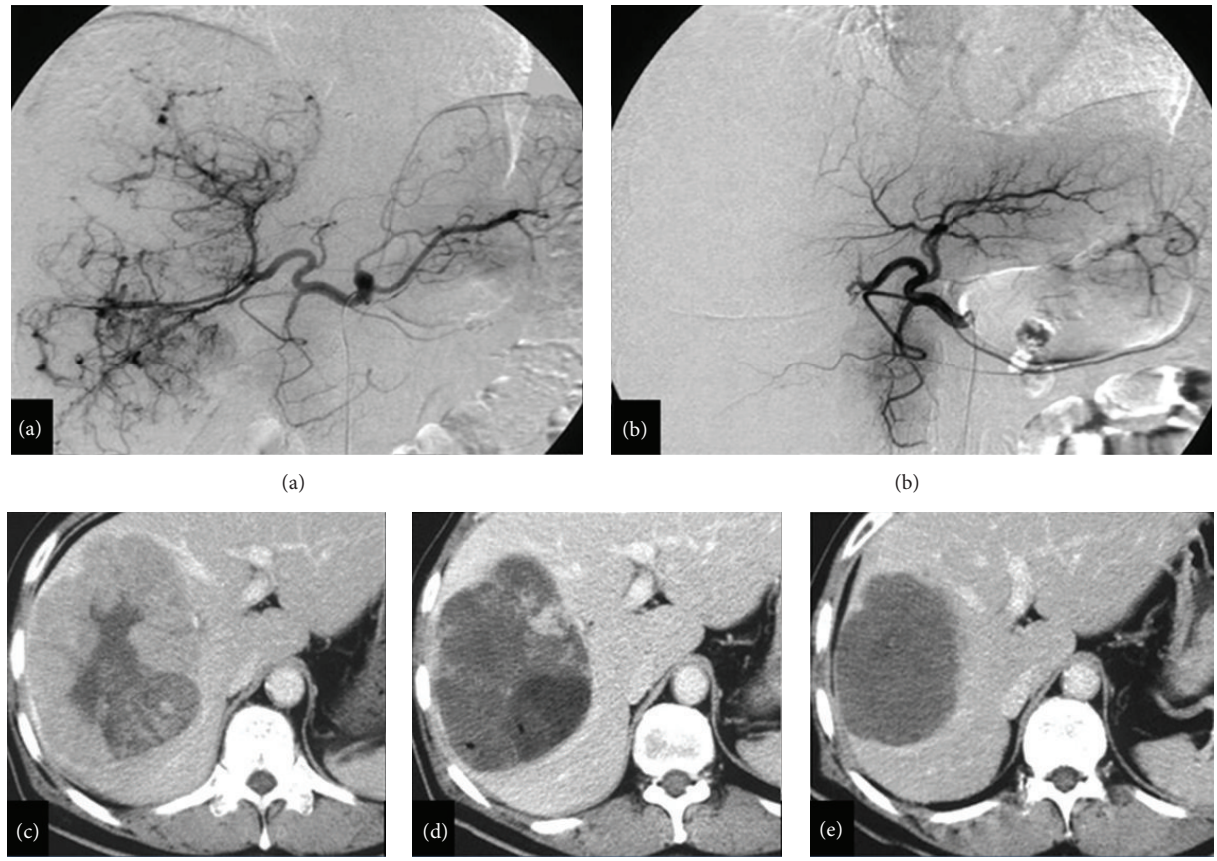

Figure 2: TACE. Large HCC treated with TACE: (a) before treatment, angiography; (b) after treatment, angiography; (c) before treatment, MDCT arterial phase; (d) 1-month assessment control after treatment, MDCT arterial phase; (e) 12 months after treatment, MDCT arterial phase.

5.2. Imaging after RFA. The aim of this kind of treatment is to generate an area of thermocoagulation larger than the tumor, by forming a necrotic scar that usually shrinks very slowly with time. This fact makes WHO criteria not applicable in the response assessment of thermal ablation [60]. Previous reports [14, 61–63] show the reduced value of unenhanced US in the evaluation of RFA efficacy, due to the similar appearance of necrotic and viable tumor tissue on US images. The use of contrast medium may help [64]. Anyway, contrast-enhanced CT or MR imaging is at present considered the most useful modalities, using as major criterion of efficacy the absence of enhancement in RF-induced necrosis. Moreover some reports suggested high confidence of these modalities in the identification of the ablation area, with only 2 mm miscalculation of the coagulated necrosis measured at histologic examination [65, 66]. On unenhanced CT images, areas treated with RFA generally appear as homogeneously hypoattenuating or heterogeneous with interspersed hyperattenuating foci in a hypoattenuating area. Contrast-enhanced CT images may show no enhancement in case of successful treatment or some area of irregular enhancement in case of incomplete ablation. In the latter case, the enhanced area may appear as a thin rim surrounding the treated lesion or as a thick nodule abutting the site of RF ablation. Local regrowths are usually seen as irregular thickening of one margin of the treated area. Peripheral recurrence may be explained by lower energy deposition and reduced heating in the locations further from the needle electrode. Moreover, tissue perfusion lowers heat accumulation by cooling, thus allowing more likely recurrence close to larger vessels abutting the site of ablation [65]. Peripheral thin and regular rim of enhancement (<1 mm) may be seen at the later phase after contrast medium administration and represents a ring of vascularized inflammatory reaction with granulation tissue surrounding necrosis [67]. This finding should never be diagnosed as regrowth, whose contrast enhancement is always thicker and irregular [62]. Wedge-shaped enhancement in the liver parenchyma adjacent to the ablation site has also been described [15] and is probably due to peripheral arterioportal shunts caused either mechanically by needle puncture or physically by thermal damage. Treatment-related complications to look for during post-RFA imaging are intrahepatic abscesses at the site of ablation, necrosis along the path of the RF electrode, and segmental dilation of intrahepatic bile ducts in contact with the ablation area.

5.3. Imaging after Microwaves. Percutaneous microwave coagulation therapy is considered to be a possible treatment of unresectable small HCCs [68, 69], due to definite tissue necrosis around the electrode and hemostatic effect of microwave irradiation [70]. Contrast-enhanced CT is commonly used to assess the complete necrosis of the tissue and possible recurrence [71, 72]. However, CT findings after HCC ablation using microwaves may be challenging and sometimes tricky. Indeed, the use of this percutaneous modality often causes an early enhancement of the normal hepatic tissue around the treated area. This postprocedural sign is likely to be a transient reaction of normal tissue to thermal damage, as it is detectable also in other procedures inducing tissue heating. On histologic specimen, this finding has been explained with a massive sinusoidal dilatation at the boundary between the coagulated area and the surrounding normal tissue, determining a peripheral granulation tissue and fibrosis after treatment [73, 74]. After treatment, an increase of arterial blood flow may occur at the margin of the treated area, leading to hepatic hypoperfusion during the arterial phase as a result of inflammation changes caused by microwaves irradiation as well as radiofrequency thermal ablation [67, 75]. Moreover, the formation of arterioportal shunts is another source of abnormal enhancement mimicking hypervascular lesions [76, 77]. The arterioportal shunts are caused by the piercing of an artery in the portal tract by the needle. Therefore, they may be recognized as wedge-shaped areas of enhancement during the arterial phase on CT [78–80] and are essentially due to the number of punctures performed rather than to thermal changes.

5.4. Imaging after TACE. This modality consists of transarterial administration of a mixture of chemotherapy and embolizing particles directly in the tumor feeding arteries, after a superselective catheterization. Contrary to normal liver, HCC receives blood supply almost entirely from the hepatic artery, and this fact allows drug accumulation preferentially into HCC lesions. CT images evaluation of tumor response to TACE is based on the assumption that the necrotic area of the tumor retains iodized oil, with enhanced foci representing viable tissue. However, beam hardening artifacts due to iodized oil retention may conceal arterial enhancement [57]. Therefore, the use of unenhanced phase is crucial to detect any additional foci of viable tumor, when compared to biphasic CT [81]. In this case, an HCC treated with TACE is to be considered as viable if showing hyperattenuation or isoattenuation on hepatic arterial phase and hypoattenuation on unenhanced and portal venous phases. A thin peripheral pseudocapsule enhanced on hepatic arterial and delayed phases may be visualized, such as other arterioportal shunts due to small hepatic arteries chemically injured iodized oil. All of these lesions differ from viable tumor for the absence of any sign of washout. Possible complications of this therapy are hepatic artery dissection or thrombosis, biloma, hepatic abscess, and embolization of nontarget vessels, which may cause gastrointestinal ulcers, skin ulcerations, and/or cholecystitis [82, 83]. Moreover, this therapy often results in a postembolization syndrome that occurs in 60–80% of patients and consists of fatigue, transient abdominal pain, ileus, fever, and increased serum levels of liver enzymes and bilirubin [84]. Different procedures have been proposed to avoid this syndrome, such as the use of drug eluting beads [85], or the replacement of chemotherapy with ethanol [86], whose imaging does not differ from the conventional TACE.

5.5. Imaging after TARE. Radioembolization is an emerging transarterial therapy for the treatment of hepatic malignancies, involving the administration of micron-sized radioactive particles featuring yttrium 90 (^{90}Y), a pure beta emitter [87] (Figure 3). Once these particles lodge in the tumor feeding arterioles, they impart a very intense local radiotherapeutic effect [88], penetrating the surrounding tissue for approximately 1 cm in diameter. Before decaying to inactive zirconium 90, the emitting particles allow the administration of up to 150 Gy to specific target areas of the liver [89]. The carrier is a microsphere ranging from 20 to 60 μm in diameter, with the radioactive element bound directly in the resin (SIR spheres) or an integral constituent of the glass (TheraSphere). The predominance of arterial blood supply to the tumor grants a preferential deposition of microspheres in the lesions, minimizing irradiation to the normal parenchyma [90]. As the other ablative therapies, TARE induces an area of coagulative necrosis and relative avascularity with an overall reduction in tumor size, as a result of the lethal insult to cancer cells [26, 91]. Follow-up imaging is usually performed with multiphase CT 30 days after treatment and at regular 3-month intervals thereafter. On unenhanced CT images, coagulative necrosis generally results in homogeneously hypoattenuating area. Although uncommon, complete disappearance of tumor with no enhancement of the treated lesion may occasionally be seen. Differently from complete response, a partial response is seen in case of viable tumor volume reduction of more than 65% [51]. Other posttreatment findings are peritumoral edema and hemorrhage, due to a sort of inflammatory reaction to the intense radiation effects of ^{90}Y. This sign is tricky, when associated with apparent lesion enlargement and tumor progression if the assessment is made on the basis of the sole lesion size [92]. Another possible pitfall is the ring enhancement, due to the preferential flow of blood vessels to the periphery of the tumors as well as the intense radiation effect. Previous studies have shown that after TARE this finding represents fibrous rather than residual viable tissue [93] and may persist for months without necessarily implying residual tumor [94]. Contralateral liver hypertrophy has also been demonstrated in patients receiving TARE, with no alteration of normal liver function [95]. Further findings after TARE are capsular retraction, hepatic fibrosis, and portal hypertension, probably due to shrinkage of the tumor with resultant scar formation and nodularity in uninvolved area [92]. Eventually, in case of lesions close to the Glisson capsule and the right pleural space, the induced radiation may cause reactive perihepatic fluid and pleural effusions [96]. Hepatic abscess, biliary dyskinesia and cholecystitis, biloma and biliary necrosis, and radiation hepatitis may all represent complications of this therapy. Also peptic ulceration and gastritis are known

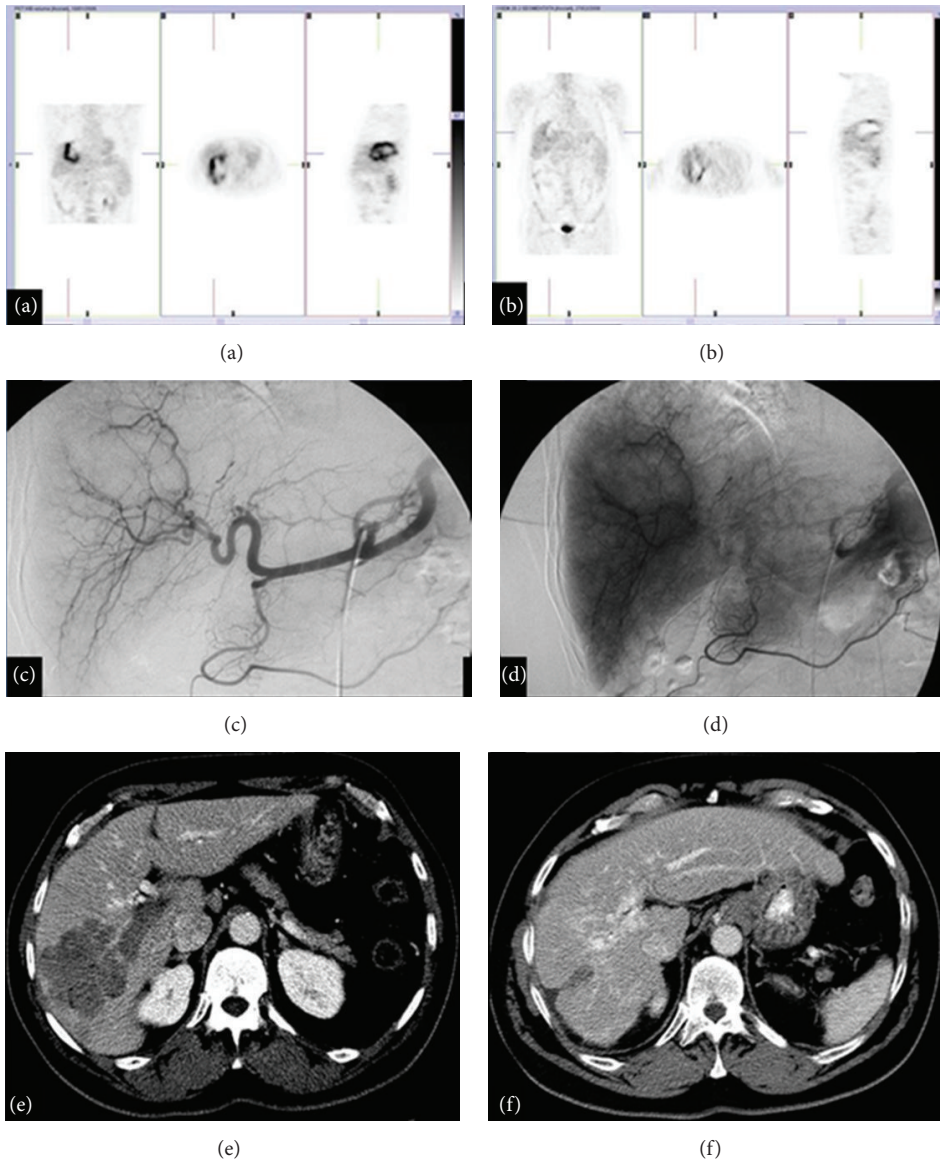

Figure 3: TARE. HCC treated with TARE: (a) before treatment, PET; (b) after treatment, PET; (c)-(d) during the procedure, angiography; (e) before treatment, MDCT arterial phase; (f) 12 months after treatment, MDCT arterial phase.

complications of radioactive ^{90}Y microsphere treatment, when deposited outside of the desired location [97].

6. Conclusion

The recent progress in HCC treatment involves the development of several locoregional therapies that allow a focused aggression on hepatic lesions, while sparing the surrounding normal parenchyma. The posttreatment evaluation of tumor response is a crucial milestone in directing the patient management, thus making the imaging appearance of treated HCC essential for accurately assessing treatment response. Therefore, the HCC appearance on multiphase CT after locoregional therapies is a challenging matter for every radiologist, who is asked to be able to distinguish the normal posttreatment alterations from residual or recurrent disease.

Disclosure

All authors of this paper declare no relationship with any company, whose products or services may be related to the subject matter of the paper.

Conflict of Interests

The authors declare that there is no conflict of interests regarding the publication of this paper.

References

[1] D. M. Parkin, F. Bray, J. Ferlay, and P. Pisani, "Global cancer statistics, 2002," *CA: A Cancer Journal for Clinicians*, vol. 55, no. 2, pp. 74–108, 2005.

[2] E. Liapi and J.-F. H. Geschwind, "Transcatheter and ablative therapeutic approaches for solid malignancies," *Journal of Clinical Oncology*, vol. 25, no. 8, pp. 978–986, 2007.

[3] A. E. Alsina, "Liver transplantation for hepatocellular carcinoma," *Cancer Control*, vol. 17, no. 2, pp. 83–86, 2010.

[4] J. M. Llovet, "Treatment of hepatocellular carcinoma," *Current Treatment Options in Gastroenterology*, vol. 7, no. 6, pp. 431–441, 2004.

[5] D. G. Farmer, M. H. Rosove, A. Shaked, and R. W. Busuttil, "Current treatment modalities for hepatocellular carcinoma," *Annals of Surgery*, vol. 219, no. 3, pp. 236–247, 1994.

[6] A. K. P. Shanbhogue, A. B. Karnad, and S. R. Prasad, "Tumor response evaluation in oncology: current update," *Journal of Computer Assisted Tomography*, vol. 34, no. 4, pp. 479–484, 2010.

[7] J. Bruix, M. Sala, and J. M. Llovet, "Chemoembolization for hepatocellular carcinoma," *Gastroenterology*, vol. 127, supplement 1, no. 5, pp. S179–S188, 2004.

[8] F. Y. Yao, R. Hirose, J. M. LaBerge et al., "A prospective study on downstaging of hepatocellular carcinoma prior to liver transplantation," *Liver Transplantation*, vol. 11, no. 12, pp. 1505–1514, 2005.

[9] J. M. Llovet, X. Mas, J. J. Aponte et al., "Cost effectiveness of adjuvant therapy for hepatocellular carcinoma during the waiting list for liver transplantation," *Gut*, vol. 50, no. 1, pp. 123–128, 2002.

[10] D. S. K. Lu, N. C. Yu, S. S. Raman et al., "Radiofrequency ablation of hepatocellular carcinoma: treatment success as defined by histologic examination of the explanted liver," *Radiology*, vol. 234, no. 3, pp. 954–960, 2005.

[11] F. Y. Yao, R. K. Kerlan Jr., R. Hirose et al., "Excellent outcome following down-staging of hepatocellular carcinoma prior to liver transplantation: an intention-to-treat analysis," *Hepatology*, vol. 48, no. 3, pp. 819–827, 2008.

[12] S. A. Curley, F. Izzo, P. Delrio et al., "Radiofrequency ablation of unresectable primary and metastatic hepatic malignancies: results in 123 patients," *Annals of Surgery*, vol. 230, no. 1, pp. 1–8, 1999.

[13] T. de Baere, D. Elias, C. Dromain et al., "Radiofrequency ablation of 100 hepatic metastases with a mean follow-up of more than 1 year," *American Journal of Roentgenology*, vol. 175, no. 6, pp. 1619–1625, 2000.

[14] L. Solbiati, S. N. Goldberg, T. Ierace et al., "Hepatic metastases: percutaneous radio-frequency ablation with cooled-tip electrodes," *Radiology*, vol. 205, no. 2, pp. 367–373, 1997.

[15] C. Dromain, T. De Baere, D. Elias et al., "Hepatic tumors treated with percutaneous radio-frequency ablation: CT and MR imaging follow-up," *Radiology*, vol. 223, no. 1, pp. 255–262, 2002.

[16] M. Mendizabal and K. R. Reddy, "Current management of hepatocellular carcinoma," *Medical Clinics of North America*, vol. 93, no. 4, pp. 885–900, 2009.

[17] A. Forner, J. M. Llovet, and J. Bruix, "Hepatocellular carcinoma," *The Lancet*, vol. 379, no. 9822, pp. 1245–1255, 2012.

[18] E. L. Kaplan and P. Meier, "Nonparametric estimation from incomplete observations," *Journal of the American Statistical Association*, vol. 53, no. 282, pp. 457–481, 1958.

[19] H. B. El-Serag and A. C. Mason, "Rising incidence of hepatocellular carcinoma in the United States," *The New England Journal of Medicine*, vol. 340, no. 10, pp. 745–750, 1999.

[20] J. Bruix and J. M. Llovet, "Major achievements in hepatocellular carcinoma," *The Lancet*, vol. 373, no. 9664, pp. 614–616, 2009.

[21] D. Franco, L. Capussotti, C. Smadja et al., "Resection of hepatocellular carcinomas—results in 72 European patients with cirrhosis," *Gastroenterology*, vol. 98, no. 3, pp. 733–738, 1990.

[22] S. Nakamura, S. Suzuki, and S. Baba, "Resection of liver metastases of colorectal carcinoma," *World Journal of Surgery*, vol. 21, no. 7, pp. 741–747, 1997.

[23] B. Ohlsson, U. Stenram, and K.-G. Tranberg, "Resection of colorectal liver metastases: 25-year experience," *World Journal of Surgery*, vol. 22, no. 3, pp. 268–277, 1998.

[24] T. Tsuzuki, A. Sugioka, M. Ueda et al., "Hepatic resection for hepatocellular carcinoma," *Surgery*, vol. 107, no. 5, pp. 511–520, 1990.

[25] G. Curro, L. Jiao, C. Scisca et al., "Radiofrequency-assisted liver resection in cirrhotic patients with hepatocellular carcinoma," *Journal of Surgical Oncology*, vol. 98, no. 6, pp. 407–410, 2008.

[26] J. Bruix and M. Sherman, "Management of hepatocellular carcinoma: an update," *Hepatology*, vol. 53, no. 3, pp. 1020–1022, 2011.

[27] K. S. Haghighi, F. Wang, J. King, S. Daniel, and D. L. Morris, "In-line radiofrequency ablation to minimize blood loss in hepatic parenchymal transection," *American Journal of Surgery*, vol. 190, no. 1, pp. 43–47, 2005.

[28] G. Germani, M. Pleguezuelo, K. Gurusamy, T. Meyer, G. Isgrò, and A. K. Burroughs, "Clinical outcomes of radiofrequency ablation, percutaneous alcohol and acetic acid injection for hepatocelullar carcinoma: a meta-analysis," *Journal of Hepatology*, vol. 52, no. 3, pp. 380–388, 2010.

[29] M.-S. Chen, J.-Q. Li, Y. Zheng et al., "A prospective randomized trial comparing percutaneous local ablative therapy and partial hepatectomy for small hepatocellular carcinoma," *Annals of Surgery*, vol. 243, no. 3, pp. 321–328, 2006.

[30] T. Livraghi, F. Meloni, M. Di Stasi et al., "Sustained complete response and complications rates after radiofrequency ablation of very early hepatocellular carcinoma in cirrhosis: is resection still the treatment of choice?" *Hepatology*, vol. 47, no. 1, pp. 82–89, 2008.

[31] N. C. Yu, S. S. Raman, Y. J. Kim, C. Lassman, X. Chang, and D. S. K. Lu, "Microwave liver ablation: influence of hepatic vein size on heat-sink effect in a porcine model," *Journal of Vascular and Interventional Radiology*, vol. 19, no. 7, pp. 1087–1092, 2008.

[32] J. M. Llovet and J. Bruix, "Systematic review of randomized trials for unresectable hepatocellular carcinoma: chemoembolization improves survival," *Hepatology*, vol. 37, no. 2, pp. 429–442, 2003.

[33] J. M. Llovet, M. I. Real, X. Montaña et al., "Arterial embolisation or chemoembolisation versus symptomatic treatment in patients with unresectable hepatocellular carcinoma: a randomised controlled trial," *The Lancet*, vol. 359, no. 9319, pp. 1734–1739, 2002.

[34] C.-M. Lo, H. Ngan, W.-K. Tso et al., "Randomized controlled trial of transarterial Lipiodol chemoembolization for unresectable hepatocellular carcinoma," *Hepatology*, vol. 35, no. 5, pp. 1164–1171, 2002.

[35] D. B. Brown, J. E. Gould, D. A. Gervais et al., "Transcatheter therapy for hepatic malignancy: standardization of terminology

and reporting criteria," *Journal of Vascular and Interventional Radiology*, vol. 20, no. 7, pp. S425–S434, 2009.

[36] R. J. Lewandowski, M. F. Mulcahy, L. M. Kulik et al., "Chemoembolization for hepatocellular carcinoma: comprehensive imaging and survival analysis in a 172-patient cohort," *Radiology*, vol. 255, no. 3, pp. 955–965, 2010.

[37] B. Atassi, A. K. Bangash, A. Bahrani et al., "Multimodality imaging following 90Y radioembolization: a comprehensive review and pictorial essay," *Radiographics*, vol. 28, no. 1, pp. 81–99, 2008.

[38] J. F. H. Geschwind, R. Salem, B. I. Carr et al., "Yttrium-90 microspheres for the treatment of hepatocellular carcinoma," *Gastroenterology*, vol. 127, pp. S194–S205, 2004.

[39] R. Salem, R. J. Lewandowski, B. Atassi et al., "Treatment of unresectable hepatocellular carcinoma with use of ^{90}Y microspheres (TheraSphere): safety, tumor response, and survival," *Journal of Vascular and Interventional Radiology*, vol. 16, no. 12, pp. 1627–1639, 2005.

[40] B. Sangro, J. I. Bilbao, J. Boan et al., "Radioembolization using 90Y-resin microspheres for patients with advanced hepatocellular carcinoma," *International Journal of Radiation Oncology Biology Physics*, vol. 66, no. 3, pp. 792–800, 2006.

[41] J. Luo, R.-P. Guo, E. C. H. Lai et al., "Transarterial chemoembolization for unresectable hepatocellular carcinoma with portal vein tumor thrombosis: a prospective comparative study," *Annals of Surgical Oncology*, vol. 18, no. 2, pp. 413–420, 2011.

[42] L. M. Kulik, B. I. Carr, M. F. Mulcahy et al., "Safety and efficacy of 90Y radiotherapy for hepatocellular carcinoma with and without portal vein thrombosis," *Hepatology*, vol. 47, no. 1, pp. 71–81, 2008.

[43] J. H. Oliver III and R. L. Baron, "Helical biphasic contrast-enhanced CT of the liver: technique, indications, interpretation, and pitfalls," *Radiology*, vol. 201, no. 1, pp. 1–14, 1996.

[44] K. Kubota, N. Hisa, T. Nishikawa et al., "Evaluation of hepatocellular carcinoma after treatment with transcatheter arterial chemoembolization: comparison of lipiodol-CT, power doppler sonography, and dynamic MRI," *Abdominal Imaging*, vol. 26, no. 2, pp. 184–190, 2001.

[45] A. S. Kierans, M. Elazzazi, L. Braga et al., "Thermoablative treatments for malignant liver lesions: 10-year experience of MRI appearances of treatment response," *American Journal of Roentgenology*, vol. 194, no. 2, pp. 523–529, 2010.

[46] S. Kim, L. Mannelli, C. H. Hajdu et al., "Hepatocellular carcinoma: assessment of response to transarterial chemoembolization with image subtraction," *Journal of Magnetic Resonance Imaging*, vol. 31, no. 2, pp. 348–355, 2010.

[47] R. L. Baron, J. H. Oliver III, G. D. Dodd III, M. Nalesnik, B. L. Holbert, and B. Carr, "Hepatocellular carcinoma: evaluation with biphasic, contrast-enhanced, helical CT," *Radiology*, vol. 199, no. 2, pp. 505–511, 1996.

[48] B. I. Choi, H. J. Lee, J. K. Man, D. S. Choi, J. B. Seo, and M. C. Han, "Detection of hypervascular nodular hepatocellular carcinomas: value of triphasic helical CT compared with iodized-oil CT," *American Journal of Roentgenology*, vol. 168, no. 1, pp. 219–224, 1997.

[49] R. Iannaccone, A. Laghi, C. Catalane et al., "Hepatocellular carcinoma: role of unenhanced and delayed phase multidetector row helical CT in patients with cirrhosis," *Radiology*, vol. 234, no. 2, pp. 460–467, 2005.

[50] C. Wald, M. W. Russo, J. K. Heimbach, H. K. Hussain, E. A. Pomfret, and J. Bruix, "New OPTN/UNOS policy for liver transplant allocation: standardization of liver imaging, diagnosis, classification, and reporting of hepatocellular carcinoma," *Radiology*, vol. 266, no. 2, pp. 376–382, 2013.

[51] P. Therasse, S. G. Arbuck, E. A. Eisenhauer et al., "New guidelines to evaluate the response to treatment in solid tumors. European Organization for Research and Treatment of Cancer, National Cancer Institute of the United States, National Cancer Institute of Canada," *Journal of the National Cancer Institute*, vol. 92, no. 3, pp. 205–216, 2000.

[52] E. A. Eisenhauer, P. Therasse, J. Bogaerts et al., "New response evaluation criteria in solid tumours: revised RECIST guideline (version 1.1)," *European Journal of Cancer*, vol. 45, no. 2, pp. 228–247, 2009.

[53] *World Health Organization (WHO) Handbook for Reporting Results of Cancer Treatment*, WHO Offset Publication no. 48, World Health Organization (WHO), Geneva, Switzerland, 1979.

[54] C. Suzuki, H. Jacobsson, T. Hatschek et al., "Radiologic measurements of tumor response to treatment: practical approaches and limitations," *Radiographics*, vol. 28, no. 2, pp. 329–344, 2008.

[55] R. Lencioni and J. M. Llovet, "Modified recist (mRECIST) assessment for hepatocellular carcinoma," *Seminars in Liver Disease*, vol. 30, no. 1, pp. 52–60, 2010.

[56] European Association for the Study of the Liver and European Organisation for Research and Treatment of Cancer, "EASL-EORTC clinical practice guidelines: management of hepatocellular carcinoma," *Journal of Hepatology*, vol. 56, no. 4, pp. 908–943, 2012.

[57] V. Yaghmai, C. Besa, E. Kim, J. L. Gatlin, N. A. Siddiqui, and B. Taouli, "Imaging assessment of hepatocellular carcinoma response to locoregional and systemic therapy," *American Journal of Roentgenology*, vol. 201, no. 1, pp. 80–96, 2013.

[58] K. Memon, L. Kulik, R. J. Lewandowski et al., "Radiographic response to locoregional therapy in hepatocellular carcinoma predicts patient survival times," *Gastroenterology*, vol. 141, no. 2, pp. 526–535, 2011.

[59] Y.-S. Kim, H. Rhim, and H. K. Lim, "Imaging after radiofrequency ablation of hepatic tumors," *Seminars in Ultrasound, CT and MRI*, vol. 30, no. 2, pp. 49–66, 2009.

[60] A. B. Miller, B. Hoogstraten, M. Staquet, and A. Winkler, "Reporting results of cancer treatment," *Cancer*, vol. 47, no. 1, pp. 207–214, 1981.

[61] Z. Amin, J. J. Donald, A. Masters et al., "Hepatic metastases: interstitial laser photocoagulation with real-time US monitoring and dynamic CT evaluation of treatment," *Radiology*, vol. 187, no. 2, pp. 339–347, 1993.

[62] S. Rossi, E. Buscarini, F. Garbagnati et al., "Percutaneous treatment of small hepatic tumors by an expandable RF needle electrode," *American Journal of Roentgenology*, vol. 170, no. 4, pp. 1015–1022, 1998.

[63] S. Rossi, M. Di Stasi, E. Buscarini et al., "Percutaneous RF interstitial thermal ablation in the treatment of hepatic cancer," *American Journal of Roentgenology*, vol. 167, no. 3, pp. 759–768, 1996.

[64] L. Solbíatí, S. N. Goldberg, T. Ierace, M. Dellanoce, T. Livraghi, and G. S. Gazelle, "Radio-frequency ablation of hepatic metastases: postprocedural assessment with a US microbubble contrast agent—early experience," *Radiology*, vol. 211, no. 3, pp. 643–649, 1999.

[65] L. Solbiati, T. Ierace, S. N. Goldberg et al., "Percutaneous US-guided radio-frequency tissue ablation of liver metastases: teatment and follow-up in 16 patients," *Radiology*, vol. 202, no. 1, pp. 195–203, 1997.

[66] S. N. Goldberg, G. S. Gazelle, C. C. Compton, P. R. Mueller, and K. K. Tanabe, "Treatment of intrahepatic malignancy with radiofrequency ablation: radiologic-pathologic correlation," *Cancer*, vol. 88, no. 11, pp. 2452–2463, 2000.

[67] T. Livraghi, S. N. Goldberg, F. Monti et al., "Saline-enhanced radio-frequency tissue ablation in the treatment of liver metastases," *Radiology*, vol. 202, no. 1, pp. 205–210, 1997.

[68] T. Seki, M. Wakabayashi, T. Nakagawa et al., "Ultrasonically guided percutaneous microwave coagulation therapy for small hepatocellular carcinoma," *Cancer*, vol. 74, no. 3, pp. 817–825, 1994.

[69] K. Ohmoto, I. Miyake, M. Tsuduki et al., "Percutaneous microwave coagulation therapy for unresectable hepatocellular carcinoma," *Hepato-Gastroenterology*, vol. 46, no. 29, pp. 2894–2900, 1999.

[70] K. Tabuse and M. Katsumi, "Application of a microwave tissue coagulation to hepatic surgery: the hemostatic effects on spontaneous repture of hepatoma and tumor necrosis," *Nippon Geka Hokan. Archiv für Japanische Chirurgie*, vol. 50, pp. 571–579, 1981.

[71] R. Murakami, S. Yoshimatsu, Y. Yamashita et al., "Treatment of hepatocellular carcinoma: value of percutaneous microwave coagulation," *American Journal of Roentgenology*, vol. 164, no. 5, pp. 1159–1164, 1995.

[72] H. Horigome, T. Nomura, K. Saso, and P. M. Itoh, "Standards for selecting percutaneous ethanol injection therapy or percutaneous microwave coagulation therapy for solitary small hepatocellular carcinoma: consideration of local recurrence," *American Journal of Gastroenterology*, vol. 94, no. 7, pp. 1914–1917, 1999.

[73] T. Fujita, K. Honjo, K. Ito et al., "Fan-shaped hepatic parenchymal damage after ethanol injection therapy for hepatocellular carcinoma: MRI appearances," *Abdominal Imaging*, vol. 24, no. 1, pp. 56–60, 1999.

[74] M. I. Ahn, Y. H. Park, J. I. Yim, and J. Yoo, "Sequential changes of sonographic and computed tomography findings in the normal rabbit liver after percutaneous ethanol injection. Correlation with pathologic findings," *Investigative Radiology*, vol. 33, no. 10, pp. 723–729, 1998.

[75] G. D. Dodd III, M. C. Soulen, R. A. Kane et al., "Minimally invasive treatment of malignant hepatic tumors: at the threshold of a major breakthrough," *Radiographics*, vol. 20, no. 1, pp. 9–27, 2000.

[76] J.-S. Yu, K. W. Kim, K. B. Sung, J. T. Lee, and H. S. Yoo, "Small arterial-portal venous shunts: a cause of pseudolesions at hepatic imaging," *Radiology*, vol. 203, no. 3, pp. 737–742, 1997.

[77] T. K. Kim, B. I. Choi, J. K. Han, J. W. Chung, J. H. Park, and M. C. Han, "Nontumorous arterioportal shunt mimicking hypervascular tumor in cirrhotic liver: two-phase spiral CT findings," *Radiology*, vol. 208, no. 3, pp. 597–603, 1998.

[78] D. Mathieu, D. Larde, and N. Vasile, "CT features of iatrogenic hepatic arterioportal fistulae," *Journal of Computer Assisted Tomography*, vol. 7, no. 5, pp. 810–814, 1983.

[79] Y. Itai, S. Furui, K. Ohtomo et al., "Dynamic CT features of arterioportal shunts in hepatocellular carcinoma," *American Journal of Roentgenology*, vol. 146, no. 4, pp. 723–727, 1986.

[80] S. J. Lee, J. H. Lim, W. J. Lee, H. K. Lim, S. W. Choo, and I. W. Choo, "Transient subsegmental hepatic parenchymal enhancement on dynamic CT: a sign of postbiopsy arterioportal shunt," *Journal of Computer Assisted Tomography*, vol. 21, no. 3, pp. 355–360, 1997.

[81] H.-C. Kim, A. Y. Kim, J. K. Han et al., "Hepatic arterial and portal venous phase helical CT in patients treated with transcatheter arterial chemoembolization for hepatocellular carcinoma: added value of unenhanced images," *Radiology*, vol. 225, no. 3, pp. 773–780, 2002.

[82] T. W. I. Clark, "Complications of hepatic chemoembolization," *Seminars in Interventional Radiology*, vol. 23, no. 2, pp. 119–125, 2006.

[83] A. J. Lee, A. S. Gomes, D. M. Liu, S. T. Kee, C. T. Loh, and J. P. McWilliams, "The road less traveled: importance of the lesser branches of the celiac axis in liver embolotherapy," *Radiographics*, vol. 32, no. 4, pp. 1121–1132, 2012.

[84] S. J. Wigmore, D. N. Redhead, B. N. J. Thomson et al., "Postchemoembolisation syndrome—tumour necrosis or hepatocyte injury?" *British Journal of Cancer*, vol. 89, no. 8, pp. 1423–1427, 2003.

[85] Y. K. Cho, J. K. Kim, M. Y. Kim, H. Rhim, and J. K. Han, "Systematic review of randomized trials for hepatocellular carcinoma treated with percutaneous ablation therapies," *Hepatology*, vol. 49, no. 2, pp. 453–459, 2009.

[86] F. Fiore, M. Del Prete, R. Franco et al., "Transarterial embolization (TAE) is equally effective and slightly safer than transarterial chemoembolization (TACE) to manage liver metastases in neuroendocrine tumors," *Endocrine*, vol. 47, no. 1, pp. 177–182, 2014.

[87] B. Gray, G. Van Hazel, M. Hope et al., "Randomised trial of SIR-Spheres plus chemotherapy vs. chemotherapy alone for treating patients with liver metastases from primary large bowel cancer," *Annals of Oncology*, vol. 12, no. 12, pp. 1711–1720, 2001.

[88] B. N. Gray, M. A. Burton, D. Kelleher, P. Klemp, and L. Matz, "Tolerance of the liver to the effects of yttrium-90 radiation," *International Journal of Radiation Oncology, Biology, Physics*, vol. 18, no. 3, pp. 619–623, 1990.

[89] J. E. Goin, R. Salem, B. I. Carr et al., "Treatment of unresectable hepatocellular carcinoma with intrahepatic yttrium 90 microspheres: factors associated with liver toxicities," *Journal of Vascular and Interventional Radiology*, vol. 16, part 1, no. 2, pp. 205–213, 2005.

[90] J. C. Andrews, S. C. Walker, R. J. Ackermann et al., "Hepatic radioembolization with yttrium-90 containing glass microspheres: preliminary results and clinical follow-up," *Journal of Nuclear Medicine*, vol. 35, no. 10, pp. 1637–1646, 1994.

[91] O. M. Ebied, M. P. Federle, B. I. Carr et al., "Evaluation of responses to chemoembolization in patients with unresectable hepatocellular carcinoma," *Cancer*, vol. 97, no. 4, pp. 1042–1050, 2003.

[92] P. D. Shreve, Y. Anzai, and R. L. Wahl, "Pitfalls in oncologic diagnosis with FDG PET imaging: physiologic and benign variants," *Radiographics*, vol. 19, no. 1, pp. 61–77, 1999.

[93] L. M. Kulik, B. Atassi, L. van Holsbeeck et al., "Yttrium-90 microspheres (TheraSphere) treatment of unresectable hepatocellular carcinoma: downstaging to resection, RFA and bridge to transplantation," *Journal of Surgical Oncology*, vol. 94, no. 7, pp. 572–586, 2006.

[94] A. L. Keppke, R. Salem, D. Reddy et al., "Imaging of hepatocellular carcinoma after treatment with yttrium-90 microspheres," *American Journal of Roentgenology*, vol. 188, no. 3, pp. 768–775, 2007.

[95] R. Salem, R. J. Lewandowski, B. Atassi et al., "Treatment of unresectable hepatocellular carcinoma with use of 90Y microspheres (therasphere): safety, tumor response, and survival," *Journal of*

Vascular and Interventional Radiology, vol. 16, no. 12, pp. 1627–1639, 2005.

[96] R. Salem and K. G. Thurston, "Radioembolization with ^{90}Yttrium microspheres: a state-of-the-art brachytherapy treatment for primary and secondary liver malignancies: part 1: Technical and methodologic considerations," *Journal of Vascular and Interventional Radiology*, vol. 17, no. 8, pp. 1251–1278, 2006.

[97] J. E. Dancey, F. A. Shepherd, K. Paul et al., "Treatment of nonresectable hepatocellular carcinoma with intrahepatic 90Y-microspheres," *Journal of Nuclear Medicine*, vol. 41, no. 10, pp. 1673–1681, 2000.

Hindawi Publishing Corporation
Gastroenterology Research and Practice
Volume 2015, Article ID 104794, 8 pages
http://dx.doi.org/10.1155/2015/104794

Clinical Study

Staging of Primary Abdominal Lymphomas: Comparison of Whole-Body MRI with Diffusion-Weighted Imaging and ^{18}F-FDG-PET/CT

Alessandro Stecco,[1] Francesco Buemi,[1] Martina Quagliozzi,[1] Mariangela Lombardi,[1] Alberto Santagostino,[2] Gian Mauro Sacchetti,[3] and Alessandro Carriero[1]

[1]*Radiology Department, "Maggiore della Carità" University Hospital, University of Eastern Piedmont, Corso Mazzini 18, 28100 Novara, Italy*
[2]*Oncohaematology Department, Sant'Andrea Hospital, Corso Mario Abbiate 21, 13100 Vercelli, Italy*
[3]*Nuclear Medicine Department, "Maggiore della Carità" University Hospital, University of Eastern Piedmont, Corso Mazzini 18, 28100 Novara, Italy*

Correspondence should be addressed to Alessandro Stecco; a.stecco@libero.it

Received 18 May 2015; Revised 22 August 2015; Accepted 23 August 2015

Academic Editor: Tatsuya Toyokawa

Background. The purpose of this study was to compare the accuracy of whole-body MRI with diffusion-weighted sequences (WB-DW-MRI) with that of ^{18}F-FDG-PET/CT in the staging of patients with primary gastrointestinal lymphoma. *Methods*. This retrospective study involved 17 untreated patients with primary abdominal gastrointestinal lymphoma. All patients underwent ^{18}F-FDG-PET/CT and WB-DW-MRI. Histopathology findings or at least 6 months of clinical and radiological follow-up was the gold standard. The Musshoff-modified Ann Arbor system was used for staging, and diagnostic accuracy was evaluated on a per-node basis. *Results*. WB-DW-MRI exhibited 100% sensitivity, 96.3% specificity, and 96.1% and 100% positive and negative predictive values (PPV and NPV), respectively. The sensitivity, specificity, and PPV and NPV of PET/CT were 95.9%, 100%, and 100% and 96.4%, respectively. There were no statistically significant differences between the two techniques ($p = 0.05$). The weighted kappa agreement statistics with a 95% confidence interval were 0.97 (0.95–0.99) between the two MRI readers and 0.87 (0.82–0.92) between the two methods. *Conclusions*. WB-DW-MRI appears to have a comparable diagnostic value to ^{18}F-FDG-PET/CT in staging patients with gastrointestinal lymphoma.

1. Introduction

The gastrointestinal (GI) tract is the most common extranodal site in lymphoma, accounting for 5% to 20% of all cases [1]. Indeed, lymphomas frequently arise in the mesenteric or retroperitoneal nodes, and the abundance of lymphoid tissue in the GI tract makes this a susceptible site for secondary involvement.

Primary GI lymphomas are, however, uncommon, comprising fewer than 5% of all (GI) cancers. Indeed, according to Dawson et al. [2], a diagnosis of primary GI lymphoma should be restricted to localized disease of stages IE and IIE, whereas Lewin et al.'s [3] system requires that patients exhibit GI symptoms or a predominant lesion.

The stomach is the most common site of primary GI lymphomas, followed by the small intestine and then the ileocaecal valve [4]. The majority of such tumours (90%) are of B-cell lineage, and T-cell lymphomas and Hodgkin's lymphoma are rare. Some histological subtypes are more often found at certain locations, for example, mucosa-associated lymphoid tissue (MALT) lymphoma in the stomach, mantle cell lymphoma (MCL) in the terminal ileum, jejunum, and colon, enteropathy-associated T-cell lymphoma (EATL) in the jejunum, and follicular lymphoma (FL) in the duodenum [5]. Multifocal tumours are particularly common in MALT lymphoma and follicular lymphoma.

Accurate diagnosis and staging of primary GI lymphomas, an especially heterogeneous group of tumours, are

fundamental for treatment stratification [6]. Staging of GI lymphomas is generally performed by means of Musshoff's modified version of Ann Arbor staging [7], with the international prognostic index being used to define the prognostic subgroups. However, the system is less than optimal for documenting certain features specific to primary GI lymphoma, in particular diffuse and incurable infiltration of the GI tract. Due to this deficiency, many staging protocols and reporting systems have been proposed, and among these the Paris staging system stands out due to its ability to record the depth of tumour infiltration and specific lymphoma spread, as well as the extent of nodal involvement [8].

Various procedures are employed in diagnosis and follow-up and to provide data for pretreatment staging, including endoscopic ultrasound (EUS), endoscopic biopsies, computed tomography (CT), magnetic resonance imaging (MRI), ^{18}F-fluorodeoxyglucose positron emission tomography (^{18}F-FDG-PET), and/or molecular markers [9]. EUS and CT are the most widely performed techniques, and CT of the chest, abdomen, and pelvis exhibits high sensitivity and specificity in staging GI lymphomas. The sensitivity and specificity of CT-based staging of FL, MCL and diffuse large B-cell lymphoma (DLBCL) can be increased even further, to 80% and 90%, respectively, by the integration of ^{18}F-FDG-PET. However, this provides no added benefit for MALT lymphomas [10]. Moreover, EUS is considered superior to CT scan in terms of locoregional staging, as it provides details of visceral wall involvement, and for the detection of perivisceral adenopathies [11].

Whole-body diffusion-weighted MRI (WB-DW-MRI) has also been extensively studied as a method of staging lymphomas [9, 12], in addition to other tumours [13, 14]. Indeed, whole-body imaging techniques can be used to assess supradiaphragmatic nodal and extranodal sites, thereby providing information vital for abdominal lymphoma staging. Despite the promise being shown by WB-DW-MRI in this area, ^{18}F-FDG-PET/CT remains the standard of reference [14]. Nevertheless, as WB-DW-MRI does not expose the patient to ionizing radiation, its validation as a GI lymphoma staging tool would be of great clinical significance. However, to the best of our knowledge there have been no studies investigating the role of WB-DW-MRI in the staging of this type of lymphoma to date.

We therefore set out to evaluate the performance of WB-DW-MRI in staging primary abdominal GI lymphomas with respect to the current preferred method, ^{18}F-FDG-PET/CT. As Paris staging has not yet been universally accepted, we elected to use the modified Ann Arbor system, using histopathological findings to confirm the diagnoses.

2. Materials and Methods

2.1. Patients. This retrospective study involved 17 untreated patients with primary abdominal GI lymphoma (12 males and 5 females; age range: 34.8–82 years, mean age: 63.1 years) diagnosed between July 2007 and February 2015. All patients underwent WB-DW-MRI and ^{18}F-FDG-PET/CT for staging purposes. Five patients also underwent EUS and nine abdominal CT scan with contrast before therapy. Diagnosis of primary GI lymphoma was confirmed histopathologically in all patients. At least 6 months of clinical and radiological follow-up was available for each patient.

According to Ann Arbor staging with Musshoff's modification, no patients were classed as stage 0 (0), two as stage I, seven as stage II, five as stage III, and three as stage IV.

All patients underwent PET/CT and MRI in the 3 weeks preceding treatment. The time interval between MRI and PET/CT scans was 0–33 days. Subsequently, 1 patient was treated by means of surgical resection and chemotherapy, while 11 received chemotherapy alone and 5 *H. pylori* eradication and chemotherapy. Of the treated patients, 9 achieved complete remission, 6 achieved partial remission, and 2 showed no response. Tables 1 and 2 show the clinicopathological features of patients and the histological classification and site of origin of the GI lymphomas diagnosed.

Informed consent was obtained from all patients and the local ethical committee approved this study.

Table 1: Clinicopathological features and sites of origin of tumours investigated.

Characteristics	Gastric	Intestinal
Mean age (yrs)	60.2	64.5
Gender		
Male	3	9
Female	2	3
Histology		
Low-grade B-cell	5	4
High-grade B-cell	0	8
Stage		
IE	2	0
IIE	3	4
IIIE	0	6
IVE	0	2
Treatment		
Surgery alone	0	0
Nonsurgical	6	10
Both	0	1
Response to treatment		
Complete remission	5	4
Partial remission	0	6
No response	0	2

Table 2: Histological classification and sites of origin.

Histology type	Gastric	Intestinal	Total
Low-grade B-cell			
MALTL*	3	5	8
Follicular lymphoma	1	4	5
High-grade B-cell			
DLBCL**	1	3	4

*MALTL, mucosa-associated lymphoid tissue lymphoma; **DLBCL, diffuse large B-cell lymphoma.

2.2. Whole-Body MRI. All patients underwent MRI on a superconductive 1.5 T magnet (Achieva, Philips, Best, Netherlands, release 2.5) using a q-body coil, with the patient positioned "feet first" on an extended anatomical coverage table featuring rolling-table technology (MobiTrak, Philips). The light visor was pointed at the orbitomeatal plane.

After multiplanar and multistack scout pulse sequence reconstruction into a whole-body scout, by means of proprietary software (MobiView, Philips), a STIR-EPI single-shot pulse sequence (diffusion-weighted imaging with background suppression, DWIBS) (TR/TE = 4284/68 ms; TI = 180 ms; matrix = 108 ∗ 67; voxel size = 5 mm; NSA = 8; thickness = 6 mm; gap =1 mm; slices = 30; FOV = 530 (RL), 341 (AP), and 180 (FH); acquisition time: 02 min 21 secs) was acquired in the axial plane. This was repeated in free breathing for up to four stacks to encompass all anatomical districts, from head to foot.

The MR protocol involved the acquisition of T2-STIR (TR/TE = 3819/165; 2 NEX; matrix = 336 ∗ 120; thickness = 6 mm; gap = 1 mm; slices = 47; FOV: 530 (RL), 265 (FH), and 328 (AP); acquisition time: 1 min 8 secs) and spin echo-T1 (TR/TE = 788/18; 1 NEX; matrix = 208 ∗ 287; thickness = 6 mm; gap = 1 mm; slices = 43; FOV: 530 (RL), 300 (AP), and 265 (FH); acquisition time: 1 min 10 secs) sequences in the sagittal and coronal planes.

2.3. PET-CT. PET-CT scans were taken on a hybrid Siemens (Siemens, Erlangen, Germany) system consisting of a lutetium oxyorthosilicate (LSO) PET scanner (HI-REZ) with Pico-3D electronics and a 16-row CT device (Somatom Sensation 16).

The PET component is a high-resolution scanner with a spatial resolution of 4.7 mm and has no septa, thus allowing 3-dimensional-only acquisition. Together with the PET system, the CT scanner is used both for attenuation correction of PET data and for localization of ^{18}F-FDG uptake in PET images. The intravenously administrated dose of ^{18}F-FDG was 3,5 mBq/Kg of body weight and imaging was performed 60 minutes after administration of the tracer.

Acquired images were reconstructed using the attenuation weighted-OSEM (ordered subset expectation maximization) iterative reconstruction, with 2 iterations, 8 subsets. Fourier rebinning was used to reduce the 3D dataset to a 2-dimensional equivalent dataset, and a 4 mm full width at half maximum Gaussian filter was applied to the image after reconstruction along the axial and transaxial directions. The data were reconstructed over a 128 ∗ 128 matrix with 5.3 mm pixel size and 2 mm slice thickness. Processed images were displayed in coronal, transverse, and sagittal planes.

3. Image Analysis

After acquisition and selection of the highest b value, the native axial images were reformatted on a stack-by-stack basis as a single 340 mm thick maximum intensity projection (MIP) image in the coronal plane, multiple 4 mm thick multiplanar reconstructions (MPRs) in the coronal plane, and multiple 4 mm thick MPRs in the sagittal plane, oriented to include the midline as well as the spine and paraspinal regions. All reformatted images were then fused by means of the smooth fusion algorithm in MobiView software (Philips) to obtain whole-body MIP and MPR images. The grey scale was subsequently inverted to enable viewing of abnormalities (increased signal) as grey areas of varying intensity against a white background, in a PET-like visualization window, as suggested by Takahara et al. [15].

All whole-body MIP and MPR images were saved in the scanner's image database in patient-specific files. The native axial slices were separated on the basis of the b value, and those acquired with b = 1,000 s/mm^2 were also saved in the image database on optimal window settings. T2-STIR and SE-T1 scan data were then merged into a single whole-body image using the same method and software.

All MR and PET/CT image sets were processed by an experienced trained radiologist, anonymized, and stored in DICOM format on a CD-ROM marked with a patient- and session-specific identification code.

MR images were read independently by two experienced MRI radiologists (A.S. and A.C. with 15 and 25 years of experience in MR imaging, resp.), both blind to each other's findings and the patient's clinical status. PET/CT images were read by a specialist with 18 years of experience in nuclear medicine (G.S.).

The three readers recorded their findings on a pre-designed spreadsheet (Excel, Microsoft, Redmond, USA) listing the following nodal and extranodal sites [16]:

(1) Abdominal GI locations: stomach, duodenum, small bowel, colon/rectum, and multiple sites.

(2) Other extranodal locations: spleen, liver, kidney, head and neck, lung, and bone.

(3) Subdiaphragmatic nodal locations: paragastric, mesenteric, para-aortic, paracaval, pelvic, and inguinal.

(4) Supradiaphragmatic nodal locations: laterocervical, axillary, supraclavicular, and mediastinal.

As Abdulqadhr et al. [17], the evaluation of possible nodal lesions was performed with MIP images of the whole-body DW sequences. The lesion was then confirmed by checking axial DW images using a value of b = 1000 mm^2/sec. A b value of 0 mm^2/sec together with b = 1000 mm^2/sec was used to rule out T2 shine-through effect [18] and to get anatomical information. The axial DW images were correlated to MIP images by references lines.

Lesions identified on DWIBS were considered positive for the disease if [18]:

(1) the major axis measurement was greater than 1 cm (on axial DWIBS sequences),

(2) their signal intensity on DWIBS was greater than that of the spinal cord,

(3) there were coalescent lymph nodes or nodal masses,

(4) lymph nodes were present in regions where there are normally no lymph nodes.

Central necrosis was considered a sign of malignancy, regardless of the size of the lymph node [19].

Extranodal lesions were identified as follows:

(1) Presence of areas of restricted diffusion at GI tract and parenchymal organs with respect to the background signal.

(2) Correlation of the above with signal abnormalities on the morphological sequences (coronal and sagittal STIR/T1w sequences).

Bone marrow signals were considered abnormal when greater than that of muscle on T2-weighted sequences and/or when presenting a "mild" restriction of diffusion on DWIBS [20].

As apparent diffusion coefficient (ADC) values for small organs and tissues are affected by respiratory motion and fail to accurately distinguish malignant from benign lesions [21], due to partial volume effects, and since inter- and intraobserver variability afflict reproducibility of the measures [22], we neither calculated nor used ADC to characterize lesion tissues. Instead, a lesion was considered positive on ^{18}F-FDG-PET/CT scans in the presence of greater focal or diffuse ^{18}F-FDG uptake than background activity in a location incompatible with normal/physiology (or unrelated to physiological sites of tracer uptake) [23, 24]. The location of ^{18}F-FDG uptake was always verified by CT. Lymph nodes with a shortest transverse diameter of ≥1 cm [23] or masses/coalescent lymph node were also considered positive.

The patients were staged by Ann Arbor staging with Musshoff's modification using the data yielded by each imaging technique. The two sets of results were then compared with each other and the results of biopsy or when this was not possible with at least 6 months of clinical and radiological follow-up (CT, MRI, and PET/CT), the standard of reference. A reduction in the size of the lesion after therapy was taken as evidence that the lesion was positive for lymphoma [22].

4. Statistical Analysis

Sensitivity, specificity, accuracy, and positive and negative predictive values were calculated for each diagnostic method on a "per-node" basis (N-staging). Analysis of the accuracy of WB-DW-MRI, ^{18}F-FDG-PET/CT, and ^{18}F-FDG-PET without CT in the assessment of the individual disease stage of each patient was also performed. Regarding the gastrointestinal lymphoma manifestation, we only calculated the ^{18}F-FDG-PET/CT and WB-DW-MRI detection rates, as their large fields of view impede the accurate staging of locoregional tumour extension (stage I).

Cohen's k statistics were used to calculate the interobserver agreement between the two MR readers and between WB-DW-MRI and ^{18}F-FDG-PET/CT. Agreement was defined as poor at $k < 0.2$, fair at $k > 0.2 < 0.4$, moderate at $k > 0.4 < 0.6$, good at $k > 0.6 < 0.8$, and very good at $k > 0.8$.

McNemar's test was used to determine the statistical significance of differences between WB-DW-MRI and ^{18}F-FDG-PET/CT interpretations. A p value of < 0.05 was regarded as statistically significant. MedCalc (MedCalc Software, Belgium) was used for all statistical analyses.

Table 3: Staging of lymphoma provided by WB-DW-MRI and ^{18}F-FDG-PET/CT.

Stage	WB-DW-MRI				
	0	I	II	III	IV
^{18}F-FDG-PET/CT					
0	2				
I		0			
II			7		
III				6	1
IV					1

5. Results

5.1. Per-Node Basis. WB-DW-MRI was true-positive for 75 (100%) of the lymphomatous node groups and true-negative for 79 (96%) of the nonmetastatic node groups, while ^{18}F-FDG-PET/CT was true-positive for 71 (94%) of the lymphomatous node groups and true-negative for 83 (100%) of the nonlymphomatous node groups. WB-DW-MRI exhibited 100% (CI 95%, 95.2% to 100%) sensitivity, 96.3% (CI 95%, 89.5% to 99.2%) specificity, and 96.1% (CI 95%, 89.1% to 99.2%) and 100% (CI 95.3% to 100%) positive and negative predictive values, respectively. The sensitivity, specificity, and PPV and NPV of ^{18}F-FDG-PET/CT were 95.9% (CI 95%, 88.6% to 99.1%), 100% (CI 95%, 95.60 to 100%), and 100% (CI 95%, 94.9% to 100%) and 96.4% (CI 95%, 90% to 99.27%), respectively.

McNemar's test revealed no statistically significant differences between ^{18}F-FDG-PET/CT and WB-DW-MRI ($p < 0.05$).

The weighted kappa statistics, with a 95% confidence interval of agreement, were 0.97 (0.95–0.99) between the two MRI readers and 0.87 (0.82–0.92) between the two methods.

5.2. Per-Patient Analysis and Gastrointestinal Lymphoma Detection Rate. Of the 17 lymphoma patients, 16 were staged the same by WB-DW-MRI and ^{18}F-FDG-PET/CT (94%). Of those 16 patients, 1 was classed as stage IV, and the remaining 15 were distributed between stages 0 and III (Figures 1 and 2, Table 3). In the case in which staging differed, WB-DW-MRI classed the patient as stage IV, predicting bone marrow (BM) invasion, while ^{18}F-FDG-PET/CT classed the patient as stage III. The bone marrow infiltration, and therefore the accuracy of the higher staging, provided by MRI, was confirmed by bone biopsy (Table 4).

In the 2 patients with low-grade MALT lymphoma, WB-DW-MRI and ^{18}F-FDG-PET/CT agreed (both stage II), but ^{18}F-FDG-PET alone predicted a far lower stage (stage 0). In the mismatched regions, enlarged lymph nodes with no F-FDG uptake were present on CT (>1 cm) (Figure 2, Table 4).

^{18}F-FDG-PET/CT and WB-DW-MRI both detected the gastrointestinal lymphoma manifestation in 10 out of

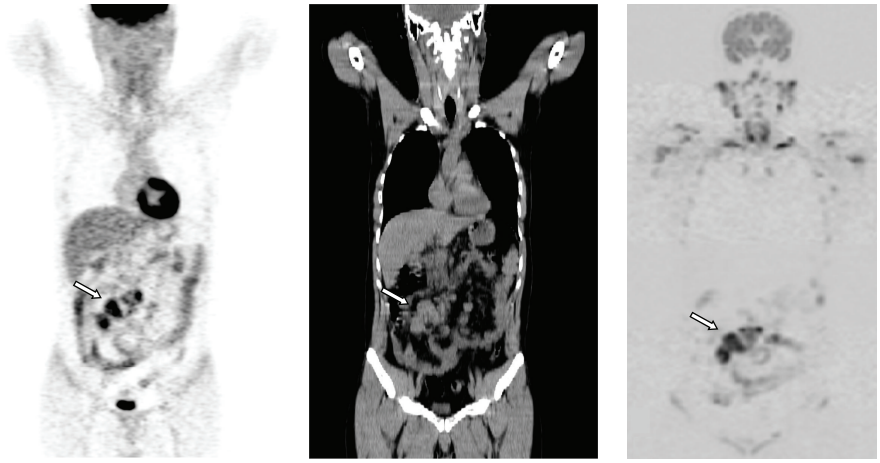

(a) (b) (c)

Figure 1: A 38-year-old man with intestinal DLBCL (diffuse large B-cell lymphoma): (a) MIP image of ^{18}F-FDG-PET, (b) coronal whole-body CT, and (c) MIP image of DWI. All techniques detected the primary intestinal lesion (arrow).

Table 4: Staging by both techniques: mismatched sites behind differences in staging with respect to standard of reference.

Patient	WB-DW-MRI	^{18}F-FDG-PET/CT	^{18}F-FDG-PET	Mismatched regions	Gold standard
Gastric MALTL*	0	0	0	Primary gastric lesion	Stage I. Positive EUB and endoscopy (ulcerated gastric lesion)
Gastric MALTL*	0	0	0	Primary gastric lesion	Stage I. Positive endoscopy
Intestinal MALTL*	II	II	0	Primary intestinal lesion, mesenteric lymph nodes	Stage II. Positive CT scan, thickened bowel wall and mesenteric lymph nodes. Radiological and clinical follow-up (partial remission after therapy on ^{18}F-FDG-PET/CT and WB-DW-MRI)
Gastric MALTL*	II	II	0	Primary gastric lesion, mesenteric, paragastric, para-aortic, and paracaval adenopathy	Stage II. Positive endoscopy. ^{18}F-FDG-PET/CT (only on CT) and WB-DW-MRI detected adenopathy but failed to find the primary lesion ^{18}F-FDG-PET negative
Intestinal DLBCL**	IV	III	III	Bone marrow involvement	Positive bone marrow biopsy

*MALTL, mucosa-associated lymphoid tissue lymphoma; **DLBCL, diffuse large B-cell lymphoma.

the 17 patients (60%), while ^{18}F-FDG-PET alone detected it in only 8 of 17 (47%). In other words, WB-DW-MRI and ^{18}F-FDG-PET/CT downstaged 2 patients classed as stage 1 by the gold standard, whereas ^{18}F-FDG-PET alone downstaged 4 patients (Table 4).

6. Discussion

To our knowledge, this is the first study to evaluate the role of WB-DW-MRI in the N-staging of primary GI lymphoma. Although it was not possible for us to confirm the diagnosis in all lymph nodes by histopathology (a common problem in radiological research, as it would be highly unethical to biopsy all suspected lesions) WB-DW-MRI staging was generally in full agreement with that provided by the standard of reference. In the majority of our cases, there were no differences between WB-DW-MRI and ^{18}F-FDG-PET/CT in this regard. However, both yielded a lower stage than the standard of reference in two patients with indolent stage 1 MALT lymphoma (Table 4), with neither PET/CT nor WB-DW-MRI being able to detect any morphologic abnormality or ^{18}F-FDG uptake/restriction of diffusivity in the known location of the gastrointestinal lymphoma in either of these two patients. ^{18}F-FDG-PET alone, on the other hand, failed to detect ^{18}F-FDG uptake in these and a further two cases (total 4 patients) with indolent MALT lymphoma (both stage II), which were successfully staged by integrating CT data (Figure 2, Table 4).

As there was a high preponderance of early-stage (I-II) indolent MALT lymphoma in our group, it is perhaps unsurprising that, overall, both ^{18}F-FDG-PET/CT and WB-DW-MRI had a GI lymphoma detection failure rate of 40%

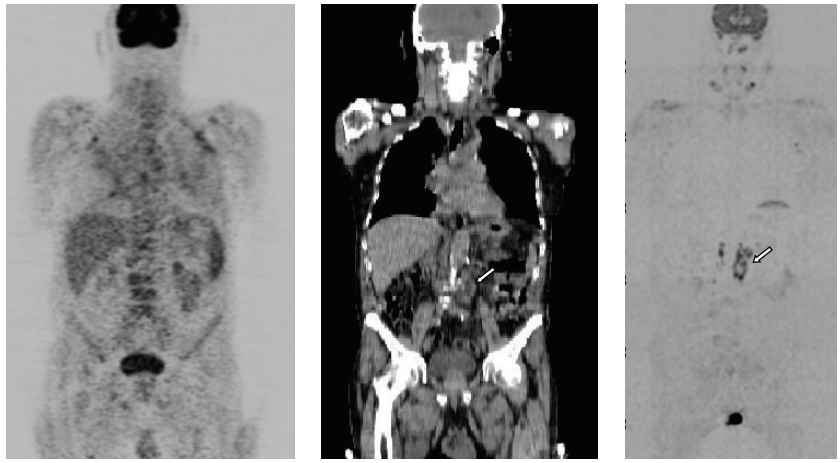

(a) (b) (c)

Figure 2: An 82-year-old man with gastric MALT lymphoma: (a) MIP image of ^{18}F-FDG-PET showing no uptake in any lymph node regions, giving stage 0; (b) coronal whole-body CT, showing multiple para-aortic lymph nodes, thus giving stage II (arrow); (c) MIP image of DWI showing the same findings, as high signal intensity in the same nodal location, giving stage II (arrow). However, all techniques, even DWI, failed to find the primary gastric lesion.

as compared to 53% with ^{18}F-FDG-PET alone. Indeed, in 33 cases of MALT lymphoma, Perry et al. [25] showed ^{18}F-FDG-PET/CT detected active disease in 100% of advanced cases (stages III-IV) but in only 42.3% of cases of early-stage disease (I-II). It seems reasonable to assume, therefore, that the early stage, small size, and low metabolism/low ^{18}F-FDG uptake were behind both the downstaging of two patients and the missed gastrointestinal lymphoma manifestations.

In our study, WB-DW-MRI detected one more patient with positive BM lesion than ^{18}F-FDG-PET/CT, correctly upstaging this patient with respect to ^{18}F-FDG-PET/CT. This finding is in line with those by Abdulqadhr et al. [17] showing that WB-DW-MRI correctly upstaged 3 patients with small lymphocytic lymphoma/chronic lymphatic leukaemia (SLL/CLL) as compared to ^{18}F-FDG-PET/CT. They postulated that the increased signal seen in SLL/CLL lesions was ascribable to the small, closely packed tumour cells causing restricted water molecule movement. However, in our two missed cases of stage 1 indolent MALT lymphoma, we failed to find any significant restriction. However, the normal focal or diffuse restriction of the small primary lesions may have been hidden by the bowel loops.

On a per-node basis, we found WB-DW-MRI to be more sensitive (100% versus 96.3%) but less specific (95.1% versus 100%) than ^{18}F-FDG-PET/CT. Overall, WB-DW-MRI detected a higher number of false-positive lymph nodes at the laterocervical, axillary, and inguinal nodal locations than ^{18}F-FDG-PET/CT, which were confirmed as reactive nodes in the follow-up. That being said, McNemar's test revealed no statistically significant differences between the two investigations, and the interobserver agreement was "very good" (>0.8).

This makes an interesting contribution to the growing debate regarding the excessive exposure to radiation during diagnostic procedures. Indeed, although ^{18}F-FDG-PET/CT is widely used in the management of lymphomas, it involves exposing patients to a substantial dose of radiation, which is of particular concern in young adults and children [26, 27] and in patients who require repeated follow-up. A nonionizing imaging technique, such as MRI, with similar functional imaging capacity would therefore be afforded an important role in this setting, especially during follow-up.

Our results, like those of Abdulqadhr et al. [17], appear to suggest a role for WB-DW-MRI, combined with ^{18}F-FDG-PET/CT, in initial staging and provided that there is agreement between the two techniques as a standalone follow-up imaging technique. This would not only be safer for patients, but also improve cost-effectiveness and total examination time, both important limitations of ^{18}F-FDG-PET/CT, in the long term. Indeed, ^{18}F-FDG-PET/CT costs roughly twice as much as WB-MRI and takes considerably longer (60 minutes of waiting time after ^{18}F-FDG injection versus 30–35 minutes) [28].

Nevertheless, there are some limitations to our study. First and foremost, it was retrospective in nature and therefore not reliant on a standardized MRI protocol. Due to the heterogeneity of the MRI protocols adopted in our institution over the years, we only considered DWIBS and STIR/T1. However, it would have been preferable to have been able to add a WB-DW-MRI protocol with axial T1w or T2w sequences, so as to shed light on the morphological characteristics of the lymph nodes at the laterocervical, axillary, and inguinal locations, and thereby potentially eliminate false-positives. However, as no such data was available for our patients, we were unable to take them into account.

Secondly, the rarity of primary GI lymphoma meant that we were only able to consider a limited number of patients. Further studies are needed, not only to confirm our findings

in a larger sample, but also to refine the staging procedure for gastric MALT lymphoma. Although indolent, this type of tumour may be multifocal [29, 30], transform to DLBCL [31], and it is difficult to diagnose, endoscopic findings being normal in the majority of cases. As multiple organs are generally involved, endoscopic biopsies usually need to be taken from multiple sites of the stomach and duodenum, encompassing both normal and abnormal regions [10, 32]. Our results indicate that this highly invasive procedure may one day be more accurately guided by DWIBS sequences, which could also prove useful by predicting the transformation of this tumour into higher-grade lymphoma (indeed, PET has already been recommended as a means of assessing the recurrence or transformation of various lymphomas [33]), although, once again, more research is necessary.

7. Conclusions

Our results suggest WB-DW-MRI as a promising technique for staging patients with primary GI lymphomas, and, pending the results of future studies and improvements to its performance, it may provide a radiation-free alternative to ^{18}F-FDG-PET/CT.

Disclosure

The paper has not been published elsewhere and is not currently under consideration by another journal.

Conflict of Interests

The authors do not have any conflict of interests regarding the publication of this paper.

References

[1] C. Freeman, J. W. Berg, and S. J. Cutler, "Occurrence and prognosis of extranodal lymphomas," *Cancer*, vol. 29, no. 1, pp. 252–260, 1972.

[2] I. M. Dawson, J. S. Cornes, and B. C. Morson, "Primary malignant lymphoid tumours of the intestinal tract. Report of 37 cases with a study of factors influencing prognosis," *British Journal of Surgery*, vol. 49, no. 213, pp. 80–89, 1961.

[3] K. J. Lewin, M. Ranchod, and R. F. Dorfman, "Lymphomas of the gastrointestinal tract: a study of 117 cases presenting with gastrointestinal disease," *Cancer*, vol. 42, no. 2, pp. 693–707, 1978.

[4] R. Herrmann, A. M. Panahon, M. P. Barcos, D. Walsh, and L. Stutzman, "Gastrointestinal involvement in non-Hodgkin's lymphoma," *Cancer*, vol. 46, no. 1, pp. 215–222, 1980.

[5] M. A. Rizvi, A. M. Evens, M. S. Tallman, B. P. Nelson, and S. T. Rosen, "T-cell non-Hodgkin lymphoma," *Blood*, vol. 107, no. 4, pp. 1255–1264, 2006.

[6] S. M. Ansell and J. Armitage, "Non-Hodgkin lymphoma: diagnosis and treatment," *Mayo Clinic Proceedings*, vol. 80, no. 8, pp. 1087–1097, 2005.

[7] K. Musshoff, "Clinical staging classification of non Hodgkin's lymphomas," *Strahlentherapie*, vol. 153, no. 4, pp. 218–221, 1977.

[8] A. Ruskoné-Fourmestroux, B. Drogosics, A. Morgner, A. Wotherspoon, and D. De Jong, "Paris staging system for primary gastrointestinal lymphomas," *Gut*, vol. 52, no. 6, pp. 912–913, 2003.

[9] G. Antoch, F. M. Vogt, L. S. Freudenberg et al., "Whole-body dual-modality PET/CT and whole-body MRI for tumor staging in oncology," *The Journal of the American Medical Association*, vol. 290, no. 24, pp. 3199–3206, 2003.

[10] P. Ghimire, G.-Y. Wu, and L. Zhu, "Primary gastrointestinal lymphoma," *World Journal of Gastroenterology*, vol. 17, no. 6, pp. 697–707, 2011.

[11] F. Di Raimondo, L. Caruso, G. Bonanno et al., "Is endoscopic ultrasound clinically useful for follow-up of gastric lymphoma?" *Annals of Oncology*, vol. 18, no. 2, pp. 351–356, 2007.

[12] A. R. Padhani, D.-M. Koh, and D. J. Collins, "Whole-body diffusion-weighted MR imaging in cancer: current status and research directions," *Radiology*, vol. 261, no. 3, pp. 700–718, 2011.

[13] C. Lin, A. Luciani, E. Itti et al., "Whole-body diffusion-weighted magnetic resonance imaging with apparent diffusion coefficient mapping for staging patients with diffuse large B-cell lymphoma," *European Radiology*, vol. 20, no. 8, pp. 2027–2038, 2010.

[14] M. E. Mayerhoefer, G. Karanikas, K. Kletter et al., "Evaluation of diffusion-weighted MRI for pretherapeutic assessment and staging of lymphoma: results of a prospective study in 140 patients," *Clinical Cancer Research*, vol. 20, no. 11, pp. 2984–2993, 2014.

[15] T. Takahara, Y. Imai, T. Yamashita, S. Yasuda, S. Nasu, and M. Van Cauteren, "Diffusion weighted whole body imaging with background body signal suppression (DWIBS): technical improvement using free breathing, STIR and high resolution 3D display," *Radiation Medicine*, vol. 4, no. 22, pp. 275–282, 2004.

[16] J. Gu, T. Chan, J. Zhang, A. Y. H. Leung, Y.-L. Kwong, and P.-L. Khong, "Whole-body diffusion-weighted imaging: the added value to whole-body MRI at initial diagnosis of lymphoma," *American Journal of Roentgenology*, vol. 197, no. 3, pp. W384–W391, 2011.

[17] G. Abdulqadhr, D. Molin, G. Åström et al., "Whole-body diffusion-weighted imaging compared with FDG-PET/CT in staging of lymphoma patients," *Acta Radiologica*, vol. 52, no. 2, pp. 173–180, 2011.

[18] D.-M. Koh and D. J. Collins, "Diffusion-weighted MRI in the body: applications and challenges in oncology," *American Journal of Roentgenology*, vol. 188, no. 6, pp. 1622–1635, 2007.

[19] C. Lin, E. Itti, A. Luciani, C. Haioun, M. Meignan, and A. Rahmouni, "Whole-body diffusion-weighted imaging in lymphoma," *Cancer Imaging*, vol. 10, pp. S172–S178, 2010.

[20] C. J. Kellenberger, S. F. Miller, M. Khan, D. L. Gilday, S. Weitzman, and P. S. Babyn, "Initial experience with FSE STIR whole-body MR imaging for staging lymphoma in children," *European Radiology*, vol. 14, no. 10, pp. 1829–1841, 2004.

[21] T. C. Kwee, T. Takahara, P. R. Luijten, and R. A. J. Nievelstein, "ADC measurements of lymph nodes: inter- and intra-observer reproducibility study and an overview of the literature," *European Journal of Radiology*, vol. 75, no. 2, pp. 215–220, 2010.

[22] E. E. Pakos, A. D. Fotopoulos, and J. P. A. Ioannidis, " ^{18}F-FDG PET for evaluation of bone marrow infiltration in staging of lymphoma: a meta-analysis," *Journal of Nuclear Medicine*, vol. 46, no. 6, pp. 958–963, 2005.

[23] B. D. Cheson, S. J. Horning, B. Coiffer et al., "Report of an international workshop to standardize response criteria

for non-Hodgkin's lymphomas. NCI sponsored international working group," *Clinical Oncology*, vol. 17, p. 1244, 1999.

[24] P. Seam, M. E. Juweid, and B. D. Cheson, "The role of FDG-PET scans in patients with lymphoma," *Blood*, vol. 110, no. 10, pp. 3507–3516, 2007.

[25] C. Perry, Y. Herishanu, U. Metzer et al., "Diagnostic accuracy of PET/CT in patients with extranodal marginal zone MALT lymphoma," *European Journal of Haematology*, vol. 79, no. 3, pp. 205–209, 2007.

[26] D. J. Brenner and C. D. Elliston, "Estimated radiation on risks potentially associated with full-body CT screening," *Radiology*, vol. 232, no. 3, pp. 735–738, 2004.

[27] B. Huang, M. W.-M. Law, and P.-L. Khong, "Whole-body PET/CT scanning: estimation of radiation dose and cancer risk," *Radiology*, vol. 251, no. 1, pp. 166–174, 2009.

[28] C. Plathow, M. Walz, M. P. Lichy et al., "Cost considerations for whole-body MRI and PET/CT as part of oncologic staging," *Der Radiologe*, vol. 48, no. 4, pp. 384–396, 2008.

[29] A. C. Wotherspoon, C. Doglioni, and P. G. Isaacson, "Low-grade gastric B-cell lymphoma of mucosa-associated lymphoid tissue (MALT): a multifocal disease," *Histopathology*, vol. 20, no. 1, pp. 29–34, 1992.

[30] S. M. Cohen, M. Petryk, M. Varma, P. S. Kozuch, E. D. Ames, and M. L. Grossbard, "Non-Hodgkin's lymphoma of mucosa-associated lymphoid tissue," *Oncologist*, vol. 11, no. 10, pp. 1100–1117, 2006.

[31] A. J. A. Deutsch, A. Aigelsreiter, P. B. Staber et al., "MALT lymphoma and extranodal diffuse large B-cell lymphoma are targeted by aberrant somatic hypermutation," *Blood*, vol. 109, no. 8, pp. 3500–3504, 2007.

[32] H. Boot, "Diagnosis and staging in gastrointestinal lymphoma," *Best Practice and Research: Clinical Gastroenterology*, vol. 24, no. 1, pp. 3–12, 2010.

[33] B. D. Cheson, B. Pfistner, M. E. Juweid et al., "Revised response criteria for malignant lymphoma," *Journal of Clinical Oncology*, vol. 25, no. 5, pp. 579–586, 2007.

Hindawi Publishing Corporation
Gastroenterology Research and Practice
Volume 2015, Article ID 159641, 7 pages
http://dx.doi.org/10.1155/2015/159641

Research Article

Assessment of Disease Activity in Small Bowel Crohn's Disease: Comparison between Endoscopy and Magnetic Resonance Enterography Using MRIA and Modified MRIA Score

Arnaldo Scardapane,[1] Annalisa Ambrosi,[1] Emanuela Salinaro,[1] Maria Elisabetta Mancini,[1] Mariabeatrice Principi,[2] Alfredo Di Leo,[2] Filomenamila Lorusso,[1] Amato Antonio Stabile Ianora,[1] and Giuseppe Angelelli[1]

[1]*Section of Diagnostic Imaging, Interdisciplinary Department of Medicine, University of Bari "Aldo Moro", Piazza Giulio Cesare 11, 70124 Bari, Italy*
[2]*Section of Gastroenterology, Department of Emergency and Organ Transplantation, University of Bari "Aldo Moro", Piazza Giulio Cesare 11, 70124 Bari, Italy*

Correspondence should be addressed to Arnaldo Scardapane; arnaldo.scardapane@gmail.com

Received 29 May 2015; Revised 11 August 2015; Accepted 19 August 2015

Academic Editor: Lorenzo Mannelli

Objectives. To retrospectively compare the results of the MRIA (magnetic resonance index of activity) with a modified MRIA (mMRIA), which was calculated excluding from MRIA formula the data of relative contrast enhancement (RCE). *Materials and Methods*. MR-E and corresponding endoscopic records of 100 patients were reviewed. MRIA, mMRIA, and SES endoscopic index were calculated for all the patients. Namely, MRIA was calculated as follows: (1.5 × wall thickening + 0.02 × RCE + 5 × intramural edema + 10 × ulcers), while mMRIA was calculated with the modified formula (1.5 × wall thickening + 5 × intramural edema + 10 × ulcers). *Results*. Mean MRIA and mMRIA values were 19.3 and 17.68, respectively ($p < 0.0001$). A significant correlation ($p < 0.0001$) was observed between MRIA and mMRIA scores and between both MR indexes and SES ($p < 0.0001$). *Conclusions*. mMRIA was comparable to MRIA in the evaluation of disease activity in Crohn's disease.

1. Introduction

Crohn's disease (CD) is a chronic progressive inflammatory disorder of the entire alimentary tract, classically involving the terminal ileum: ileitis is observed in 90% of the patients with small-intestinal CD, who in turn constitute 30–40% of all CD patients [1].

The disease is characterized by a relapsing and remitting course (flare-ups followed by clinical remission), posing the problem of repeated follow-ups over time for the assessment of disease activity.

To assess the severity of clinical disease activity, composite scores such as Crohn's Disease Activity Index (CDAI) or the Harvey-Bradshaw Index are used [2].

Ileocolonoscopy has been recognized as the gold standard for the evaluation of lesions in the colon and terminal ileum. To assess the severity of endoscopic inflammation, Crohn's Disease Endoscopic Index of Severity (CDEIS), the Simplified Endoscopy Score (SES-CD), or, in the postoperative setting, the Rutgeerts score was developed for use in clinical trials. However, there are several drawbacks related to the invasiveness, procedure-related discomfort, risk of bowel perforation,

and relatively poor patient acceptance; moreover, it cannot always be complete in small bowel examination [2, 3]. Small bowel imaging, therefore, plays a vital role in diagnosing and phenotyping CD, thereafter assessing disease activity and complications [4]. MR enterography (MR-E) of the small bowel, thanks to the lack of ionizing radiation, along with very high soft-tissue contrast and multiplanar images has high diagnostic accuracy in the evaluation of luminal and extraluminal abnormalities [5].

A recent study, by proving evidence that the magnitude of quantitative MR changes (wall thickening, presence of edema and ulcers, and contrast signal intensity) closely parallels the severity of endoscopic lesions, allowed the creation of an MR index of activity (MRIA). The authors also demonstrated that MRIA is highly correlated with endoscopic scores [6].

In this paper, we have calculated a modified MRIA score (mMRIA) removing from the calculation suggested by Rimola et al. the data related to the relative contrast enhancement of bowel wall in order to correlate this score to MRIA and endoscopic score. Our purpose was to verify if this modified score, which is calculated from unenhanced images, might be used with the same accuracy compared to MRIA with possible advantages in pediatric patients, in the case of proven intolerance to gadolinium-based contrast and in subjects with severe renal failure and in repeated follow-up examination.

2. Materials and Methods

2.1. Study Population. During the period between March 2013 and March 2015, 100 patients aged between 16 and 81 were retrospectively enrolled in this study. Inclusion criteria were the following: (1) histologically proven Crohn's disease of the terminal ileum, (2) availability of a complete colonoscopy with terminal ileum exploration, (3) lack of surgical intervention related to Crohn's disease, and (4) MR-E performed within 60 days from endoscopy.

Disease duration ranged from 3 to 100 months (average 37 months). According to their treatment patients were divided into the following groups: (1) untreated patients (32/100), (2) patients assuming mesalazine (14/100), (3) patients assuming immunomodulators (31/100), and (4) patients assuming biological drugs (23/100). Our series was divided into two more groups related to the use of systemic corticosteroids (39/100 cases).

The informed consents of all the patients were available for both colonoscopy and MR-E. The study was approved by the Local Ethical Committee.

2.2. Endoscopic Evaluation. In this study, the endoscopic records of the 100 patients were reviewed. MR-E was performed between 4 and 60 days (mean 48 days) from endoscopy. In 28/100 cases it was performed before ileocolonoscopy, while in 72/100 patients MR-E followed endoscopy. Endoscopic exams were performed by a board certified gastroenterologist with 10 years of experience in performing ileocolonoscopy. For calculating the SES-CD, the intestine was divided into five segments: the ileum, the right colon, the transverse colon, the left colon, and the rectum. The degree of disease involvement in each of the five segments was determined by the assessment of four parameters: presence and size of ulcers (score 0–3), extent of ulcerated surface (score 0–3), extent of affected surface (score 0–3), and presence and type of narrowing (score 0–3) [7]. Each bowel segment may have values between 0 and 12 while the overall SES score is calculated as the sum of each segment's score and may range from 0 to 60. Both overall and terminal ileum scores were calculated in our series and disease activity categories were assessed according to the overall SES score (Table 1).

Table 1: Endoscopic activity of Crohn's disease according to SES scores.

Overall SES score	Crohn's disease activity
0–2	Disease in remission
3–6	Mild disease activity
7–15	Moderate disease activity
>15	Severe disease activity

2.3. Magnetic Resonance Enterography Technique. All MR-E were performed on a 1.5-Tesla MR unit (Philips Achieva 1.5 T A-series, Koninklijke Philips Electronics N.V., Eindhoven, The Netherlands) with a 4-channel phased-array body coil in the prone position.

Patients were asked to take oral laxatives at variable times and personalized doses to cleanse the bowel and to fast an overnight before the exam.

On the day of the examination, 45–55 min before the MR, each patient received orally a solution of biphasic contrast medium, previously prepared by dissolving 250–300 mL of 18% mannitol in 1500 mL of water in order to achieve a 3.5%–4% solution.

Inhibition of bowel peristalsis was achieved by injecting 10 mL/mg N-butyl scopolamine (Buscopan, Boehringer Ingelheim, Florence, Italy) intramuscularly before starting the MR examination.

The imaging protocol consisted of the following breath-hold sequences (Table 2):

(1) Coronal, axial, and sagittal 2D balanced turbo-field echo (BTFE): matrix 256 × 256; slice number 40; thickness 8 mm, with 4 mm overlap; shortest TE/TR; flip angle 90°; FOV 350–450; and acquisition time 21 s/sequence.

(2) Coronal and axial T2W single shot turbo spin echo (SSh-TSE): thickness 4-5 mm; TE 100 ms; shortest TR; flip angle 90°; matrix 320 × 320; FOV 350–450 mm; and breath-hold acquisition.

(3) Axial T2W single shot turbo spin echo SPAIR (SSh-TSE-SPAIR): thickness 4-5 mm; TE 100 ms; shortest TR; flip angle 90°; matrix 320 × 320; FOV 350–450 mm; and breath-hold acquisition.

(4) Coronal T1w high-resolution isotropic volume (THRIVE): matrix 256 × 256; slice number 100; thickness 2 mm; SENSE factor 4; shortest TE/TR; flip angle 10;

Table 2: MRE sequences.

Sequence	Plane	Thickness/overlap	FOV	TR/TE (ms)	FA
Balanced turbo-field echo	Ax./Cor./Sag.	8/4 mm	350–450	Shortest/shortest	90°
T2 single shot	Ax./Cor.	4-5/0 mm	350–450	Shortest/100	90°
T1 high resolution isotropic volume (THRIVE)	Ax./Cor./Sag.	4/2 mm	350–450	Shortest/shortest	10°

FOV 350–450; acquisition time 19 s/sequence; coronal and axial T1w high-resolution isotropic volume (THRIVE). This sequence was acquired before and after i.v. administration of 0.15 mL/Kg of gadolinium diethylene-triamine penta acetic acid (Gd-DTPA) 0.5 M followed by 20 of saline solution with a scan delay of 35, 70, and 120 seconds.

(5) THRIVE acquisitions in the axial and sagittal plane: matrix 256 × 256; slice number 100; thickness 2 mm; SENSE factor 4; shortest TE/TR; flip angle 10; FOV 350–450; acquisition time 19 s/sequence.

2.4. Image and Statistical Analysis. Two radiologists experienced in abdominal MR imaging (AS with 10 years of experience and AASI with 15 years of experience identified throughout the paper as R1 and R2) who were unaware of endoscopic findings and results independently reviewed the examinations.

The analysis was performed using a dedicated postprocessing workstation DICOM viewer (OsiriX imaging software), examining the images from all sequences.

For all the examinations MRIA (magnetic resonance index of activity) and mMRIA (modified MRIA) of the terminal ileum were calculated by both the readers.

MRIA was calculated according to previous paper by Rimola et al. with the following formula:

1.5 × wall thickness (mm) + 0.02 × RCE + 5 × edema + 10 × ulceration (where RCE corresponds to the relative contrast enhancement) [6].

The mMRIA was obtained by the same calculation, excluding the data related to relative contrast enhancement (0.02 × RCE), using the following formula: 1.5 × wall thickness (mm) + 5 × edema + 10 × ulceration.

Quantitative measurements (wall thickness, RCE) were obtained from the most thickened loop. The presence of mucosal ulceration was defined as deep depressions in the mucosal surface within the thickened wall (Figure 1), and the presence of mural edema was defined as the high intensity signal on T2-weighted sequences relative to the psoas muscle's signal intensity (Figure 2).

Then relative contrast enhancement (RCE) was calculated according to the following formula: RCE = [(WSI postgadolinium − WSI pregadolinium)/(WSI pregadolinium)] × 100 × (SD noise pregadolinium/SD noise postgadolinium), where SD noise pregadolinium corresponds to the average of three SD of the signal intensity measured outside of the body before gadolinium injection, and SD noise postgadolinium corresponds to the SD of the same noise after gadolinium administration.

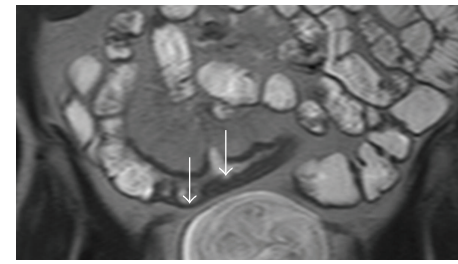

Figure 1: MRE, T2W coronal image. Ulcerations were diagnosed when irregular mucosal depressions were recognized within a thickened loop (arrow).

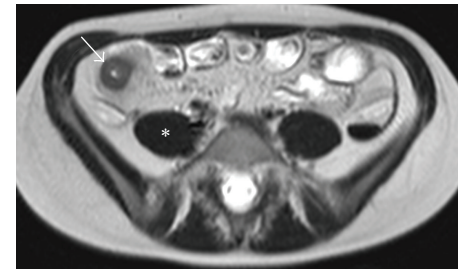

Figure 2: MRE, T2W axial image. Edema was diagnosed when the involved loops (arrow) showed higher signal intensity compared with psoas muscle (∗) in T2W images.

Cohen K test was used to calculate the interobserver agreement between R1 and R2 in recognizing qualitative MR findings such as wall ulceration and edema and to estimate agreement between endoscopy and MR-E. The quantitative evaluations such as wall thickness, RCE, MRIA, and mMRIA were compared between the two readers using the paired samples and two-sample Student's t-test, while the MRIA/mMRIA correlation was calculated using Pearson's correlation. The correlation between MRIA/mMRIA and endoscopic SES index was explored by Spearman's rank correlation. Statistic tests were performed using the software STATA/IC 14.

3. Results

Endoscopic evaluations and MR-E were considered adequate to the diagnosis in all the cases.

Endoscopy demonstrated the disease in all the patients. A terminal ileitis was diagnosed in 58/100 cases and ileocolitis in 23/100 patients, while Crohn's colitis was recognized in 19/100 patients. Overall SES ranged from 0 to 47 (mean 11.23, SD 8) while SES of terminal ileum ranged from 0 to 12 (mean 4.2; SD 3.3). On the basis of endoscopy a complete

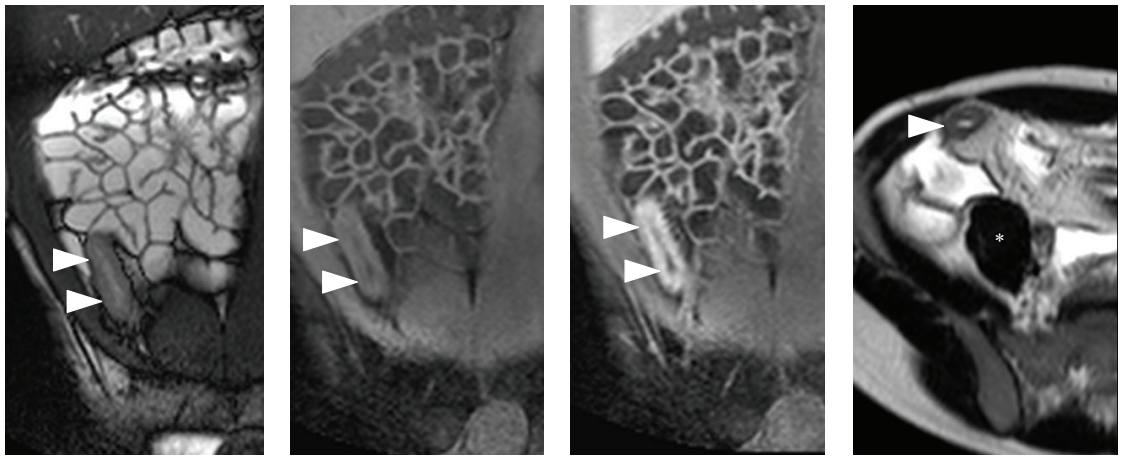

Figure 3: MR-E of a patient with terminal ileitis (ileal SES score 10; overall SES score 15). (a) Coronal B-TFE image. (b) Unenhanced coronal THRIVE image. (c) CE-coronal THRIVE. (d) Axial SSh-T2 image. MR-E shows a 10 mm thick, hyperenhancing, and ulcerated terminal ileum (arrowheads). T2 sequence demonstrates mural edema as terminal ileum (arrowheads) shows higher signal intensity than psoas muscle (∗). MRIA = 31.4; mMRIA = 30.

Table 3: Disease activity of patients' series according to SES values.

SES group	Number of patients
Disease in remission	3
Mild disease activity	27
Moderate disease activity	51
Severe disease activity	19

remission (score 0–2) was diagnosed in 3/100 patients (3%), a mild disease activity (score 3–6) in 27/100 (27%) cases, a moderate activity (7–15) in 51/100 (51%) patients, and a severe disease (>15) in the remaining 19/100 (19%) patients (Table 3). Both the readers demonstrated the involvement of the terminal ileum in 75/100 patients, while the terminal ileum was considered normal in 25/100 cases.

Ulcerations were recognized in 52/100 patients by R1 and in 50/100 cases by R2 ($K = 0.85$) while mural oedema was diagnosed in 57/100 cases by R1 and in 60/100 by R2 ($K = 0.83$). Mean wall thickness was not statistically different between R1 (mean 7.44; SD 3.16) and R2 (mean 7.31; SD 3.2). MRIA and mMRIA indexes calculated on CE MR-E were not different between the two readers ($p > 0.05$); namely, MRIA ranged from 3.78 to 38.17 (mean 19.13; SD 10.68) for R1 and from 4.78 to 39.45 (mean 19.014; SD 10.47) for R2, while mean mMRIA ranged from 3 to 37.5 (mean 17.7; SD 10.38) for R1 and from 4.5 to 37 (mean 17.48; SD 10.07) for R2 (Figure 3). Paired samples t-test demonstrated a statistically significative difference between MRIA and mMRIA for both the readers ($p < 0.0001$) (Figure 4). In addition, MRIA and mMRIA showed a strong correlation between each other (Pearson's $r = 0.99$; $p < 0.0001$) (Figure 5).

In our series, overall SES, ileal SES, and disease activity groups showed a strong correlation with MRIA and mMRIA. Correlation coefficients, which are summarized in Table 4,

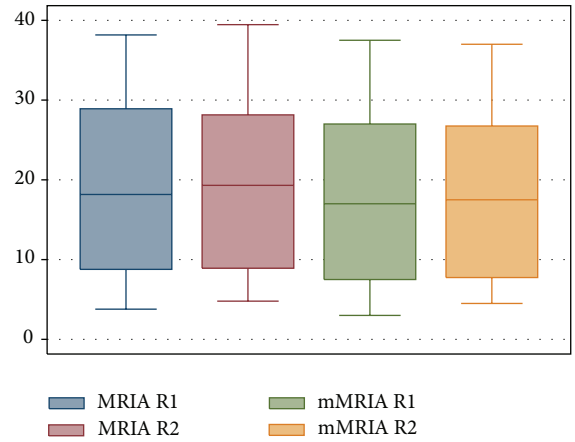

Figure 4: Box-plot of MRIA and mMRIA values of our series.

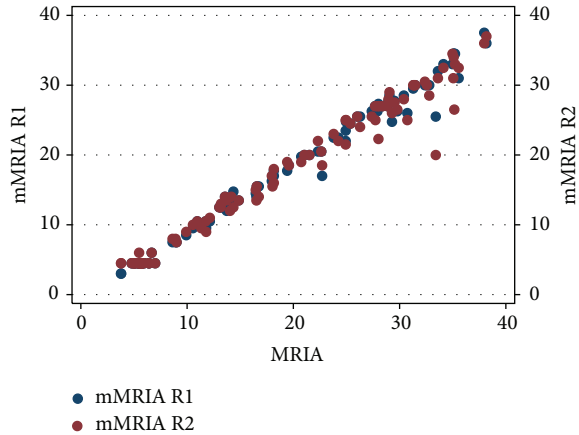

Figure 5: Scatter plot diagram demonstrating a strict correlation between MRIA and mMRIA values for both the reviewers.

Table 4: Correlation coefficients between MRIA, mMRIA, and endoscopic findings for R1 and R2.

	Overall SES	Ileal SES	Disease activity groups
MRIA R1	0.5965*	0.3683*	0.5872*
mMRIA R1	0.5940*	0.3637*	0.5899*
MRIA R2	0.6037*	0.3708*	0.6031*
mMRIA R2	0.5931*	0.3851*	0.5920*

* $p < 0.0001$.

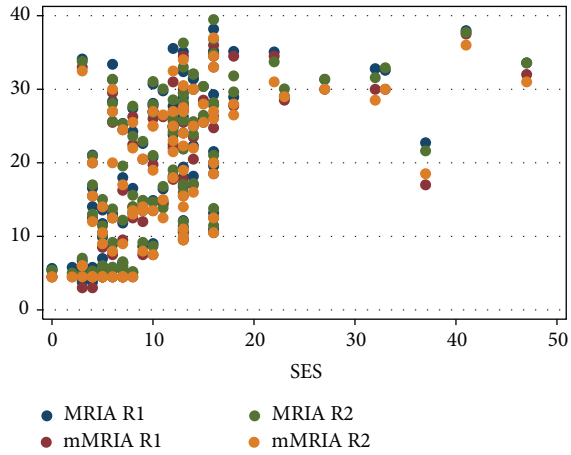

Figure 6: Scatter plot diagram of MRIA and mMRIA versus overall SES values.

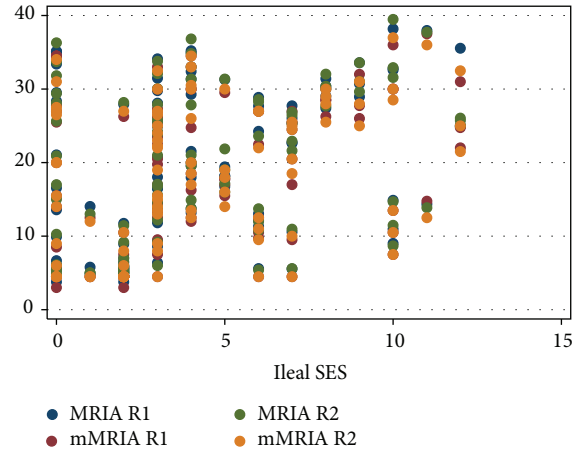

Figure 7: Scatter plot diagram of MRIA and mMRIA versus ileal SES values.

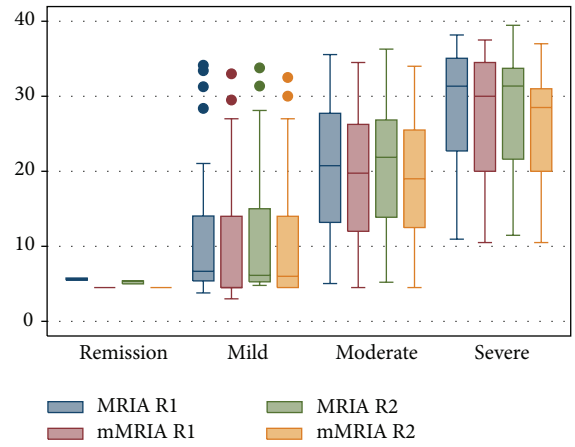

Figure 8: Box-plot diagram of MRIA and mMRIA values related to disease activity groups for both R1 and R2.

were statistically significative for R1 and R2 (Table 4, Figures 6–8).

The one-way ANOVA comparing patients assuming different treatments showed significantly lower values of MRIA and mMRIA in patients without any treatment ($p = 0.049$), while no differences were found for subjects assuming mesalazine, immunomodulators, or biological drugs. In addition, MRIA and mMRIA values were significantly higher in patients using systemic corticosteroids for both the readers (R1: $p = 0.018$ and 0.035; R2: $p = 0.016$ and 0.033).

4. Discussion

In this study we compared the accuracy of MRIA to mMRIA which is calculated from unenhanced images only and we found that these two scores can be calculated with a very good interobserver agreement and have the same degree of correlation with the SES endoscopic score. To monitor disease activity and to guide appropriate treatment, CD patients require multiple imaging examinations repeatedly [8]. Cross-sectional techniques have advanced the ability to diagnose, classify, and monitor CD [9]; the desirable imaging modality would be one that is reproducible, free of ionizing radiation, and well tolerated. MR-E is a noninvasive technique not relying on ionizing radiation, showing high values of sensitivity and specificity in CD assessment [10] and nowadays the standard protocol is based on morphologic unenhanced images and on dynamic fast 3D spoiled gradient echo T1 fat-suppressed postcontrast sequence that evaluates the pattern of bowel wall enhancement [11].

Many studies stress the importance of evaluating the pattern of contrast enhancement of bowel wall, to assess disease activity [12]. Dambha et al., in a recent study in 2014, point out that intense mucosal enhancement postintravenous gadolinium is typical of active disease and that gadolinium administration identifies acute inflammatory change [13]. According to them, mucosal hyperenhancement has occasionally been found to be the only feature of recurrent disease in the absence of typical imaging findings [13]. Furthermore, in a study by Macarini et al., a significant reduction in wall thickness and contrast enhancement is considered the most reliable finding for predicting clinical remission in patients treated for active disease [10]. Other authors suggest assessing wall thickness and presence of edema in T2 sequence images as an initial global appraisal and only adding a basal and contrast enhanced T1 sequence in case an abnormality is detected [14]. Existing MRI activity scores generally include the evaluation of the pattern of contrast enhancement [6, 15–19]. Because the location of CD lesions in the intestine has a characteristic skip pattern, in which segments with severe

ulcerative lesions can be adjacent to others with normal mucosa, Rimola et al. evaluated the MR findings associated with lesions of different endoscopic severity in a segment-by-segment analysis and also as a global MR index of activity (MRIA). MR changes found to be associated with disease activity and severity included edema, presence of ulcers, wall thickening, and relative contrast enhancement [6].

The aim of our paper was to compare MRIA to a modified index (mMRIA) calculated from unenhanced sequences. We found that mMRIA was statistically different from MRIA but it showed a very strong correlation with MRIA. In addition, mMRIA and MRIA demonstrated a comparable significative correlation with the endoscopic index of disease activity in the terminal ileum and with the disease activity calculated on the basis of SES score. As expected untreated patients (with clinical remission or mild disease activity) and patients using systemic corticosteroid (usually not responding to standard therapy) showed, respectively, lower and higher value of MRIA/mMRIA scores, while we did not find any difference among the remaining treatment groups. Probably the evaluation of multiple follow-up exams might put a light on the role of MR activity indexes in the evaluation of therapy efficacy. This experience shows that a reliable calculation of an MR based activity index can be achieved using unenhanced scans without any accuracy issue. However, despite these promising results, it should be remembered that the morphologic mural changes, the hyperintensity in T2-weighted sequences, and contrast enhancement are the expression different phenomena. Namely, T2-hyperintensity is due to mural edema, while contrast enhancement is related to wall hypervascularity and increased vascular permeability which frequently but not necessarily overlap [6, 17]. For this reason CE sequences and consequent patterns of mural contrast enhancement still play a crucial role in the assessment of Crohn's disease, namely, in the first assessment of the disease. On the other hand, RCE has a little effect on the MRIA calculation and it is not surprising that MRIA and mMRIA perform the same if compared with endoscopy as mMRIA actually constitutes the biggest part of MRIA score.

Our experience demonstrates that the calculation of a reliable index to assess Crohn's disease activity may be done with an unenhanced MR-E. According to these results, contrast injection could be avoided without concerns in patients needing repeated follow-up exams who generally show a better acceptance for unenhanced exams; furthermore, these findings can be really helpful with obvious advantages for pediatric patients and in case of renal failure or proven allergic reaction to Gd-based agents.

Our study has some limitations mostly related to its retrospective nature: firstly, our sample is inhomogeneous as patients had different disease durations and were following different treatments which might be responsible for anatomical changes we could not appreciate in a single MR exam. Secondly, the time slot between MR-E and endoscopy was variable leading to discrepancies between endoscopy and MR-E. Lastly, differing from previous studies, a complete per-segment and per-patient evaluation could not be done since the lack of a dedicate distension of the colon with oral contrast only allowed a reliable evaluation of the sole terminal ileum.

5. Conclusions

The results of this study show that the proposed mMRIA score provides a promising tool for assessing CD severity of the terminal ileum with a strong correlation with MRIA score and with endoscopy. The use of the mMRIA that is obtained from unenhanced images might be useful in different clinical settings such as follow-up exams, pediatric patients, and subjects with chronic renal failure or proven intolerance to Gd-based contrast media. Anyhow, further prospective studies are required to confirm mMRIA utility on both small bowel and colonic loops and to investigate its accuracy as a predictor of treatment efficacy in repeated studies.

Conflict of Interests

The authors declare that there is no conflict of interests regarding the publication of this paper.

References

[1] K. Horsthuis, P. C. F. Stokkers, and J. Stoker, "Detection of inflammatory bowel disease: diagnostic performance of cross-sectional imaging modalities," *Abdominal Imaging*, vol. 33, no. 4, pp. 407–416, 2008.

[2] B. Pariente, J. Cosnes, S. Danese et al., "Development of the Crohn's disease digestive damage score, the Lemann score," *Inflammatory Bowel Diseases*, vol. 17, no. 6, pp. 1415–1422, 2011.

[3] J. Panés, R. Bouzas, M. Chaparro et al., "Systematic review: the use of ultrasonography, computed tomography and magnetic resonance imaging for the diagnosis, assessment of activity and abdominal complications of Crohn's disease," *Alimentary Pharmacology & Therapeutics*, vol. 34, no. 2, pp. 125–145, 2011.

[4] S. Taylor, S. Mallett, G. Bhatnagar et al., "METRIC (MREnterography or ulTRasound in Crohn's disease): a study protocol for a multicentre, non-randomised, single-arm, prospective comparison study of magnetic resonance enterography and small bowel ultrasound compared to a reference standard in those aged 16 and over," *BMC Gastroenterology*, vol. 14, article 142, 2014.

[5] J.-M. Benitez, M.-A. Meuwis, C. Reenaers, C. Van Kemseke, P. Meunier, and E. Louis, "Role of endoscopy, cross-sectional imaging and biomarkers in Crohn's disease monitoring," *Gut*, vol. 62, no. 12, pp. 1806–1816, 2013.

[6] J. Rimola, S. Rodriguez, O. García-Bosch et al., "Magnetic resonance for assessment of disease activity and severity in ileocolonic Crohn's disease," *Gut*, vol. 58, no. 8, pp. 1113–1120, 2009.

[7] M. Daperno, G. D'Haens, G. Van Assche et al., "Development and validation of a new, simplified endoscopic activity score for Crohn's disease: the SES-CD," *Gastrointestinal Endoscopy*, vol. 60, no. 4, pp. 505–512, 2004.

[8] T. Fujii, M. Naganuma, Y. Kitazume et al., "Advancing magnetic resonance imaging in crohn's disease," *Digestion*, vol. 89, no. 1, pp. 24–30, 2014.

[9] A. Athanasakos, A. Mazioti, N. Economopoulos et al., "Inflammatory bowel disease—the role of cross-sectional imaging techniques in the investigation of the small bowel," *Insights into Imaging*, vol. 6, no. 1, pp. 73–83, 2015.

[10] L. Macarini, L. P. Stoppino, A. Centola et al., "Assessment of activity of Crohn's disease of the ileum and large bowel: proposal

for a new multiparameter MR enterography score," *Radiologia Medica*, vol. 118, no. 2, pp. 181–195, 2013.

[11] S. H. Kim, "Computed tomography enterography and magnetic resonance enterography in the diagnosis of Crohn's disease," *Intestinal Research*, vol. 13, no. 1, pp. 27–38, 2015.

[12] D. J. M. Tolan, R. Greenhalgh, I. A. Zealley, S. Halligan, and S. A. Taylor, "MR enterographic manifestations of small bowel Crohn disease," *Radiographics*, vol. 30, no. 2, pp. 367–384, 2010.

[13] F. Dambha, J. Tanner, and N. Carroll, "Diagnostic imaging in Crohn's disease: what is the new gold standard?" *Best Practice and Research: Clinical Gastroenterology*, vol. 28, no. 3, pp. 421–436, 2014.

[14] J. Rimola, I. Ordás, S. Rodriguez et al., "Magnetic resonance imaging for evaluation of Crohn's disease: validation of parameters of severity and quantitative index of activity," *Inflammatory Bowel Diseases*, vol. 17, no. 8, pp. 1759–1768, 2011.

[15] A. Laghi, O. Borrelli, P. Paolantonio et al., "Contrast enhanced magnetic resonance imaging of the terminal ileum in children with Crohn's disease," *Gut*, vol. 52, no. 3, pp. 393–397, 2003.

[16] R. N. Low, I. R. Francis, D. Politoske, and M. Bennett, "Crohn's disease evaluation: comparison of contrast-enhanced MR imaging and single-phase helical CT scanning," *Journal of Magnetic Resonance Imaging*, vol. 11, no. 2, pp. 127–135, 2000.

[17] F. Maccioni, A. Bruni, A. Viscido et al., "MR imaging in patients with Crohn disease: value of T2- versus T1-weighted gadolinium-enhanced MR sequences with use of an oral superparamagnetic contrast agent," *Radiology*, vol. 238, no. 2, pp. 517–530, 2006.

[18] J. Florie, M. N. J. M. Wasser, K. Arts-Cieslik, E. M. Akkerman, P. D. Siersema, and J. Stoker, "Dynamic contrast-enhanced MRI of the bowel wall for assessment of disease activity in Crohn's disease," *The American Journal of Roentgenology*, vol. 186, no. 5, pp. 1384–1392, 2006.

[19] N. Gourtsoyiannis, N. Papanikolaou, J. Grammatikakis, G. Papamastorakis, P. Prassopoulos, and M. Roussomoustakaki, "Assessment of Crohn's disease activity in the small bowel with MR and conventional enteroclysis: preliminary results," *European Radiology*, vol. 14, no. 6, pp. 1017–1024, 2004.